DESIGNING NOVEL HOST MATERIALS FOR BLUE PHOSPHORESCENT ORGANIC LIGHT-EMITTING DIODES

DISSERTATION

Zur Erlangung des akademischen Grades

eines Doktors der Naturwissenschaften (Dr. rer. nat)

im Fach Chemie der Fakultät für Biologie, Chemie und Geowissenschaften

der Universität Bayreuth

vorgelegt von

Michael Rothmann

geboren in München / Deutschland

Bayreuth, 2009

Die vorliegende Arbeit wurde in der Zeit von Januar 2006 bis November 2009 am Lehrstuhl für Makromolekulare Chemie I der Universität Bayreuth unter Betreuung von Prof. Dr. Peter Strohriegl angefertigt.

Vollständiger Abdruck der von der Fakultät für Biologie, Chemie und Geowissenschaften der Universität Bayreuth genehmigten Dissertation zur Erlangung des akademischen Grades Doktor der Naturwissenschaften (Dr. rer. nat.).

Datum der Einreichung der Dissertation:	27. November 2009
Datum des wissenschaftlichen Kolloquiums:	18. März 2010

Prüfungsausschuss:

Vorsitzender:	*Prof. Dr. Karlheinz Seifert*
Erstgutachter:	*Prof. Dr. Peter Strohriegl*
Zweitgutachter:	*Prof. Dr. Mukundan Thelakkat*
	Prof. Dr. Helmut Alt

„Dem Licht muß notwendigerweise Finsternis vorangegangen sein.“

Giacomo Girolamo Casanova

Table of Contents:

Summary

The overall efficiency of an organic light-emitting diode (OLED) is always limited to the efficiency of its individual components. The most important component is the emission layer, where excitons are formed and light is generated. This thesis deals with the improvement of one class of OLED component, namely host materials for blue phosphorescent emitters. Three generations of 1,3,5-triazine-based materials with varying donor-substituents are presented in this work. In the first generation carbazole units are bound to the triazine core. The second generation consists of triazines with diarylamino substituents. The third generation compounds are a combination of disubtituted triazines from the first two generations and a phenoxy-carbazole unit. While the first and second generation comprise substituents that are directly bound to the triazine core, in the third generation triazines the phenylcarbazole-donor is attached via a nonconjugated ether bond. Within each generation various properties are tailored to fulfill the complex profile of requirements for host materials.

Known nucleophilic substitution reactions were further improved to enable the efficient synthesis of novel host materials in very high purity and high yields. The sequential replacement of the chlorines of cyanuric chloride is dependent on temperature, actual ring substitution and the nature of the nucleophile. Effective methods were developed to yield asymmetrically substituted triazines in a controlled manner.

The thermal properties, including the thermal stability to enable the processing by vapor deposition and the glass forming properties to result in a morphological stability of prepared thin emission layers, were controlled by systematic investigation of different substitution patterns. Thus, glass transition temperatures up to 170 °C are presented. Studies of the long term stability of amorphous host films, carried out for several materials, revealed its importance for long term efficient devices.

The electrochemical properties of the novel compounds were investigated by cyclic voltammetry to study the energetic position of the HOMO and the LUMO as well as the stability of the material upon oxidation and reduction. Using this method the injection properties of the materials were determined. The blocking of activated positions resulted in reversible redox behavior. Furthermore the ionization potential was decreased for the third generation triazines to yield an improved hole injection into these materials. Additionally computational calculations were carried out to understand and further improve the energy levels by substituent exchange. This led directly to the development of bipolar host materials with separated hole and electron transport units within one molecule. Furthermore single carrier devices were fabricated to demonstrate the benefits of the transport bipolar characteristics.

For the efficient operation of a device the triplet energy of the host material has to be higher compared to the emitter. First generation triazines exhibit triplet energies up to 2.96 eV and therefore enable the use of light and middle blue phosphorescent emitters. Second generation triazines comprise exceptionally high triplet energies up to 3.24 eV. These are amongst the highest values reported in the literature and facilitate the use of deep blue phosphorescent emitters. For hosts of the third generation the triplet energy depends on the choice of the triazine moiety. They are therefore suited for light and deep blue emitter. Extensive photo physical characterizations of all materials have been carried out in solutions, neat films and doped films. Energy transfer experiments with several emitters additionally gained valuable information about the compatibility of host and guest molecules

All generations of triazines are tested as host material in OLEDs. The optimization of the device configurations was carried out by combinatorial evaporation. The sequential adaption of layer thickness and composition helped to improve the device performance. The stepwise optimization of the host material properties resulted in an enduring progression concerning the luminance and efficiency. For the third generation triazines 11.5 % external quantum efficiency and a high brightness of 33000 cd/m^2 were achieved.

Zusammenfassung

Die Gesamteffizienz einer organischen Leuchtdiode (OLED) wird durch die Effizienzen ihrer Einzelkomponenten, aus denen sie aufgebaut ist, bestimmt. Der wichtigste Bestandteil ist die Emitterschicht, in der Exzitonen gebildet werden und Licht erzeugt wird. Diese Dissertation beschäftigt sich mit der Optimierung einer Klasse an OLED Materialien, genauer den Matrixmaterialien für blaue Phosphoreszenzemitter. In dieser Arbeit werden drei Generationen von 1,3,5-Triazinen mit verschiedenen Donorsubstituenten vorgestellt. In der ersten Generation sind Carbazoleinheiten direkt an den Triazinkern geknüpft und bei der zweiten Generation wurden diese durch Diarylaminogruppen ersetzt. Die dritte Generation ist eine Kombination aus den disubstituierten Triazinen der ersten beiden Generationen und einer Phenoxycarbazoleinheit. Während in den ersten beiden Generationen die Donorsubstituenten direkt an den Kern gebunden sind, so ist in der dritten Generation der Phenoxycarbazoldonor nicht konjugiert über eine Etherbrücke angebunden. Innerhalb einer jeden Generation werden verschiedene Eigenschaften maßgeschneidert um dem komplexen Anforderungsprofil der Matrixmaterialien gerecht zu werden.

Hierzu wurden bekannte nukleophile Substitutionen weiter verbessert, um Matrixmaterialien effizient, hochrein und in guten Ausbeuten herzustellen. Das schrittweise Ersetzen von Chlorsubstituenten des Cyanursäurechlorides ist abhängig von der Reaktionstemperatur, des Substitutionsmusters am Ring und der Natur des Nukleophils. In dieser Arbeit wurden effektive Methoden entwickelt, um asymmetrisch-substituierte Triazine in kontrollierter Weise zu erhalten.

Die thermischen Eigenschaften, welche die thermische Stabilität und die Glasbildungseigenschaften beinhalten, wurden durch systematisches Untersuchen von verschiedenen Substitutionsmustern kontrolliert. Eine hohe thermische Stabilität ermöglicht das physikalische Aufdampfen der Materialien. Gute Glasbildungseigenschaften führen zu morphologisch stabilen Emissionsschichten. Hierzu werden Verbindungen mit hohen

Glasübergangstemperaturen von bis zu 170°C vorgestellt. Untersuchungen zur Langzeitstabilität von amorphen Matrixmaterialfilmen, die für verschiedene Materialien durchgeführt wurden, demonstrieren die Bedeutung für eine hohe Lebensdauer und Effizienz der Bauteile.

Die elektrochemischen Eigenschaften der neuen Verbindungen wurden hinsichtlich der Lage der HOMO und LUMO Energieniveaus sowie der Stabilität der Materialien gegen Oxidation und Reduktion untersucht. Weiterhin wurden mit dieser Methode die Injektionseigenschaften gegenüber den Ladungsträgern bestimmt. Das Blockieren von reaktiven Positionen am Molekül resultierte reversiblem Redoxverhalten. Zusätzlich wurden Computerberechnungen durchgeführt um die Lage oder Verschiebung der Energieniveaus zu verstehen und durch Substituentenaustausch weiter zu verbessern. Das führte zur Entwicklung von bipolaren Matrixmaterialien, bei denen innerhalb eines Moleküls separate Einheiten für den Loch- und Elektronentransport vorhanden sind. Es wurden ‚Single-Carrier-Devices' hergestellt um die Vorteile der beschriebenen bipolaren Transportcharakteristik der Materialien aufzuzeigen.

Für einen effizienten Betrieb der OLED zu gewährleisten muss weiterhin das Tripletniveau des Matrixmaterials höher sein als das Tripletniveau des Emitters. Die Triazine der ersten Generation zeigen Triplettenergien von bis zu 2.96 eV und sind deshalb für leicht- und mittelblaue Emitter geeignet. Die Triplettniveaus der zweiten Triazingeneration sind mit bis zu 3.24 eV außerordenlich hoch. Das sind Werte, die sich unter den höchsten jemals in der Literatur vorgestellten Triplettenergien befinden. Bei den Verbindungen der dritten Generation hängt die Lage des Tripletniveau von der Wahl der Triazineinheit ab. Sie sind deshalb sowohl für leicht- als auch für tiefblaue Emitter geeignet. An den Materialien wurden intensive photophysikalische Untersuchungen sowohl in Lösungs als auch als auch an reinen und dotierten Filmen durchgeführt. In Energietransferexperimenten dotierter Schichten konnten wertvolle Informationen bezüglich Effizienz und Verträglichkeit der Matrix-Emitter Kombinationen gewonnen werden.

Vertreter aus allen Triazingenerationen wurden als Matrixmaterialien in OLEDs getestet. Die Optimierung der Bauteile erfolgte durch kombinatorische Aufdampfexperimente, wobei sowohl die Schichtdickenabhängigkeit als auch der Dotiergrad variiert wurde. Durch die generationsweise Optimierung der Matrixmaterialien konnten die Leuchtdichten und die Effizienzen der OLEDs stetig verbessert werden. In der dritten Generation wurden eine externe Quantenausbeute von 11.5% und eine maximale Leuchtdichte von 33000 cd/m^2 erreicht.

2 Introduction

Since C. W. Tang and S. A. van Slyke reported the first multilayer organic light-emitting diodes (OLEDs) in 1987, research groups around the world made tremendous progress in the understanding and manufacture of those devices.[1] Nowadays several companies fabricate full color OLED displays. The market for these flat-screen displays is worth billions of Euros per year. But there is another upcoming lucrative market for organic LEDs in white lighting applications. A recent study showed that about 20 % of the total primary energy is consumed by lighting.[2] This enormous amount of energy mainly originates from the use of inefficient light sources like incandescent lamps, which turn about 95 % of the energy into heat. Considering the concerns about global warming, Germany as well as many other states legislated for a general ban on inefficient light sources.[3] Well-established replacements like halogen lamps and compact fluorescent lights are equally inefficient or slightly better and generate about 20 lm/W or 60 lm/W, respectively. Only inorganic LEDs enable efficiencies beyond 120 lm/W but since they are spotlights they are not well suited as general lighting source. In the past years it has been shown with great effort that OLEDs are on the best way to become a serious competitor in the lighting market. In early 2009, the lighting companies OSRAM and PHILIPS commercialized first OLED panels whereon designers presented prototypes of desk lamps and visions of transparent luminescent windows (Figure 1).

Figure 1: (left to right) OSRAM white light OLED panel; Prototype desk lamp by I. Maurer; Vision of transparent OLED windows; (source: http://www.osram.de). This visionary study impressively illustrates one major advantage of OLEDs: the possibility of a large-area source of diffuse light.

Not only in industrial development departments but also in academic research various strategies have been developed to improve known OLED devices. Very recently K. Leo and co-workers reported a white organic light-emitting diode with fluorescent tube efficiency of 90 lm/W.[4] This step towards highly efficient lighting was only possible due to the discovery of efficient phosphorescent emitters by Forrest and Thompson in 1998.[5] From spin statistics it is known that the ratio of singlet and triplet excitons is 1:3 in small organic molecules.[6] Thus taking all loss pathways into account the maximum external quantum efficiency (EQE) of a fluorescent OLED is limited to 5 %.[7] In contrast to that an OLED that harvests singlet and triplet excitons can theoretically reach an EQE of about 20 %. For a single-color emitting system this goal was reached surprisingly early. In 2001 Forrest and co-workers presented a green OLED with 19 % EQE.[7] In the last decade several reports of 20% EQE or even slightly more emerged in scientific literature. Nowadays also red and blue OLEDs with high EQEs are well described.[8,9] However the EQE is not the only important measure for OLEDs. Especially for lighting applications the power efficiency is considered to be more important. That means additional device optimizations concerning charge carrier injection and transport have to be taken into account. In consideration of competing with modern and future lighting tubes power efficiencies above 100 lm/W are desirable. OLED lighting projects funded by the U.S. Department of Energy are intended to achieve 150 lm/W until 2015.[10]

In order to generate white light several possibilities are discussed. The most popular involves a red-green-blue (RGB) color-mixing system, where the single colors are either organized horizontally or vertically. In the horizontal approach the output spectrum can be adjusted during the operation due to the separation of the colors. This is a major advantage over the vertical stack, where the output-color is fixed once the device is fabricated. However the horizontal stack design is complicated and therefore expensive in fabrication.[11] This limits its application. The vertical approach on the other hand is ideal for a cheap large area processing. The disadvantage of this design is related to the different aging of the three sub-colors. This may result in a color shift during the lifetime of the device. Generally speaking, the lifetime of OLED materials is still a major goal toward the commercial success of the devices. Especially the blue emitting systems tend to degrade

faster than other components.[12] This fact emphasizes the importance of the further improvement of existing blue emitting systems or the development of novel ones. In Figure 2 a newly published white OLED stack by K. Leo and co-workers is compared to the first published multi-layer OLED by C. W. Tang and S. A. van Slyke. This shows the increasing complexity in this field.

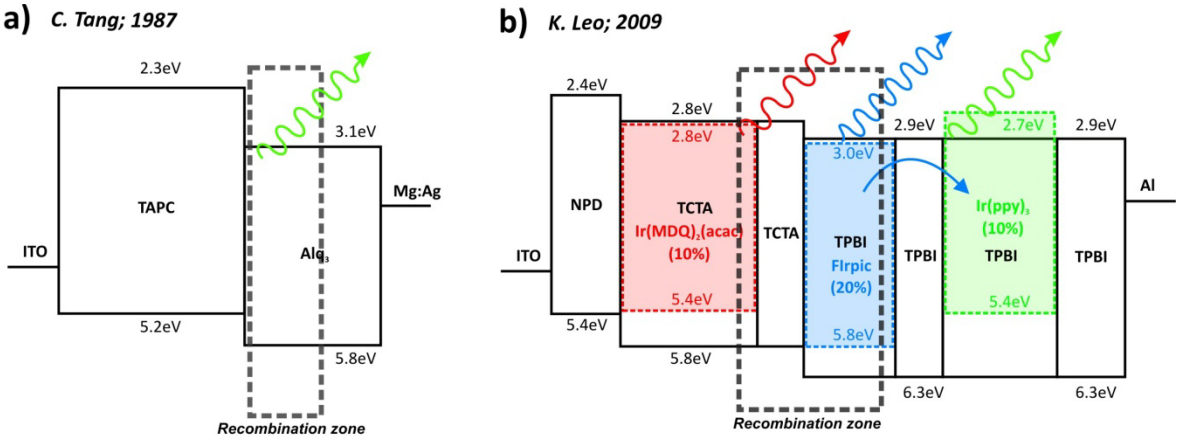

Figure 2: Energy diagram of: **a)** first published multi-layer OLED by C. Tang consisting of a hole conducting layer of TAPC, an electron conducting layer of Alq_3; **b)** state-of-the-art multi-layer white OLED stack by K. Leo and co-workers consisting of a hole and electron conducting layer as well as a complex emission layer comprising three phosphorescence emitting host guest systems (explanation of abbreviations in the respective chapter).

The Tang-device consisted of 2 layers, where TAPC acts as hole conductor and Alq_3 serves as electron conductor and emitter. This is mainly because the injection barrier for electrons from Alq_3 to TAPC is very high (0.8 eV) and therefore all excitons are generated in the Alq_3 layer. In vast contrast to that the Leo-device is a 7-layer stack involving 3 doped emission layers which are separated by thin organic layers. The charge carrier balance is extremely important in this setup to yield pure white emission. Excitons have to be generated in a narrow recombination zone and the separating layers must only permit a exciton transfer from blue to green. This illustrates the complexity of this highly optimized OLED stack. The replacement of one material would result in a complete re-design of the whole stack to guarantee efficient white emission.

OLED setup and working principle

In general there are two predominant methods to fabricate OLEDs. The organic material is either deposited from the gas phase or from solution. The vapor deposition technique is limited to small organic molecules, which can be thermally evaporated in high vacuum. Processing from solution on the other hand is also possible with high molecular weight polymers. However it is very challenging to fabricate a multi-layer organic device from solution.[13] For this purpose vapor deposition methods are very powerful. Therefore almost all state-of-the-art OLEDs are deposited from the gas phase.

The simplest setup of an organic light emitting diode is composed of an organic emissive layer, which is sandwiched between two electrodes. The first device of this kind was published by R. Friend and co-workers in 1990.[14] The device consisted of a 70 nm thick poly(p-phenylene vinylene) (PPV) layer, an indium-tin oxide bottom contact and a top contact of aluminum (Figure 3a). Although this simple OLED exhibits a poor performance regarding brightness and efficiency it exemplifies its working principle.

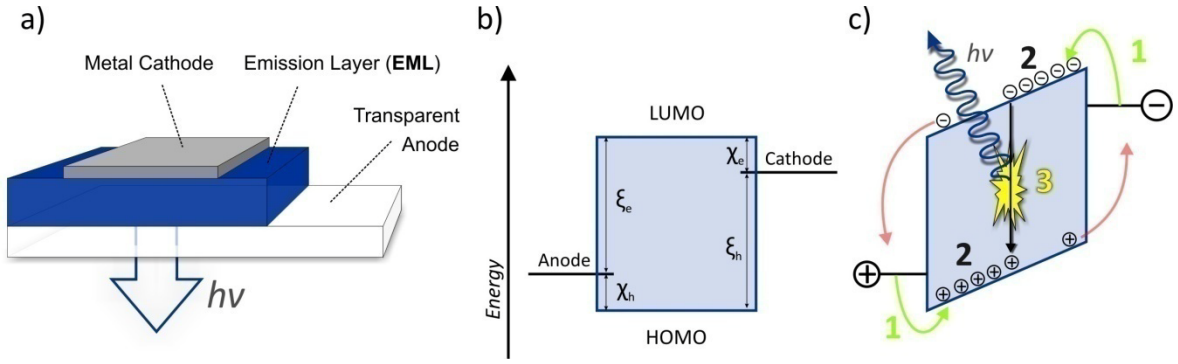

Figure 3: a) Schematic of a single-layer OLED consisting of transparent anode, emission layer (EML) and metal cathode; **b)** energy diagram of a single-layer OLED: χ_h: hole injection barrier from the anode to the HOMO of the EML; χ_e: electron injection barrier from the cathode to the LUMO of the EML; ξ_h and ξ_e: injection barriers for hole and electron from the respective counter electrode in reverse-biasing mode; **c)** energy diagram of a single-layer OLED upon applying an electric field; including three essential OLED processes: 1) injection 2) transport and 3) recombination of holes (⊕) and electrons (Θ), exciton diffusion and emission.

In Figure 3b) the energy diagram of a single layer OLED is illustrated. The injection barriers in conduction direction, χ_e for electrons and χ_h for holes, symbolize the potential difference from the Fermi level of the electrode to the lowest unoccupied molecular

orbital (LUMO) and the highest occupied molecular orbital (HOMO) of the organic material respectively. In reverse direction these barriers are symbolized by ξ_e and ξ_h. The ratio of χ to ξ is a measure for the injection balance of the diode.[15] Although the HOMO and LUMO levels are shown as line in the schematic they can be considered as a narrow Gaussian-like distribution of states.[16] Figure 3c shows the energy diagram of a single-layer OLED upon applying an electric field. The illustration includes three essential processes in an operating device, which are: the injection of charge carriers (1), the transport of hole (⊕) and electron (Θ) (2) and the formation of an exciton, exciton diffusion and its emissive decay (3).

Charge carrier injection (1)

The injection of a hole or an electron into an organic material means its oxidation or reduction respectively. As shown in Figure 3b), there are certain injection barriers χ_h and χ_e for these processes. For an efficient injection of holes and electrons they have to be as low as possible. Ideally the surface contacts are ohmic, which requires energy barriers below 0.3 eV.[17] Regarding this case the operation of the OLED is space-charge limited and no longer injection limited.[18] Additionally the injection barriers for holes and electrons should be equal to guarantee charge carrier balance in the emission layer. The injection process can be understood as a hopping process of a charge carrier from the Fermi level of the metal into tail states of the organic material.[19,20] The most common anode material for OLEDs is indium-tin oxide (ITO), which is sputtered onto a glass substrate. It is transparent and exhibits a low resistivity. The Fermi energy of ITO strongly depends on the pretreatment of the material and varies from 4.2 eV to 4.8 eV.[21] Therefore an ohmic contact is possible if the HOMO of the organic is below 5.1 eV. To avoid too strong limitations in material choice, the use of polymeric injection layers is widespread. Especially poly(3,4-ethylenedioxythiophene):poly(4-styrenesulfonate) (PEDOT:PSS) is well described in literature and enables ohmic injection into materials with HOMO energies up to 5.8 eV.[22] The variety of cathode metals is larger than for anode materials. Very favorable is a relatively low work function of the metal, like that of the alkaline earth

metals barium (Φ = 2.7 eV), calcium (Φ = 2.9 eV) or magnesium (Φ = 3.5 eV). The vast disadvantage of these metals is their reactivity. Therefore they are often capped with aluminum (Φ = 4.0 eV) or silver (Φ = 4.3 eV). Because the injection barrier of most aluminum/organic interfaces is too large for ohmic behavior, the injection properties can be increased by the introduction of a thin lithium fluoride interlayer.[23] The LiF/Al cathode allows good electron injection into most organic electron conductors.

Charge carrier transport (2)

Once holes and electrons are injected into an organic layer they will propagate to the cathode and the anode respectively, due to the external electric field. This propagation can be understood as a series of redox processes. Considering the hole transport, an oxidized molecule acts as electron acceptor for a neutral neighboring molecule which acts as electron donor. Thus, on molecular level, a hole is a radical cation while an electron is a radical anion. This means, an electron is either transferred from the LUMO to the LUMO (electron transfer) or from the HOMO to the HOMO (hole transport) of two neighboring molecules. The transfer itself is interpreted as hopping.[24] The propagation speed of the charge carriers thereby is limited by the intrinsic mobility of the material. Additionally, it is influenced by the existence of trap states within the layer. These traps are energetically more favorable sites, which result from impurities, dopants and/or defects.[16] Therefore the mobility is high in perfect organic crystals and low in amorphous materials.

Charge carrier recombination, exciton diffusion and emission (3)

In order to emit light, a hole and an electron must recombine and form an exciton. The recombination can be regarded as a reaction between hole and electron, which is driven by the Coulomb interaction. At this point it is important to know that depending on the spin of the electrons, either singlet or triplet excitons are formed. There are 4 possible spin configurations, which can result from the recombination of 2 electrons with undefined spin (Figure 4).

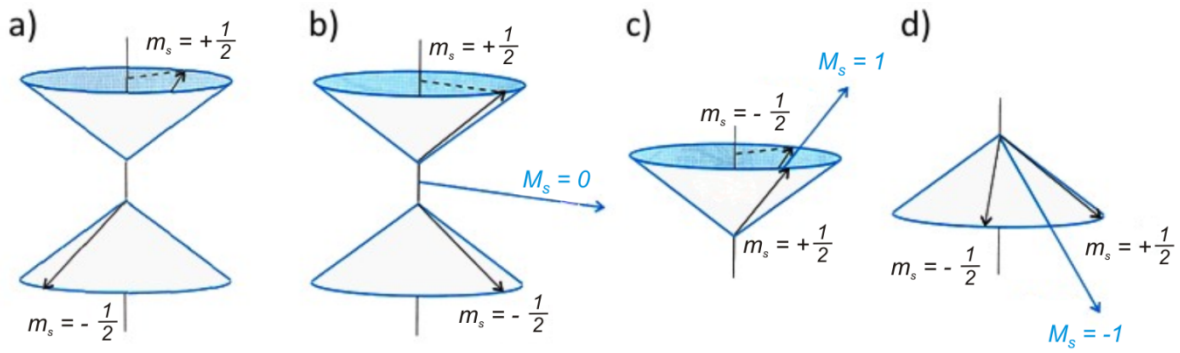

Figure 4: Possible spin configurations for the recombination of two electrons with anti-parallel spin (a) or parallel spin (b-d). While a) represents the singlet state, b)-d) are three possible triplet configurations.

If the spins (m_s) of two electrons are anti-parallel to each other, the total angular momentum (M_s) of the system is 0. This equates to a singlet exciton (Figure 4a). If the two spins are parallel the total angular momentum of the system can be +1, 0 and -1. Although the total angular momentum of configuration a) and b) are both 0, they represent different states. Since, in an OLED all injected electrons exhibit random spin all 4 configurations are possible. Thus the ratio of singlet to triplet excitons is 1 to 3. Once the exciton is formed, it can either undergo radiative decay or diffuse within the organic material. The typical lifetime of singlet or triplet exciton is in the range of nanoseconds or microseconds rerspectively. This can be translated into a typical diffusion length of about 10 nanometers. The diffusive energy transfer can be subdivided into two non-radiative mechanisms, the so-called Förster and Dexter transfer types, depending on the different intermolecular interaction. The Förster mechanism is a dipolar transfer between an excited donor molecule and a non-excited acceptor. Therefore the existence of a spectral overlap between donor-emission and acceptor-absorption is essential. Depending on the transfer efficiency the energy can be transferred over a distance of several nanometers. In contrast to that Dexter energy transfer is an electron transfer mechanism and therefore has a short range. Since the electrons are transferred by hopping an orbital overlap of donor and acceptor molecules is essential. The spin symmetry is persevered in this case, which means that both singlet and triplet excitons can be transferred. On the other side, a triplet-triplet exchange by Förster transfer in not possible. It is limited to singlet-singlet transfer in general and triplet-singlet transfer in individual cases.[25]

The emissive decay of the exciton is mainly influenced by its spin configuration. The electronic processes described in the following are summarized in Figure 5. For most organic molecules the triplet-singlet transition is spin-forbidden and therefore a very slow process. Thus the energy of a triplet is lost by non-radiative processes. The singlet-singlet transition on the other hand can be a very efficient emissive decay in organic molecules. This process is called fluorescence. In contrast to that triplet-singlet emission (phosphorescence) is only efficient if a high spin-orbit coupling within the molecule is present and the transition becomes partly allowed. This is achieved by the presence of a heavy metal atom, like iridium or platinum, in the molecule. Therefore these organometallic complexes are able to harvest singlet as well as triplet excitons and a theoretical quantum efficiency of 100% can be achieved. To obtain this it is essential that the singlet excitons are efficiently converted into triplet excitons by inter system crossing (ISC).

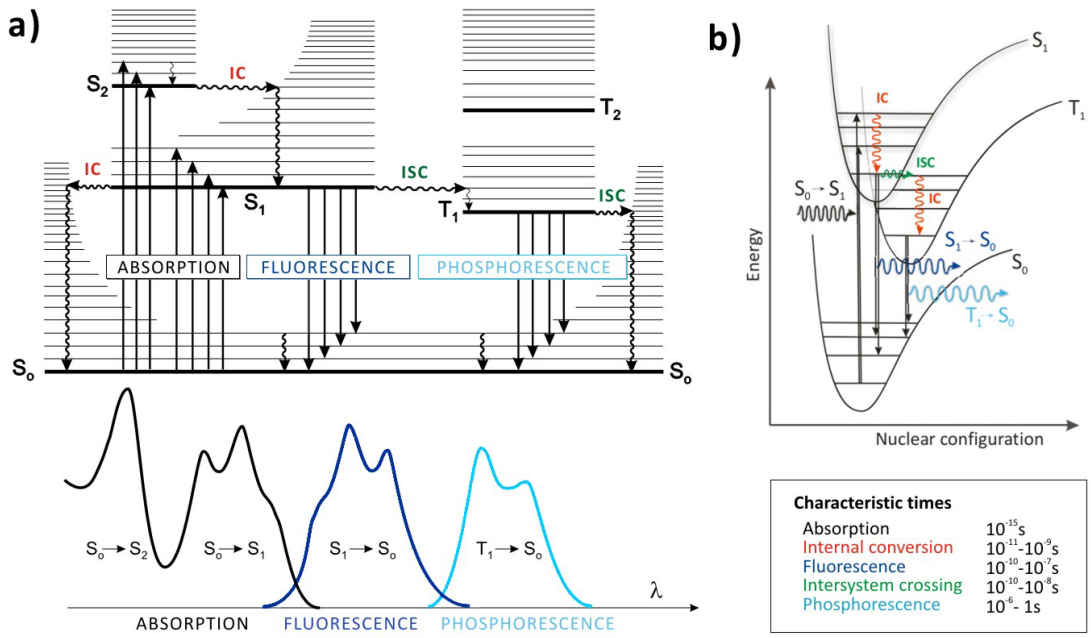

Figure 5: a) Perrin-Jablonski diagram and relative positions of absorption, fluorescence and phosphorescence in optical spectroscopy;[26] **b)** Potential diagram including ground state S_0 and the excited states S_1 and T_1; vertical electronic transitions follow the Franck-Condon principle. Both diagrams include the electronic transitions: absorption (S_0-S_1), fluorescence (S_1-S_0) and phosphorescence (T_1-S_0) as well as internal conversion (IC) and inter system crossing (ISC).

In figure 5a the relative positions of absorption, fluorescence and phosphorescence signals are shown. These electronic processes always follow the Franck-Condon principle of vertical transition (Figure 5b). While the transition is in progress the nuclear configuration does not change. Therefore the absorption actually is the transition from the vibrational ground state $S_{0,0}$ into several vibrationally excited $S_{1,n}$ states, according to the relative position and shape of the potential energy curves. This results in a characteristic splitting of the absorption signal, depending on the probability of each transition. Hence, in an idealized system the fluorescence occurs from the $S_{1,0}$ and state shows the same splitting ('mirror image' rule). At room temperature the fluorescence is generally red shifted to the absorption. This effect is called Stokes shift. Even more pronounced is this effect, if the dipole moment of excited state and ground state are different. In this case, energy is often lost due to solvent relaxation. This generally results in a lower quantum efficiency. The same effects are applicable for the phosphorescence. To populate the triplet $T_{1,0}$ state it is necessary to change the spin configuration by inter system crossing (ISC). The ISC-rate depends exponentially on the singlet-triplet gap and requires vibrational coupling of the two states. In organic molecules the energy difference is between 1 eV and 0.5 eV, whereas in organometallic complexes it can be close to zero. However there are possibilities of obtaining high ISC rates in organic materials. This is possible, if either the T_2 state is close to the S_1 state and allows efficient coupling. Furthermore, if the n-π* transition is more pronounced than the π -π* transition ISC becomes more probable.[27]

In summary, the external quantum efficiency η_{ext} of an organic light emitting diode can be expressed by the product of the single efficiencies.[7]

$$\eta_{ext} = \eta_{int} \ \eta_{ph} = \gamma \ \eta_{ex} \ \Phi_p \ \eta_{ph} \qquad (1)$$

Here, γ is the charge carrier balance factor, which is ideally equal to 1 and expresses the ratio of injected electrons to holes. The fraction of formed excitons η_{ex}, which emit light reaches a theoretical maximum of 1 for phosphorescent emitters and Φ_p is the intrinsic quantum efficiency for the emissive decay. The photon out-coupling efficiency η_{ph} depends on the used substrate and is about 20 % for glass with a refractive index of 1.5. In order to reach an internal efficiency η_{int} of 100 % it is essential that a phosphorescent

emitting system is used. Additionally the injection and transport properties for holes and electrons should be similar to obtain a perfect charge carrier balance. Therefore it is usually necessary to use a more complex device architecture than the single-layer setup shown in Figure 3a. Modern multi-layer OLEDs comprise additional injection, transport and blocking layers for both charge carriers. A schematic of a multi-layer OLED setup is presented in Figure 6.

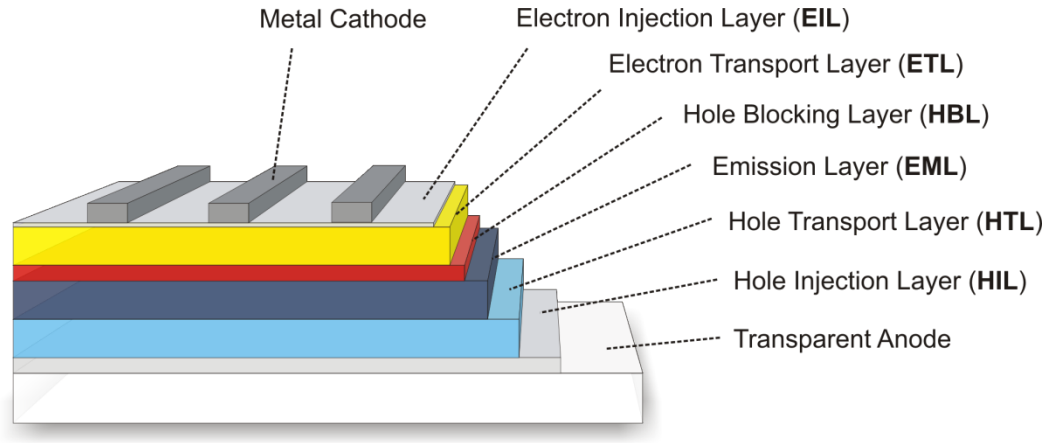

Figure 6: Typical setup of a multi-layer OLED comprising injection, transport, blocking and emission layers.

Each layer plays a decisive role in highly efficient OLED devices. The hole (HTL) and electron transport layers (ETL) should exhibit high mobilities in order to increase the charge carrier and exciton density in the emission layer (EML) and therefore achieve a high luminance. In modern phosphorescent small molecule OLEDs (SM-OLEDs) the emission layer consists of a host and the luminescent guest. The guest has to be a highly efficient emitter, while the host has to dilute the guest to prevent self quenching. The host usually is responsible for the transport of the charge carriers, exciton formation and energy transfer to the emitter. Generally the hole mobility is higher than the electron mobility in most EMLs. To handle the excess of holes often a hole blocking layer (HBL) is incorporated. To reduce the injection barriers in the device to a minimum the selection of individual materials for each setup is essential. For hole and electron transport materials as well as blocking materials there is a large number of possibilities to choose from. The selection of the host-guest system often determines the efficiency and is therefore an important aspect which is described in the following section.

OLED Materials

As described in the preceding chapter OLED materials can be divided in mainly 4 classes: hole transport materials (1), electron transport materials (2), host or matrix materials (3) and emitters (4). Although each class has to fulfill individual requirements there are general needs for all OLED materials. First of all the materials have to fit to the processing procedure. For most SM-OLEDs this involves the fabrication by thermal evaporation. Therefore the materials must exhibit a high thermal stability and the ability to evaporate thermally in high vacuum. Another essential requirement to guarantee the operational stability of the device is the ability to from a morphologically stable amorphous layer.[28] This ability guarantees that the emitter stays uniformly diluted in the matrix to minimize the effect of concentration quenching. In addition the absence of grain boundaries, which may act as trap states, makes the use of organic glasses as OLED materials advantageous.[29,16] In order to obtain organic glasses, several points have to be taken into account. An important fact is to avoid strong intermolecular forces like hydrogen bonding or π-π stacking between the molecules. Furthermore the introduction of bulky substituents leads to a larger intermolecular distance and a hindrance in packing and therefore an amorphous behavior. On the other hand the increased distance separates the conducting units from each other and results in a decreasing charge carrier mobility. Another possibility to design organic glasses is the synthesis of asymmetric molecules. With this method the number of conformers is increased and the high amount of energy needed for the crystallization favors the stability of amorphous films.[28,30] Furthermore the morphological stability of an amorphous film strongly depends on the glass transition temperature (T_g) of the material. In a first approximation the T_g should exceed the operational temperature by at least 50 °C to guarantee morphological stability.[31,32] The injection and transport properties are different for all classes of materials and therefore described separately.

Hole Transport Materials

Most hole-transporting materials reported so far contain electron donating aromatic amino groups Among the aromatic amines the triphenylamino moieties are the most common ones. In Figure 7 a selection of frequently used HT-materials is presented.

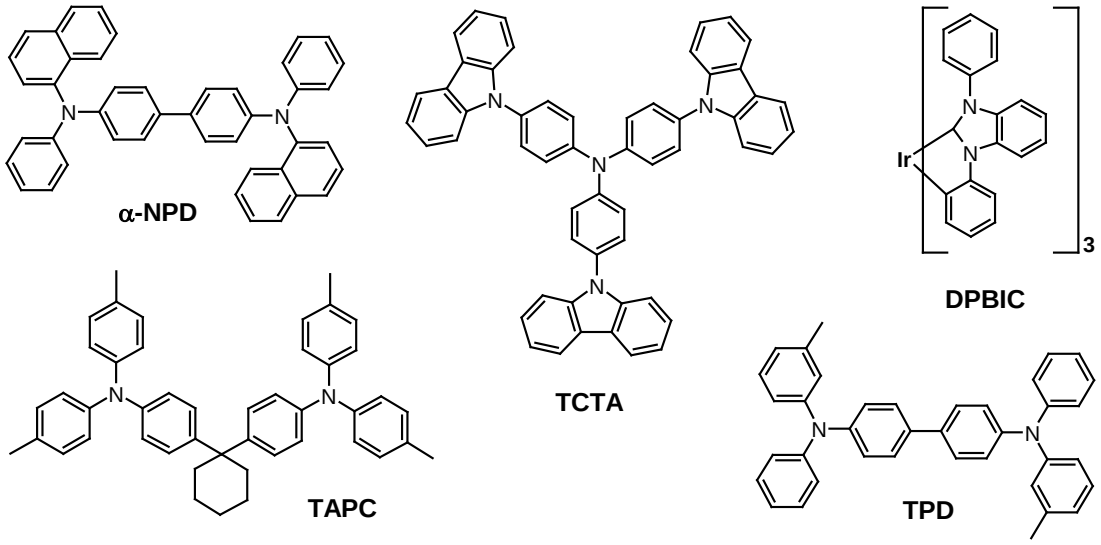

Figure 7: Selection of hole transport materials: N,N'-di(naphtha-1-yl)-N,N'-diphenyl-benzidine (**α-NPD**), 4,4',4''-tris(carbazol-9-yl)triphenylamine (**TCTA**), tris[(3-phenyl-1H-benzimidazol-1-yl-2(3H)-ylidene)-1,2-phenylene]-Iridium (**DPBIC**), 1,1'-bis(4'-(N,N'-di(p-tolyl)aminophenyl)cyclohexane (**TAPC**), N,N'-bis(3-methylphenyl)-N,N'-diphenyl-benzidine (**TPD**) (left-to-right and top-to-bottom)

As described previously one important requirement for OLED materials is the ability to form stable amorphous films. Since the T_g is a measure for the long-term stability high values are desirable. The triphenylamino containing material TPD (T_g = 60°C) exhibits the lowest glass transition temperatures of the selection shown in figure 7. Although the temperature is increased to 78 °C for TAPC both materials form meta-stable amorphous films.[28] The T_g of the naphthyl-substituted NPD (100 °C) is high enough to prevent crystallization of an amorphous film.[30] The glass formation properties of TCTA (T_g = 150 °C) are even better due to its space-filling star-shaped structure. Another important criterion, especially for HTL and ETL materials, is the charge carrier mobility. Since the mobility is generally high in ordered systems like crystals, amorphous films usually exhibit significantly lower values by several orders of magnitudes. However, within common hole conductors (figure 7) TAPC shows the highest mobility values with $1*10^{-2}$ $cm^2V^{-1}s^{-1}$.[33] TPD

and TCTA exhibit values that are lower by one order of magnitude, while the mobility of NPD and DPBIC is in the range of 10^{-4} $cm^2V^{-1}s^{-1}$.[34,37] Good hole injection properties on the other hand require a small energy gap between work-function of the anode and HOMO of the HTL. The HOMO values of TPD, DPBIC, TAPC and NPD are in the range of 5.2 eV to 5.4 eV and well situated for hole injection from ITO or an organic injection layer.[35,36] The carbazole moiety of TCTA is responsible for the relatively low HOMO of 5.8 eV which results in worse injection properties. Besides these general requirements for HTL materials, for blue phosphorescent OLEDs another property becomes important. Especially when the recombination zone is close to the HTL-EML interface excitons may diffuse into the HTL layer, if the triplet energy of the HTL material is lower than that of the host-guest system of the EML. The subsequent exciton decay in the HTL is a very effective efficiency loss pathway.[37] Regarding the triplet energies of the presented hole transport materials only DPBIC ($E(T_1\text{-}S_0)$ = 2.96 eV) and TAPC ($E(T_1\text{-}S_0)$ = 2.87 eV) exhibit large enough energy gaps for blue OLEDs. The energies of NPD and TPD are 2.29 eV and 2.34 eV respectively and therefore too low for blue OLEDs. In this case the application of an exciton blocking interlayer allows the use of NPD or TPD as HTL materials. In summary TAPC is a perfect choice for highly efficient blue OLEDs, but due to its morphological instability its not suited for long lifetime OLEDs. For this purpose DPBIC is a better compromise despite its lower hole mobility.

Electron Transport Materials

In contrast to HTL materials electron conductors often comprise electron deficient heterocycles, like pyridines, pyrimidines, quinoxalines, imidazoles, oxadiazoles, triazoles or triazines. However the most common ETL materials are Alq_3 and BCP (Figure 8) as well as 4-biphenyloxolato-aluminum-bis(2-methyl-8-hydroxychinolinato)4-phenylphenolate (BAlq), which is also a metal-organic complex.[38] In Figure 8 a selection of frequently used ETL-materials is presented.

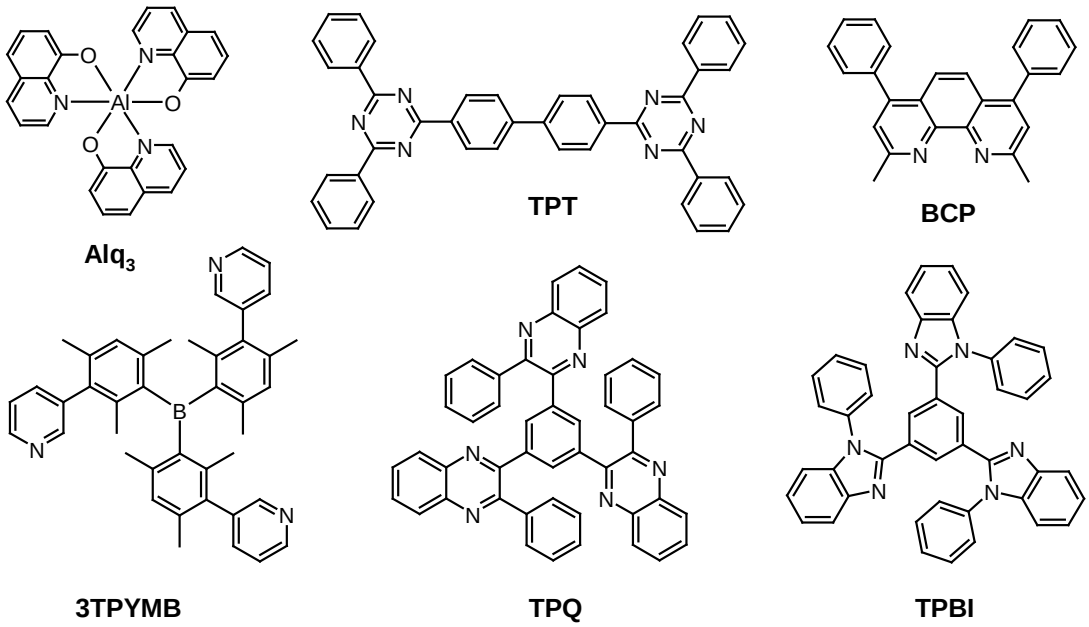

Figure 8: Selection of electron transport materials: tris(8-hydroxychinoline)aluminum (**Alq_3**), 4,4'-bis-(2-(4,6-diphenyl-1,3,5-triazinyl))-1,1'-biphenyl (**TPT**), 2,9-dimethyl-4,7-diphenyl-1,10-phenanthroline (**BCP**), tris(3-(3-pyridyl)-mesityl)borane (**3TPYMB**), 1,3,5-tris(3-phenylquinoxaline-2-yl)benzene (**TPQ**), 1,3,5-(tris(N-phenylbenzimidazol-2-yl)-benzene (**TPBI**).

In general ETL materials have to fulfill similar requirements as described for hole conducting materials. Regarding the properties of Alq_3 it is remarkable that it is one of the most common ETL materials. The electron mobility is very low (10^{-6} $cm^2V^{-1}s^{-1}$) and for most green and all blue EML systems an efficient hole/exciton blocker has to be employed due to the low triplet bandgap of Alq_3.[39] BCP, which is either used as electron conductor or as hole blocker, possesses a triplet energy of only 2.5 eV.[40] The values for the electron mobility vary from values of $1*10^{-3}$ $cm^2V^{-1}s^{-1}$ to $5*10^{-6}$ $cm^2V^{-1}s^{-1}$.[41,42] The injection properties from a LiF/Al cathode into both materials are good since they exhibit LUMO levels of 3.0 eV (BCP) and 2.9 eV (Alq_3). TPBI exhibits a higher triplet energy (2.74 eV) than Alq_3 and BCP but a similarly low electron mobility of 10^{-5} $cm^2V^{-1}s^{-1}$.[43] Phenylquinoxalines are able to form stable organic glasses with transition temperatures above 147 °C and exhibit an electron mobility of 10^{-4} $cm^2V^{-1}s^{-1}$. Another class of material with a high electron mobility are triazines. In a comparison of TPT with Alq_3 its electron mobility was nearly 2 orders of magnitude higher.[44] However the triplet energies of TPQ and TPT are below 2.5 eV. The influence of the charge carrier balance and triplet energy of the ETL on the efficiency of an OLED was studied by So and co-workers.[45] They found that the application

of 3TPYMB, which has an electron mobility of 10^{-5} $cm^2V^{-1}s^{-1}$ and a higher triplet energy than BCP, yielded an OLED quantum efficiency that was nearly doubled compared to a BCP-ETL device. In summary all standard ETL materials need exciton blocking interlayers close to the EML due to their low triplet energies. Only TPBI and 3TPYMB might stand alone in light blue emitting devices.

Phosphorescent Emitting Material

In order to generate white light a three color red-green-blue (RGB) approach is most common. All colors within the triangle spanned by the three colors can be generated. Since for display applications it is desirable to possess a large color space, the single colors should be close to the national television standards committee (NTSC) chromaticity. For white light applications, where the emission color is always a mixture, it is more important to span a triangle which includes the pure white region of the color diagram. The CIE (Commission Internationale de l'Éclairage) diagram in figure 9a shows the triangle spanned by the NTSC red, green and blue.

Also illustrated in figure 9a are the spectral color curve (dotted line) and the black body curve (red line). The latter describes the temperature-dependent emission color of a black body. A temperature of 5200-6000 K represents a pure white. Lower temperatures result the emission of a warm white, while higher temperatures yield a cold blue-shifted white. In figure 9b three typical phosphorescent emitters including their emission in solution are displayed. The red phosphor $Ir(MDQ)_2(acac)$ exhibits perfect emission properties (CIE x 0.64, y 0.34) concerning the chromaticity. The CIE coordinates of the green emitter $Ir(ppy)_3$ are slightly below the NTSC green, but still fulfill the requirements. The phosphorescent complex FIrpic however is only light blue (CIE x 0.17, y 0.32; λ_{max} 473 nm; $E(T_1\text{-}S_0)$ = 2.65 eV) and therefore reduces the possible emission colors of a RGB device.

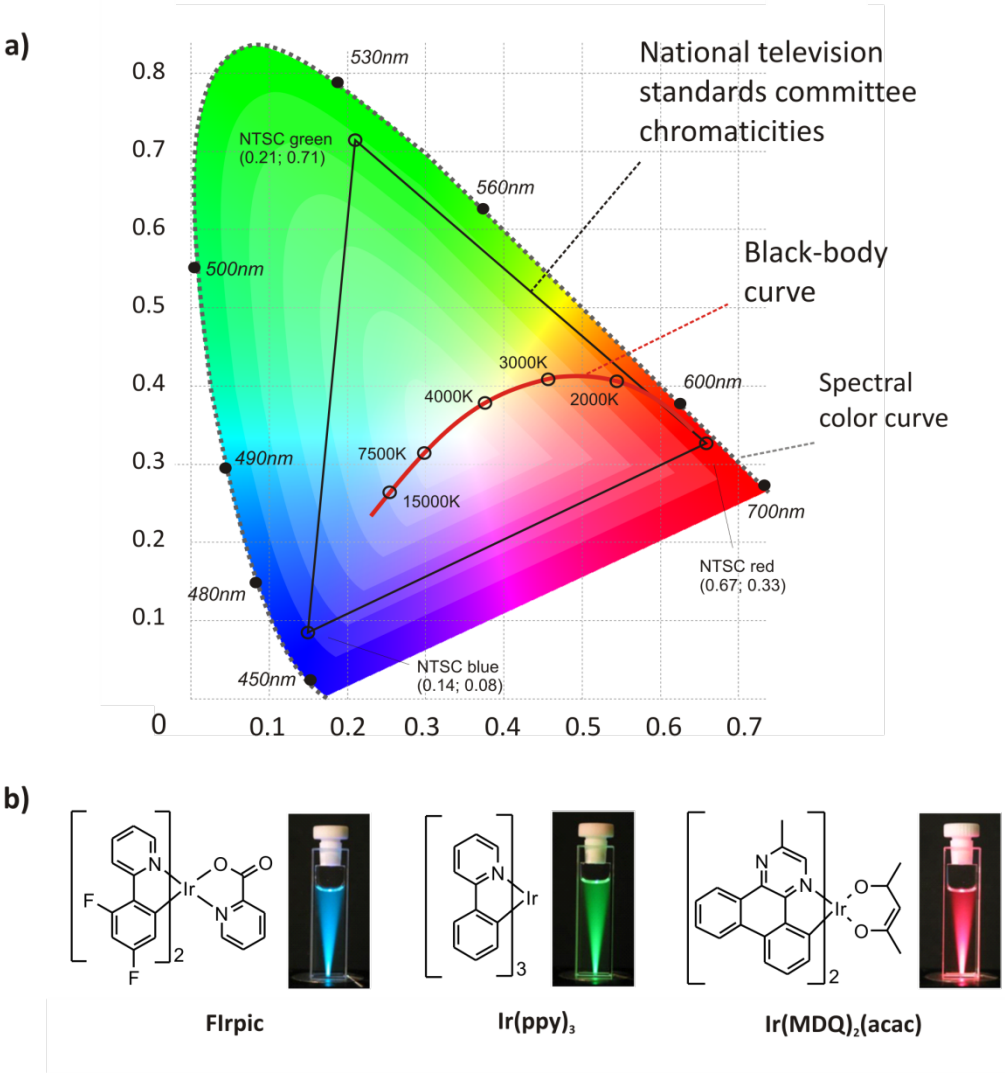

Figure 9: a) CIE color diagram including the chromaticities of the national television standards committee (NTSC), the black body curve (red line) and spectral color curve (dotted line); **b)** three phosphorescent emitters: bis(4,6-di-fluorophenyl)-pyridinato-*N*,C^2)picolinato-iridium(III) (FIrpic , blue; x 0.17, y 0.32), tris(phenylpyridium)-iridium(III) ($Ir(ppy)_3$, green, x 0.27, y 0.63; λ_{max} 510 nm; $E(T_1\text{-}S_0)$ = 2.42 eV) and (2-methyldibenzo[f,h]quinoxalino(C^2, N'))-Iridium(III) acetylacetonate ($Ir(MDQ)_2(acac)$, red, x 0.64, y 0.34).

Recently Leo and co-workers presented a highly efficient white OLED comprising these three emitters (figure 2).[4] Due to the light blue color of FIrpic the resulting white emission was situated in the warm white to yellow region (CIE x 0.45, y 0.47). This highlights the necessity of deeper blue phosphorescent emitters for white organic light-emitting diodes. Since phosphorescent emitters are most efficient in diluted host-guest systems, the development of a suitable host for novel deep blue emitters is as important as the emitter-design itself.

Host Materials for Phosphorescent Emitters

Since the quantum efficiency of neat phosphorescent emitter films is low due to self quenching, the dilution of the emitter is one major task of host materials.

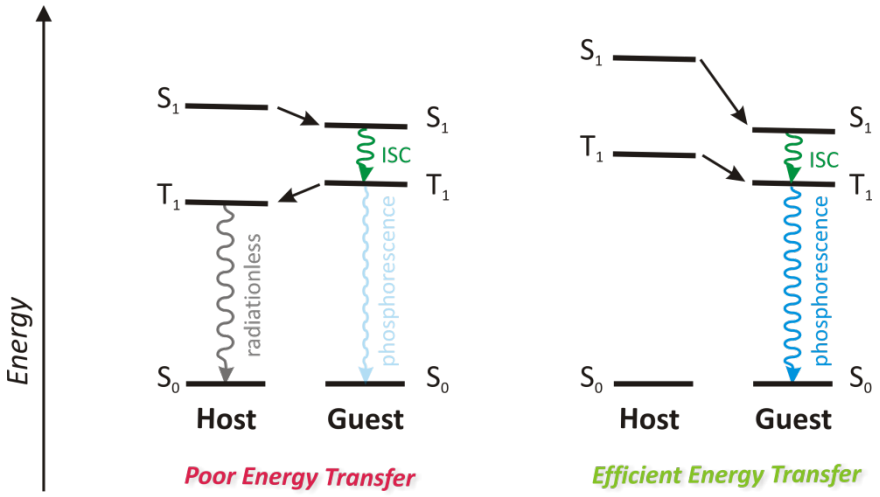

Figure 10: Comparison of poor (left) and optimal energy level alignment (right) of phosphorescent host-guest systems. Energy back transfer from guest to host yields poor phosphorescent quantum efficiency due to the low triplet energy of the host (left), while efficient energy confinement on the guest results in high quantum yields.

In figure 10 a comparison of two host-guest systems with either poor (left case) or efficient energy transfer is shown. For efficient energy transfer both, the singlet and triplet energies of the host have to be higher than those of the guest. Only this case guarantees the confinement of all excitons on the emitter and the efficiency of the system is equal to the intrinsic quantum efficiency of the emitter. The left case in figure 10 shows poor energy transfer from host to guest. This involves only transfer of singlets to the guest, followed by a subsequent inter system crossing. Due to the lower triplet energy of the host the energy is back transferred to the T_1 level and decays radiationless, which results in low quantum yields for the emitting system. This demonstrates the importance of a suitable host. For blue phosphorescent emitters with triplet energies of 2.65 eV (FIrpic) the host should exhibit a triplet bandgap of at least 2.75 eV to guarantee an efficient exciton confinement. Deep blue emitters ($E(T_1\text{-}S_0) > 2.8$ eV) therefore require hosts with bandgaps close to 2.9 eV. Keeping this in mind, when designing host molecules, raises the question of suitable building blocks for these materials. Figure 11 comprises the triplet

energies and phosphorescence wavelengths of a selection of one-, two- and three-membered conjugated ring systems.

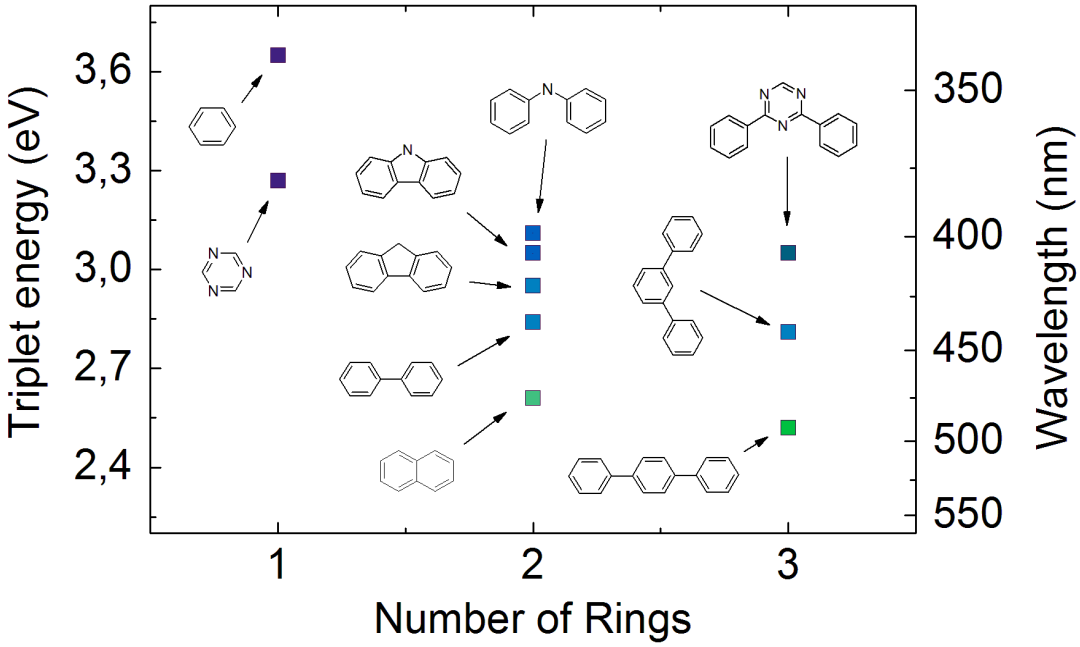

Figure 11: Triplet energy (left ordinate) and phosphorescence wavelength (right ordinate) of conjugated molecules depending on the number of ring. (top to bottom) System with one ring: benzene, triazine; two rings: diphenylamine, carbazole, fluorene, biphenyl, naphthalene; three rings: diphenyltriazine, m-terphenyl, p-terphenyl. The color of the phosphorescence is implied in the full squares.

It is striking that the $E(T_1\text{-}S_0)$ drops considerably in the line of benzene, biphenyl and p-terpehnyl. Since the triplet energy of aromatic hydrocarbons usually decreases upon substitution, even biphenyl ($E(T_1\text{-}S_0)$ = 2.82 eV) can be ruled out as possible building block.[46,47] Even more pronounced is the decrease in the triplet bandgaps for fused aromatic hydrocarbons. Naphthalene for example exhibits a triplet energy of only 2.62 eV.[48] Only diphenylamine and carbazole, which exhibit triplet energies of 3.11 eV and 3.06 eV respectively, are reliable candidates regarding the 2-ring systems.[49] One approach to increase the triplet energy of larger ring systems is the *meta*- or *ortho*-linkage of the involved units to decrease the conjugation. Thus the triplet energy of m-terphenyl is 0.25 eV higher than for the linear p-terphenyl.[47] If electron deficient heterocycles like triazines are incorporated the triplet energy of the system increases. Since the triplet energy drops upon aggregation of the molecules molecular glasses are most desirable

candidates for phosphorescent hosts. Figure 12 comprises a series of substituted carbazole based host materials.

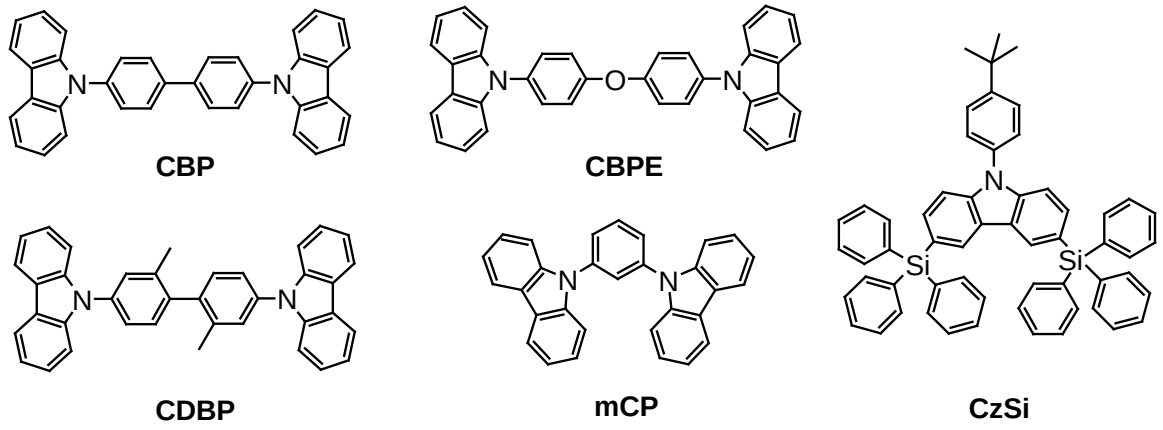

Figure 12: Selection of carbazole-based host materials: 4,4'-bis(9-carbazolyl)-biphenyl (**CBP**), bis(4-(carbazol-9-yl)phenyl)ether (**CBPE**), 4,4'-bis(carbazol-9-yl)-2,2'-dimetyhl-biphenyl (**CDBP**), 1,3-bis(carbazol-9-yl)-benzene (**mCP**), 9-(4-tert-butylphenyl)-3,6-di-triphenylsilyl)-carbazole (**CzSi**).

CBP is one of the most commonly used host materials for phosphorescent emitters. However the triplet energy of CBP ($E(T_1\text{-}S_0) = 2.56$ eV)[50] is too low for efficient blue phosphorescent OLEDs. Therefore CBP is mainly used as host for red and green emitters. Several researchers presented proposals how to increase the triplet energy of carbazole based host materials. Tokito and co-workers published one suggestion where the conjugation of the biphenyl, which is the triplet-limiting building block, was reduced by the introduction of two methyl groups in 2- and 2'-position. In the resulting material CDBP the dihedral angle between the two phenyl rings is increased and the conjugation is therefore decreased. This results in a triplet energy of 2.79 eV and an efficient confinement of excitons on the light blue emitter FIrpic.[51] The EQE of an OLED comprising a CDBP:FIrpic emission layer was doubled from 5 % to 10.1 % compared to a CBP:FIrpic device.[52] In the host material mCP presented by Holmes et al. the biphenyl unit was replaced by a single phenyl ring with two carbazoles attached meta to each other.[38] This yields a triplet energy of 2.9 eV. The EQE of a mCP:FIrpic device was increased to 7.5 %. The host material CzSi, a substituted phenyl-carbazole, exhibits a triplet energy of 3.02 eV which is very close to the intrinsic energy of carbazole.[53] This is possible due to the almost perfect 90°C dihedral angle between carbazole and phenyl. The bulky side-groups are

necessary to obtain an amorphous host material (T_g = 131°C). Additionally the electrochemical stability benefits from the blocking of the 3- and 6-position, since unsubstituted carbazoles undergo dimerisation reactions.[54,55] However the bulky triphenylsilyl groups negatively influence the charge carrier transport properties of CzSi. Nevertheless CzSi:FIrpic devices reach an EQE of 16 %.[53] The coupling of two phenylcarbazole units connected by non-conjugating bridges, like ethers or methylene units, was published by D. Ma and co-workers.[56] Similar to CzSi, CBPE exhibits a high triplet energy ($E(T_1\text{-}S_0)$ = 3.02 eV) and good glass forming properties (compared to CBP and mCP), which reveals the potential of non-conjugated bond as bridging unit for high triplet energy host materials.

For many phosphorescent emitters a concentration between 3% and 12% yields the most efficient host-guest system in an OLED. Baldo et al. demonstrated the dependence of the $Ir(ppy)_3$ concentration in a CBP matrix on the efficiency of the OLED.[57] A maximum EQE was found for concentrations of 6 % - 8 %. This means that the host material mainly transports the charge carriers. Therefore host materials, which strongly favor either hole or electron transport lead to an accumulation of charge carriers at the corresponding interface. This makes it necessary to incorporate additional blocking layers next to the EML to confine charge carriers and excitons to the emission layer. However, even if no excitons are lost to the neighboring layer the triplet exciton concentration is high in such a narrow recombination zone and favors triplet-triplet or triplet-polaron interaction.[58,59] These processes are supposed to be efficient loss pathways. Therefore a broad recombination zone situated in the middle of the EML is desirable.

Recently bipolar host materials have attracted the attention of several researchers. Such bipolar materials must permit the formation of stable radical cations and anions within the molecule. Additionally proper HOMO and LUMO levels are necessary to accept holes and electrons from the neighboring layers. This task is often solved by the fusion of electron and hole conducting moieties in one molecule. Aromatic amines and carbazoles are commonly used as hole transporting unit while electron deficient heterocycles or

phosphine-oxides are the most prominent electron transporting units. Figure 13 shows a selection of bipolar host material from the literature.

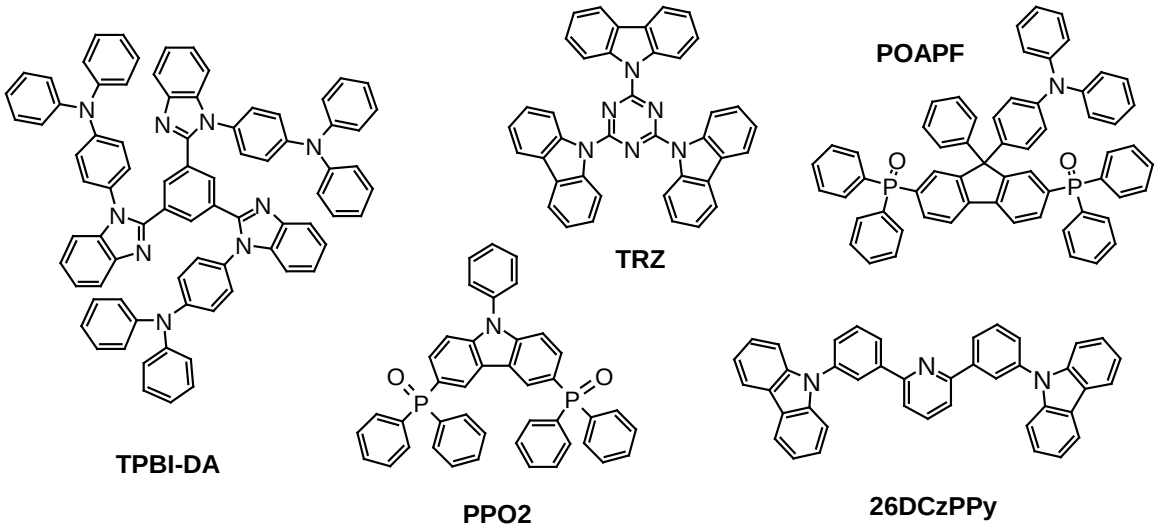

Figure 13: Selection of bipolar host materials: 1,3,5-tris(N-(4-diphenylaminophenyl)benzimidazol-2-yl)benzene (**TPBI-DA**), 2,4,6-tricarbazol-9-yl-1,3,5-triazine (**TRZ-3Cz**), 2,7-(bis(diphenylphosphoryl)-9-(4-(N,N-diphenylamino)phenyl)-9-phenylfluorene (**POAPF**), 3,6-bis(diphenylphosphoryl)-9-phenylcarbazole (**PPO2**), 2,6-bis(3-(carbazol-9yl)phenyl)pyridine (**26DCzPPy**).

Since the number of bipolar hosts for blue phosphorescent emitters is very limited, figure 13 also comprises two materials for green emitters. In TPBI-DA the well-known electron-transporting core TPBI is combined with 3 diphenylamine groups. [60] Since the triplet level of TPBI itself is only 2.74 eV, also TPBI-DA ($E(T_1\text{-}S_0)$ = 2.70 eV) lacks sufficient triplet energy for blue phosphors. In OLEDs with the green dye $Ir(ppy)_2(acac)$ the quantum efficiency was tripled to 15 % compared to the TPBI device due to a broadening of the recombination zone. In TRZ-3Cz the donor and acceptor moieties are directly bound to each other.[61] The triplet therefore decreases to a value of 2.81 eV although the two isolated moieties exhibit triplet energies above 3 eV. This behavior is typical for conjugated donor acceptor system. Due to the relatively low triplet, the authors decided to use TRZ-3Cz only in combination with green $Ir(ppy)_3$. The resulting OLEDs yielded 10 % EQE. In a study by Adachi and co-workers the bipolar transport characteristics of several carbazole substituted heterocycles were investigated.[62] The triazine-containing material TRZ-3Cz featured the best bipolar transport in the series. Kido et al. combined an electron deficient pyridine unite with two phenylcarbazoles to yield the bipolar material

26DCzPPy.[63] Although the moieties were bound meta to each other the relatively large conjugated system exhibits a triplet energy of only 2.71 eV. However the presented OLEDs with blue FIrpic reached external quantum efficiencies of 24 %. This value is among the highest reported values for FIrpic based OLEDs. The bipolar character of 26DCzPPy additionally decreases the efficiency roll-off at high brightness. Therefore the efficiency at 1000 cd/m^2 is still above 22 %. Another interesting class of bipolar materials are phosphine-oxide substituted donor molecules. POAPF consists of a fluorene core with phosphine-oxide and triphenylamine substituents, which are responsible for the transport.[64] The triplet energy of this material of 2.75 eV is defined by the relatively large fluorene-core. Although the EQE of FIrpic devices (20.2 %) is not as high as for 26DCzPPy the material enables bipolar transport. Very recently another bipolar phosphine-oxide containing material (PPO2) was published.[65] Due to the fact that the carbazole core is the largest conjugated system the triplet energy is 3.02 eV. This enables the fabrication of deep blue OLEDs with a PPO2 host. The resulting OLEDs with tris((3,5-difluoro-4-cyanophenyl)pyridine) iridium (FCNIr; CIE x 0.15, y 0.16; E(T_1-S_0) = 2.8 eV) yielded external quantum efficiencies up to 18 %.

In summary the application of bipolar host materials for blue phosphorescent OLEDs holds great potential concerning the efficiency of the device due to a more balanced charge carrier transport. Until now only very few bipolar materials with high enough triplet energies for blue phosphors are known.

3 References

[1] C. W. Tang and S. A. van Slyke, *Appl. Phys. Lett.*, **1987**, *51*, 913.

[2] A. Misra, P. Kumar, M. N. Kamalasanan, and S. Chandra, *Semicond. Sci. Technol.*, **2006**, *21*, R35.

[3] „Gesetz über die umweltgerechte Gestaltung energiebetriebener Produkte“; BGBI Absatz I, S. 258.

[4] S. Reineke, F. Lindner, G. Schwartz, N. Seidler, K. Walzer, B. Luessem and K. Leo, *Nature*, **2009**, *459*, 234.

[5] M. A. Baldo, D. F. O'Brien, Y. You, A. Shoustikov, S. Sibley, M. E. Thompson, S. R. Forrest, *Nature (London)*, **1998**, *395*, 151.

[6] M. Segal, M. A. Baldo, R. J. Holmes, S. R, Forrest, Z. G. Soos, *Phys. Rev. B*, **2003**, *68*, 075211.

[7] C. Adachi, M. A. Baldo, M. E. Thompson, S. R. Forrest, *J. Appl. Phys.*, **2001**, *90*, 5048.

[8] J. Huang, T. Watanabe, K. Ueno, Y. Yang, *Adv. Mater.*, **2007**, *19*, 739–743.

[9] N. Chopra, J. Lee, Y. Zheng, S.-H. Eom, J. Xue, F. So, *Appl. Phys. Lett.*, **2008**, *93*, 143307.

[10] http://www.reuters.com/article/pressRelease/idUS206286+17-Jun-2008+BW20080617 (date: October 25, 2009)

[11] B. C. Krummacher, V.-E. Choong, M. K. Mathai, S. A. Choulis, F. So, F. Jermann, T. Fiedler, M. Zachau, *Appl. Phys. Lett.*, **2006**, *88*, 113506.

[12] S. Tonzani, *Nature*, **2009**, *459*, 312.

[13] M. C. Gather, A. Koehnen, A. Falcou, H. Becker, K. Meerholz, *Adv. Funct. Mater.*, **2007**, *17*, 191.

[14] J. H. Burroughes, D. D. C. Bradley, A. R. Brown, R. N. Marks, K. Mackay, R. H. Friend, P. L. Burn, A. B. Holmes, *Nature*, **1990**, *347*, 539.

[15] D. Hertel, C. D. Müller, K. Meerholz, *Chem. Unserer Zeit*, **2005**, *39*, 336.

[16] R. Schmechel, H. von Seggern, *Phys. Stat. Sol (A)*, **2004**, *201*, 1215.

[17] M. A. Lampert, P. Mark, *Current Injection in Solids* (Academic, New York, 1970).

[18] C. Giebeler, H. Antoniadis, D. D. C. Bradley, Y. Shirota, *Appl. Phys. Lett.*, **1998**, *72*, 2448.

[19] V. I. Arkhipov, E. V. Emelianova, Y. H. Tak, H. Bässler, *J. Appl. Phys.*, **1998**, *84*, 848.

[20] M. A. Baldo, S. R. Forrest, *Phys. Rev. B.*, **2001**, *64*, 085201.

[21] J. S. Kim, M. Granström, R. H. Friend, N. Johansson, W. R. Salaneck, R. Daik, W. J. Feast, F. Cacialli, *J. Appl. Phys.*, **1998**, *84*, 6859.

[22] D. Poplavsky, J. Nelson, D. D. C. Bradley, *Appl. Phys. Lett.*, **2003**, *83*, 707.

[23] L. S. Hung, C. W. Tang, M. G. Mason, *Appl. Phys. Lett.*, **1997**, *70*, 152.

[24] H. Bässler, *Phys. Stat. Sol. B*, **1993**, *175*, 15.

[25] M. A. Baldo, M. E. Thompson, S. R. Forrest, *Nature*, **2000**, *409*, 750.

[26] B. Valeur, *Molecular Fluorescence: Principles and Applications*, Wiley-VCH, **2001**.

[27] K. Müllen (Ed.), U. Scherf (Ed.), *Organic Light-emitting Devices*, Wiley-VCH, **2006.**

[28] P. Strohriegl, J. V. Grazulevicius, *Adv. Mater.,* **2002,** *14*, 1439-1452.

[29] Y. Shirota, *J. Mater. Chem.,* **2000**, *10*, 1-25.

[30] B. E.Koene, D. E. Loy, W. E. Thompson, *Chem. Mater.,* **1998**, *10*, 2235-2250.

[31] G. Adam and J. H. Gibbs, *J. Chem. Phys.*, **1965**, *43*, 139.

[32] K. Naito and A. Miura, *J. Phys. Chem.*, **1993**, *97*, 6240.

[33] P. M. Borsenberger, L. Pautmeier, R. Richert, H. Bässler, *J. Chem. Phys.*, **1991**, *94*, 8276.

[34] M. Stoll, J. F. Janus, D. M. Pai, *J. Phys. Chem.*, **1984**, *88*, 4704.

[35] Y. Zhu, A. P. Kulkarni, S. A. Jenekhe, *Chem. Mater.*, **2005**, *17*, 5225.

[36] A. J. Mäkinen, I. G. Hill, R. Shashidhar, N. Nikolov, Z. H. Kafafi, *Appl. Phys. Lett.*, **2001**, *75*, 557.

[37] J. Lee, N. Chopra, S.-H. Eom, Y. Zheng, J. Xue, F. So, J. Shi, *Appl. Phys. Lett.*, **2008**, *93*, 123306.

[38] R. J. Holmes, S. R. Forrest, Y.-J. Tung, R. C. Kwong, J. J. Brown, S. Garon, M. E. Thompson, *Appl. Phys. Lett.*, **2003**, *82*, 2422.

[39] T. C. Wong, J. Kovac, C. S. Lee, L. S. Hung, S. T. Lee, *Chem. Phys. Lett.*, **2001**, *334*, 61.

[40] V. I. Adamovich, S. R. Cordero, P. I. Djurovich, A. Tamayo, M. E. Thompson, B. W. D'Andrade, S. R. Forrest, *Org. Elect.*, **2003**, *4*, 77.

[41] S.-J. Su, T. Chiba, T. Takeda, J. Kido, *Adv. Mater.*, **2008**, *20*, 2125.

[42] M. K. Fung, Z. Xie, S. T. Lee, L. S. Hung, J. Shi, Y. Q. Li, *Adv. Mater.*, **2002**, *14*, 1317.

[43] M. E. Kondakova, T. D. Pawlik, R. H. Young, D. J. Giesen, D. Y. Kondakov, C. T. Brown, J. C. Deaton, J. R. Lenhard, K. P. Klubek, *J. Appl. Phys.*, **2008**, *104*, 094501.

[44] R. A. Klenkler, H. Aziz, A. Tran, Z. D. Popovic, G. Xu, *Org. Elect.*, **2008**, *9*, 285.

[45] N. Chopra, J. Lee, Y. Zheng, S.-H. Eom, J. Xue, F. So, *Appl. Phys. Lett.*, **2008**, *93*, 143307.

[46] G. N. Lewis, M. Kasha, *J. Am. Chem. Soc.*, **1944**, *66*, 2100.

[47] J. S. Brinen, J. G. Koren,W. G. Hodgson, *J. Chem. Phys.,***1966***,* 44, 3095.

[48] M. Yanagidate, K. Takayama, M. Takeuchi, J. Nishimura, H. Shizuka, *J. Phys. Chem.*, **1993**, *91*, 8881.

[49] J. E. Adams, W. W. Mantulin, J. R. Huber*, J. Am. Chem. Soc.*, **1973**, *95*, 5477.

[50] C. Adachi, R. C. Kwong, P. I. Djurovich, V. I. Adamovich, M. A. Baldo, M. E. Thompson, S. R. Forrest, *Appl. Phys. Lett.*, **2001**, *79*, 2082.

[51] I. Tanaka, Y. Tabata, S. Tokito, *Chem. Phys. Lett.*, **2004**, *400*, 86.

[52] S. Tokito, T. Ilijma, Y. Suzuri, H. Kita, T. Tsuzuki, F. Sato, *Appl. Phys. Lett.*, **2003**, *83*, 569.

[53] M.-H. Tsai, H.-W. Lin, H.-C. Su, T.-H. Ke, C.-C. Wu, F.-C. Fang, Y.-l. Liao, K.-T. Wong, C.-I. Wu, *Adv. Mater.*, **2006**, *18*, 1216.

[54] J. F. Ambrose, R. F. Nelson, *J. Electrochem. Soc.*, **1968**, *115*, 1159.

[55] J. F. Ambrose, L. L. Carpenter, R. F. Nelson, *J. Electrochem. Soc.*, **1975**, *122*, 876.

[56] J. H. Hongmei, Y. Dai, X. Ou, J. Wang, S. Tao, X. Zhang, P. Wang, D. Ma, *J. Phys. Chem.*, **2009**, *113*, 6761.

[57] M. A. Baldo, S. Lamansky, P. E. Burrows, M. E. Thompson, S. R. Forrest, *Appl. Phys. Lett.*, **1999**, *75*, 4.

[58] S. Reineke, K. Walzer, K. Leo, *Phys. Rev. B*, **2007**, *75*, 125328.

[59] M. A. Baldo, C. Adachi, S. R. Forrest, *Phys. Rev. B*, **2000**, *62*, 10967.

[60] S.-Y. Takizaw, V. A. Montes, P. Anzenbacher, *Chem. Mater.*, **2009**, *21*, 2452.

[61] H. Inomata, K. Goushi, T. Masuko, T. Knno, T. Imai, H. Sasabe, J. J. Brown, C. Adachi, *Chem. Mater.*, **2004**, *16*, 1285.

[62] K. Son, M. Yahiro, T. Imai, H. Yoshizaki, C. Adachi, *Chem. Mater.*, **2008**, *20*, 4439.

[63] H. Sasabe, S.-J. Su, J. Kido, *Chem. Mater.*, **2008**, *20*, 1691.

[64] F.-M. Hsu, C.-H. Chien, C.-F. Shu, C.-H. Lai, C.-C. Hsieh, K.-W. Wang, P.-T. Chou, *Adv. Funct. Mater.*, **2009**, *19*, 2834.

[65] S. O. Jeon, K. S. Yook, C. W. Joo, J. Y. Lee, *Adv. Funct. Mater.*, **2009**, published online; DOI: 10.1002/adfm.200901274

4 Aim of the Thesis

The aim of this thesis was the synthesis and characterization of novel host materials for blue phosphorescent emitters and their application in organic light-emitting diodes.

The introduction in the preceding chapter demonstrates the importance of appropriate host materials for phosphorescent emitters in order to gain highly efficient OLEDs. The requirements which are essential to fulfill this task are summarized in figure 1 right. The class of donor-substituted triazines was chosen for this purpose. Since the requirements for material synthesis are simple and effective procedures combined with large quantities we were looking for a simple synthesis with a small number of required steps. Therefore nucleophilic substitution of cyanuric chloride seems to be the perfect choice to yield substituted 1,3,5-triazines. In order to obtain high yields and very pure products the procedures have to be adjusted to the respective donor moiety.

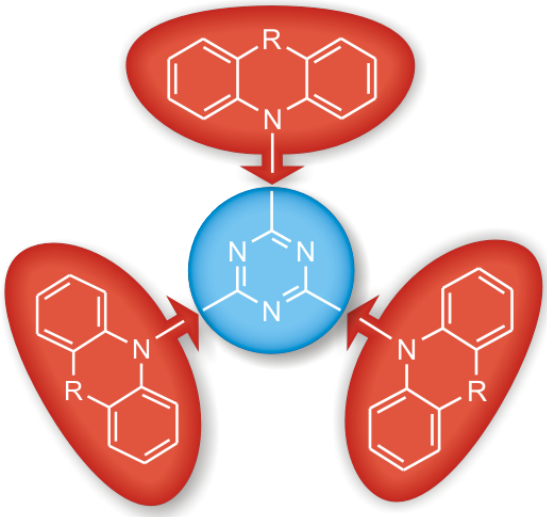

Requirements for host materials:

- Triplet energy higher than 2.8 eV
- Efficient energy transfer to the emitter
- High thermal stability
- Stable amorphous morphology and high T_g
- Good electron and hole/electron transport and injection properties

Figure 1: left: Schematic of a donor-substituted triazine host material. The central triazine core (blue) is electron deficient, while the donor-substituent (red) is electron-rich. Due to directly bound donor the electron deficiency of the core is decreased. **Right:** List of requirements for OLED host materials.

Since the choice of the donor-substituent determines the material properties efficient tailoring of their photo physical, thermal and electronic characteristics is a main target of

this work. Upon thorough determination of the mentioned properties important structure-property relationships are drawn. Additionally to demonstrate the benefits of the novel materials organic light-emitting diodes were fabricated and investigated.

5 Overview of the Thesis

The thesis contains five publications. Four of them are presented in chapters 6 to 9 and one appears as appendix in chapter 10. All chapters deal with the synthesis and characterization of host materials for blue phosphorescent emitters and the application of those materials as hosts in blue organic light-emitting diodes (OLEDs). To fulfill the specific requirements of a host material concerning thermal, photo physical and charge carrier transport properties the class of substituted triazines was chosen. All materials presented in the following comprise an electron-deficient 1,3,5-triazine core that was connected to up to three electron-rich substituents. Figure 1 illustrates three typical structures which are included in the thesis.

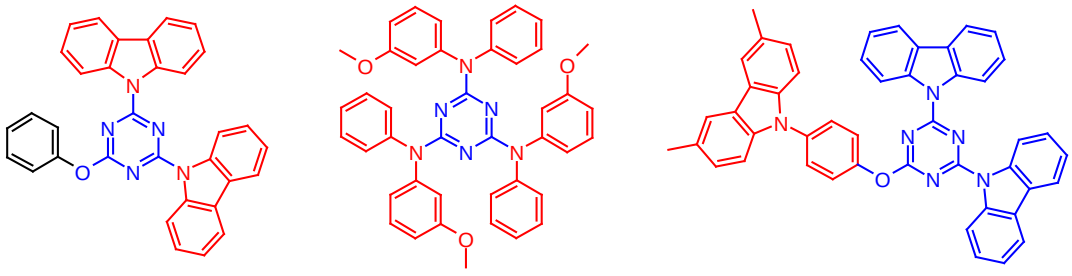

1st generation *2nd generation* *3rd generation*

Figure 1: One example of the first, second and third generation of triazine based host materials. Each molecule comprises an electron-deficient moiety (blue) and an electron-rich moiety (red). Electronically neutral parts are black. In the first and second generation the donor part (carbazole or diarylamine) is directly connected to the acceptor part (triazine core). In the third generation acceptor and donor moieties are separated by a non-conjugated ether bond.

Since the materials should be applied in blue phosphorescent organic light-emitting diodes, the most essential requirement is a high enough triplet energy of the host material. Therefore electron-rich substituents with varying π-conjugated systems were attached to the triazine core in order to optimize the photo physical properties, like the triplet energy as well as the energy levels of the highest occupied and the lowest unoccupied molecular orbitals (HOMO and LUMO). The materials that evolved from this thesis can be classified into three generations. The first generation is suitable for light and middle blue phosphorescent emitters with triplet energies up to 2.70 eV. Materials of this

generation have at least one carbazole attached to the triazine core. The second generation of hosts exhibits very high triplet levels and is therefore well suited for emitters with triplet energies up to 3.0 eV and has at least on diarylamine-substituent in common. All third generation triazines have one phenoxy-carbazole attached to the core. By the variation of the remaining two substituents the triplet bandgap can be varied. Within each generation the thermal properties, including thermal stability and glass forming properties, were tailored through different substitution patterns. Typical examples of each generation including a classification of the triplet energy are schematically shown in Figure 2.

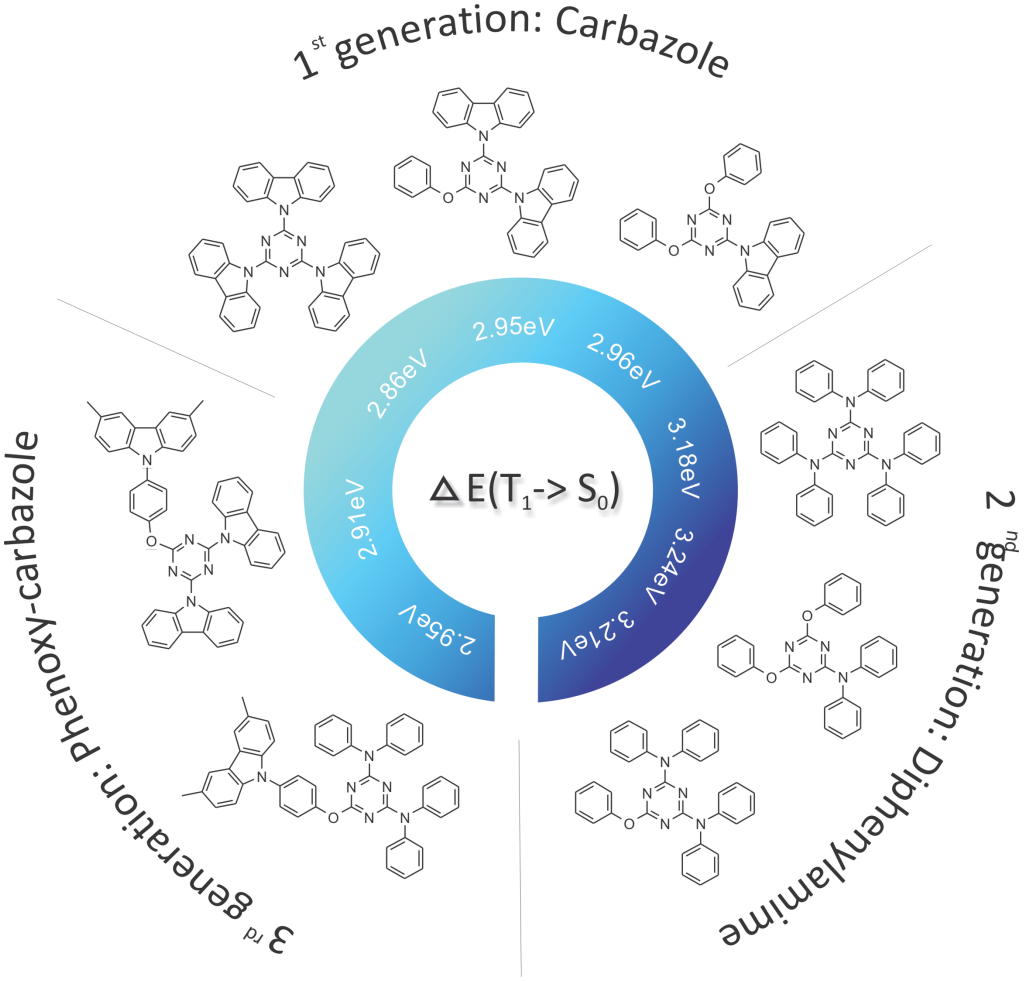

Figure 2: Schematic illustration of the triplet energy in dependence of the donor-substituent attached to the triazine core. First generation triazines comprising one to three carbazoles with triplet energies suitable for light and middle blue emitters. Second generation triazines comprising one to three diphenylamine units with triplet energies suitable for deep blue emitters. Third generation triazines with an non-conjugated phenoxy-carbazole moiety are suitable for light to deep blue emitters, depending on the donor which is directly bound to the triazine core.

Since the triazine host materials of all generations comprise either diarylamino or phenoxy substituents the synthetic strategy was optimized for the first generation and applied in the following generations. The most effective way to obtain donor-substituted triazines is the sequential replacement of the chlorines of cyanuric chloride by nucleophiles. The degree of substitution is dependent on temperature, actual ring substitution and the nature of the nucleophile. The different synthetic possibilities are summarized in Figure 3. The details concerning synthesis and characterization are found in the respective chapters.

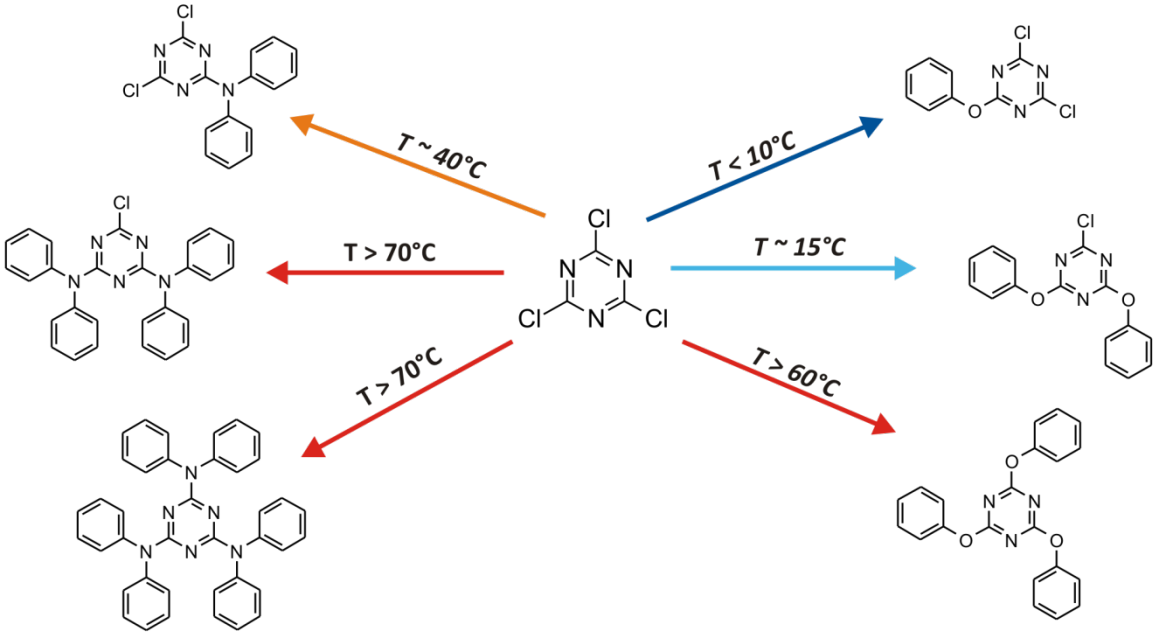

Figure 3: Schematic of one-, two and threefold substitution of cyanuric chloride. The reaction with diarylamines follows mainly a stoichiometric control. Only for mono-substituted triazines the temperature has to be kept below 40°C. In contrast to that the reaction with phenols follows mainly a temperature control. The mono-substitution can only be efficiently stopped at this stage, when temperatures below 10°C are maintained. For twofold substitutions the temperature should be kept at 15°C, while the threefold reaction is most effective at high temperatures.

All materials are characterized regarding their thermal, photo physical and electronic properties. Additionally computational calculations concerning the electronic levels are carried out to help to understand electron distributions and transport properties of the materials. Finally OLEDs or single carrier devices are presented to prove the effectiveness of each class of materials. A short summary of the three parts (three generations of triazine hosts) of this thesis is given in the following.

The first part of the thesis includes the synthesis of carbazolyl-substituted triazine host materials (1st generation) by nucleophilic substitution. Furthermore the characterization and application of the triazines as host material in a blue phosphorescent OLED is presented. The degree of carbazole substitution defines the triplet energy, since the electron withdrawing character of the triazine affects three, two or just one carbazole unit. The glass forming properties are tailored by the application of two different concepts. The first one involves the asymmetric substitution of up to two carbazole units with phenoxy units. This results in materials with a reduced tendency to crystallize. Secondly, the methyl-substitution of the carbazole and the phenoxy groups yielded molecular glasses. Furthermore, the ability of carbazolyl-triazines as host materials in blue phosphorescent OLEDs is demonstrated. One publication dealing with this class of materials is found in chapter 6.

The second part of the thesis is about the synthesis, characterization and application of diphenylamino- and iminodibenzyl-substituted triazines (2nd generation) as host material for phosphorescent emitter. This part benefits from the experiences I gained in the first part. The thermal properties of these triazines are tailored using the same concepts that were effective for carbazolyl-triazines. In contrast to the carbazole groups the intrinsic triplet of diphenylamine is higher; hence the triplet bandgap of diphenylamino-triazines is increased drastically. Therefore the 2nd generation triazines are also suitable as host for deep blue emitters. One publication deals with the synthesis and tailoring of the individual properties as well as the application of the material in OLEDs (chapter 7). In another publication one diphenylamino-triazine is used to study the effect of an electric field on excitons in deep blue host/guest systems (chapter 10).

In the last part, the synthesis and characterization of the 3rd generation triazines are presented. In contrast to the preceding generations, which have donor substituent directly attached to the triazine core, these materials comprise an additional phenoxy-carbazole donor moiety attached via a non-conjugated ether bond. This electron-rich unit strongly enhances the hole transport and injection properties. In two publications the influence of different substituted triazine moieties on the triplet energy, electronic levels and the

thermal properties is investigated. One publication introduces this class of materials and emphasized one material and its bipolar transport characteristics (chapter 8). Another publication focuses on the comparison of several materials of this class concerning the photo physical as well as electronic properties and is highlighted by OLED results (chapter 9).

In the following, the key results of each publication are summarized in order to connect the individual publications. Similarities to and improvements over preceding generations are also in the focus of the following chapter. Detailed information about each class can be found in the respective chapters.

First generation of triazine-based host materials: Carbazolyl-substituted triazines (chapter 6)

In this chapter the synthesis of seven triazine based host materials, which are synthesized by nucleophilic substitution, is described. Since the literature known symmetric tris-carbazolyl-triazine is highly crystalline it is necessary to find a way to yield less crystalline material. We found that asymmetrical substitution of the triazine core with two different units is the best way to reduce crystallinity. Either a mixture of two methylsubstituted carbazoles (TRZ1) or a combination of carbazole and phenol groups (TRZ2-7) is used to yield asymmetry. Furthermore when 3-methylcarbazole or 3,5-dimethylphenol are used as substituents, molecular glasses are obtained. In Figure 4 the chemical structures which are subject of this part are summarized.

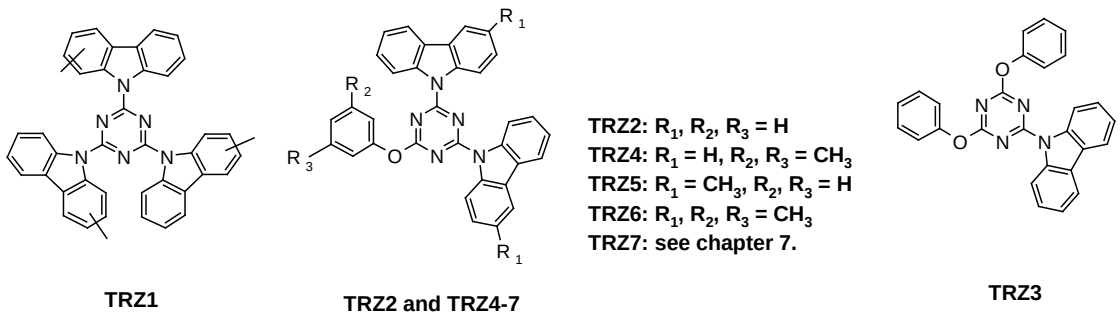

Figure 4: Chemical structure of seven triazine based host materials of the first generation hosts.

The trend to less crystallinity is observed best in the group of mono-phenoxy triazines. 2,4-Biscarbazolyl-6-phenoxy-1,3,5-triazine (TRZ2) shows crystalline behavior in the DSC experiment, which means that upon cooling of the melt crystallization is detected. In contrast to that TRZ4, which has additional methyl groups attached to the phenol, remains amorphous upon cooling, but crystallizes upon subsequent heating. For the triazines TRZ5 and TRZ6 the degree of methyl-substitution is further increased, which results in amorphous behavior upon cooling and subsequent heating. The glass transition temperatures of these two triazines range from 85 °C to 90 °C and is doubled to 170 °C for TRZ7, a “dimeric” structure with two biscarbazolyl units attached to resorcinol. The DSC scans of TRZ1, representing a crystalline material, and TRZ7, an organic glass, are shown in Figure 5.

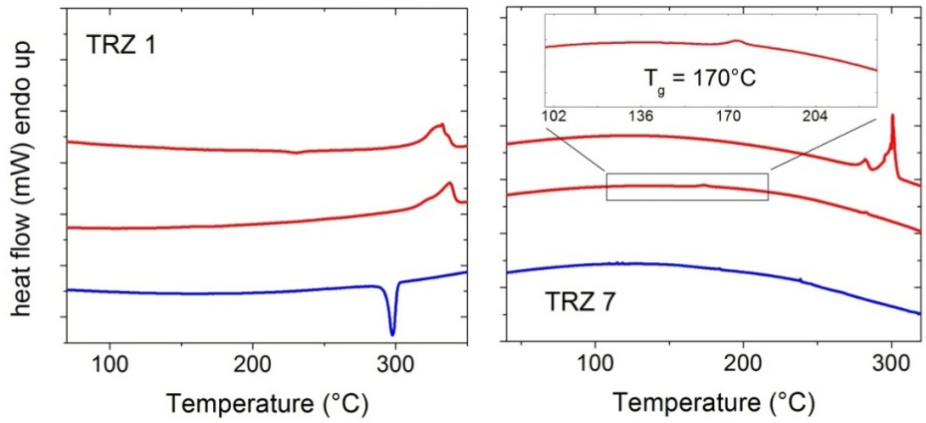

Figure 5: DSC traces of TRZ1 and TRZ7. Shown are the first heating (top red line), second heating (middle red line) and first cooling trace (bottom blue line) at a scan speed of 10K/min.

The photo physical properties are determined by absorption, fluorescence and phosphorescence spectroscopy. The optical bandgaps are estimated from the absorption edge of the absorption spectrum. We found that the bandgap energy increases with decreasing carbazole content. The wavelength of the fluorescence maximum follows the same trend. Since the triplet energy of a host material has to be higher compared to the emitter, this is the most important optical value. It is determined from the first highest energetic maximum of the phosphorescence spectrum. For triazines TRZ1-3 the triplet bandgap also increases with decreasing number of carbazoles and reaches values of 2.86 eV, 2.95 eV and 2.96 eV, respectively. Additionally energy transfer experiments are

carried out to illustrate the effectiveness of the host material. Therefore a neat host film and an emitter-doped host film are excited at the absorption maximum of the host. The pure emission of the guest is observed if the energy transfer in the doped film is efficient. Figure 6 comprises the optical properties of TRZ1.

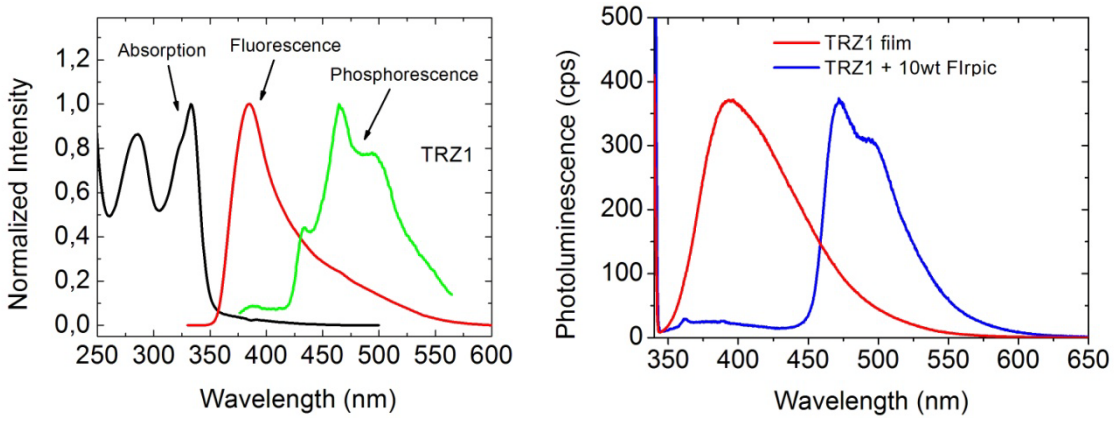

Figure 6: Left: Photo physical properties of TRZ1 in a neat film, including absorption (black line), fluorescence (red line) and phosphorescence (green line). Absorption and fluorescence are measured at room temperature using standard spectroscopic methods, while phosphorescence is measured at 5K using time-gated spectroscopy. **Right:** Energy transfer experiment; Fluorescence spectra of a neat TRZ1 film and a FIrpic-doped TRZ1 film excited at the absorption maximum of TRZ1. On excitation of the neat film the emission of TRZ1 is detected (red line), while for the doped film the emission of FIrpic is observed (blue line) due to efficient energy transfer from host to guest.

In order to demonstrate the potential of this class of materials two OLEDs with TRZ2 as host and FIrpic as guest are fabricated. In the first device TRZ2 is used additionally as hole blocker, while device 2 comprises DBFSi (for the structure see chapter 7) as hole blocker. The external quantum efficiency (EQE) as well as the luminous efficiency of both devices are plotted versus the voltage in Figure 7 left. The device configuration of device 2, including calculated HOMO and LUMO values of each material, is shown on the right side of Figure 7. From the energy diagram it is clear that DBFSi is a more efficient hole blocker than TRZ2 due to its lower HOMO level. Therefore the EQE and luminous efficiency of device 2 (EQE = 12.1 %) are higher compared to device 1 (EQE = 6.7 %).

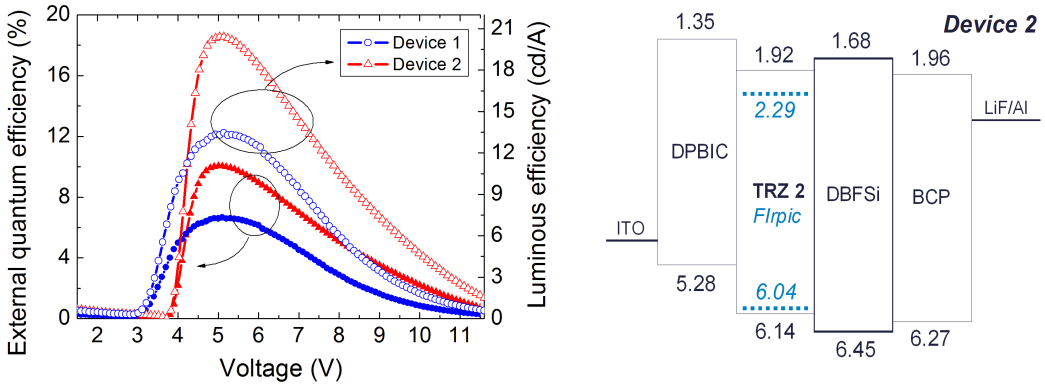

Figure 7: Left: External quantum efficiency-voltage-luminous efficiency characteristics of two OLED devices. **Right:** Device configuration of device 2. HOMO and LUMO values are extracted from density functional theory (DFT) calculations. For detailed information about the materials used in this device see chapter 6.

The electro chemical behavior of TRZ2 is investigated by cyclic voltammetry and compared the behavior of one 3rd generation triazine. Additionally the transport characteristics are determined in single carrier devices within this comparison. Those results are presented in chapter 8.

Second generation of triazine-based host materials: Diphenylamino- and iminodibenzyl-substituted triazines (chapters 7 and 10)

This chapter concerns the synthesis of seven diarylamino-substituted triazines, their characterization and application as host in blue phosphorescent OLEDs. The synthesis of these compounds takes benefit of the work on carbazolyl-triazines in chapter 6. The nucleophilic substitutions are controlled by temperature and stoichiometry and yield four symmetric and three asymmetric triazines. Since 2,4,6-tris-(diphenylamino)-1,3,5-triazine (ATRZ1) is highly crystalline and does not allow the preparation of an amorphous film for further investigations the potential of this class of triazines was overlooked for a long time. Using similar techniques as described for the first generation triazines we succeeded in the preparation of diarylamino-substituted triazines with amorphous behavior. Their chemical structures are shown in Figure 8.

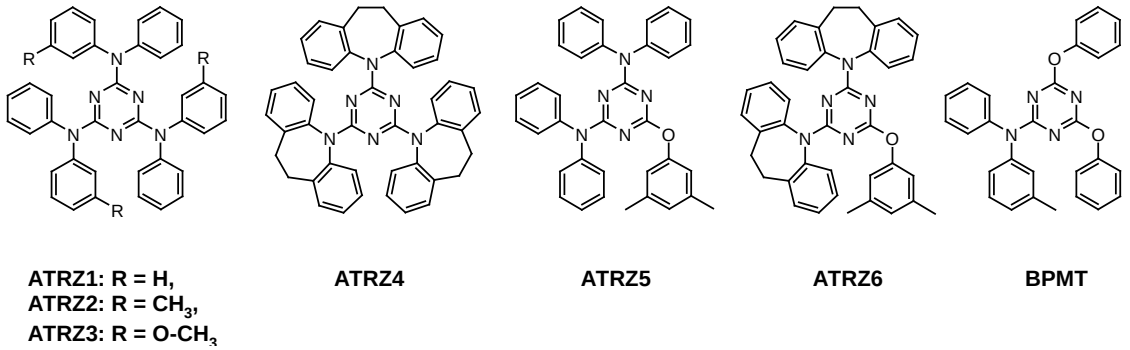

Figure 8: Chemical structure of seven triazine based host materials of the second generation.

The DSC first and second heating and cooling scans of ATRZ1 (Figure 9 left) reveal the crystalline nature of this compound. From the very sharp exothermic crystallization transition upon cooling it can be estimated that ATRZ1 forms a highly ordered crystalline film and is therefore not suited as host material for OLEDs. To obtain less crystalline materials the diphenylamine unit is methyl or methoxy substituted in the *meta*-position. Similar to the first generation triazines the substitution of diphenylamine by phenoxy groups results in amorphous behavior of ATRZ5 and BPMT. The glass transition temperatures of all diphenylamine-triazines are relatively low due to the flexible amino-group. Therefore the rigid iminodibenzyl unit in ATRZ4 and ATRZ6 is introduced to increase the T_g. In Figure 9 the two heating and cooling DSC traces of ATRZ1 and ATRZ6 are shown.

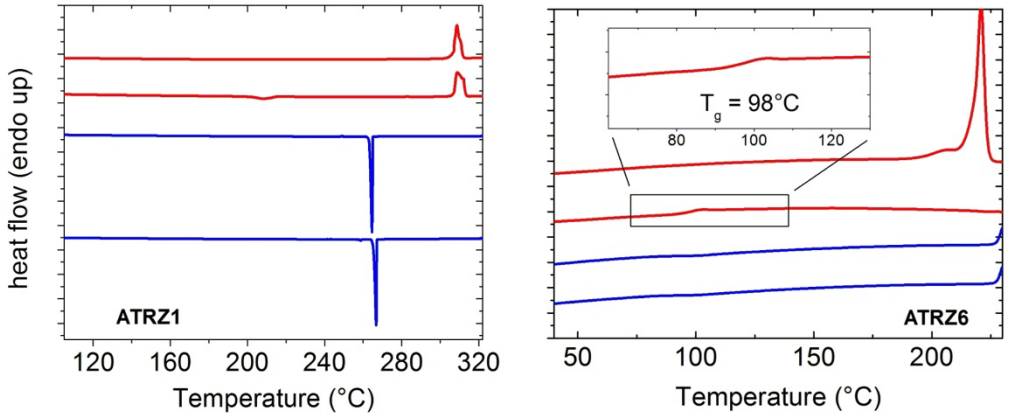

Figure 9: DSC traces of highly crystalline ATRZ1 and amorphous ATRZ6. Shown is the first heating (top red line), second heating (second red line), first cooling trace (top blue line) and second cooling trace (bottom blue line) at a scan speed of 10K/min.

Since diphenylamine and iminodibenzyl exhibit a smaller π-conjugated system compared to carbazole the triplet and singlet bandgaps of the resulting molecules exceed those of the triazine compounds presented in the preceding chapter. The singlet bandgaps range from 3.95 eV to 3.98 eV for the five diphenylamino-triazines. The values of the two iminodibenzyl-triazines are even higher and exceed 4.25 eV. Exceptionally high triplet energies in the range of 3.18 eV (ATRZ3) to 3.24 eV (BPMT) are obtained for all diphenylamino-triazines. Those values are amongst the highest values reported in the literature. Exemplarily the photo physical characterization of ATRZ2 is presented in Figure 10.

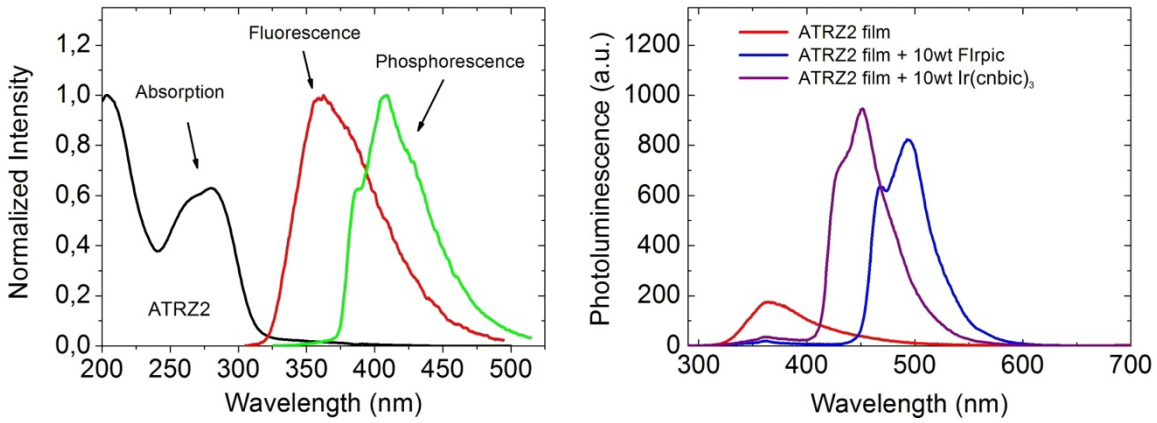

Figure 10: Left: Photo physical properties of ATRZ2 in a neat film, including absorption (black line), fluorescence (red line) and phosphorescence (green line). Absorption and fluorescence are measured at room temperature using standard spectroscopic methods, while phosphorescence is measured at 5K using time-gated spectroscopy. **Right:** Energy transfer experiment; Fluorescence spectra of a neat ATRZ2 film and two doped ATRZ2 films excited at the absorption maximum of ATRZ2. On excitation of the neat film the emission of ATRZ2 is detected (red line), while for the doped films the emission of FIrpic (blue line) and of $Ir(cnbic)_3$ (violet line) is observed due to energy transfer from host to guest.

The extraordinary high triplet energies of the diphenylamino-triazines enable the use of deep blue emitters like iridium-tris(1-cyanophenyl-3-methylbenzimidazolin-2-yilidene-C,$C^{2'}$ ($Ir(cnbic)_3$). This is verified by an energy transfer experiment shown in Figure 10. On excitation of the $Ir(cnbic)_3$-doped film at the absorption maximum of ATRZ2, the emission of $Ir(cnbic)_3$ (violet line) is detected.

The capability of diphenylamino-triazines as host material for blue phosphorescent emitters in OLEDs was investigated using a combinatorial approach. The best results are

found for the following device configuration: α-NPD (30 nm) / host:FIrpic (30 nm; 12 %) / BAlq (30 nm). ATRZ3 and ATRZ5 are used as host materials in device 1 and device 2 respectively. Figure 11 comprises the current efficiency-voltage characteristics (left) and the electroluminescence spectrum (right) of both devices. The electroluminescence spectrum of both devices exhibits pure FIrpic emission. The fact that no contribution of NPD is detected indicates that the recombination zone is centered in the EML or closer to the EML-ETL interface. The current efficiency of 14.1 cd/A is good when taking into account that no exciton blocking layers are used at the EML interfaces and the transport materials BAlq and NPD exhibit lower triplet energies than the emitter.

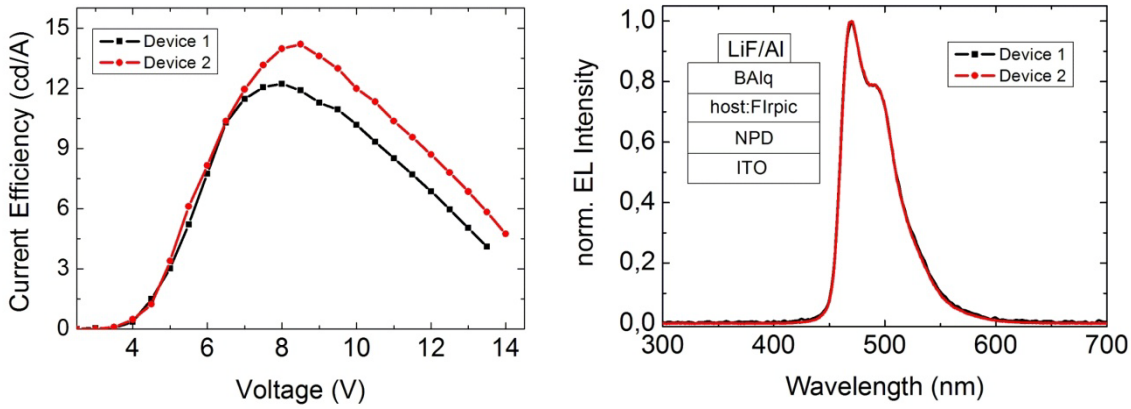

Figure 11: Left: Current efficiency-voltage characteristics of both devices. **Right:** Device configuration of the devices is shown in the inset. Electroluminescence spectrum of both devices at a luminance of 100 cd/m^2. For detailed information about the materials used in this device see chapter 7.

Additional to these results another diphenylamino-triazine BPMT was subject of investigations regarding the electric field dependence of Coulomb-stabilized excitons in deep blue host:guest systems (chapter 10). Here the photoluminescence intensity of the emitter Ir(cnbic)$_3$ in a device setup, where the host:guest layer is sandwiched between ITO/SiOx (10 nm) and SiOx (125 nm)/Al electrodes, upon applying an electric field is investigated. The emitter is excited with a laser pulse and the PL spectrum is recorded. The various host:guest systems that are compared are categorized in two heterostructures. In type I structures (BPMT:Ir(cnbic)$_3$) the emitter is enclosed by the host with respect to their electronic levels. In the Type II structure the HOMO of the emitter is lower than that of the host DPBIC. In Figure 12 the electronic levels of the

heterostructures and the PL intensity of the different devices at different electric fields is shown.

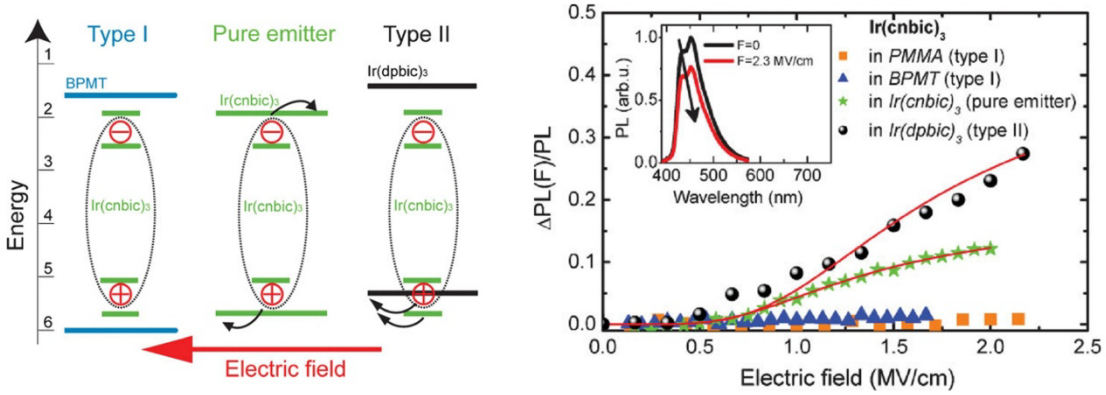

Figure 12: Left: Scheme of the energy levels of the different samples, taking into account the exciton binding energy of the emitter molecule. The curved arrows show possible exciton separation processes upon application of the external electric field. This results in the transfer of an electron or a hole to the surrounding molecules which constitute the host material. **Right:** Field induced relative quenching plotted as a function of the applied electric field. The data points are obtained integrating on the PL spectrum of the emitter molecule ($Ir(cnbic)_3$). Four different samples are reported in which $Ir(cnbic)_3$ is dispersed in: PMMA (orange squares), BPMT (blue triangles), $Ir(cnbic)_3$ (green stars) and DPBIC (black dots).

In the type I system there are no energy accepting levels upon exciton dissociation. In the pure emitter both the HOMO and LUMO of the surrounding emitter molecules provide a density of states for charge separation. The type II structure promotes exciton dissociation by hole transfer. Therefore the emission intensity of $Ir(cnbic)_3$ in BPMT is independent of the applied electric field. In contrast to that the PL intensity decreases about 15 % for the pure emitter device and about 30 % for the type II heterostructure upon applying an electric field of 2.3 MV/cm. These results demonstrate how important the specific tailoring of the electronic levels of the host material is with respect to the emitter.

Third generation of triazine-based host materials: Phenoxy-carbazole substituted triazines (chapters 8 and 9)

In chapters 8 and 9 a series of phenoxy-carbazole substituted triazine host material (PCTrz, PCTrz2 and PCTrz3) is presented. Here the intention was to design bipolar host materials. The non-conjugated ether bond, which connects the two moieties, separates the

oxidation- and reduction-sites of the molecule. This strict separation of donor and acceptor part is different to the triazines of the first and second generation, in which the donor groups are directly bound to the triazine core. The donor strength of those directly attached groups is decreased. In this generation of host materials both cases are present, since the acceptor moiety consists of a donor-substituted triazine core. The chemical structures of PCTrz, PCTrz2 and PCTrz3 are shown in Figure 13.

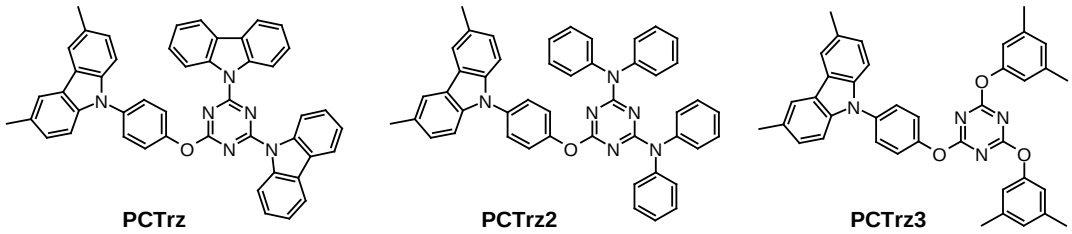

Figure 13: Chemical structure of the three triazine based host materials of the third generation.

The triazine-based PCTrz is subject of a detailed comparison to the first generation material TRZ2 (2,4-dicarbazolyl-6-phenoxy-1,3,5-triazine), since the triazine moiety is the same in both materials. In cyclic voltammetry experiments we found that the LUMO levels of both materials are similar, but the HOMO of PCTrz is 0.5 eV higher compared to that of TRZ2 (see Figure 16). This can be explained by the additionally attached phenoxy-carbazole moiety of PCTrz, which is separated from the electron-deficient triazine core and is therefore electron-richer than the carbazoles directly bound to the triazine core. Furthermore density functional theory calculations (DFT) of the electronic levels revealed that the HOMO and LUMO levels are perfectly separated in PCTrz (Figure 14 right). This is in accordance to the estimations of the LUMO levels of both moieties by the addition of the bandgap energy to the HOMO measured in electrochemistry. Here the LUMO of the triazine moiety is 0.3 eV lower than for the phenoxy-carbazole moiety. Thus, the hole and electron transporting moieties are successfully separated from each other in PCTrz. To investigate the influence on the injection and transport properties single carrier devices are fabricated and measured. Figure 14 comprises the current density-voltage characteristics of PCTrz and TRZ2 devices.

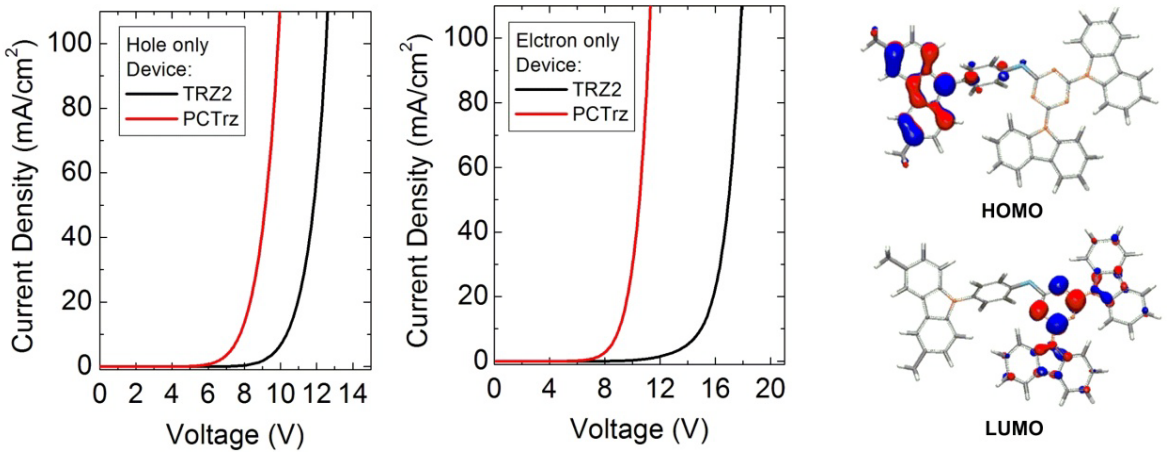

Figure 14: Left: Current density-voltage characteristics of the hole-only devices of PCTrz (red line) and TRZ2 (black line). **Middle:** Current density-voltage characteristics of the electron-only devices of PCTrz (red line) and TRZ2 (black line). **Right:** Spatial distribution of the HOMO and LUMO levels of PCTrz extracted from DFT calculations.

The hole-only devices clearly demonstrate the improved injection properties into PCTrz. However, the electron-only device also reveals an improved performance for PCTrz. The reason for this is currently not fully understood. Since the LUMO levels are very similar it can be speculated that the transport properties of PCTrz are responsible for the improved characteristics. Another hint for this can be found in the higher electron transfer rate, which is extracted from computational calculations. In summary it can be stated that PCTrz exhibits bipolar transport properties.

In chapter 9 the investigations concerning the bipolar character of third generation triazines are discussed in more detail. Additionally the thermal, electrical and optical properties within the series of triazine hosts shown in Figure 13 are described. Since the number of hole transporting phenoxy-carbazole units per triazine core is kept constant, the thermal properties of the three compounds are mainly defined by the rigidity and flexibility of the triazine substituent. Consequently, PCTrz exhibits the highest melting- crystallization- and glass transition temperatures (T_g = 148 °C) due to the rigid carbazole substituent. The glass transitions of PCTrz2 and PCTrz3 are lower (at 109 °C and 89 °C respectively) due to their more flexible amine and phenoxy groups. It is noteworthy that PCTrz3 is obtained as amorphous material from the synthesis and it was not possible to observe crystallization of the material at any time.

The optical characterization of the three compounds revealed very interesting aspects. The absorption spectrum of each material is almost the exact addition of the absorption of the two parts of the respective host molecule. The photoluminescence spectra of cyclohexane solutions showed almost similar emission of the phenoxy-carbazole moiety. Since the triazine moieties exhibit larger bandgaps than the phenoxy-carbazole, it can be assumed that the energy that is absorbed by the triazine part undergoes intramolecular transfer to the phenoxy-carbazole. However, the spectra of neat films showed a different behavior. In all PL spectra, but especially for PCTrz, an additional red-shifted peak was detected. This peak is attributed to an intermolecular charge transfer complex caused by aggregation. To prove this statement concentration dependent fluorescence spectroscopy of PCTrz diluted in a PMMA matrix was carried out. Figure 15 comprises a comparison of the neat film photoluminescence spectra at room temperature and at 10K.

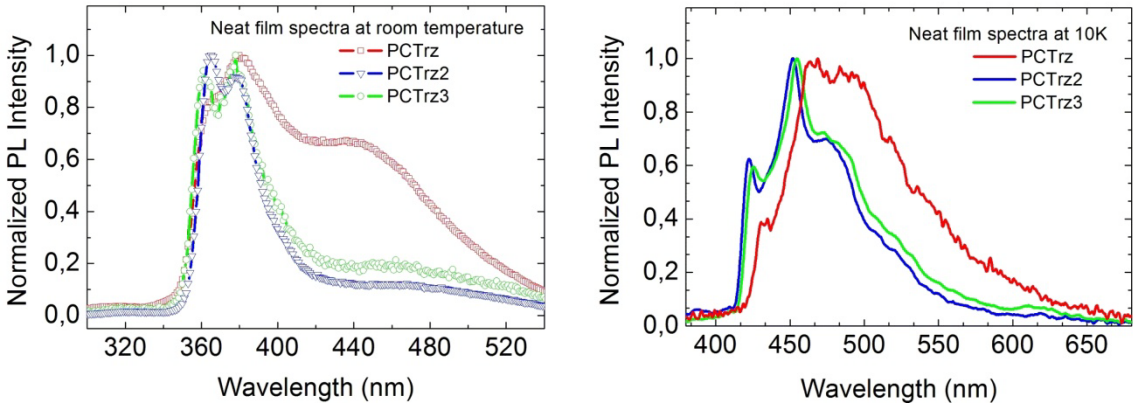

Figure 15: Left: Neat film fluorescence spectra of PCTrz (red line), PCTrz2 (blue line) and PCTrz3 (green line) at room temperature. **Right:** Neat film time gated low temperature phosphorescence spectra of PCTrz (red line), PCTrz2 (blue line) and PCTrz3 (green line) measured at a temperature of 10K.

Further evidence for the CT-complex arises from the phosphorescence spectrum of PCTrz. It is significantly broader compared to PCTrz2 and PCTrz3 and comprises less intensity. This evidences that the population of the CT-state is favored over the triplet state. Although the 0-0 phosphorescence transitions of all materials are very similar (in the range from 2.94 eV for PCTrz2 to 2.88 eV for PCTrz) it was found in quantum efficiency measurement that PCTrz2-based host:guest films comprise the highest efficiency.

Since the phenoxy-carbazole moiety is kept constant for the series of materials the position of the LUMO levels and the resulting electron injection properties can be studied for different electron transporting triazine moieties. The ionization potentials of the three materials are almost identical in cyclic voltammetry experiments. This can be explained by the fact that the oxidation takes place at the phenoxy-carbazole moiety and is further supported by density functional theory calculations of the electronic levels. In contrast to that the LUMO levels strongly differs for the three materials. The HOMO and LUMO levels of the respective parts of the triazine hosts as well as their optical bandgaps are shown in an illustration in Figure 16.

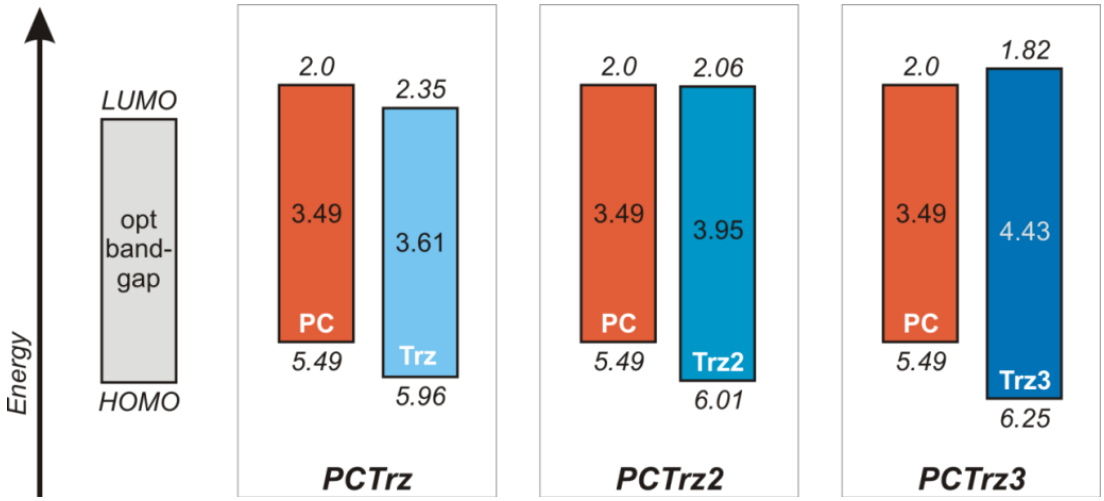

Figure 16: Schematic of the HOMO, LUMO and optical bandgap values for the respective moieties of each triazine host material. The HOMO values are measured by cyclic voltammetry, while the LUMO is estimated (HOMO minus opt. bandgap). Since the donor and acceptor parts of each host material are separated by a non-conjugated ether bridge they are regarded as isolated moieties. Therefore the two parts are individually characterized by cyclic voltammetry. The phenoxycarbazole moiety is more easily oxidized and therefore represents the hole conduction part of the molecule. In contrast to the LUMO values of the triazine moieties are different in each material.

Here it becomes clear that the oxidation of all materials takes place at the phenoxy-carbazole part. Therefore the hole injection of the third generation triazines is increased due to the higher HOMO levels. While the reduction of PCTrz is confined on the triazine moiety, that of PCTrz2 and PCTrz3 can be clearly assigned to one moiety. Nevertheless it is speculated that the reduction of PCTrz2 favorably takes place at the triazine moiety. To demonstrate the potential of phenoxy-carbazole substituted triazines as host material for blue phosphorescent emitters OLEDs with the following configuration were fabricated:

ITO / PEDOT / p-doped DPBIC 35nm / DPBIC 20nm / 15% LBE in PCTrz2 30nm / PYD2 10nm / Alq_3 50nm / LiF / AL. The luminance-voltage-current density characteristics and the external quantum efficiency-voltage-current efficiency characteristics of the OLED with PCTrz2 as host is shown in Figure 17.

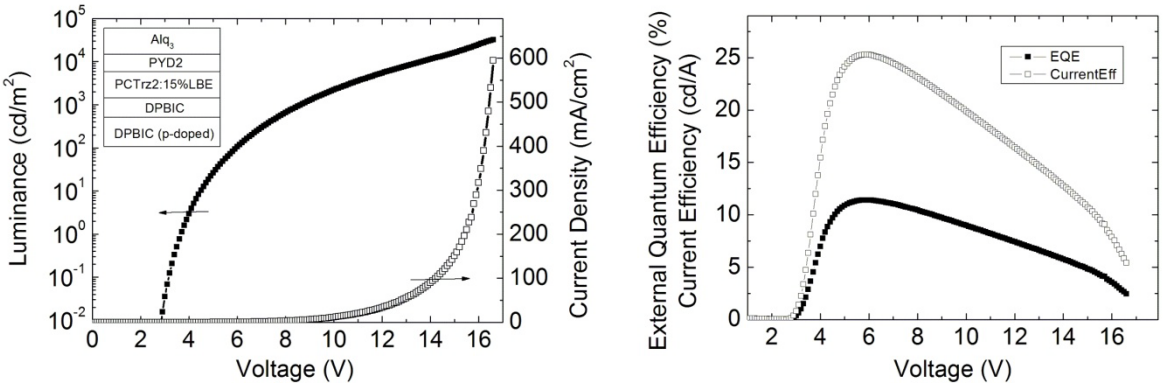

Figure 17: Left: Luminance-voltage-current density characteristics of an OLED with PCTrz2 as host; **Right:** External quantum efficiency-voltage and current efficiency-voltage characteristics of an OLED with PCTrz2 as host; **Inset**: device configuration.

The device reaches a maximum luminance of 33000 cd/m^2 at 16.6 V. The threshold voltage of 2.8 V indicates injection without barrier. The maximum external quantum efficiency of 11.5 % is reached at 100 cd/m^2. This corresponds to a current efficiency of 25 cd/A. It is further notable that the EQE remains high over a wide voltage range. Therefore at a luminance of 1000 cd/m^2 the EQE is still at 10.2 %.

In summary we conclude that the substitution of the phenoxy groups of first and second generation triazines by phenoxy-carbazole leads to better injection and transport properties as well as an improved OLED performance in third generation triazine based host materials.

Patent applications.

In addition to the five publications presented in chapters 6-10, two patents were prepared during the period of this thesis.[*] Both patents were published on April 30, 2009. The first patent (WO 2009/053346 A1) deals with the "Use of diphenylamino-bis(phenoxy) and bis(diphenylamino)-phenoxytriazine compounds in OLEDs". The title of the second patent (WO 2009/053278 A1) is: "Use of substituted tris(diphenylamino)-triazine compounds in OLEDs".

[*] Inventors: Evelyn Fuchs (BASF SE); Nicolle Moonen (BASF SE); Christian Lennartz (BASF SE); Peter Strohriegl (Universität Bayreuth); Michael Rothmann (Universität Bayreuth); Applicant: BASF SE

Individual contributions to joint publications

In the following, the contributions of the individual authors to the papers are specified.

Chapter 6

This work is submitted to *Chemistry of Materials* with the title:

"Donor-substituted 1,3,5-Triazines as Host Materials for Blue Phosphorescent Organic Light-Emitting Diodes"

by **Michael M. Rothmann**, Stephan Haneder, Enrico Da Como, Christian Lennartz, Christian Schildknecht and Peter Strohriegl.

I synthesized and characterized all the materials for this publication. I investigated the thermal and optical properties, except the low temperature spectroscopy. I was involved in the OLED processing and I wrote the publication.

Stephan Haneder and Enrico Da Como carried out the low temperature time-gated spectroscopy. Chrisitan Lennartz did the computational calculations. Christian Schildknecht and Christian Bonsigniore fabricated the OLEDs. Peter Strohriegl supervised the project and corrected the manuscript.

Chapter 7

This work is intended for submission to *Chemistry of Materials* with the title:

"Novel 1,3,5-Triazine-based Host Materials for Deep Blue Phosphorescent Emitters"

by **Michael M. Rothmann**, Stephan Haneder, Enrico Da Como and Peter Strohriegl.

I synthesized and characterized all the materials for this publication. I investigated the thermal and optical properties, except the low temperature spectroscopy. I fabricated and characterized the OLED and I wrote the publication.

Stephan Haneder and Enrico Da Como carried out the low temperature time-gated spectroscopy. Peter Strohriegl supervised the project and corrected the manuscript.

Chapter 8

This work is submitted to *Chemical Communications* with the title:

"Designing a bipolar host material for blue phosphorescent OLEDs: Phenoxy-carbazole substituted triazine"

by **Michael M. Rothmann**, Evelyn Fuchs, Christian Schildknecht, Nicolle Langer, Christian Lennartz, Ingo Münster, and Peter Strohriegl.

I synthesized and characterized all the materials for this publication. I investigated the thermal, optical and electrochemical properties. I was involved in the processing of the single carrier devices and I wrote the publication.

Christian Lennartz did the computational calculations. Christian Schildknecht and Christian Bonsigniore fabricated single carrier devices. Nicolle Langer and Evelyn Fuchs were involved in the scientific discussion and corrected the manuscript. Peter Strohriegl and Ingo Münster supervised the project and corrected the manuscript.

Chapter 9

This work is intended for submission to *Journal of Materials Chemistry* with the title:

"Designing bipolar host materials for blue phosphorescent OLEDs: A Series of Phenoxy-carbazole substituted 1,3,5-Triazines"

by **Michael M. Rothmann**, Sebastian T. Hoffmann, Anna Köhler Gerhard Wagenblast, Christian Lennartz, Soichi Watanabe, and Peter Strohriegl.

I synthesized and characterized all the materials for this publication. I investigated the thermal, optical and electrochemical properties and I wrote the publication.

Christian Lennartz did the computational calculations. Soichi Watanabe fabricated the OLEDs. Gerhard Wagenblast was involved in some photo physical measurements. Sebastian Hoffmann carried out the low temperature time-gated spectroscopy Anna Köhler and Peter Strohriegl supervised the project and corrected the manuscript.

Chapter 10: Appendix

This work is published in *Advanced Functional Materials* (**2009**, *19*, 2416-2422) with the title:

"Effect of Electric Field on Coulomb-Stabilized Excitons in Host/Guest Systems for Deep-Blue Electrophosphorescence"

by Stephan Haneder, Enrico Da Como, Jochen Feldmann, **Michael M. Rothmann**, Peter Strohriegl, Christian Lennartz, Oliver Molt, Ingo Münster, Christian Schildknecht and Gerhard Wagenblast.

This work appears as appendix, since all the work concerning electric field dependant spectroscopy was carried out by Stephan Haneder and Enrico Da Como. Stefan Haneder wrote the publication.

I synthesized and characterized the deep blue host material BPMT, which was used in the study. I was involved in the scientific discussion and corrected the manuscript. Christian Lennartz, Oliver Molt, Christian Schildknecht and Gerhard Wagenblast provided the blue phosphorescent emitter, carried out computational calculations and were responsible for the evaporation of the devices. Ingo Münster, Jochen Feldmann and Peter Strohriegl supervised the project and corrected the manuscript.

6 Donor-substituted 1,3,5-Triazines as Host Materials for Blue Phosphorescent Organic Light-Emitting Diodes

Michael M. Rothmann,† Stephan Haneder,‡ Enrico Da Como,‡ Christian Lennartz, § Christian Schildknecht, § Peter Strohriegl,†*

† Makromolekulare Chemie I and Bayreuther Institut für Makromolekülforschung, University of Bayreuth, 95440 Bayreuth, (Germany),

‡ Photonics and Optoelectronics Group, Department of Physics and CeNS Ludwig-Maximilians-Universität, 80799, Munich (Germany)

§ BASF SE, 67056, Ludwigshafen (Germany)

* Corresponding author. Email: peter.strohriegl@uni-bayreuth.de

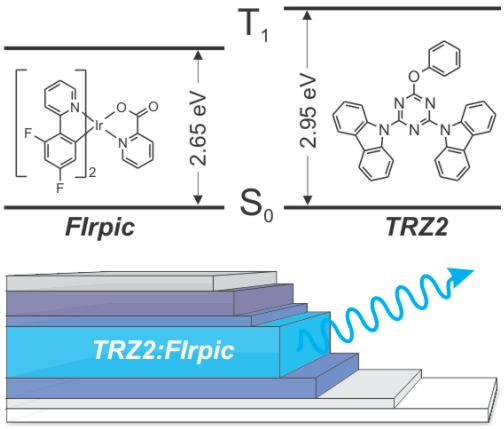

submitted to *Chemistry of Materials*

Abstract.

A series of new donor-substituted 1,3,5-triazines (**TRZ 1-7**) has been prepared by nucleophilic substitution of cyanuric chloride with carbazole, 3-methylcarbazole, phenol and 3,5-dimethylphenol. These s-triazines have been investigated as host material for blue phosphorescent light-emitting diodes (OLEDs). All triazine based hosts were characterized regarding their optical and thermal properties. Different substitution patterns resulted in high glass transition temperatures (T_g) of up to 170°C and triplet energies ($\Delta E(T_1\text{-}S_0)$) of up to 2.96 eV. The application as host material for the blue phosphor bis(4,6-difluorophenylpyridinato-N,C2)picolinato-iridium(III) (FIrpic) yielded maximum current efficiencies up to 21 cd/A.

Keywords.

Triazine, electroluminescence, OLED, blue phosphorescence, molecular glasses

Introduction.

Since the discovery of efficient phosphorescent emitters for organic light emitting diodes (OLED) by Forrest and Thompson many groups face the challenge to develop suitable new materials for phosphorescent OLEDs.[1,2] In most small molecule-based OLEDs the emitting layer consists of a phosphorescent dye which is doped into a host material to avoid concentration quenching and to optimize the charge balance. High efficiencies are only obtained when the energy is efficiently transferred from the host the phosphorescent dye. For an efficient transfer the triplet energy of the host material has to be higher than that of the guest.[3] This becomes more challenging for host materials used in combination with blue phosphorescent emitters, where triplet energies larger than 2.8 eV are required. In general the electron mobility of many organic hosts is much lower than the hole mobility due to the fact that they mainly consist of strong electron donors like aromatic carbazoles or amines.[4] In contrast to that electron transport materials often contain electron deficient heterocycles. Triazines for example are known to be good electron conductors and therefore have been used as electron transport layer in OLEDs [5,6,7]. However the hole transport properties of most triazines are not sufficient for their use as host material in OLEDs. Recent developments of new matrix materials for phosphorescent organic light emitting diodes often focus on the synthesis of bipolar materials.[8,9] In a study of Inomata et al. donor-substituted 2,4,6-tris(diarylamino)-1,3,5-triazines were presented as matrix material and electron conductor for OLEDs.[10] The combination of electron accepting triazines and electron donating diarylamine resulted in bipolar transport.[11] They proved to be a good host material for the green phosphorescent emitter tris(2-phenylpyridine)iridium ($Ir(ppy)_3$). The highest triplet energy was presented for 2,4,6-tris(carbazolyl)-1,3,5-triazine ($\Delta E(T_1\text{-}S_0)$ = 2.81 eV). An OLED with 2,4,6-tris(carbazolyl)-1,3,5-triazine as host and $Ir(ppy)_3$ as guest have shown a maximum quantum efficiency of 10.2 %.

Other OLED relevant properties like the electro-chemical properties of s-triazines[12] or the ab initio calculated molecular orbitals and triplet energies[13] are described for this class of materials and show their potential as host materials for OLEDs. In a recent work the electric

field induced quenching on the phosphorescence intensity of a deep-blue triplet emitter dispersed in a donor substituted triazine is described.[14]

Another essential requirement for the successful operation of OLEDs, which is often neglected, is the ability of the material to form stable amorphous films.[15] This property guarantees that the emitter stays uniformly diluted in the matrix to minimize the effect of concentration quenching. In addition the absence of grain boundaries, which may act as trap states, makes the use of organic glasses as OLED materials advantageous.[16,17] In order to obtain organic glasses, several points have to be taken into account. An important fact is to avoid strong intermolecular forces like hydrogen bonding or π-π stacking between the molecules. Furthermore the introduction of bulky substituents leads to a larger intermolecular distance and a hindrance in packing and therefore an amorphous behavior. On the other hand the increased distance separates the conducting units from each other and results in decreasing charge carrier mobility. Another possibility to design organic glasses is the synthesis of asymmetric molecules. With this method the number of conformers is increased and the high amount of energy needed for the crystallization favors the stability of amorphous films.[15,18]

In this paper we describe the successful combination of high triplet energies and amorphous behavior for donor substituted triazines. This was achieved by the introduction of substituted carbazoles and by the successive replacement of up to two carbazoles by phenoxy groups (Scheme 1). This yielded asymmetric materials with glass transition temperatures up to 170 °C and triplet energies up to 2.96 eV. The device performance of two triazines as host materials for the blue phosphor FIrpic is presented

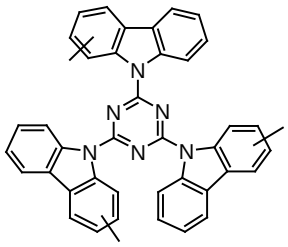

TRZ 1

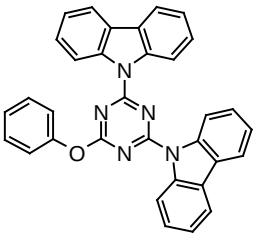

TRZ 2

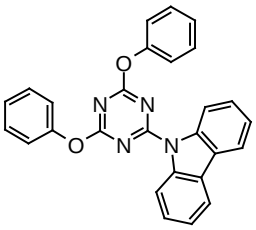

TRZ 3

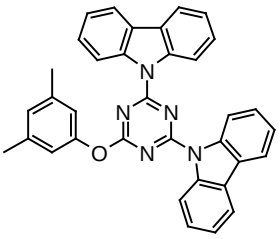

TRZ 4

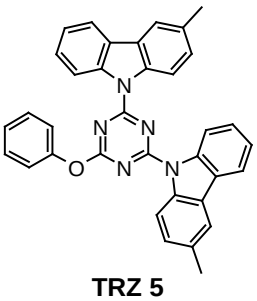

TRZ 5

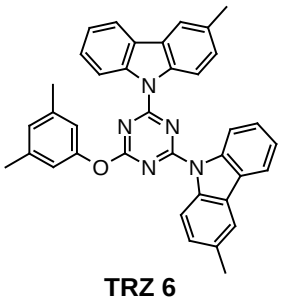

TRZ 6

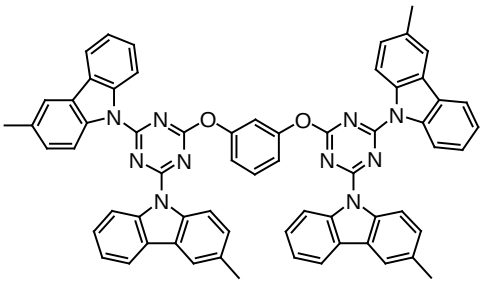

TRZ 7

Scheme 1: Structures of the donor substituted triazines **TRZ 1-7**.

Experimental Section.

Materials. All commercially available reagents were purchased from Aldrich and used without further purification. The synthesis of tris[(3-phenyl-1H-benzimidazol-1-yl-2(3H)-ylidene)-1,2-phenylene]-Iridium (DPBIC) and 2,8-bis(triphenylsilyl)-dibenzofuran (DBFSi) is described in the literature.[19, 20]

2,4,6-Tris(methylcarbazole-9'-yl)-1,3,5-triazine (**TRZ 1** is a statistical mixture of a triazines core with 2- and 3-methyl-carbazole substituents). A mixture of 2-methylcarbazole (1.45 g, 8.0 mmol) and 3-methylcarbazole (1.45 g, 8.0 mmol) was dissolved in dry THF (100 ml) under argon atmosphere in a two-necked round bottom flask equipped with a septum inlet

and three way stopcock. n-Buthyllithium (1.6 M in hexane solution) (1.6 M) (9.37 ml, 15 mmol) was added drop wise to the methylcarbazole solution and the mixture was stirred for 10 minutes. In a separate three-necked round bottom flask equipped with a septum inlet, three way stopcock and condenser cyanuric chloride (0.83 g. 4.5 mmol) was dissolved in dry THF (60 ml) under argon. The carbazole-lithium solution was added dropwise to the cyanuric chloride solution using a transfer canula within 15 minutes. The reaction mixture was refluxed for 6 h. After cooling to room temperature 40 ml of water were added. The product was filtered off, washed with water, hexane and diethyl ether and further pre-purified by hot filtration from ethanol. Recrystallization from a chlorobenzene/hexane mixture yielded in 1.7 g (61 %) of **TRZ 1** as white crystalline solid. ^{1}H NMR (250 MHz, d^{4}-THF): δ (ppm) 8.96 (m, 6H), 8.02 (m, 6H), 7.31 (m, 9H), 2.53 (s, 4.3H), 2.38 (s, 4.7H). EI-MS: m/z 618 (100, M^{+}), 309 (30, M^{2+}).

2,4-Bis(carbazol-9'-yl)-6-chloro-1,3,5-triazine (1a). Carbazole (1.42 g, 8.5 mmol) was dissolved in dry THF (50 ml) under argon in a two-necked round bottom flask equipped with a septum inlet and three way stopcock. n-Butyllithium (1.6 M in hexane solution) (5.0 ml, 8.0 mmol) was added dropwise to the methylcarbazole solution and the mixture was stirred for 10 minutes. In a separate three-necked round bottom flask equipped with a septum inlet, three way stopcock and condenser cyanuric chloride (0.74 g, 4.0 mmol) was dissolved in dry THF (20 ml) in an argon atmosphere. The carbazole lithium solution was added dropwise to the cyanuric chloride solution using a transfer canula within 10 minutes. The reaction mixture was refluxed for 6 hours. After cooling to room temperature 40 ml of water were added. The product was filtered off, washed with water, hexane and diethyl ether and further purified by hot filtration from ethanol, to yield 1.2 g (68 %) of **1a** as white crystalline solid. mp: 231 °C. ^{1}H NMR (250 MHz, $CDCl_3$): δ (ppm) 8.92 (d, 4H), 8.06 (d, 4H), 7.56-7.40 (m, 8H). EI-MS: m/z 445 (100, M^{+}), 192 (90), 166 (100).

2,4-Bis(3'-methylcarbazol-9'-yl)-6-chloro-1,3,5-triazine (1b). This compound was synthesized by a procedure similar to that of **1a** except that 3-methylcarbazole was used instead of carbazole. Yield: 1.5 g (78 %) as white solid. mp: 235 °C. ^{1}H NMR (250 MHz,

$CDCl_3$): δ (ppm) 8.81 (d, 2H), 8.66 (d, 2H), 7.92 (d, 2H), 7.72 (s, 2H), 7.41-7.33 (m, 4H), 7.22 (d, 2H), 2.50 (s, 6H). EI-MS: m/z 473 (100, M^+), 237 (20, M^{2+}), 180 (15).

2,4-Bisphenoxy-6-chloro-1,3,5-triazine (2). Cyanuric chloride (3.68 g, 20 mmol) was dissolved in acetone (200 ml) and cooled to 15°C. In a separate flask phenol (3.76 g, 40 mmol) was reacted with sodium hydroxide (1.60 g, 40 mmol) in water (200 ml). After the formation of the sodium phenolate was complete the solution was cooled to 15 °C and added dropwise to the cyanuric chloride solution. The reaction mixture was stirred at temperatures below 15 °C for 8 hours before 200 ml of water were added. The white precipitate was filtered and washed with water and ethanol. The product was purified by recrystallization from hexane to yield 5.8 g (85 %) as white crystals. ^{1}H NMR (250 MHz, $CDCl_3$): δ (ppm) 7.42-7.35 (m, 4H), 7.28-7.22 (m, 2H), 7.13 (d, 4H). EI-MS: m/z 299 (100, M^+).

2,4-Bis(carbazol-9'-yl)-6-phenoxy-1,3,5-triazine (TRZ 2). In a two necked round bottom flask 2,4-bis(carbazol-9'-yl)-6-chloro-1,3,5-triazine (**1a**) (0.89 g, 2 mmol) was dissolved in chloroform (20 ml). In a separate flask phenol (0.23 g, 2.4 mmol) and sodium hydroxide (0.095 g, 2.4 mmol) were dissolved in 10 ml water at room temperature and stirred for 10 minutes until the solution was added to the **1a**. Tetrabutylammonium bromide (12 mg, 0.04 mmol) and dibenzo-18-crown-6 (14 mg, 0.04 mmol) were added as phase transfer catalysts. The mixture is heavily stirred for 8 hours at 70 °C. After cooling to room temperature, addition of 20 ml water and extraction with diethyl ether, the organic phase was washed with water and dried over magnesium sulfate. The solvent was removed under reduced pressure and the product was purified by recrystallization from a hexane/ THF mixture to yield 0.40 g (40 %) of **TRZ 2** as white crystalline solid. ^{1}H NMR (250 MHz, $CDCl_3$): δ (ppm) 8.74-8.70 (m, 4H), 8.04-8.00 (m, 4H), 7.60 (d, 2H), 7.44-7.36 (m, 11H). EI-MS: m/z 503 (100, M^+), 337 (50), 166 (40).

2-(Carbazol-9'-yl)-4,6-bisphenoxy-1,3,5-triazine (TRZ 3). This compound was synthesized by a procedure similar to that of **1a** except that the ratio carbazole to triazine was 1.2 to 1. Yield: 0.77 g (90 %) as white crystalline solid. ^{1}H NMR (250 MHz, $CDCl_3$): δ (ppm) 8.07 (d, 2H), 7.89 (d, 2H), 7.60-7.53 (m, 4H), 7.46-7.41 (m, 2H), 7.36-7.25 (m, 6H), 7.13-7.07 (m, 2H). EI-MS: m/z 430 (100, M+), 337 (100), 166 (50).

2,4-Bis(carbazol-9'-yl)-6-(3',5'-dimethylphenoxy)-1,3,5-triazine (TRZ 4). This compound was synthesized by a procedure similar as described for **TRZ 2**. 3,5-dimethylphenol was used instead of phenol. Yield: 0.92 g (86 %) as white crystalline solid. ^{1}H NMR (250 MHz, $CDCl_3$): δ (ppm) 8.78-8.74 (m, 4H), 8.05-8.01 (m, 4H), 7.41-7.29 (m, 8H), 7.09 (s, 1H), 7.04 (s, 2H), 2.44 (s, 6H). EI-MS: m/z 531 (70, M^+), 365 (100), 166 (50), 105 (40).

2,4-Bis(3'-methylcarbazol-9'-yl)-6-phenoxy-1,3,5-triazine (TRZ 5). This compound was synthesized by a procedure similar as described for **TRZ 2**. Instead of 2,4-bis(carbazol-9'-yl)-6-chloro-1,3,5-triazine (**1a**) 2,4-bis(3'-methylcarbazol-9'-yl)-6-chloro-1,3,5-triazine (**1b**) was used. Yield: 0.92 g (86 %) as white crystalline solid. ^{1}H NMR (250 MHz, $CDCl_3$): δ (ppm) 8.72-8.68 (m, 2H), 8.59 (d, 2H), 7.99-7.95 (m, 2H), 7.79 (s, 2H), 7.57 (d, 2H), 7.45-7.33 (m, 7H), 7.14 (d, 2H), 2.52 (s, 6H). EI-MS: m/z 531 (100, M^+), 351 (30), 180 (30).

2,4-Bis(3'-methylcarbazol-9'-yl)-6-(3',5'-dimethylphenoxy)-1,3,5-triazine (TRZ 6). This compound was synthesized by a procedure similar as described for **TRZ 2**. Instead 2,4-bis(carbazol-9'-yl)-6-chloro-1,3,5-triazine (**1a**) 2,4-bis(3'-methylcarbazol-9'-yl)-6-chloro-1,3,5-triazine (**1b**) was used. 3,5-dimethylphenol was used instead of phenol. Yield: 0.86 g (81 %) as white crystalline solid. ^{1}H NMR (250 MHz, $CDCl_3$): δ (ppm) 8.70-8.68 (m, 2H), 8.59 (d, 2H), 7.97-7.94 (m, 2H), 7.78 (s, 2H), 7.57 (d, 2H), 7.45-7.33 (m, 4H), 7.10 (s, 1H), 7.04 (s, 2H), 2.50 (s, 6H), 2.43 (s, 6H). EI-MS: m/z 559 (100, M^+), 379 (50), 180 (35).

Bis(4,6-di(3'-methylcarbazol-9'-yl)-1,3,5-triazin-2-yl)resorcinol (TRZ 7). This compound was synthesized by a procedure similar as described for **TRZ 2**. Instead of 2,4-bis(carbazol-9'-yl)-6-chloro-1,3,5-triazine (**1a**) 2,4-bis(3'-methylcarbazol-9'-yl)-6-chloro-1,3,5-triazine (**1b**) was used. Instead of phenol resorcinol was used. The ratio of triazine to resorcinol to sodium hydroxide was changed to 1:2.4:2.2 (mmol). Yield: 0.47 g (48 %) as white solid. mp: 300°C. ^{1}H NMR (250 MHz, $CDCl_3$): δ (ppm) 8.74 (d, 4H), 8.58 (d, 4H), 7.93 (d, 4H), 7.74 (s, 4H), 7.60 (s, 1H), 7.50 (d, 2H), 7.42-7.25 (m, 9H), 7.21-7.13 (d, 4H), 2.49 (s, 12H). NMR. EI-MS: m/z 984 (100, M^+), 804 (20), 492 (40, M^{2+}), 180 (100).

Characterization. 1H-NMR spectra were recorded on a Bruker AC-250 spectrometer at 250 MHz. All NMR-data given are given as chemical shifts δ (ppm) downfield from $Si(CH_3)_4$. MS

spectra were obtained on a Finnigan Mat 8500, MAT 112 S Varian machine using EI-ionisation. Melting points and glass transition temperature determination was carried out on a Perkin Elmer Diamond DSC at a heating/cooling rate of 10 K/min under nitrogen atmosphere. Thermographimetric analysis (TGA) was performed on a Mettler Toledo TGA/SDTA851e machine at a heating rate of 10 K/min in nitrogen atmosphere.

UV-Vis absorption spectra were recorded on a Hitachi U-3000 spectrometer. Photoluminescence spectra were obtained using a Shimadzu Spectrofluorophotometer RF-5301PC. UVASOL solvents purchased from Merck were used to prepare solutions and films for optical characterization. The phosphorescence spectra were obtained with a time gated PL setup described elsewhere.[14] In brief, thin film samples were mounted in liquid helium cold finger cryostat and excited by laser pulses (500 ps) at 337 nm. The detection of phosphorescence was accomplished by a gated micro-channel-plate (MCP) with a time-gated detection window delayed with respect to the photoexciting pulse. For the experiments presented here, the detection started 500 ns after the pulse and for a time interval of 1 ms.

OLED fabrication. The organic layers were deposited by thermal evaporation in high vacuum ($<10^{-6}$ mbar) onto indium-tin-oxide (ITO, 10 ohm/square) pre-coated glass substrates. Prior to use the ITO glass was degreased using organic solvents and cleaned using an UV-ozon oven for 30 minutes. The organic layers and the metal cathode were evaporated without breaking the vacuum.

Computational Calculations. The transport levels of the materials used were determined via density functional calculations. For the ionization potential and the electron affinity first the geometry of the neutral as well as the charged states were optimized using the BP86-functional[21,22] in combination with a split-valence basis set (SV(P)) including polarization functions on all heavy atoms[23]. For iridium an effective core potential was employed.[24] For the energetics single point calculations at the optimized geometries using the same functional in combination with a valence triple zeta basis set (TZVP)[25] were conducted. To account for dielectric solid state effects a UPS/IEPS-calibrated version of the conductor like

screening model (COSMO)[26] was used in conjunction with the single point calculations. All calculations were carried out with the turbomole program package.[27]

Results and Discussion.

Synthesis. Previously reported 2,4,6-triscarbazolyl-1,3,5-triazine [10] is highly crystalline with a melting point of 465 °C. Several attempts have been made to reduce the crystallinity of triscarbazolyl-triazines. The substitution of the s-triazine core with three 2-methylcarbazole units or three 3-methylcarbazoles still yielded materials with a high tendency to crystallize. Furthermore we synthesized unsymmetrically substituted triscarbazolyl triazines. In a two step synthesis, we were able to prepare various compounds with either two methylcarbazoles and one carbazole unit or three different methylcarbazole units. This strategy resulted in materials with slightly decreased crystallization tendencies. However the glass formation properties of these triazines were still poor. We found that a stoichiometric mixture of 2-methylcarbazole and 3-methylcarbazole (1:1) as substituents was the most effective way to obtain a less crystalline material. **TRZ 1** is synthesized by nucleophilic substitution of cyanuric chloride with a 1:1 mixture of 2- and 3-methyl substituted carbazoles (see Scheme 2). The ^{1}H-NMR spectrum of **TRZ 1** confirmed that the carbazoles are incorporated in an almost equimolar ratio.

The synthesis of the unsymmetrical triazines **TRZ 2** to **TRZ 7** followed a different route. To obtain these compounds at least two steps are required. For all materials except for **TRZ 3**, the first synthetic step was a substitution of cyanuric chloride with carbazole or 3-methylcarbazole. The number of carbazole substituents was controlled by the ratio of carbazole and triazine. This is possible due to the stepwise deactivation of the chlorine atoms at the triazine core after substitution with an electron donating carbazole unit. Therefore the reaction can be efficiently stopped at this step and yields of 68 % (**1a**) and 78 % (**1b**) were obtained. In the second step **1a** and **1b** were reacted with phenol and 3,5-dimethylphenol to yield triazines **TRZ 2** and **TRZ 5** as well as **TRZ 4** and **TRZ 6**, respectively. In contrast to that phenoxy substitutions mainly follow a temperature control.[28] The synthesis of intermediate **2** was carried out at temperatures below 15 °C to suppress the

three-fold substitution and yielded 85 %. The substitution of **2** with carbazole yielded the triazine **TRZ 3**. For the synthesis of triazine **TRZ 7** the diol resorcinol was reacted with **1b**.

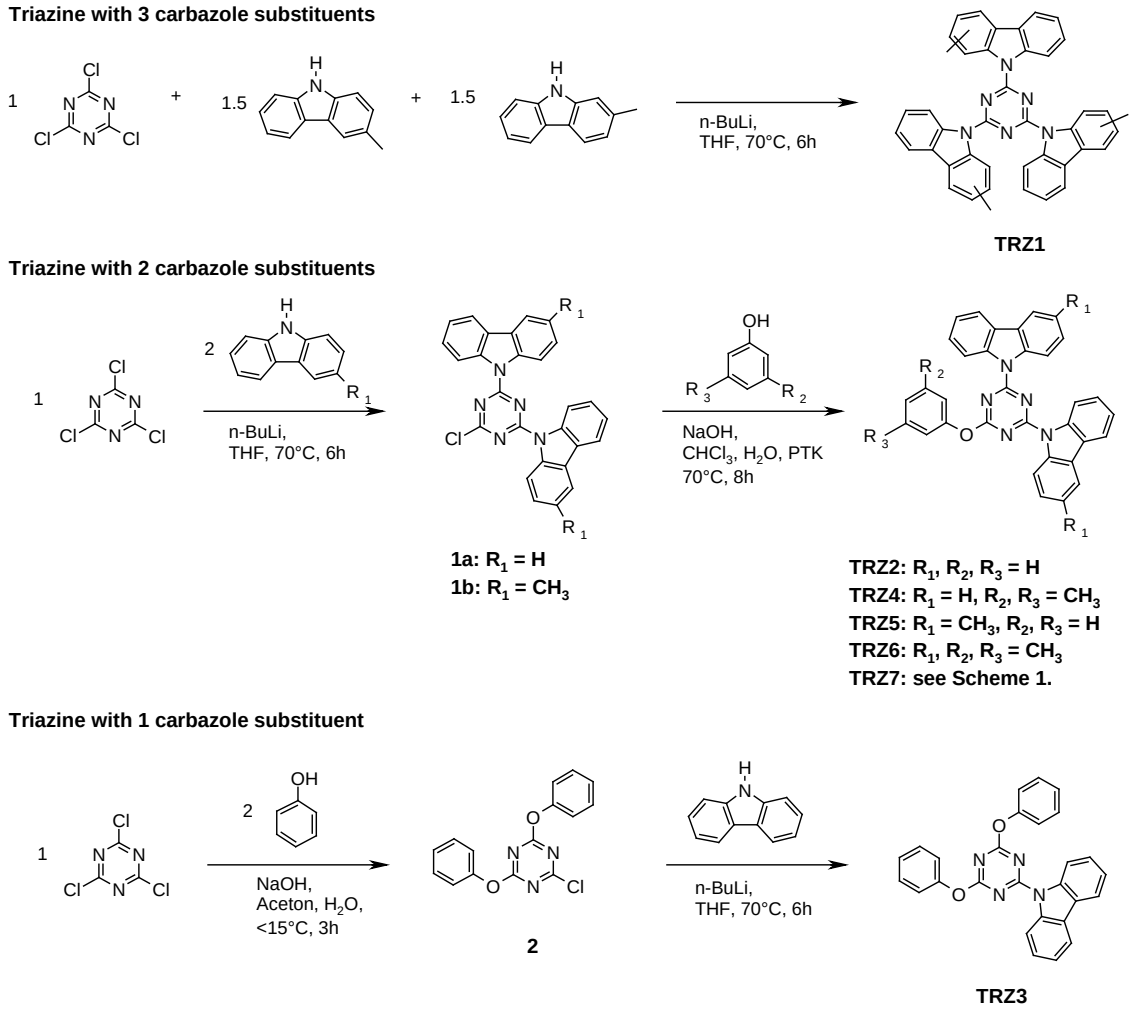

Scheme 2: Synthesis of donor substituted triazines **TRZ 1-7**.

Thermal characterization. The thermal properties of the novel triazines were investigated by differential scanning calorimetry (DSC), and their thermal stability was examined by thermogravimetric analysis (TGA). In both experiments the heating and cooling rate was 10 K/min. The data are shown in Table 1. The first and second heating as well as the first cooling curves of **TRZ 1**, **TRZ 4** and **TRZ 5** are shown in figure 1.

Table 1: Thermal properties of triazines TRZ 1-TRZ 7

Product	T_g [°C]	T_m [°C]	T_c [°C]	T_d [°C]
TRZ 1	-	335	295	372
TRZ 2	80[a]	219	135	356
TRZ 3	-	248	186	307
TRZ 4	83	210	127[b]	310
TRZ 5	85	147[c]	-	364
TRZ 6	90	171[c]	-	386
TRZ 7	170	301[c]	-	399

* T_g: glass-transition temperatures, T_m: melting temperatures, T_c: crystallization temperatures and T_D: onset temperatures of decomposition
[a] Observed only after very fast cooling of the melt.
[b] Observed only upon heating
[c] Observed only in the first heating scan.

All triazines exhibit a melting peak during the first DSC heating cycle. The melting temperatures range from 147 °C for **TZR 5** to 335 °C for **TRZ 1** (see figure 1). **TRZ 1**, **TRZ 2** and **TRZ 3** crystallize upon cooling in the DSC. **TRZ 4** forms a glass upon cooling and a glass transition can be observed in the subsequent heating cycle at 83 °C. On further heating **TRZ 4** crystallizes at 127 °C and exhibits a melting at 210 °C (see figure 1). **TRZ 5**, **TRZ 6** (see figure 1) and **TRZ 7** also form glasses on cooling. In contrast to **TRZ 4** these triazines stay amorphous in the following heating and cooling cycles. The glass transition temperatures of **TRZ 5** (85 °C) and **TRZ 6** (90 °C) are slightly higher than that of **TRZ 4**. The higher molecular weight of the dimeric compound **TRZ 7** results in a much higher T_g of 170 °C. The thermal behavior can be reproduced in multiple cycles. The glass transition of **TRZ 2** was determined in a separate experiment. The material was heated above its melting temperature and afterwards cooled very fast using liquid nitrogen to yield a supercooled melt. On subsequent heating in the DSC a T_g was observed at 80 °C followed by a crystallization peak at 121 °C and melting peak at 219 °C. However it was not possible to observe a glass transition of **TRZ 1** and **TRZ 3** using this technique. These experiments demonstrate that it is possible to get stable glasses from these triazine compounds.

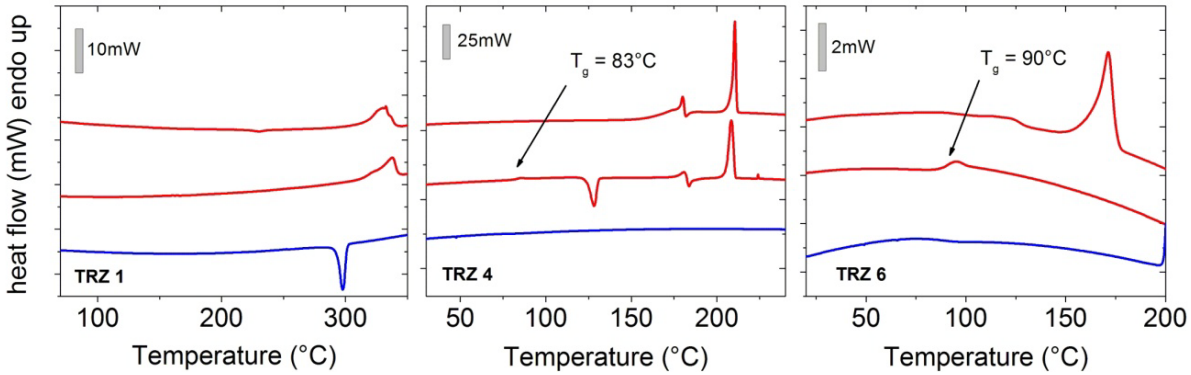

Figure 1: First heating cycle (top line), second heating cycle (middle line) and first cooling cycle (bottom line) of **TRZ 1**, **TRZ 4** and **TRZ 6** (left to right).

All compounds exhibit a high thermal stability in the TGA experiment. The decomposition temperatures range from 307°C to 399°C for **TRZ 3** and **TRZ 7** respectively. This enables thermal evaporation without decomposition. It was possible to yield amorphous films by spin coating or thermal evaporation from all triazine host materials. Films of **TRZ 1** and **TRZ 3** tended to crystallize after several hours to days. All other films were long time stable.

Optical properties. The absorption, fluorescence and phosphorescence spectra of **TRZ 1** - **TRZ 3** films (150nm) on quartz are shown in figure 2. The spectra show typical examples of triazines with three, two and one carbazole group. The spectra of **TRZ 4 - TRZ 7** are very similar to those of **TRZ 2** with a little bathochromic shift due to the inductive effect of the methyl groups attached to the carbazole. By comparing the absorption spectra of three triazines it can be observed that the lowest energetic absorption maximum is shifted from 333 nm to 320 nm with increasing amount of phenoxy substituents. From the absorption edge of these spectra the optical bandgap can be estimated. **TRZ 1** has the lowest bandgap of 3.54 eV. **TRZ 2** and **TRZ 3** have bandgap values of 3.61 eV and 3.75 eV respectively. In the non-gated room temperature PL spectra we observe the fluorescence of the compounds and the bathochromic shift is even more pronounced. The fluorescence of **TRZ 1** is relatively broad with a maximum at 385 nm. The spectrum of **TRZ 2** has two sharp peaks with almost the same height at 372 nm and 389 nm and a broad red shifted shoulder. The fluorescence of **TRZ 3** is narrower with a maximum at 351 nm. The hypsochromic shift can be assigned to the electron withdrawing effect of the triazine on the single carbazole. In

TRZ 3 the effect is very pronounced since only one carbazole unit is present. The hypsochromic shift becomes smaller in **TRZ 2** and **TRZ 1** with two and three carbazole units connected to the central triazine.

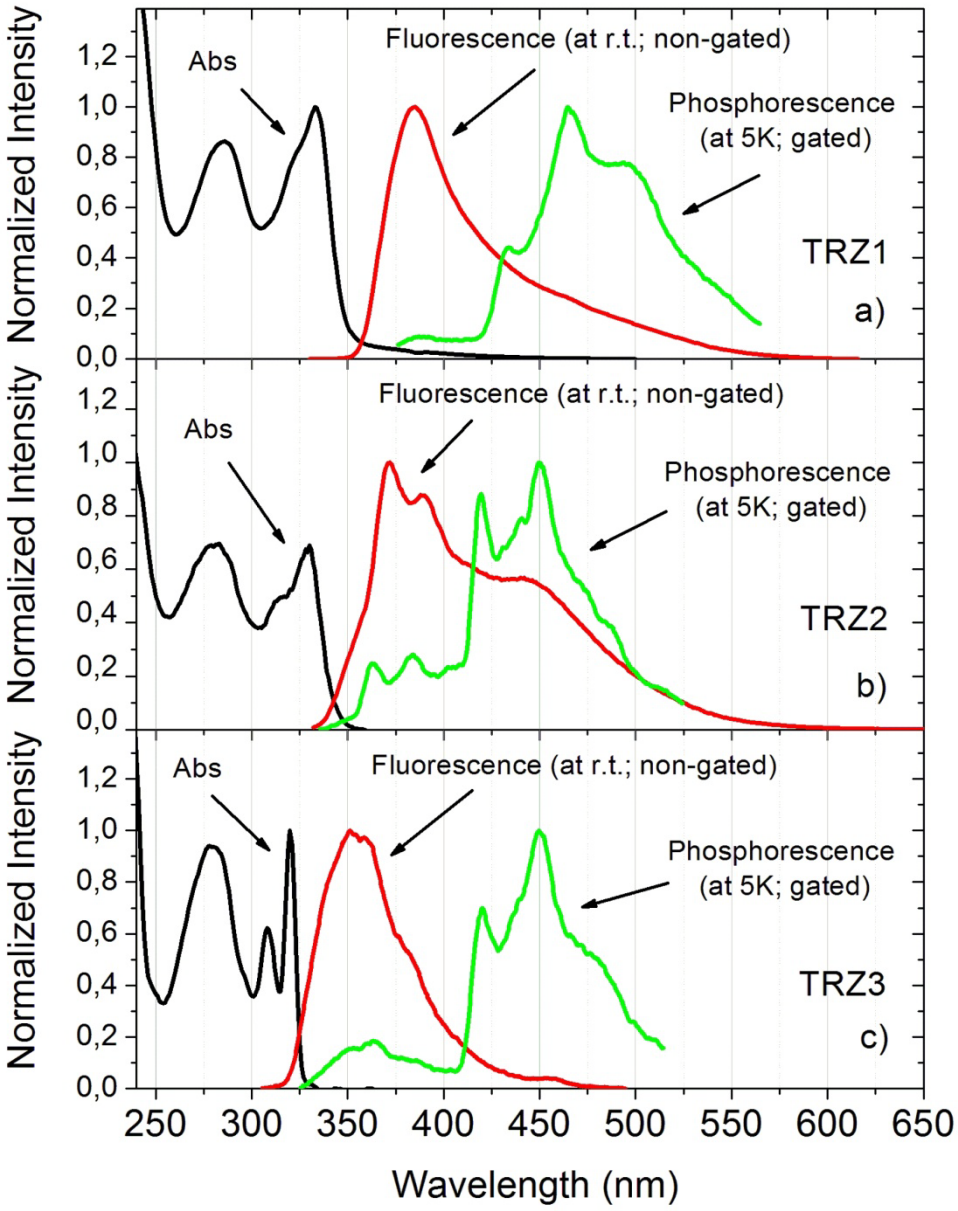

Figure 2: Photo physical properties of **TRZ 1**, **TRZ 2** and **TRZ 3** in neat films, including absorption (black line), fluorescence (red line) and phosphorescence (green line). Absorption and fluorescence are measured at room temperature using standard spectroscopic methods, while phosphorescence is measured at 5K using time-gated spectroscopy

For the application as host material in OLEDs the triplet level of the host must be higher compared to the guest. The triplet energy of selected triazines was determined from neat

film time-gated phosphorescence spectra of neat films at T = 5K. In this experiment the detection of the phosphorescence spectrum is achieved by recording the PL several hundred ns after the laser pulse, i.e. after the prompt fluorescence has decayed and in the presence of the long-lived phosphorescence. The triplet energy was obtained from the first vibronic transition of the red shifted phosphorescence spectrum. All spectra exhibited a vibronic progression up to the 0-2 peak. **TRZ 1** shows a 0-0 phosphorescence transition at 433 nm (2.86 eV) and a maximum at 465 nm. Values of 420 nm (2.95 eV) and 419 nm (2.96 eV) for **TRZ 2** and **TRZ 3** are determined for the respective 0-0 transitions. In contrast to the fluorescence the difference of the first phosphorescence maximum of **TRZ 2** and **TRZ 3** is only 1 nm. These maxima are centered at 450 nm and correspond to the 0-1 transition. The weak signals between 320 nm and 400 nm may result from delayed fluorescence of the host materials as suggested by the good energy overlap with the prompt fluorescence spectra (dashed lines). From the high triplet energy values it can be estimated that efficient exothermic energy transfer from all the presented TRZ host to blue phosphors such as FIrpic (2.65 eV) is possible.

Phosphorescent Organic Light-Emitting Diodes. Two OLEDs with the configurations shown in figure 3 were fabricated to demonstrate the potential of donor-substiuted triazines as host material for blue phosphorescent emitters. For this purpose **TRZ 2** was chosen as representative material for this class. On top of indium-tin-oxide (ITO) poly(thiophene-3-[2-(2-methoxyethoxy)ethoxy]-2,5-diyl) was used as hole-injection layer followed by 35 nm of DPBIC p-doped with molybdenum(VI) oxide as hole-transporting layer. An additional 10 nm thick layer of DPBIC followed as exciton and electron blocker. The 20 nm thick emission layer consisted of **TRZ 2** doped with 8% (device 1) or 16% (device 2) FIrpic. In device 1 **TRZ 2** was used as hole-blocking layer (5 nm) followed by 20 nm 2,9-Dimethyl-4,7-diphenyl-1,10-phenanthroline (BCP) as electron transporting material. In device 2 the hole-blocking and electron-conduction layers consisted of 5 nm DBFSi and 40 nm BCP. The devices were finalized by deposition of LiF (0.7 nm)/ Al (100 nm) cathode.

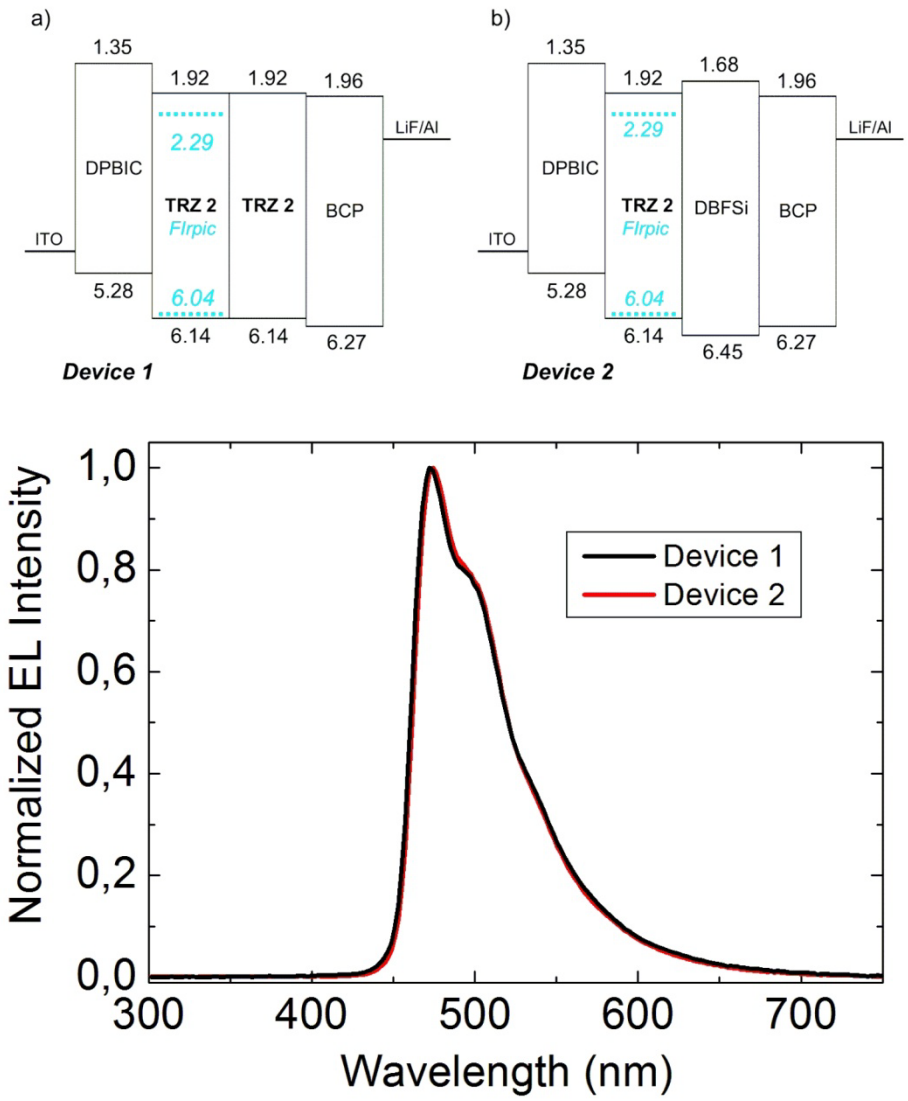

Figure 3: Top: Energy level diagram of device 1 and device 2; Ionization potentials and electron affinity levels of the different materials are indicated. The dotted lines represent the levels of the emitter FIrpic. The HOMO and LUMO levels were extracted from density functional theory (DFT) calculations. **Bottom:** Electroluminescent spectra of device 1 and device 2 at 10 mA/cm^2.

In literature the bipolar transport characteristics of a carbazol substituted triazine were reported.[10] Therefore we consider it very important that exciton blocking layers are used on both sides of the emission layer. In our setup DPBIC is used as exciton and electron blocker on the hole conduction side. The blocker on the electron conduction side was varied. In device 1 the host material **TRZ 2** itself was used. DBFSi which was employed in device 2 acts both as effective hole and exciton blocker.

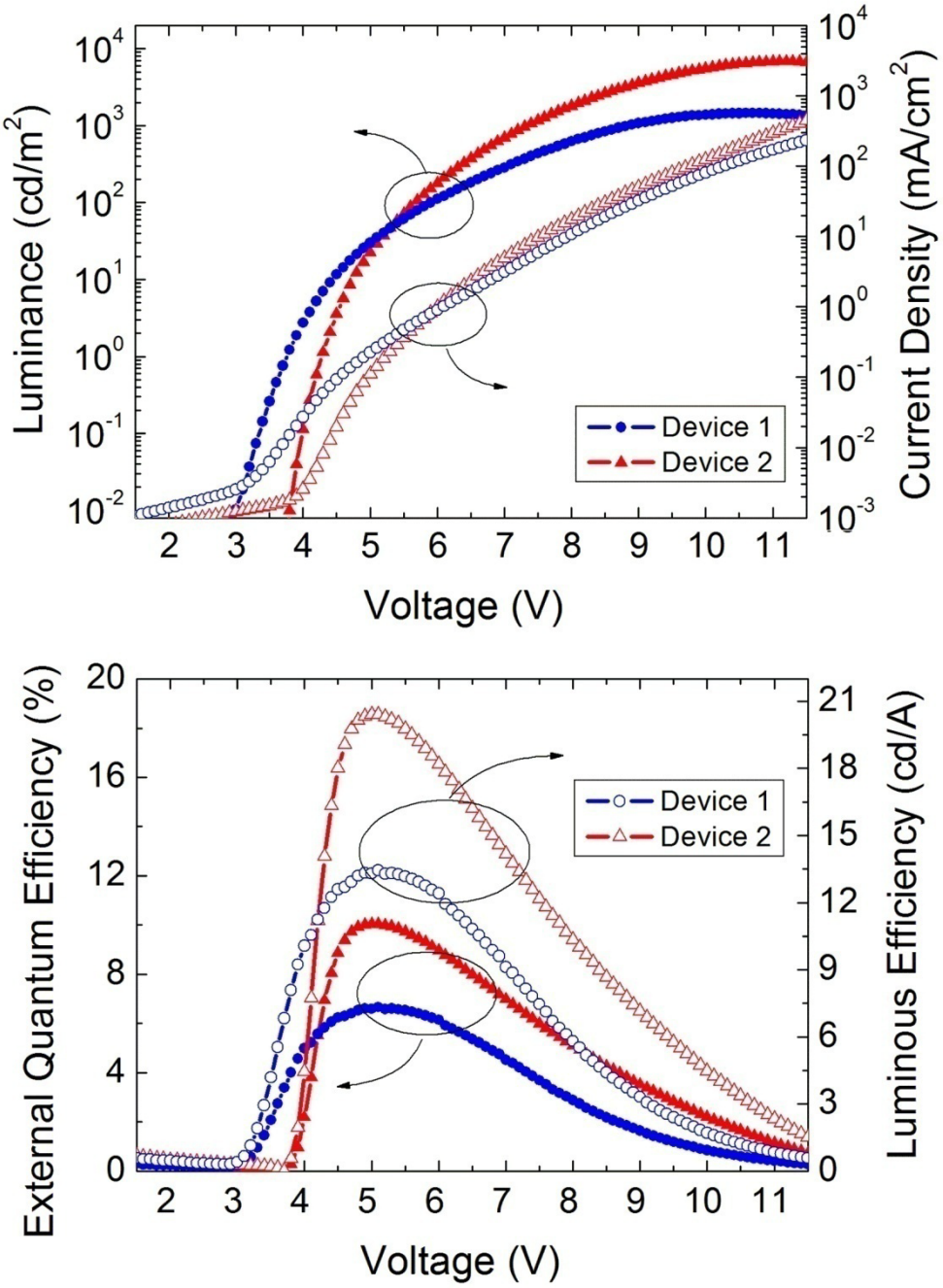

Figure 4: Top: Luminance-voltage (solid symbols) and current-voltage (open symbols) characteristics of devices 1 (blue circles) and device 2 (red triangles), Bottom: external quantum efficiency-voltage (solid symbols) and luminous efficiency-voltage plots (open symbols) of devices 1 (blue circles) and device 2 (red triangles)

Figure 3 considers the electroluminescence spectra of both devices at a current density of 10 mA/cm^2. Both spectra show a pure emission of FIrpic with a maximum at 473 nm and CIE coordinates of x = 0.17 and y = 0.32. Figure 4 (top) displays the current density-voltage-

luminance characteristics of the devices. The device with **TRZ 2** as hole and excition blocking material (device 1) exhibited a 0.8 V lower turn-on voltage. This voltage increase can be attributed to the application of DBFSi as blocking layer which exhibits a higher LUMO level than **TRZ 2** (see figure 3). This results in an additional injection barrier. On the other side the current density and the luminance curves were steeper in device 2. Maximum luminances of 6900 cd/m^2 and 1500 cd/m^2 were reached at 11 V for device 2 and device 1 respectively. The higher value of device 2 was attributed to the more effective exciton blocking of DBFSi. Figure 4 (bottom) shows the external quantum efficiency (EQE) and current efficiency plotted versus the voltage. Here the efficiency of the different blockers is even more pronounced. Device 2 exhibts a maximum EQE value of 10.2 % at 22 cd/m^2. The maximum luminous and power efficiencies are 20.4 cd/A and 13.2 lm/W respectively. At a luminesence of 100 cd/m^2 an EQE of 9.5 % and a luminous efficiency of 19.2 cd/A were reached. The efficiencies of device 1 were significantly lower. Maximum external quantum, luminous and power efficiencies of 6.7 %, 12.6 cd/A and 8.7 lm/W were reached at 5.1 V, 5.1 V and 4.4 V respectively. These much lower values highlight the importance of a suitbale hole/exciton blocking layer in this device setup. These results demonstrate the potential of donor-substituted triazines as host materials for blue phosphorescent OLEDs.

Conclusions.

In this paper we presented a series of new matrix materials based on the concept of donor-substituted triazines with three, two and one carbazole unit. The thermal properties, especially the glass formation, were controlled by different substitution patterns and amorphous host materials with transition temperatures up to 170 °C are obtained. This guarantees a long-term morphological stability. The triplet energies of the triazines were in the range from 2.86 eV to 2.96 eV. The potential of this class of materials as hosts for blue phosphors has been tested. A maximum brightness of 6900 cd/m^2 and a maximum external quantum efficiency of 10.2 % were reached using the blue emitter FIrpic. These first results show that the donor substituted of triazines hold great potential as host materials for blue OLEDs.

Acknowledgement.

We thank C. Bonsignore for his support during the preparation and characterization of the light emitting diodes. Our special thanks go to I. Bauer for supporting us during synthesis and characterization of the host materials. We also like to thank Dr. Ingo Münster, Dr. Evelyn Fuchs and Dr. Nicolle Langer for scientific discussions. We are grateful to the BMBF for financial support through the project OPAL 2008.

References

[1] Baldo, M. A.; O'Brien, D. F.; You, Y.; Shoustikov, A.; Sibley, S.; Thompson, M. E.; Forrest, S. R. *Nature (London)*, **1998**, 395, 151-154.

[2] Yersin, H., Ed. *Highly Efficient OLED's with Phosphorescent Materials*; Wiley-VCH: Weinheim, Germany, **2008**.

[3] Tanaka, I.; Tabata, Y.; Tokito, S.; *Chem. Phys. Lett.* **2004**, *400*, 86-89.

[4] D'Andrade, B. W.; Datta, S.; Forrest, S. R.; Djurovich, P.; Polikarpov, E., Thompson, M. E.; *Org. Elec.,* **2005**, 6, 11-20.

[5] Fink, R.; Frenz, C.; Thelakkat, M.; Schmidt, H.-W.; *Macromol.* **1997***, 30*, 8177-8181.

[6] Fink, R.; Heischkel, Y.; Thelakkat, M.; Schmidt, H.-W.; Jonda, C. Hueppauff, M.; *Chem. Mater.* **1998***, 10*, 3620-3625.

[7] Richard, A.; Klenklera, H. A.; Tranc, A.; Popovic, D. Z.; Xu, G.; *Org. Elect.* **2008***, 9*, 285-290.

[8] Su, S.-J.; Sasabe, H.; Takeda, T.; Kido, J.; *Chem. Mater.* **2008***, 20*, 1691–1693.

[9] Su, S.-J.; Chiba, T.; Takeda, T.; Kido, J.; *Adv. Mater.* **2008***, 20*, 5951-5953.

[10] Inomata, H.; Goushi, K.; Masuko, T.; Konno, T.; Imai, T.; Sasabe, H.; Brown, J. J.; Adachi, C.; *Chem. Mater.* **2004***, 16*, 1285-1291.

[11] Son, K.; Yahiro, M.; Imai, T.; Yoshizaki, H.; Adachi, C.; *Chem. Mater.* **2008**, *20*, 4439-4446.

[12] Selby, T. D.; Stickley, K. R.; Blackstock, S. C.; *Org. Lett.* **2000**, *2*, 171-174.

[13] Chu, T.; Ho, M.; Chen, J.; Chen, C.; *Chem. Phys. Lett.* **2005**, *415*, 137-140.

[14] Haneder, S.; Da Como, E.; Feldmann, J.; Rothmann, M. M.; Strohriegl, P.; Lennartz, C.; Molt, O.; Münster, I.; Schildknecht, C.; Wagenblast, G.; *Adv. Funct. Mater.* **2009**, *19*, 2416-2422.

[15] Strohriegl, P.; Grazulevicius, J. V.; *Adv. Mater.* **2002,** *14*, 1439-1452.

[16] Shirota, Y.; *J. Mater. Chem.* **2000**, *10*, 1-25.

[17] Schmechel, R.; Von Seggern,; H.; *Phys. Stat. Sol. (A)* **2004,** *201*, 1215-1235.

[18] Koene, B. E.; Loy, D. E. Thompson W. E.; *Chem. Mater.* **1998**, *10*, 2235-2250.

[19] Bolt, M.; Lennartz, C.; Prinz, M.; Schmidt, H.-W.; Thelakkat, M.; Baete, M.; Neuber, C.; Kowalsky, W.; Schildknecht, C.; Johannes, H.-H.; WO Patent **2005** 019373.

[20] Langer, N.; Kahle, K.; Lennartz, C.; Molt, O.; Fuchs, E.; Rudolph, J.; Schildknecht, C.; Watanabe, S.; Wagenblast, G.; WO Patent **2009**, 003898.

[21] Perdew, J. P.; *Phys. Rev. B* **1986**, *3319*, 8822.

[22] Becke, A. D.; *Phys. Rev. A* **1988**, *36*, 3098.

[23] Schäfer, A.; Horn, H.; Ahlrichs, R.; *J. Chem. Phys.* **1992,** *9*, 2571.

[24] Andrae, D.; Haeussermann, U.; Dolg, M.; Stoll, H.; Preuss, H.; *Theor. Chim. Acta* **1990**, *77*, 123.

[25] Schäfer, A.; Huber, C.; Ahlrichs, R.; *J. Chem. Phys.* **1994**, *100*, 5829.

[26] Klamt, A.; *J. Phys. Chem.* **1995**, *99*, 2224.

[27] Ahlrichs, R.; Bär, M.; Häser, M.; Horn, H.; Cölmel, C.; *Chem. Phys. Lett.* **1989**, *162*, 165.

[28] Schaefer, F. C.; Thurston, J. T.; Dudley, J. R.; *J. Am. Chem. Soc.* **1951**, *73*, 2990-2992.

7 Novel 1,3,5-Triazine-based Host Materials for Deep Blue Phosphorescent Emitters

Michael M. Rothmann,[a] Stephan Haneder,[b] Enrico Da Como,[b] Peter Strohriegl,[a]

[a] Makromolekulare Chemie I and Bayreuther Institut für Makromolekülforschung, University of Bayreuth, 95440 Bayreuth, (Germany),

[b] Photonics and Optoelectronics Group, Department of Physics and CeNS Ludwig-Maximilians-Universität, 80799, Munich (Germany)

to be submitted to *Chemistry of Materials*

Abstract.

A series of new donor-substituted 1,3,5-triazines (**ATRZ 1-6**) has been prepared by nucleophilic substitution of cyanuric chloride with diphenylamine, 3-methyldiphenylamine, 3-methoxydiphenylamine iminodibenzyl and 3,5-dimethylphenol. All triazine based hosts were characterized regarding their optical and thermal properties. Amorphous behaviour with glass transition temperatures (T_g) of up to 98°C were obtained for all derivatives. We found exceptionally high triplet energies ($\Delta E(T_1\text{-}S_0)$) ranging from 3.18 eV to 3.21 eV. Furthermore organic light-emitting diodes with **ATRZ 3** and **ATRZ 5** as host material and FIrpic as phosphorescent guest comprise maximum current efficiencies of 14.2 cd/A.

Keywords.

Triazine, electroluminescence, OLED, deep blue phosphorescence, molecular glasses.

Introduction.

For more than one decade the discovery of phosphorescent emitters by Forrest and Thompson stimulated the development of new materials for phosphorescent organic light emitting diodes.[1,2] To avoid self-quenching the emitter has to be diluted in a host material.[3] Therefore the efficiency of this type of OLEDs is often determined by the choice of an appropriate host material, which has to transfer the energy to the emitter. This assumes that the triplet energy of the host is higher compared to the emitting guest.[4] This task gets more challenging when host materials for blue phosphorescent emitters are in the focus of interest, where host triplet energies larger than 3.0 eV are required. Classical host materials based on carbazole are intrinsically limited to triplet energies of about 3 eV.[5] Meanwhile it has been shown that substituted N-phenylcarbazoles, for example 9-(4-tert-butylphenyl)-3,6-di-triphenylsilyl)-carbazole (CzSi, $E(T_1\text{-}S_0)$ = 3.02 eV)[6] or bis(4-(carbazol-9-yl)phenyl)-ether (CBPE, $E(T_1\text{-}S_0)$ = 3.02 eV)[7] reach triplet bandgaps close to their intrinsic limit. In order to provide host materials with even larger bandgaps the conjugation within the molecule has to be further decreased. Ideally only the conjugation length should not exceed one phenyl ring very much. Thus the number of possible building blocks becomes limited. In the past organo-silane compounds have been regarded as promising materials with ultra high bandgaps.[8] OLEDs using a p-bis(triphenylsilyl)benzene host and Iridium(III) bis(4',6'-difluorophenylpyridinato)tetrakis(1-pyrzolyl)borate (FIr6) as emitter with power efficiencies of 20 lm/W have been reported.[9] Nevertheless, one major disadvantage of UGH materials is their very low lying highest occupied molecular orbital (HOMO) far below 6 eV. Hole injection into such materials becomes difficult. Due to a lack of conjugated units the transport properties are also limited. This is often compensated by the use of high doping concentrations.

We recently reported unsymmetrically substituted triazines with electron rich carbazole units and their use as host materials in blue phosphorescent OLEDs. The triplet energies of these triazines reached values of up to 2.96 eV for 2,4-dicarbazolyl-6-phenoxy-1,3,5-triazine.[10]

A few years ago Inomata et al. presented a symmetric 2,4,6-triscarbazolyl-1,3,5-triazine with a triplet energy of 2.81 eV.[11] Furthermore 2,4,6-tris(diphenylamino)-1,3,5-triazine was synthesised but however no phosphorescence spectrum was measured due to the polycrystalline character of the material. Ab inito calculations of Chu et al. claimed that the triplet energy of 2,4,6-tris(diphenylamino)-1,3,5-triazine should be 0.25 eV higher than for the carbazole analogue.[12] Additionally the authors expect very good transport behaviour for 2,4,6-tris(diphenylamino)-1,3,5-triazine due to the low dipole moment of the molecule. Recently we have published investigations about the field induced phosphorescence quenching of a deep blue emitter embedded in two different host materials, where one host materials was 2,4-bisphenoxy-6-(3-methyldiphenylamino)-1,3,5-triazine (BPMT).[13] The material has good glass forming properties which enables spectroscopic investigations of neat films. A triplet energy of 3.24 eV was measured by low temperature time-gated phosphorescence spectroscopy. This proved that of diphenylamino-substituted triazines exhibit exceptionally high triplet bandgaps.

In this publication we describe the synthesis of a series of diphenylamine and iminodibenzyl substituted triazines. By the application of different substitution pattern we succeeded in the preparation of materials with good glass forming properties and glass transition temperatures up to 98 °C. Therefore it was possible to investigate the photophysical properties of neat films. Furthermore two OLEDs with diphenylamino-triazine host materials are presented.

Experimental.

Materials. All commercially available reagents were purchased from Aldrich and used without further purification.

2,4,6-Tris-(diphenylamino)-1,3,5-triazine (ATRZ 1). Diphenylamine (5.92 g, 35.0 mmol) was dissolved in 100 ml of dry THF under argon atmosphere in a two-necked round bottom flask equipped with a septum inlet and three-way stopcock. n-Butyllithium (21.8 ml 35.0 mmol, 1.6-M hexane solution) was added dropwise to the diphenylamine solution at room temperature and the mixture was stirred for 10 minutes. In a separate three-necked round bottom flask equipped with a septum inlet, three-way stopcock and condenser cyanuric chloride (1.84 g, 10.0 mmol) was dissolved in 100 ml dry THF under argon atmosphere. The lithium-diphenylamide solution was added dropwise to the cyanuric chloride solution within 15 minutes using a transfer canula. The reaction mixture was refluxed for 6 h. After cooling to room temperature water (200 ml) was added. The product was filtered, washed with water, hexane and diethyl ether and further purified by hot filtration from ethanol. Recrystallization from a chlorobenzene/hexane mixture yielded in 3.55 g (61%) of **ATRZ 1** as white crystalline solid. ^{1}H NMR (250 MHz, $CDCl_3$): δ (ppm) 7.16-7.09 (m, 24H), 7.06-7.02 (m, 6H). EI-MS: m/z = 582 (100, M^+), 309 (30, M^{2+}).

2,4,6-Tris-(3-methyldiphenylamino)-1,3,5-triazine (ATRZ 2). This compound was synthesized by the procedure described for **ATRZ 1** except that 3-methyldiphenylamine was used instead of diphenylamine. Yield: 3.81 g (64%) as white crystalline solid.^{1}H NMR (250 MHz, $CDCl_3$): δ (ppm) 7.15-7.08 (m, 9H), 7.05-6.82 (m, 18H), 2.17 (s, 9H). EI-MS: m/z = 624 (100, M^+), 312 (10, M^{2+}).

2,4,6-Tris-(3-methoxydiphenylamino)-1,3,5-triazine (ATRZ 3). This compound was synthesized by the procedure described for **ATRZ 1** except that 3-methoxydiphenylamine was used instead of diphenylamine. Yield: 3.43 g (51%) as white crystalline solid. ^{1}H NMR (250 MHz, $CDCl_3$): δ (ppm) 7.16-6.95 (m, 18H), 6.76-6.55 (m, 9H), 3.63 (s, 9H). EI-MS: m/z = 672 (100, M^+), 474 (20).

2,4,6-Tris-(iminodibenzyl)-1,3,5-triazine (ATRZ 4). This compound was synthesized by the procedure described for **ATRZ 1** except that iminodibenzyl was used instead of diphenylamine. Yield: 3.43 g (51%) as white crystalline solid.^{1}H NMR (250 MHz, $CDCl_3$): δ (ppm) EI-MS: m/z = 660 (100, M^+), 330 (25, M^{2+}).

2,4-Bis-(diphenylamino)-6-chloro-1,3,5-triazine. Diphenylamine (3.38 g, 20.0 mmol) was dissolved in 100 ml of dry THF under argon atmosphere in a two-necked round bottom flask equipped with a septum inlet and three-way stopcock. n-Butyllithium (12.5 ml, 1.6M hexane solution) was added dropwise to the diphenylamine solution at room temperature and the mixture was stirred for 10 minutes. In a separate three-necked round bottom flask equipped with a septum inlet, three-way stopcock and condenser cyanuric chloride (1.84 g, 10.0 mmol) was dissolved in 100 ml dry THF under argon atmosphere. The lithium-diphenylamide solution was added dropwise to the cyanuric chloride solution within 10 minutes using a transfer canula. The reaction mixture was refluxed for 6 hours. After cooling to room temperature water (200 ml) was added. The product was filtered, washed with water, hexane and diethyl ether and further purified by hot filtration from ethanol and liquid chromatography using a hexane/THF (3/1, V/V) as eluent, to yield 3.48 g (77%) of 2,4-Bis-(diphenylamino)-6-chloro-1,3,5-triazine as white crystalline solid. ^{1}H NMR (250 MHz, $CDCl_3$): δ (ppm) 7.33-7.22 (m, 8H), 7.21-7.05 (m, 12H). EI-MS: m/z = 448 (100, M^+), 414 (90).

2,4-Bis-(iminodibenzyl)-6-chloro-1,3,5-triazine. This compound was synthesized by the procedure described for 2,4-Bis-(diphenylamino)-6-chloro-1,3,5-triazine except that iminodibenzyl was used instead of diphenylamine. Yield: 3.43 g (51%) as white crystalline solid.^{1}H NMR (250 MHz, $CDCl_3$): δ (ppm) EI-MS: m/z = 618 (100, M^+), 309 (30, M^{2+}).

2,4-Bis-(diphenylamino)-6-(3,5-dimethylphenoxy-1,3,5-triazine (ATRZ 5). In a two necked round bottom flask 2,4-bis-(diphenylamino)-6-chloro-1,3,5-triazine (2.25 g, 5.0 mmol) was dissolved in 70 ml of acetone. In a separate flask 3,5-dimethylphenol (0.61 g 6.5 mmol) and sodium hydroxide (0.23 g, 5.7 mmol) were dissolved in 50 ml of a acetone-water mixture (1/1, V/V) at room temperature and stirred for 15 minutes until the solution was added drop wise to the 2,4-Bis-(diphenylamino)-6-chloro-1,3,5-triazine solution. The mixture is refluxed for 8 hours. After cooling to room temperature water (50 ml) was added. The

product was filtered, washed with water and diethyl ether and further purified by liquid chromatography using a hexane/ethyl acetate (7/1, V/V) as eluent, to yield 2.15 g (80%) of **ATRZ 5** as white crystalline solid. ^{1}H NMR (250 MHz, $CDCl_3$): δ (ppm) 7.24-7.07 (m, 20H), 6.69 (s, 1H), 6.67 (s, 2H), 2.21 (s, 6H). EI-MS: m/z = 534 (100, M^+), 367 (50), 167 (15).

2,4-Bis-(iminodibenzyl)-6-(3,5-dimethylphenoxy)-1,3,5-triazine (ATRZ 6). This compound was synthesized by the procedure described for **ATRZ 5**. 2,4-bis-(iminodibenzyl)-6-chloro-1,3,5-triazine was used instead of 2,4-bis-(diphenylamino)-6-chloro-1,3,5-triazine. Yield: 2.15 g (80%) as white crystalline solid. ^{1}H NMR (250 MHz, $CDCl_3$): δ (ppm) EI-MS: m/z = 587 (100, M^+), 393 (20).

Characterization. ^{1}H-NMR spectra were recorded on a Bruker AC-250 spectrometer at 250 MHz. All NMR-data are given as chemical shifts δ (ppm) downfield from $Si(CH_3)_4$. MS spectra were obtained on a Finnigan Mat 8500, MAT 112 S Varian machine using EI-ionisation. Melting points and glass transition temperature determination was carried out on a Perkin Elmer Diamond DSC at a heating/cooling rate of 10 K/min under nitrogen atmosphere. Thermographimetric analysis (TGA) was performed on a Mettler Toledo TGA/SDTA851e machine at a heating rate of 10 K/min in nitrogen atmosphere.

UV-Vis absorption spectra were recorded on a Hitachi U-3000 spectrometer. Photoluminescence spectra were obtained using a Shimadzu Spectrofluorophotometer RF-5301PC. UVASOL solvents purchased from Merck were used to prepare solutions and films for optical characterization. The phosphorescence spectra were obtained with a time gated PL setup described elsewhere.[13] In brief, thin film samples were mounted in a liquid helium cold finger cryostat and excited by laser pulses (500 ps) at 337 nm. The detection of phosphorescence was accomplished by a gated micro-channel-plate (MCP) with a time-gated detection window delayed with respect to the photo exciting pulse. For the experiments presented here, the detection started 500 ns after the pulse and for a time interval of 1 ms.

OLED fabrication. The organic layers were deposited by thermal evaporation in high vacuum ($3*10^{-6}$ mbar) onto indium-tin-oxide (ITO, 30 ohm/square) pre-coated glass

substrates (purchased from Merck) using different shadow masks to evaporate thickness gradients. The setup of the combinatorial vapor deposition chamber is described elsewhere.[14] Prior to use the ITO glass was degreased using organic solvents and cleaned using oxygen plasma for 10 minutes.

Results and discussion.

Synthesis. The structures and the synthetic route to all donor substituted triazines **ATRZ 1-6** are summarized in Scheme 1. The symmetrical triazines are obtained by a nucleophilic substitution of cyanuric chloride with diphenylamine (**ATRZ 1**), 3-methyl-diphenylamine (**ATRZ 2**), 3-methoxy-diphenylamine (**ATRZ 3**) or iminodibenzyl (**ATRZ 4**) in one step. For the unsymmetrically substituted triazines or a two-step synthesis is required. The first step involves a twofold nucleophilic substitution of cyanuric chloride. The degree of substitution was controlled by the ratio of carbazole and diphenylamine or iminodibenzyl. This is possible due to the stepwise deactivation of the chlorine atoms at the triazine core after each substitution with an electron donating diarylamino unit. The reaction of cyanuric chloride with two equivalents of diphenylamine leads to the disubstituted intermediate in 77 % yield. In the second step the remaining chlorine is substituted with 3,5-dimethylphenol to yield the triazines **ATRZ 5** and **ATRZ 6**.

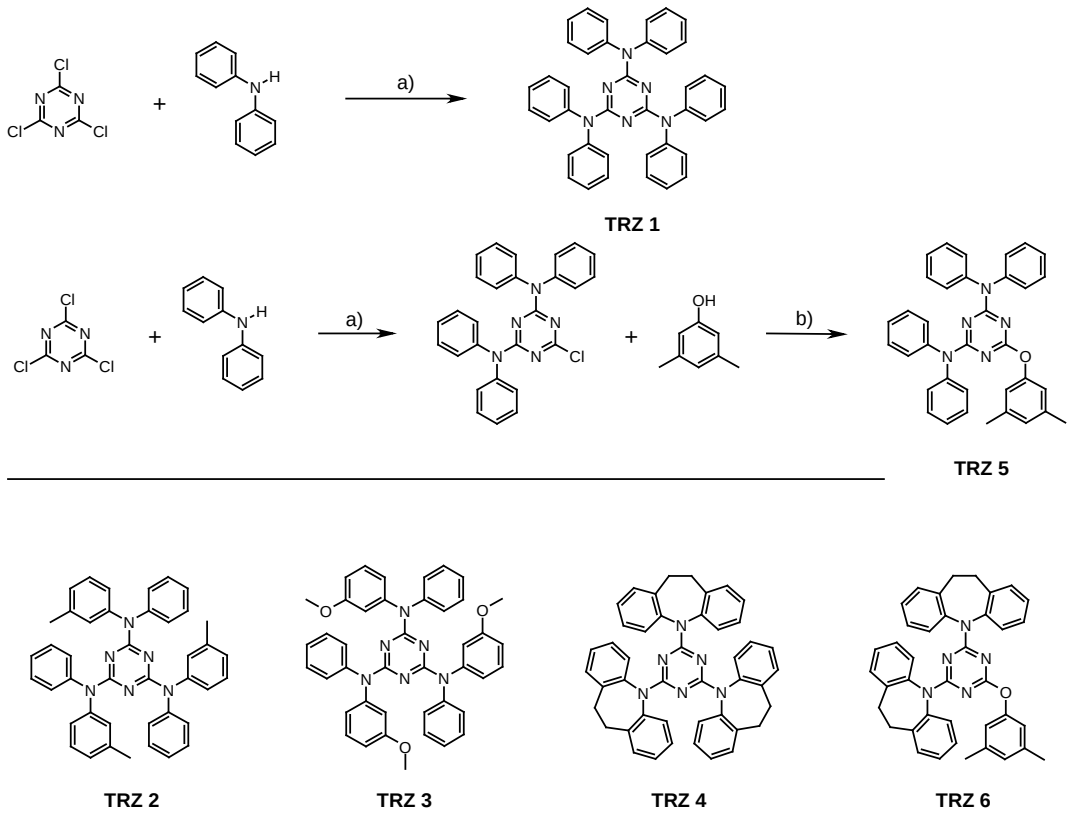

Figure 1: Synthetic route and structures of substituted triazines ATRZ 1-6; Conditions: a) n-BuLi, THF, 70°C, 6h; b) NaOH, acetone, water, 60°C, 8h.

Thermal properties. To investigate the thermal properties differential scanning calorimetry (DSC) and thermogravimetric analysis (TGA) were used. In both experiments the heating and cooling rate was 10 K/min The thermal properties of triazines **ATRZ 1-6** are summarized in table 1. In figure 2 the DSC curves of triazines **ATRZ 1**, **ATRZ 2** and **ATRZ 3** are shown. The first heating cycle of **ATRZ 1** shows a melting at 308 °C (60 kJ/mol). Upon cooling the very sharp exothermic peak at 268 °C (50 kJ/mol) indicates a very fast crystallization. However, during the second and further heating cycles **ATRZ 1** exhibits an additional exothermic peak at 208 °C (9 kJ/mol). This indicates that a small part of the sample remains amorphous during cooling, despite the fast crystallization. The melting and crystallization behavior remains the same in further cycles. The thermal behavior of **ATRZ 2** is similar to that of **ATRZ 1** with much lower transition temperatures. All heating cycles exhibit an endothermic peak at 175 °C (38 kJ/mol). Upon cooling a broad exothermic peak is observed with a maximum at 102 °C (24 kJ/mol) which point to a complex crystallization process of **ATRZ 2** The second and further heating cycles show an additional exothermic peak at 119 °C (4 kJ/mol).

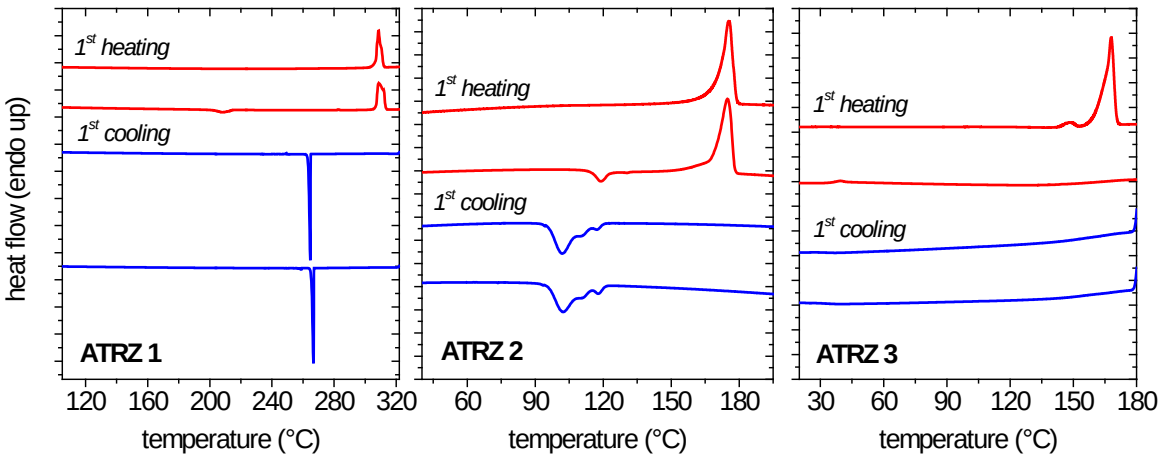

Figure 2: DSC traces of ATRZ1 (left), ARTZ2 (middle) and ATRZ (right). Shown are the first heating (top red line), second heating (second red line) as well as first cooling trace (first blue line) and second cooling scan (bottom blue line) at a scan speed of 10K/min.

On comparing the thermal behaviour of **ATRZ 1** and **ATRZ 2** it is clear that the tendency to crystallise is significantly lower for **ATRZ 2**. In contrast to **ATRZ1** and **ATZR2**, **ATRZ 3** shows

the typical behavior of an organic glass. Only during the first heating cycle a melting is observed at 168 °C (46 kJ/mol). Further heating and cooling cycles shows that the sample remains completely amorphous with a glass transition at 37 °C. This series of triazines demonstrates that the trend towards crystallization can be effectively be reduced by appropriate substitution. While **ATRZ 1** is a highly crystalline material the space filling *meta*-methoxy groups of **ATRZ 3** efficiently hinders intermolecular interaction and therefore **ATRZ 3** shows amorphous behavior. The thermal properties of the asymmetric **ATRZ 5** differ from the other triazines. The sample melts upon heating at 184 °C (35 kJ/mol)) and remains amorphous (T_g = 54°C) upon cooling. During the second heating cycle the sample crystallizes at 109°C (27 kJ/mol) followed by a endothermic melting peak at 184 °C. The relatively low glass transition temperatures of **ATRZ 3** and **ATRZ 5** are attributed to the flexibility of the diphenylamino groups. The symmetric triazine **ATRZ 4** has a similar thermal behavior as **ATRZ 1** with high melting (280 °C) and crystallization temperatures (180 °C). Its glass transition temperature can only be detected after very fast cooling of the melt using liquid nitrogen. Nevertheless, the T_g of 88 °C is significantly higher due to the more rigid substituent iminodibenzyl. **ATRZ 6** with 2 iminodibenzyl groups and one phenoxy group on the other hand exhibits the properties of an organic glass and a T_g of 98 °C, which is the highest glass transition temperature in this series of triazines. This behavior can be assigned to the rigidity of iminodibenzyl and the asymmetry of the molecule.

All triazines exhibit a high thermal stability. The onset of decomposition ranges from 303 °C to 312 °C. Additionally the triazines **ATRZ 1** and **ATRZ 4** sublimed during the TGA experiment starting at temperatures 10 °C below their melting temperature. A mass loss of 100 % is detected in those two cases.

Table 1: Thermal properties of triazines ATRZ 1-ATRZ 6

Host	T_g [°C]	T_m [°C]	T_c [°C]	T_d [°C]
ATRZ 1	-	308	268	291[d]
ATRZ 2	39 [a]	175	102	306
ATRZ 3	37	168 [b]	-	304
ATRZ 4	88 [a]	280	180	270 [d]
ATRZ 5	54	184	109 [c]	312
ATRZ 6	98	221[b]	-	303

[*] T_g: glass-transition temperatures, T_m: melting temperatures, T_c: crystallization temperaturesand T_D: decomposition temperatures (initial loss of mass (5%) was observed)

[a] Only detectable after very fast cooling of the melt (using liquid nitrogen) and subsequent measurement with 10 K/min under nitrogen atmosphere

.[b] Observed only in the first heating scan.[c] Observed upon heating.

[d] Onset of sublimation

It was possible to yield amorphous films by spin coating or thermal evaporation for all triazine host materials, except **ATRZ 1**. Neat films of **ATRZ 2** and **ATRZ 4** tend to crystallize within 24 hours. All other films stayed amorphous for several months. However, evaporated host-guest films (5-15% guest) of all triazines, except **ATRZ 1**, exhibited good morphological long-term stability. No crystallization could be observed for at least 3 months.

Optical properties. To investigate the optical properties of the donor substituted triazines absorption and emission spectra of spin-coated films were recorded. **ATRZ 1** was not included since it was not possible to prepare an amorphous film. Figure 3 depicts absorption, fluorescence and phosphorescence film spectra of the triazines **ATRZ 2**, **ATRZ 5** and **ATRZ 6**. The photo physical data of triazines **ATRZ 2-6** are summarized in table 2. The absorption spectrum of **ATRZ 2** exhibits two maxima. The intensity of the maximum at 279 nm is higher than the one at 264 nm. **ATRZ 5**, which is substituted with one phenoxy and two diphenylamino units, shows a similar optical behaviour with the difference, that the absorption peak at 278 nm has almost the same height as the peak at 264 nm. In

contrast to that the absorption spectrum of **ATRZ 6** comprises one peak at 263 nm. The optical bandgaps are estimated from the absorption edge. The bandgaps of **ATRZ 2** and **ATRZ 5** are almost identical at wavelengths of 314 nm (3.95 eV) and 310 nm (3.98 eV), while for **ATRZ 6** a significantly higher bandgap of 4.29 eV is determined.

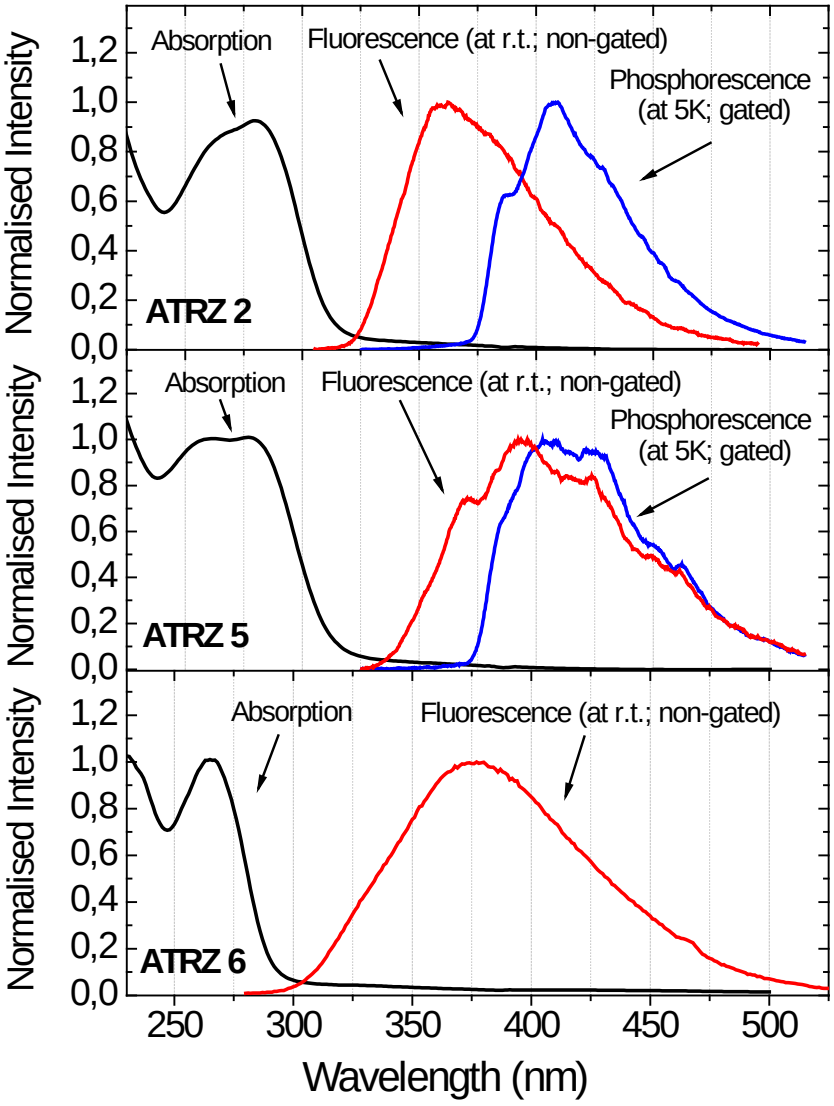

Figure 3: Photo physical properties of ATRZ1(top), ATRZ5 (middle) and ATRZ5 (bottom) in a neat film, including absorption (black line), fluorescence (red line) and phosphorescence (blue line). Absorption and fluorescence are measured at room temperature using standard spectroscopic methods, while phosphorescence is measured at 5K using time-gated spectroscopy.

The emission of non-gated spectra at room temperature can be assigned to fluorescence. The emission of all triazines, except **ATRZ 5,** is broad and unstructured. The maxima of the fluorescence signals range from 364 nm to 388 nm (see table 2). The triplet energy of the

diphenylamino-triazines was determined from time-gated phosphorescence spectra of neat films at T = 5K. In this experiment the detection of the phosphorescence spectrum is achieved by recording the PL several hundred ns after the laser pulse, i.e. after the prompt fluorescence has decayed and in the presence of the long-lived phosphorescence. The triplet energy was obtained from the first vibronic transition of the red shifted phosphorescence spectrum. **ATRZ 2** shows a 0-0 phosphorescence transition at 387 nm (3.20 eV) and a maximum at 408 nm, which can be attributed to the 0-1 transition. The behavior of **ATRZ 5** is similar but the 0-0 transition is less pronounced at slightly lower wavelength (3.21 eV). The maximum is centered at 402 nm and correspond to the 0-1 transition. The behavior of **ATRZ 3** is close to that of **ATRZ 2** with slightly lower triplet energy of 3.18 eV. For both iminodibenzyl-triazines the phosphorescence signal was too weak for an accurate determination of the triplet energy.

The HOMO levels of all triazines have been determined from neat film samples by ultra-violet photoelectron spectroscopy in air (Riken Keiki AC-2) and are summarized in table 2. For the tris-diphenylamino-triazines **ATRZ 2** and **ATRZ 3** very similar values of 5.88 eV and 5.87 eV were found. **ATRZ5**, in which one diphenylamine unites is substituted by a phenol exhibits a slightly lower HOMO value of 5.95 eV. This can be attributed to the stronger influence of the electron deficient triazine core on only two diphenylamino groups compared to three groups in **ATRZ 2** and **ATRZ 3**. The tris-iminodibenzyl-triazine **ATRZ 4** features a significantly higher HOMO at 5.67 eV. This is consistent with earlier observations by Koene et al., [15] where the HOMO was shifted about -0.2 eV when iminodibenzyl was used instead of diphenylamine as electron-donating unit in substituted 1,4-benzenes. The asymmetric triazine **ATRZ 6** exhibits a little lower HOMO compared to **ATRZ 4** due to the stronger influence of the triazine on the two iminodibenzyls.

The LUMO values were estimated by subtraction of the optical bandgap energy from the ionization potential. Since the diphenylamino-triazines exhibit almost identical bandgap energies the LUMOs range from 1.93 eV to 1.97 eV. The bandgaps of both iminodibenzyl derivatives are 0.3 eV larger than those of **ATRZ2-4**. In combination with their higher HOMO values the LUMO values for **ATRZ 4** and **ATRZ 6** are 1.40 eV and 1.42 eV

respectively. Regarding these high LUMO levels we expect that these two materials are efficient electron blockers. For this reason they were not tested in OLEDs as host materials.

Phosphorescent Organic Light-Emitting Diodes. The methoxy-substituted **ATRZ 3** was tested as host material in OLEDs and compared to the asymmetric material **ATRZ 5.** The OLEDs had the following configurations: On top of indium-tin-oxide (ITO) a 30 nm thick hole transporting layer consisting of N,N'-di(naphtha-1-yl)-N,N'-diphenyl-benzidine (α-NPD), followed by a 30 nm thick emission layer, which consisted of **ATRZ 3** (device 1) or **ATRZ 5** (device 2) doped with 12 % iridium(III) bis(4,6-di-fluorophenyl)-pyridinato-*N*,C^2)picolinat (FIrpic), and a 4-biphenyloxolato-aluminum-bis(2-methyl-8-hydroxychinolinato)-4-phenylphenolate (BAlq) electron-transport/hole-blocking layer (30 nm) were evaporated. The devices were finalized by deposition of LiF (0.7 nm)/ Al (150 nm) cathode. A schematic of the OLED setup is illustrated in the inset in figure 4a. The current density-voltage-luminance characteristics and the current efficiency-voltage characteristics of both devices are illustrated in Figure 4b and 4c. The electroluminescence spectra (Figure 4a) of both devices show a pure FIrpic emission with a maximum at 470 nm (CIE x. 0.17, y. 0.31). The device with **ATRZ 3** as host materials exhibits a somewhat lower threshold voltage (3.7 V) compared to the **ATRZ 5**-device (3.8 V). This is attributed to the lower HOMO level of **ATRZ 5**. Maximum luminance values of 1700 cd/m^2 (device 1) and 1900 cd/m^2 (device 2) are obtained at 13.0 V and 13.5 V respectively. The current efficiency of device 2 reaches a maximum of 14.2 cd/A at 8.5 V (180 cd/m^2), while a slightly lower maximum current efficiency of 12.2 cd/A (8 V) is obtained for device 1. These first device results demonstrate the potential of this class of donor-substituted triazines as host material for blue phosphorescent emitter.

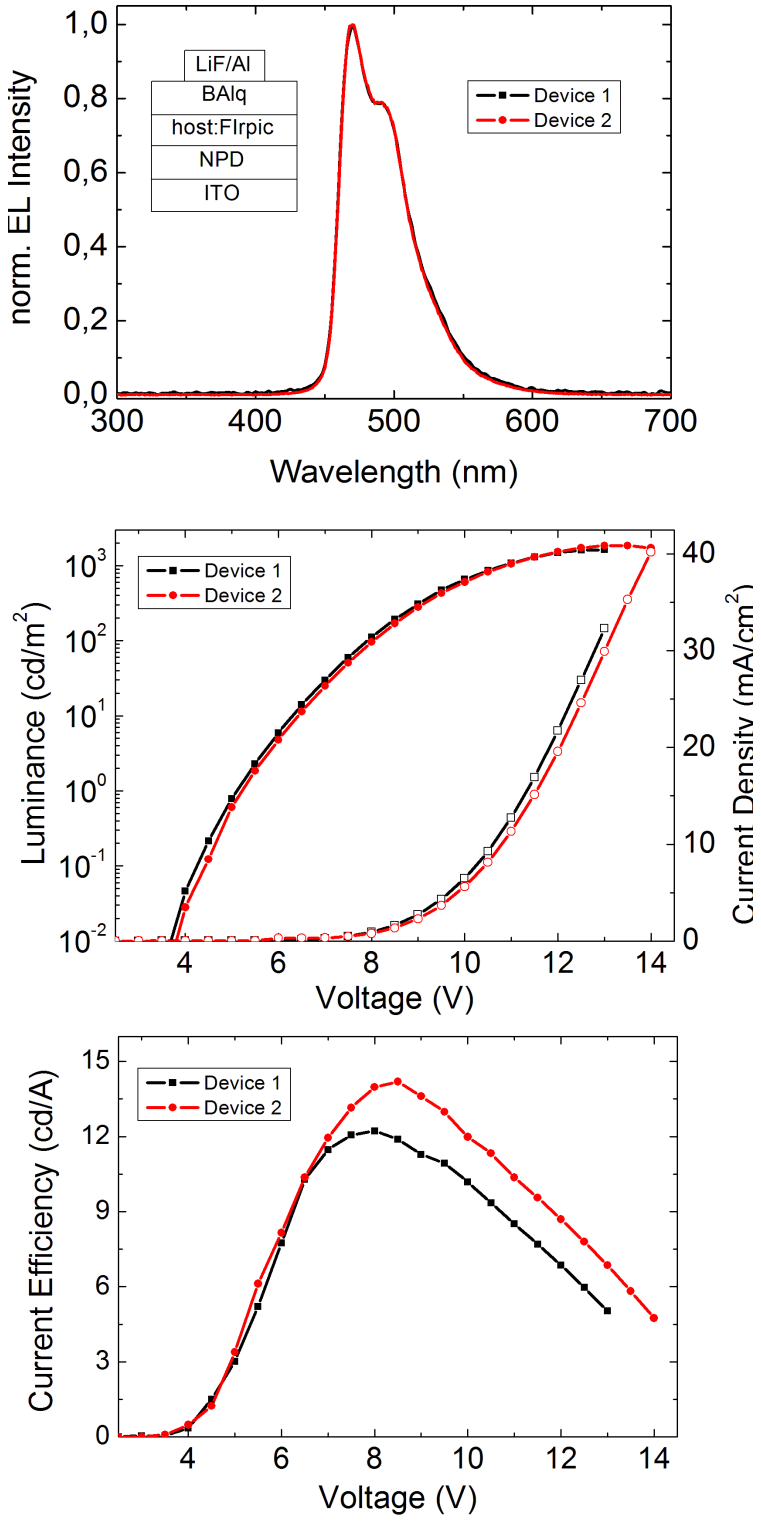

Figure 4: a) Electroluminescence spectra (inset: device setup of both devices), **b)** current density-voltage-luminance characteristics and **c)** the current efficiency-voltage characteristics of devices 1 (squares, ATRZ3 host material) and device 2(circles, ATRZ5 host material).

Conclusions

We have successfully tailored the glass forming properties of diarylamino-substituted triazines utilizing different substitution patterns. Therefore it was possible to investigate the neat film photo physical properties of diphenylamino-substituted triazines. We found exceptionally high triplet energies for all diphenylamino-triazine. The triplet bandgap values obtained by low-temperature phosphorescence spectroscopy are in the range from 3.18 eV to 3.21 eV. First studies of the OLED properties of two triazines as host materials in blue phosphorescent OLEDs were carried out and gained current efficiencies of up to 14.2 cd/A.

Acknowledgement

We thank I. Bauer for supporting us during synthesis and characterization of the host materials. We also like to thank Dr. Ingo Münster, Dr. Evelyn Fuchs and Dr. Nicolle Langer for fruitful discussions. We are grateful to the BMBF for financial support through the project OPAL 2008 (Grant No. 13N8992).

References

[1] Baldo, M. A.; O'Brien, D. F.; You, Y.; Shoustikov, A.; Sibley, S.; Thompson, M. E.; Forrest, S. R. *Nature (London)*, **1998**, 395, 151-154.

[2] Yersin, H., Ed. *Highly Efficient OLED's with Phosphorescent Materials*; Wiley-VCH: Weinheim, Germany, **2008**.

[3] C. Adachi, M. A. Baldo, M. E. Thompson, S. R. Forrest, J. Appl. Phys., 2001, 90, 5048-5051.

[4] Tanaka, I.; Tabata, Y.; Tokito, S. *Chem. Phys. Lett.* **2004**, *400*, 86-89.

[5] Adams, J. E.; Mantulin, W. W.; Huber, J. R.; *J. Am. Chem. Soc.* **1973**, *95*, 5477.

[6] Tsai, M.-H.; Lin, H.-W.; Su, H.-C.; Ke, T.-H.; Wu, C.-C.; Fang, F.-C.; Liao, Y.-L.; Wong, K.-T.; Wu, C.-I.; *Adv. Mater.* **2006**, *18*, 1216.

[7] Hongmei, J. H.; Dai, J.; Ou, X.; Wang, J.; Tao, S.; Zhang, X.; Wang, P.; Ma, D.; *J. Phys. Chem.* **2009**, *113*, 6761.

[8] Ren, X.; Li, J.; Holmes, R. J.; Djurovich, P. I.; Forrest, S. R.; Thompson, M.E.; *Chem. Mater.*, **2004**, *16*, 4743-4747.

[9] Eom, S.-H.; Zheng, Y.; Chopra, N.; Lee, J.; So, F.; Xue*, J.; Appl. Phys. Lett.*, **2008**, *93*, 133309.

[10] Rothmann, M. M.; Haneder, S.; Da Como, E.; Lennartz, C.; Schildknecht, C.; Strohriegl, P.; *submitted to Chem. Mater.* **2009**,.

[11] Inomata, H.; Goushi, K.; Masuko, T.; Konno, T.; Imai, T.; Sasabe, H.; Brown, J. J.; Adachi, C.; *Chem. Mater.* **2004**, *16*, 1285.

[12] Chu, T.-Y.; Ho, M.-H.; Chen, J.-F.; Chen, C.-H.; *Chem. Phys. Lett.* **2005**, *415,* 137.

[13] Haneder, S.; Da Como, E.; Feldmann, J.; Rothmann, M. M.; Strohriegl, P.; Lennartz, C.; Molt, O; Münster, I.; Schildknecht, C.; Wagenblast, G.; *Adv. Funct. Mater.* **2009**, *19*, 2416-2422.

[14] Thelakkat, M.; Schmitz, C.; Neuber, C.; Schmidt, H-W. *Macromol. Rapid Commun.* **2004**, *25*, 204-223.

[15] Koene, B. E. ; Loy, D. E.; Thompson, M. E.; *Chem. Mater.* **1998**, *10*, 2235-2250.

8 Designing a bipolar host material for blue phosphorescent OLEDs: Phenoxy-carbazole substituted triazine

Michael M. Rothmann,[a] Evelyn Fuchs,[b] Christian Schildknecht,[b] Nicolle Langer,[b] Christian Lennartz,[b] Ingo Münster,[b] and Peter Strohriegl[a]*

[a] Makromolekulare Chemie I and Bayreuther Institut für Makromolekülforschung, University of Bayreuth, 95440 Bayreuth, (Germany),

[b] BASF SE, 67056, Ludwigshafen (Germany)

* Corresponding author. Email: peter.strohriegl@uni-bayreuth.de

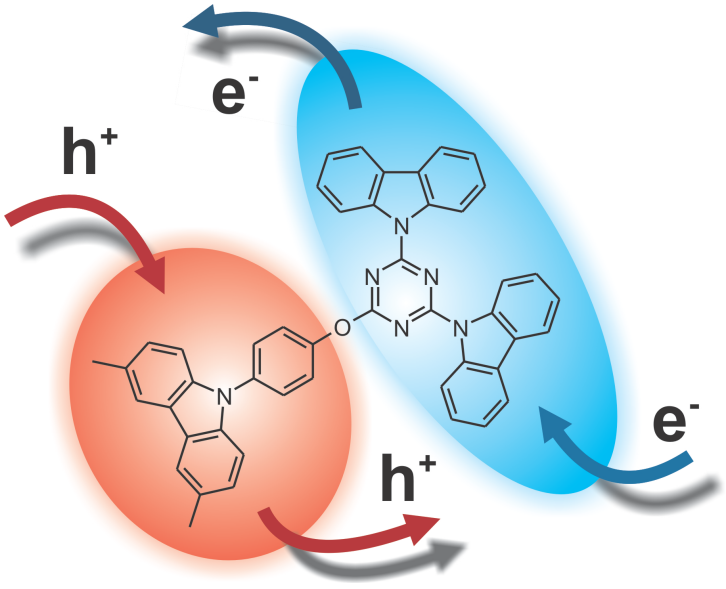

submitted to *Chemical Communications*

Abstract.

A novel phenoxy-carbazole substituted triazine host material (PCTrz) was synthesized. PCTrz exhibits a high triplet bandgap of 2.91 eV and a high glass transition temperature of 148 °C. A non-conjugated ether bond separates the oxidation- and reduction-site in the molecule. Good charge carrier transport properties in single carrier devices prove the potential as host for blue phosphorescent OLEDs.

Since the first multilayer organic light emitting diode (OLED) was published by Tang and van Slyke 20 years ago OLED materials and device setups have undergone many improvements.[1,2,3] Nowadays full color displays and OLED lighting applications are in the focus of research. One major step towards highly efficient OLEDs was the discovery of phosphorescent emitters which can harvest both singlet and triplet excitons and can reach the theoretical quantum efficiency limit of 100%.[4] To avoid concentration quenching the emitter has to be embedded in a suitable host. In order to confine all excitons to the emitter the triplet energy of the host has to be higher than that of the emitter. This is still a rather challenging task for material researchers, especially in the blue spectral region. Besides the large triplet bandgap materials have to fulfill further requirements like thermal, electrochemical and morphological stability to provide easy processing and long term stability. For efficient OLEDs well balanced charge carrier transport and a broad recombination zone are desirable. This task is most likely solved by the design of a bipolar material. However, when donor and acceptor moieties form one conjugated molecule the triplet energy will drop dramatically.[5] This is often prevented by *meta* linkage of the two moieties.[6] The use of electron accepting N-heterocycles like triazines as electron transporters in OLEDs is well described.[7,8] One approach to enhance the hole conduction of 1,3,5-triazines involves the introduction of donor substituents.[9] 2,4,6-Tricarbazolyl-1,3,5-triazine is an example for this class of materials, which exhibits bipolar transport properties.[10] However, its ionization potential (IP = 6.0 eV) might be too large for good hole injection and therefore results in high onset voltages and a recombination zone close to the interface of hole transport layer and emission layer (HTL/EML). Up to now, only few bipolar hosts with triplet energies larger than 2.8 eV, which are suitable for blue phosphorescent emitters, are known.[11]

Recently we reported a series of donor substituted triazine host materials with high triplet energies and good OLED performance.[12] However, the hole injection and transport properties of those triazines were limited and yielded a recombination zone close to the HTL/EML interface. Thus enhanced hole injection properties are desired and supposed to improve the charge carrier balance and the OLED performance.

In this work we present 2-(4-(3,6-dimethylcarbazol-9-yl)-phenoxy)-bis-4,6-biscarbazolyl-1,3,5-triazine PCTrz as a new bipolar host material for blue phosphorescent OLEDs. PCTrz comprises one hole conducting phenoxy-carbazole and one electron deficient biscarbazolyl-triazine moiety, which are connected by an ether bond, which breaks the conjugation between the two parts of the molecule. This was proved by cyclic voltammetry and density functional theory calculations. The separation of the oxidation- and reduction-site results in a “monodisperse molecular mixed host” which combines good transport properties for both types of charges. The triplet energy of PCTrz was measured at 10K embedded in a PMMA matrix. The high value of 2.91 eV proves the potential as host material for blue phosphorescent emitters. The material exhibits high thermal stability and good sublimation properties. The glass transition temperature of 148°C ensures morphological stability of the host-guest emission layer during the operation of the device. The synthesis of PCTrz is outlined in Scheme 1.

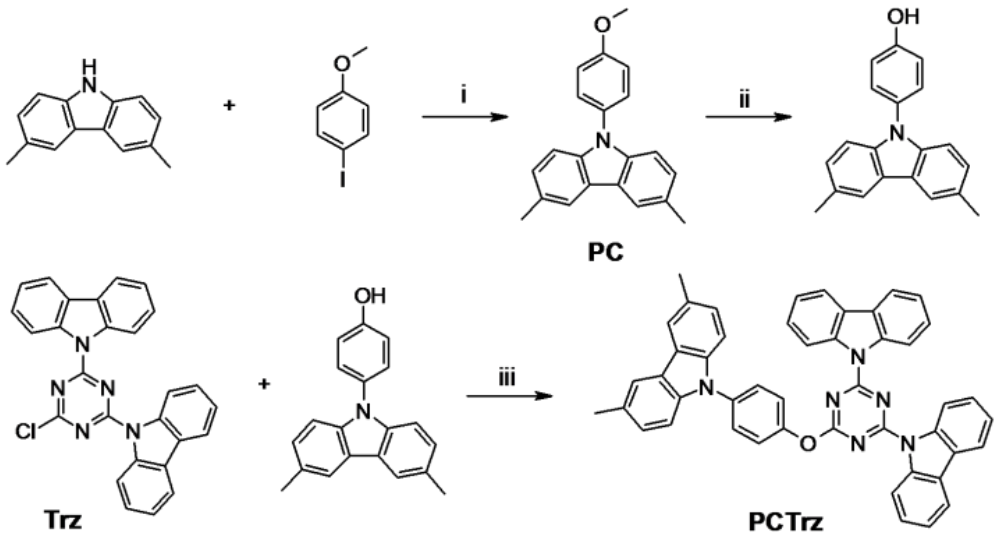

Scheme 1: Synthesis of 2-(4-(3,6-dimethylcarbazol-9-yl)-phenoxy)-bis-4,6-biscarbazolyl-1,3,5-triazine PCTrz: i) CuI, K_3PO_4, trans-1,2-diamino-cyclohexane, dioxane, 120°C, 18h, 68%; ii) BBr_3, CH_2Cl_2, -78°C, 12h, 92%; iii) NaOH, H_2O, dioxane, 100°C, 6h, 80%.

The donor part is prepared by *Goldberg* reaction of 3,6-dimethylcarbazole and 4-iodoanisole followed by methyl ether cleavage with boron tribromide to yield 9-(4-hydroxyphenyl)-3,6-dimethylcarbazole in 62% yield. The synthesis of 2-chloro-4,6-

biscarbazolyl-1,3,5-triazine (Trz) is described elsewhere.[12] Finally, PCTrz is prepared by a nucleophilic substitution at the triazine core in 80% yield.

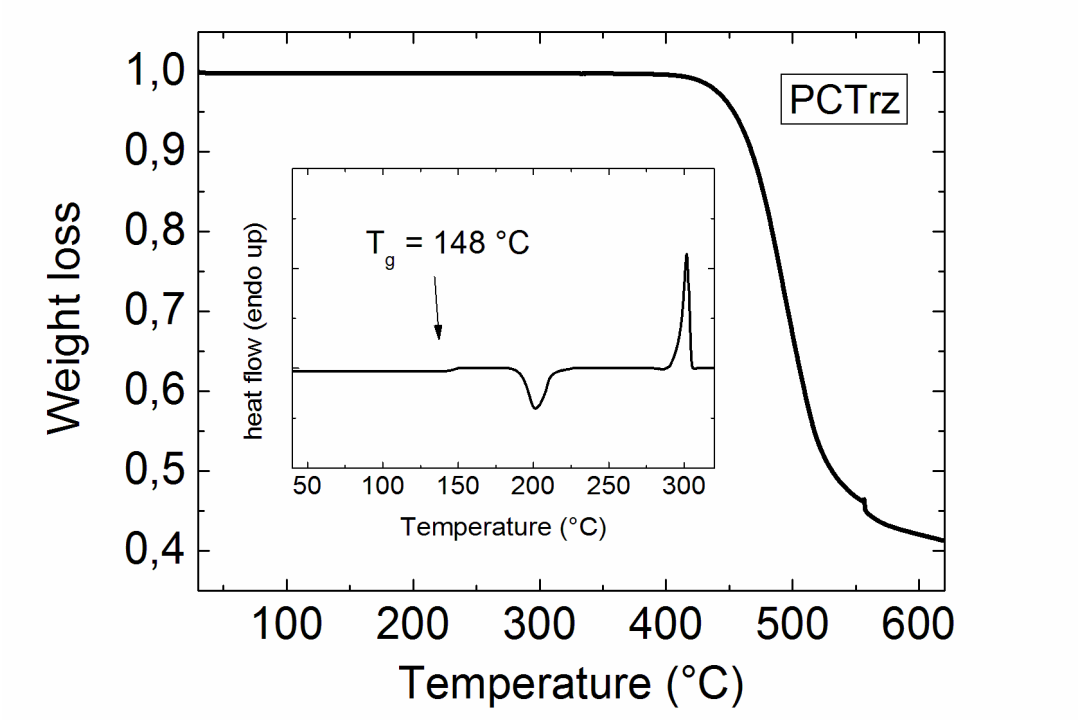

Figure 1: Thermal characterization of PCTrz: TGA curve (10K/min; N_2); inset: second DSC scan (10K/min; N_2; after; fast cooling of the melt at 40K/min)

The thermal properties of PCTrz were investigated using thermogravimetric analysis (TGA) and differential scanning calorimetry (DSC). The TGA curve in Figure 1 illustrates thermal stability up to at least 400 °C. A weight loss of 1 % (T_D^1) is observed at 425 °C while T_D^5 is reached at a temperature of 453 °C. This value is more than 150 °C above the sublimation temperature of PCTrz and therefore substantiates its very high thermal stability. The morphological stability of an amorphous film strongly depends on the glass transition temperature (T_g) of the material. The T_g should exceed the operational temperature by 50 °C to guarantee morphological stability.[13,14] Regarding the temperature requirements of potential technological applications for OLEDs[15] a T_g of more than 110 °C should be high enough to prevent the crystallization of an amorphous film during operation. In the inset in Figure 1 the second DSC heating scan of PCTrz is shown. The T_g is observed at 148 °C followed by an exothermic peak at 201 °C which is assigned to the crystallization of the material. The endothermic peak at 301 °C corresponds to the melting of the sample. These

thermal properties, especially the high T_g, fit very well into the profile of requirements for a host material.

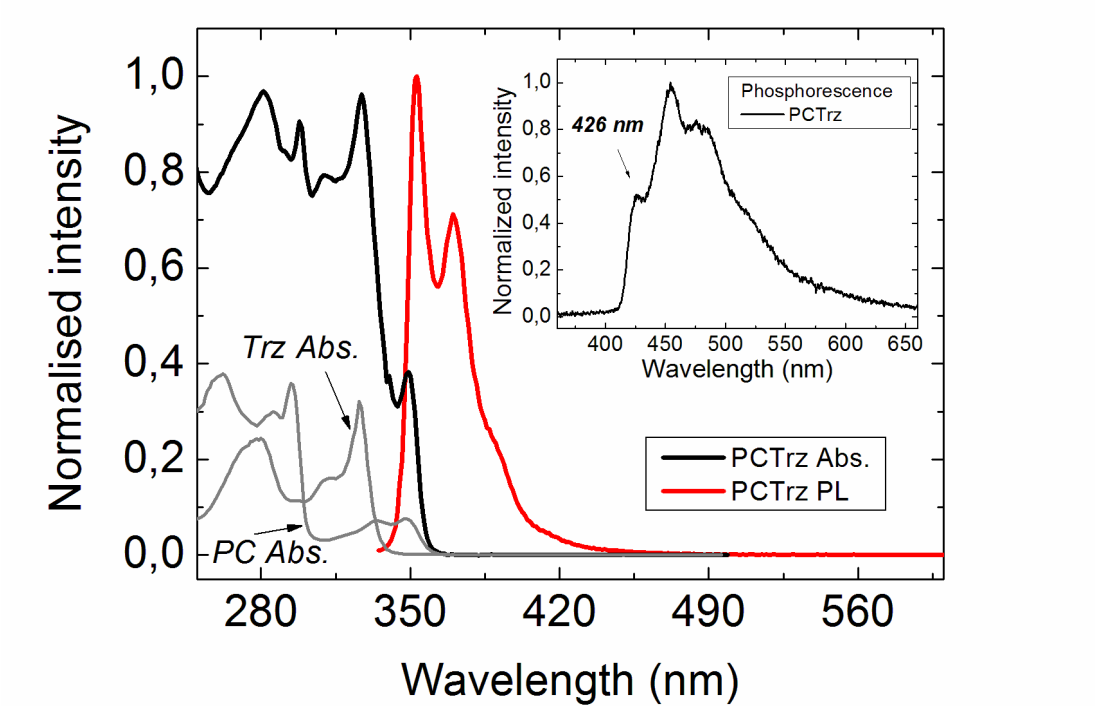

Figure 2: Absorption of PCTrz (black line), PC (grey line) and Trz (grey line) as well as fluorescence (red line) in cyclohexane solution at room temperature. **Inset**: phosphorescence of PCTrz at 10K.

The absorption and fluorescence spectra measured in cyclohexane solution are given in Figure 2. The absorption spectrum of PCTrz is an almost perfect addition of the absorption of its two parts 2-chloro-4,6-biscarbazolyl-1,3,5-triazine (Trz) and 9-(4-methoxyphenyl)-carbazole (PC) (grey line and grey dotted line in Figure 2). Therefore the lowest energetic maximum at 349 nm is attributed to the phenoxy-carbazole moiety. The next stronger maximum at 327 nm is attributed to the π-π^* transition of the carbazole moiety of the carbazolyl-triazine. The optical bandgap was estimated from the absorption edge of the lowest energetic maximum at 359 nm (3.45 eV). On excitation at 349 nm or lower wavelengths the fluorescence of PCTrz is detected. It consists of two maxima at 353 nm and 370 nm as well as a shoulder at 390 nm. This fluorescence behavior is equal to that of phenylcarbazole with a small hypsochromic shift due to the strong electron accepting character of the triazine which is located *para* to the carbazole. However, the influence of the triazine is only weak due to the non-conjugated ether bond.

In contrast to that the two carbazoles which are directly bound to the triazine are strongly influenced and possess a more electron deficient character. It can be supposed that the energy which is absorbed by the carbazolyltriazine part undergoes intramolecular transfer to the phenoxy-carbazole part. Therefore, only the fluorescence of this moiety is detected. To determine the triplet energy of PCTrz a phosphorescence spectrum (see inset in Figure 2) of a film (120 nm) consisting of 10 % PCTrz and 90 % PMMA was measured at a temperature of 10K. The triplet energy is obtained from the first vibronic transition of the phosphorescence spectrum. PCTrz shows a 0-0 phosphorescence transition at 426 nm (2.91 eV) and a maximum centered at 472 nm which correspond to the 0-1 transition. From this high triplet energy value it can be assumed that exothermic energy transfer to most blue phosphorescent emitters is possible.

In order to demonstrate the improved hole injection properties of PCTrz compared to other carbazole substituted triazines,[12] cyclic voltammetry (CV) and single carrier device (SCD) measurements were carried out. The electrochemical behavior upon oxidation and reduction was studied in CH_2Cl_2 and THF solution respectively (see Figure S1; ESI†). Both oxidation and reduction processes of PCTrz exhibit reversible behavior in multi-scan experiments. The oxidation is observed at a half-wave potential of 0.68 V (vs. Fc/Fc^+). This result is in contrast to the irreversible oxidation of donor-substituted triazines without phenoxy-carbazole moiety like TRZ2 (structure in inset in Figure 3). Furthermore, the oxidation of TRZ2 was observed at distinctly higher potential (1.16 V vs Fc/Fc^+). Therefore the oxidation wave of PCTrz at 0.68 V is attributed to the oxidation of the phenoxy-carbazole moiety. This is supported by the similar oxidation behavior of 9-(4-methoxyphenyl)-3,6-dimethylcarbazole (PC). The perfectly reversible oxidation behavior can be explained by the blocking of the reactive 3- and 6-position of the phenoxy-carbazole, since it is known that unprotected carbazoles undergo side-reactions upon oxidation.[16] The reduction of PCTrz is observed at a half wave potential of -2.61 V (vs. Fc/Fc^+). Due to the similarity to the reduction of TRZ2 it is attributed to the reduction of the triazine moiety. Furthermore these results are invigorated by computational calculations of the electron density distribution of the HOMO and LUMO (see Figure 3 bottom). It was found that the electron density is centered on the HOMO of the phenoxy-carbazole moiety, while the

LUMO is mainly confined on the triazine ring. These results substantiate the successful separation of electron accepting and donating counterparts. The oxidation and reduction potentials of PCTrz can be translated to a IP of 5.48 eV and a electron affinity (EA) of 2.20 eV, respectively. The decreased HOMO of PCTrz compared to TRZ2 should yield improved hole injection properties. The I-V-characteristics of the hole-only devices is presented in Figure 3 (left). Additionally the electron-only device characteristic is shown in Figure 3 (right).

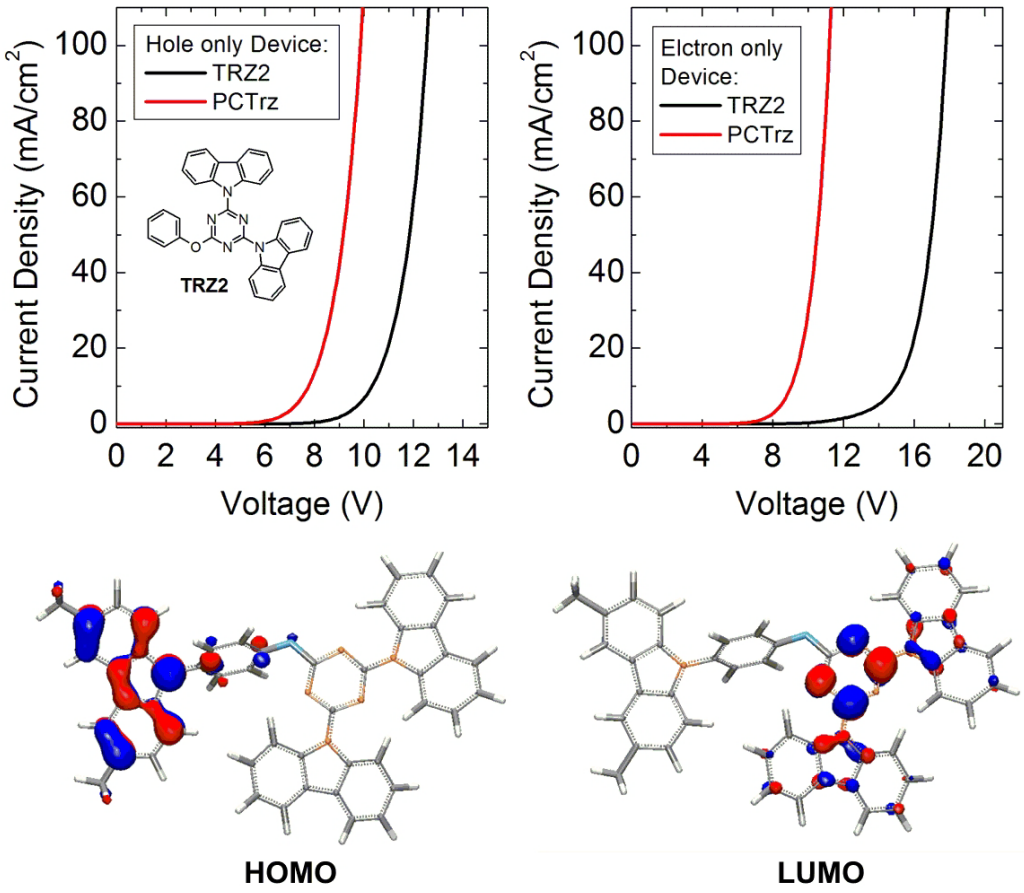

Figure 3: TOP: I-V-characteristics: (left) hole-only devices and (right) electron-only devices of TRZ2 compared to PCTrz; **BOTTOM**: calculated spatial distribution of HOMO and LUMO energy densities of PCTrz.

The charge transport properties of PCTrz were investigated with single carrier devices with the following configuration: hole-only-device: ITO /HIL (80 nm) /NPD:MoO_3 (p-doped, 35 nm) /NPD (10 nm) /PCTrz (30 nm) /NPD (10 nm) /NPD:MoO_3 (p-doped, 35 nm) /Al; electron-only-device: ITO /BCP:Cs_2CO_3 (n-doped, 70 nm) /BCP (10 nm) /PCTrz (30 nm) /BCP (10 nm) /BCP:Cs_2CO_3 (n-doped, 30 nm) /Al. For the electron-only devices the n-doped BCP

(HOMO = 6.5 eV) effectively prevents the injection of holes from the ITO anode (4.8 eV) and enhances the electron injection and transport. In a similar way the p-doped NPD prevented the injection of electrons from the cathode in case of the hole-only devices and enhances the hole injection and transport. In Figure 3 (top) the current density-voltage (I-V)-characteristics of hole- and electron-only-devices of PCTrz and TRZ2 are compared. From the hole-only-device characteristics it can be seen that the turn on voltage of the PCTrz device is about 2.5 V lower compared to that of TRZ2. Also at current-densities of 100 $mAcm^{-2}$ the difference in voltage is about 2.5 V. This behavior can be understood with respect to the smaller IP of PCTrz which facilitates the hole injection from the hole transporting NPD layer. From the I-V curves of the electron-only devices it can be seen that the device with PCTrz exhibits a much lower threshold voltage. At current densities of 100 $mAcm^{-2}$ the difference in voltage is as high as 7 V. This behavior cannot be explained by a restrained injection as the LUMO levels are very similar for both materials. Therefore we speculate that a different packing behavior (morphology) might favor electron transport in PCTrz. In total this new class of materials holds great potential for the use in blue phosphorescent OLEDs. Further tests in OLEDs are ongoing and will be published soon.

In summary we have designed a new bipolar host material, which contains a phenoxy-carbazole that is separated from the biscarbazolyl-triazine by a non-conjugated ether bond. PCTrz exhibits a very high thermal stability and its glass forming properties are excellent. The T_g of 148 °C is high enough to ensure morphological stability in OLED applications. Results from cyclic voltammetry and computational calculations proved the separation of the oxidation- and reduction-site. The charge carrier injection and transport properties were significantly improved compared to donor-substituted triazines like TRZ2.

We thank C. Bonsignore for his support during the preparation and characterization of the single carrier devices. We also like to thank S. Hoffmann for recording the phosphorescence spectrum. We are grateful to the BMBF for financial support through the project OPAL 2008 (Grant No. 13N8992).

References

[1] C. W. Tang and S. A. van Slyke, *Appl. Phys. Lett*, **1987**, *51*, 913.

[2] H. Yersin (Ed.), *Highly Efficient OLED's with Phosphorescent Materials*; Wiley-VCH: Weinheim, Germany, **2008**.

[3] S. Reineke, F. Lindner, G. Schwartz, N. Seidler, K. Walzer, B. Luessem and K. Leo, *Nature*, **2009**, *459*, 234.

[4] M. A. Baldo, D. F. O'Brian,Y. You, A. Shoustikov, S. Sibley, M. E. Thompson and S. Forrest, *Nature*, **1998**, *395*, 151.

[5] D. J. Cowley,I. Pasha, *J. Chem. Soc. Perkin Trans. II*, **1983**, 1139.

[6] S.-J. Su, H. Sasabe, T. Takeda,J. Kido*, Chem. Mater*, **2008**, *20*, 1691.

[7] R. Fink, Y. Heischkel, M. Thelakkat, H.-W. Schmidt, C. Jonda and M. Hüppauff, *Chem. Mater.*, **1998**, *10*,3620.

[8] R. Klenker, H. Aziz, A. Tran, Z. D. Popovic and G. Xu, *Org. Elect.*, **2008**, *9*, 285.

[9] H. Inomata, K. Goushi, T. Masuko, T. Konno, T. Imai, H. Sasabe, J. J. Brown and C. Adachi, *Chem. Mater.*, **2004**, *16*, 1285.

[10] K. S. Son, M. Yahiro, T. Imai, H. Yoshizaki and C. Adachi, *Chem. Mater.*, **2008**, *20*, 4439.

[11] S. O. Jeon, K. S. Yook, C. W. Joo and J. Y. Lee, Adv. Funct. Mater., 2009, available online (DOI: 1002/adfm.200901274)

[12] M. M. Rothmann, S. Haneder, E. Da Como, C. Schildknecht, C. Lennartz and P. Strohriegl, *Chem. Mater.*, submitted.

[13] G. Adam and J. H. Gibbs, *J. Chem. Phys.*, **1965**, *43*, 139.

[14] K. Naito and A. Miura, *J. Phys. Chem.*, **1993**, *97*, 6240.

[15] H. Aziz, Z. D. Popovic and N.-X. Hu, *Appl. Phys. Lett.*, **2002**, *81*, 370.

[16] J. F. Ambrose, L. L. Carpenter, R. F. Nelson, *J. Electrochem. Soc.*, **1975**, *122*, 876.

Supporting Information for:

Designing a bipolar host material for blue phosphorescent OLEDs: Phenoxy-carbazole substituted triazine

Michael M. Rothmann,[a] *Evelyn Fuchs,*[b] *Christian Schildknecht,*[b] *Nicolle Langer,*[b] *Christian Lennartz,*[b] *Ingo Münster,*[b] *and Peter Strohriegl**[a]

[a] Makromolekulare Chemie I and Bayreuther Institut für Makromolekülforschung, University of Bayreuth, 95440 Bayreuth, (Germany),

[b] BASF SE, 67056, Ludwigshafen (Germany)

* Corresponding author. Email: peter.strohriegl@uni-bayreuth.de

submitted to *Chemical Communications*

Electrochemical properties - Cyclic voltammetry (CV)

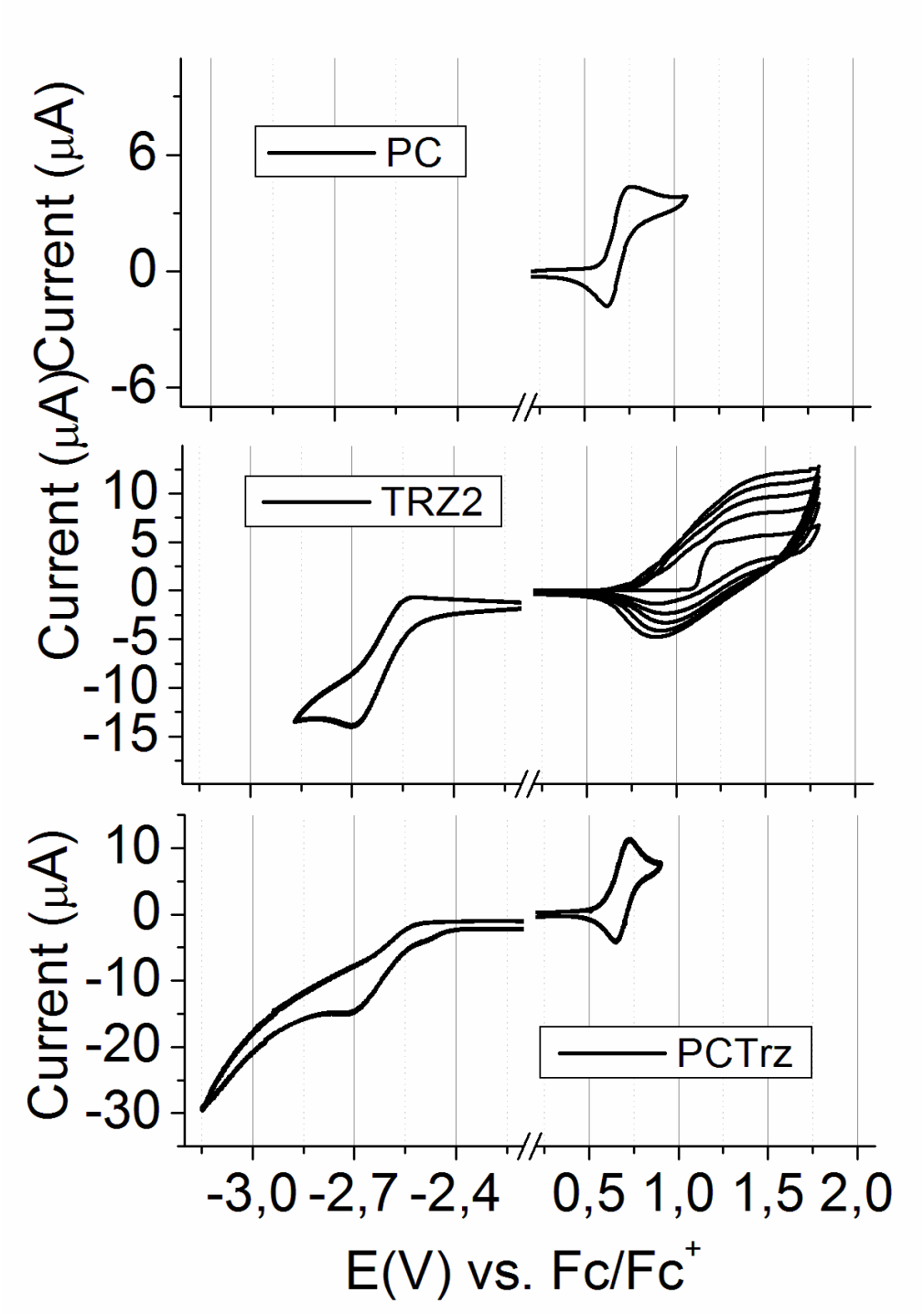

Figure S1: Reduction and oxidation potentials vs Fc/Fc^+ of PC, TRZ2 and PCTrz in THF (5 cycles; 50 mV/s) and DCM (5 cycles; 50 mV/s), respectively.

Table S1: Electrochemical potentials as well as HOMO and LUMO values of PC, TRZ2 and PCTrz**.**

	PC	TRZ2	PCTrz
E_{ox} (V) vs Fc/Fc^+	0.69	1.16	0.68
E_{red} (V) vs Fc/Fc^+	-	-2.61	-2.60
HOMO (eV)	5.49	5.96	5.48
LUMO (eV)	-	2.19	2.20

Synthesis and characterization of intermediates and final compound PCTrz.

Materials. All commercially available reagents were purchased from Aldrich and used without further purification. The synthesis of 2,4-biscarbazolyl-6-chloro-1,3,5-triazine is described elsewhere.[1]

Characterization. ^{1}H-NMR spectra were recorded on a Bruker AC-300 at 300 MHz. All NMR-data given are given as chemical shifts δ (ppm) downfield from $Si(CH_3)_4$. MS spectra were obtained on a Finnigan Mat 8500, MAT 112 S Varian machine using EI-ionization. Melting points and glass transition temperature determination was carried out on a Perkin Elmer Diamond DSC at a heating/cooling rate of 10 K/min under nitrogen atmosphere. Thermographimetric analysis (TGA) was performed on a Mettler Toledo TGA/SDTA851e machine at a heating rate of 10 K/min under nitrogen atmosphere. UV-Vis absorption spectra were recorded on a Hitachi U-3000 instrument. Photoluminescence spectra were obtained using a Shimadzu Spectrofluorophotometer RF-5301PC. UVASOL solvents purchased from Merck were used to prepare solutions and films for optical characterization. Cyclovoltammetry measurements were carried out in absolute solvents measuring at a platinum working electrode versus a $Ag/AgNO_3$ reference electrode. Each measurement was calibrated against an internal standard (ferrocene/ferrocenium redox system).

Single carrier device fabrication. The organic layers were deposited by thermal evaporation in high vacuum ($<10^{-6}$ mbar) onto indium-tin-oxide (ITO, 10 ohm/square) pre-coated glass substrates. Prior to use the ITO glass was degreased using organic solvents and cleaned

using an UV-ozon for 30 minutes. The organic layers and the metal cathode were evaporated without breaking the vacuum.

Computational Calculations. The transport levels of the materials used were determined via density functional calculations. For the ionization potential and the electron affinity first the geometry of the neutral as well as the charged states were optimized using the BP86-functional[2,3] in combination with a split-valence basis set (SV(P)) including polarization functions on all heavy atoms[4]. For iridium an effective core potential was employed.[5] For the energetics single point calculations at the optimized geometries using the same functional in combination with a valence triple zeta basis set (TZVP)[6] were conducted. To account for dielectric solid state effects a UPS/IEPS-calibrated version of the conductor like screening model (COSMO)[7] was used in conjunction with the single point calculations. All calculations were carried out with the turbomole program package.[8]

9-(4-Methoxyphenyl)-3,6-dimethylcarbazole (PC). 3,6-Dimethylcarbazole (3.90 g, 20 mmol), 4-iodanisole (5.15 g, 22 mmol), copper(I)-iodide (0.38 g, 2 mmol), potassium phosphate (4.24 g, 20 mmol) and (trans)-1,2-diaminocyclohexane (0.23 g, 2 mmol) were dissolved in 80 ml dry dioxane before the reaction mixture was refluxed for 14 hours in an argon atmosphere. After cooling to room temperature the mixture was filtered to remove all inorganic salts and the solvent was removed under reduced pressure. The crude product was purified with liquid chromatography using a hexane/THF (10/1; V/V) eluent to yield 9-(4-methoxyphenyl)-3,6-dimethylcarbazol (4.01 g, 13.6 mmol) as white solid. (Yield: 68 %). ^{1}H NMR (300 MHz, $CDCl_3$, δ): 7.90.(s, 2H), 7.44 (d, 2H), 7.21 (m, 4H), 7.10 (d, 2H), 3.91 (s, 3H), 2.54 (s, 6H); ^{13}C NMR (75 MHz, $CDCl_3$, δ): 158.6, 139.8, 130.8, 128.7, 128.3, 126.9, 123.1, 120.1, 114.9,.109.3, 55.6, 21.4; EI-MS (m/z (%)): 301 (100) [M^+], 286 (25);

9-(4-Hydroxyphenyl)-3,6-dimethylcarbazole. 9-(4-Methoxyphenyl)-3,6-dimethyl-carbazole (3.45 g, 11.5 mmol) was dissolved in dry dichloromethane (60 ml) under argon and cooled to -78°C before boron tribromide (8.80 ml of a 1M solution in dichloromethane, 12.6 mmol) was added dropwise. The mixture was allowed to warm to room temperature under

stirring. After the addition of water (20 ml) the organic phase was collected and the solvent was removed under reduced pressure. The crude product was purified with liquid chromatography using a hexane/THF (7/1; V/V) eluent to yield 9-(4-hydroxyphenyl)-3,6-dimethylcarbazol (3.03 g, 10.6 mmol) as white solid. (Yield: 92 %) ^{1}H NMR (300 MHz, $CDCl_3$, δ): 7.89 (s, 2H), 7.39-7.37 (d, 2H), 7.20 (m, 4H), 7.03-7.00 (d, 2H), 5.03 (s, 1H), 2.54 (s, 6H); ^{13}C NMR (75 MHz, $CDCl_3$, δ): 154.6, 139.8, 130.9, 128.8, 128.6, 127.0, 123.1, 120.1, 116.4, 109.3, 21.4;EI-MS (m/z (%)): 286 (100) [M^+];

2,4-Biscarbazolyl-6-(4-(3,6-dimethylcarbazol-9-yl)phenoxy)-1,3,5-triazine (PCTrz). 4-Hydroxyphenyl-3,6-dimethylcarbazole (0.77 g, 2.67 mmol) and sodium hydroxide (0.10 g, 2.5 mmol) were dissolved in a water/dioxane mixture (20 ml, 1/1 (V/V)) at room temperature and stirred for 10 minutes until the solution was added to a solution of 2,4-biscarbazolyl-6-chloro-1,3,5-triazine (0.99 g, 2.23 mmol) in dioxane (40 ml). The mixture is stirred for 8 hours at 70°C. After cooling to room temperature and addition of water (20 ml) the solid is filtered and washed with water and ethanol. The crude product is further purified by recrystallisation from a hexane/ THF mixture and sublimation to yield 2,4-Biscarbazolyl-6-(4-(3,6-dimethylcarbazol-9-yl)phenoxy)-1,3,5-triazine (PCTrz) (1.24 g, 80 %) as white crystalline solid. ^{1}H NMR (300 MHz, $CDCl_3$-F_3CCOOD, δ): 8.73-8.70 (m, 4H), 8.08-8.05 (m, 4H), 7.96 (s, 2H), 7.78 (d, 2H), 7.64 (d, 2H), 7.44-7.40 (m, 10H), 7.28-7.25 (m, 2H), 2.59 (s, 6H); ^{13}C NMR (75 MHz, $CDCl_3$-F_3CCOOD, δ): 171.5, 164.9, 150.4, 139.2, 138.5, 136.6, 129.6, 128.2, 127.3, 127.2, 126.8, 124.0, 123.7, 123.6, 120.3, 119.8, 117.4, 109.4, 21.3; EI-MS (m/z (%)): 696 (100) [M^+], 530 (30) [$M^+ - C_{12}H_8N$], 348 (30) [M^{2+}], 166 (30) [$C_{12}H_8N$ (carbazole)]; T_m: 301 °C; T_g: 148 °C; $T_d{}^1$: 425 °C;

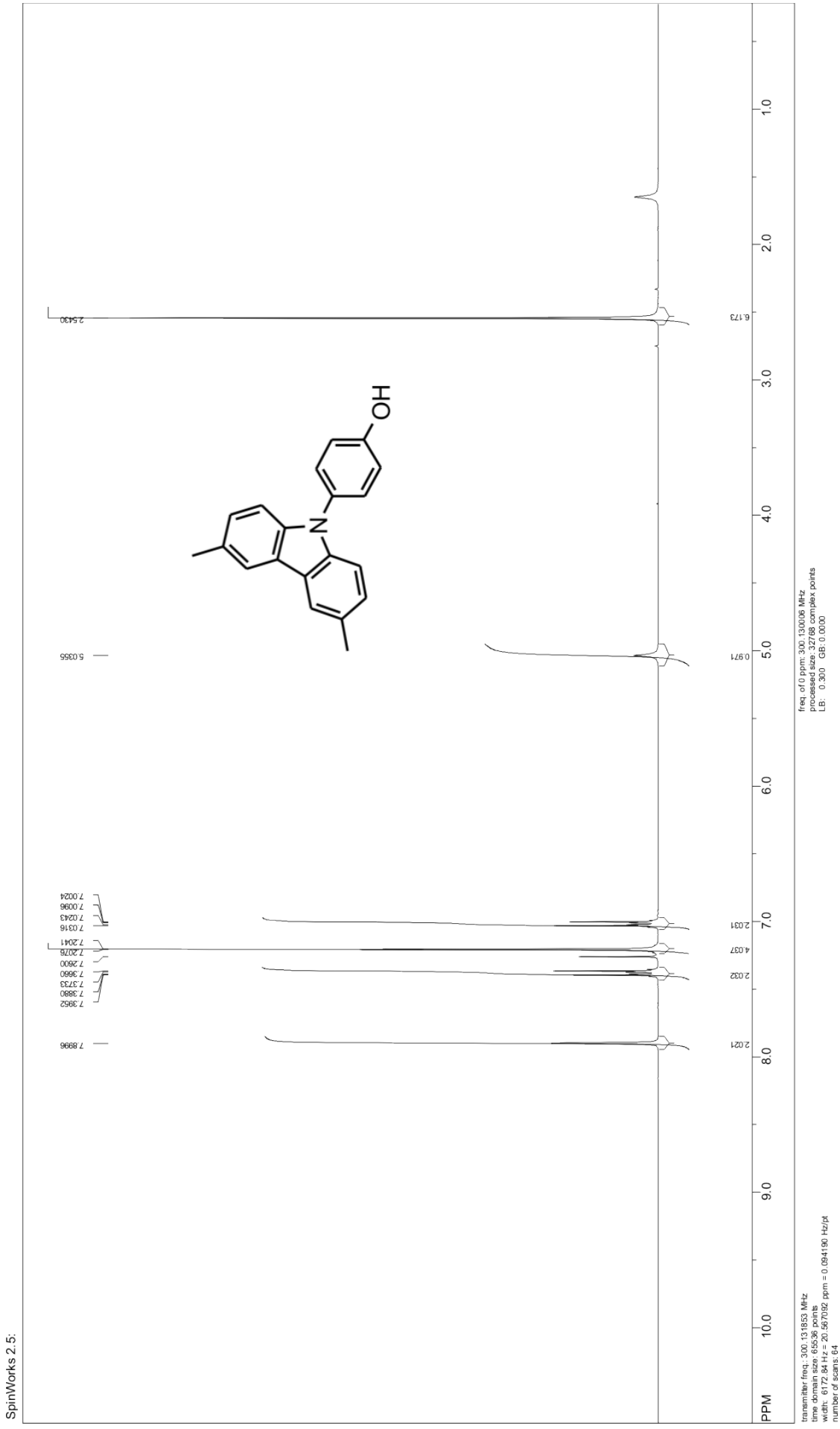
SpinWorks 2.5:
OH
N
2.5430
5.0355
7.8996
7.3962
7.3880
7.3733
7.3660
7.2600
7.2078
7.2041
7.0316
7.0243
7.0096
7.0024
6.173
0.971
2.031
4.037
2.032
2.021
PPM
1.0
2.0
3.0
4.0
5.0
6.0
7.0
8.0
9.0
10.0
transmitter freq.: 300.131853 MHz
time domain size: 65536 points
width: 6172.84 Hz = 20.567092 ppm = 0.094190 Hz/pt
number of scans: 64
freq. of 0 ppm: 300.1300106 MHz
processed size: 32768 complex points
LB: 0.300 GB: 0.0000

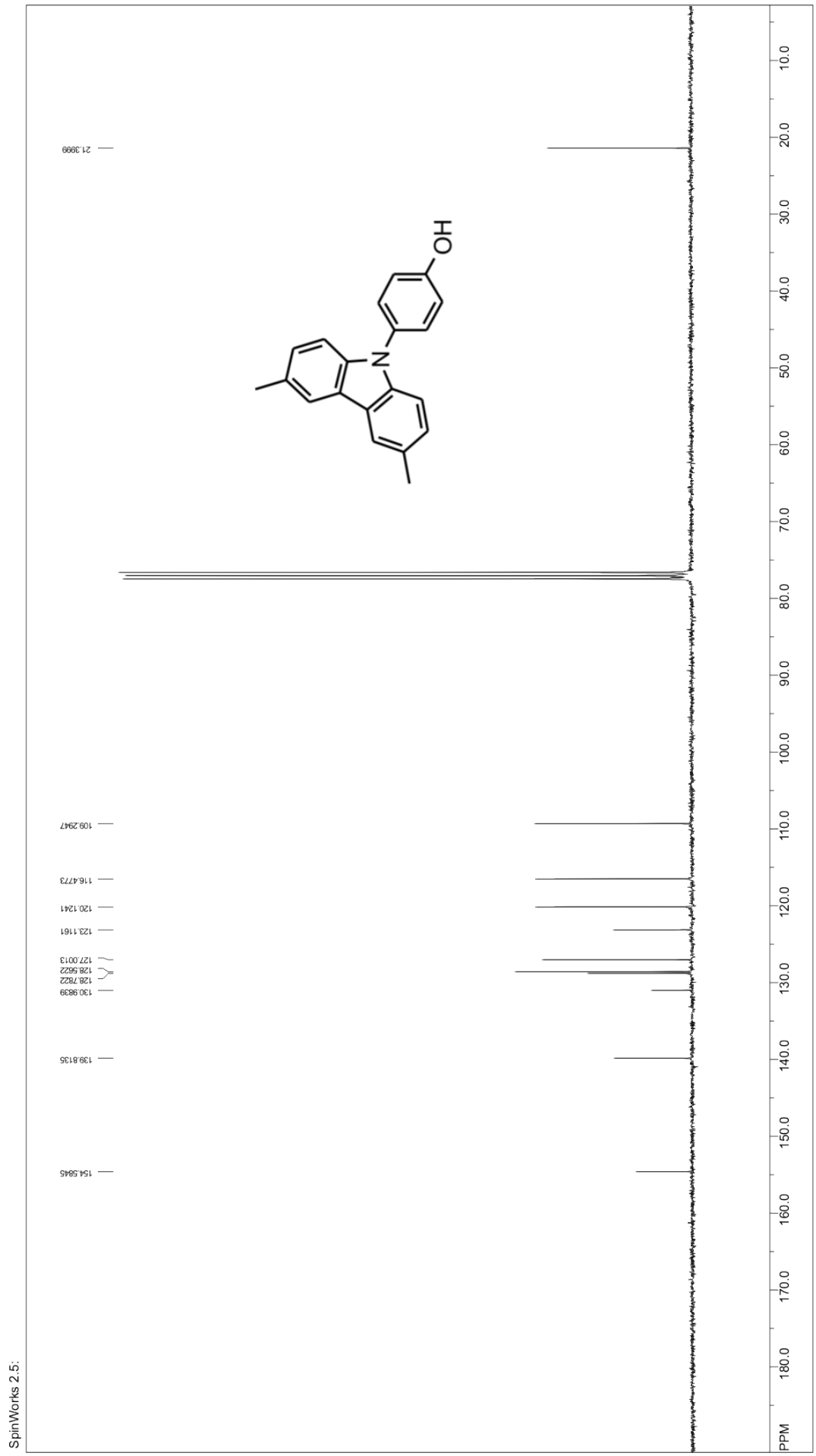
SpinWorks 2.5:
21.3899
109.2947
116.4773
120.1241
123.1161
127.0013
128.5622
128.7822
130.9839
139.8135
154.5845
OH
N
PPM
180.0
170.0
160.0
150.0
140.0
130.0
120.0
110.0
100.0
90.0
80.0
70.0
60.0
50.0
40.0
30.0
20.0
10.0
transmitter freq.: 75.475295 MHz
time domain size: 65536 points
width: 17985.61 Hz = 238.297995 ppm = 0.2744439 Hz/pt
number of scans: 2048
freq. of 0 ppm: 75.467749 MHz
processed size: 32768 complex points
LB: 1.000 GB: 0.0000

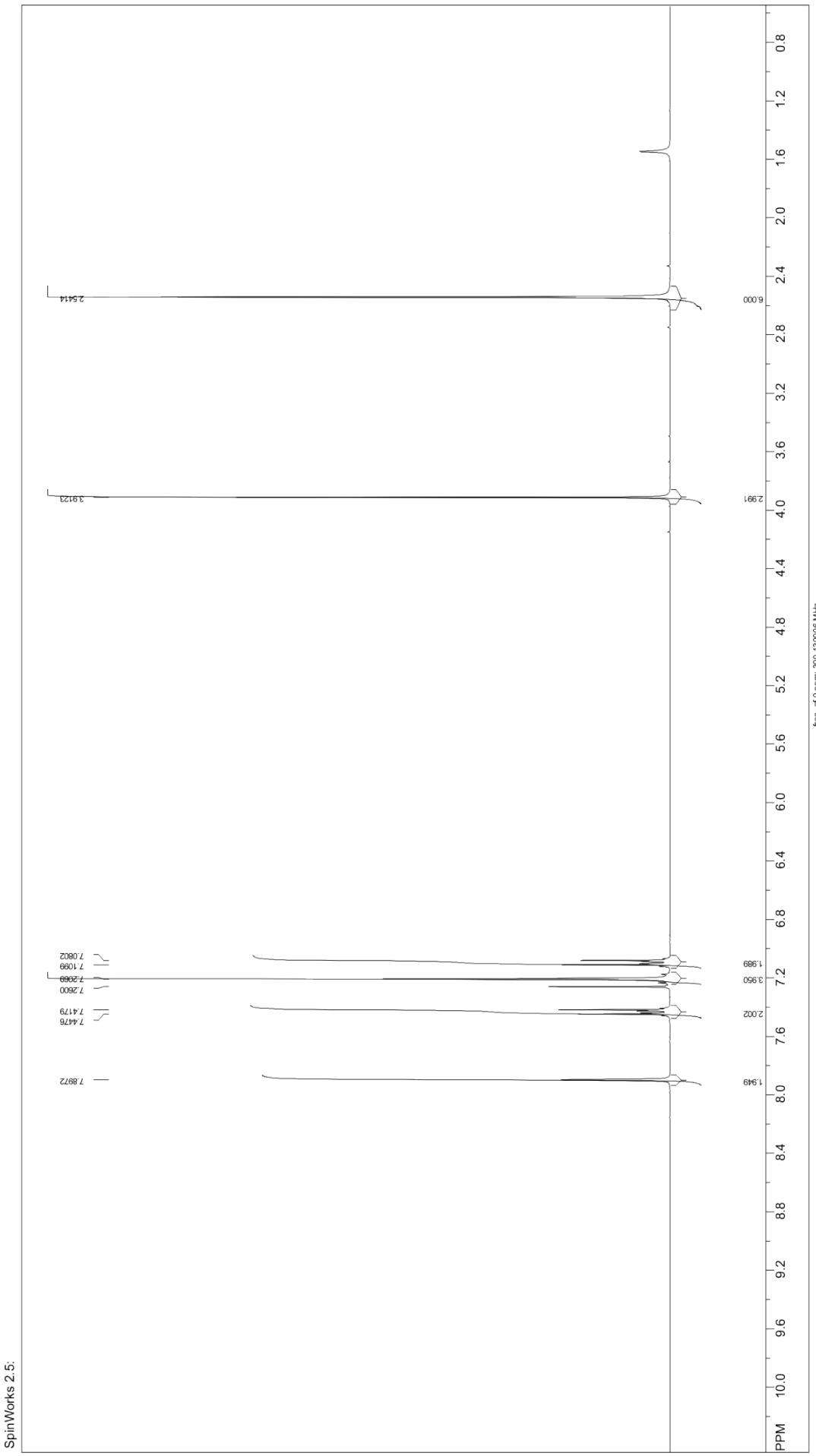
SpinWorks 2.5:
PPM
10.0
9.6
9.2
8.8
8.4
8.0
7.6
7.2
6.8
6.4
6.0
5.6
5.2
4.8
4.4
4.0
3.6
3.2
2.8
2.4
2.0
1.6
1.2
0.8
2.5414
3.9123
7.0802
7.1099
7.2069
7.2600
7.4179
7.4476
7.8972
6.000
2.991
1.989
3.950
2.002
1.949
freq. of 0 ppm: 300.130006 MHz
processed size: 32768 complex points
LB: 0.300 GB: 0.0000
transmitter freq.: 300.131863 MHz
time domain size: 65536 points
width: 6172.84 Hz = 20.567092 ppm = 0.094190 Hz/pt
number of scans: 64

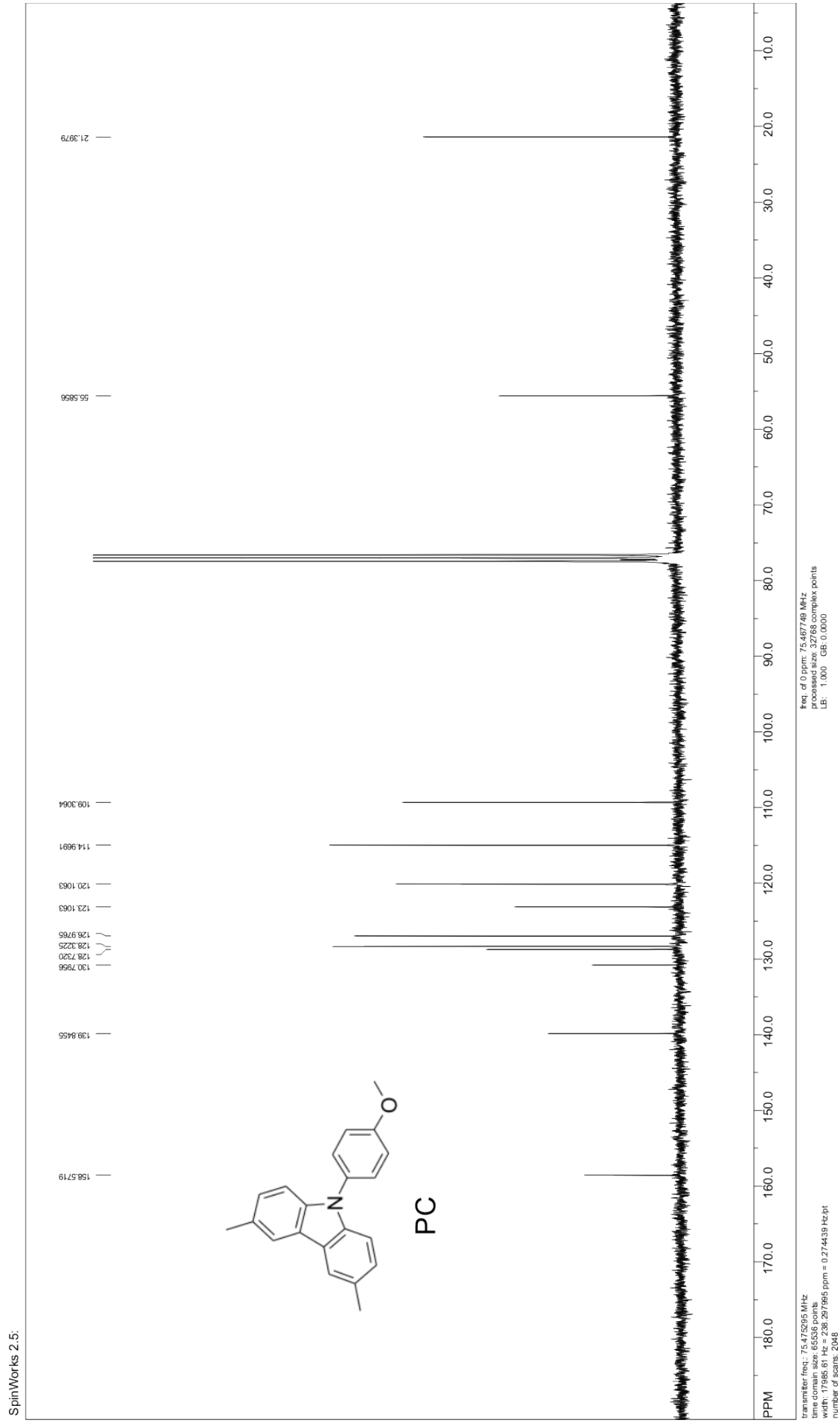
SpinWorks 2.5:
21.3979
55.5856
109.3064
114.9691
120.1063
123.1063
126.9765
128.3225
128.7320
130.7956
138.8455
158.5719
PC
PPM
10.0
20.0
30.0
40.0
50.0
60.0
70.0
80.0
90.0
100.0
110.0
120.0
130.0
140.0
150.0
160.0
170.0
180.0
transmitter freq.: 75.475295 MHz
time domain size: 65536 points
width: 17985.61 Hz = 238.297995 ppm = 0.274439 Hz/pt
number of scans: 2048
freq. of 0 ppm: 75.467749 MHz
processed size: 32768 complex points
LB: 1.000 GB: 0.0000

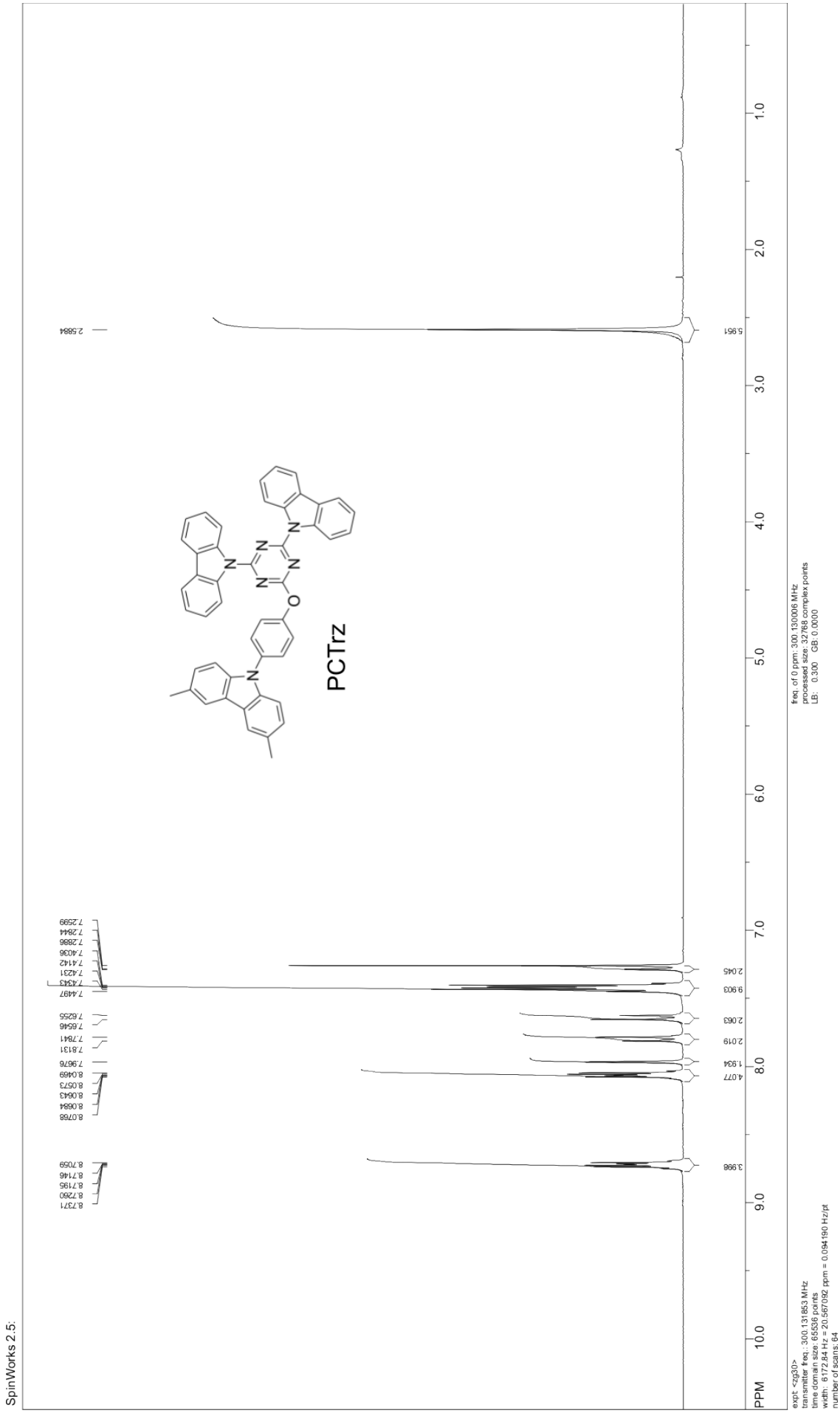
SpinWorks 2.5:
PCTrz
PPM
10.0
9.0
8.0
7.0
6.0
5.0
4.0
3.0
2.0
1.0
8.7371
8.7260
8.7195
8.7146
8.7059
8.0768
8.0694
8.0643
8.0573
8.0469
7.9676
7.8131
7.7841
7.6546
7.6255
7.4497
7.4343
7.4231
7.4142
7.4036
7.2886
7.2844
7.2599
2.5884
3.998
4.077
1.934
2.019
2.063
9.903
2.045
5.961
expt: <zg30>
transmitter freq.: 300.131863 MHz
time domain size: 65536 points
width: 6172.84 Hz = 20.567092 ppm = 0.094190 Hz/pt
number of scans: 64
freq. of 0 ppm: 300.130006 MHz
processed size: 32768 complex points
LB: 0.300 GB: 0.0000

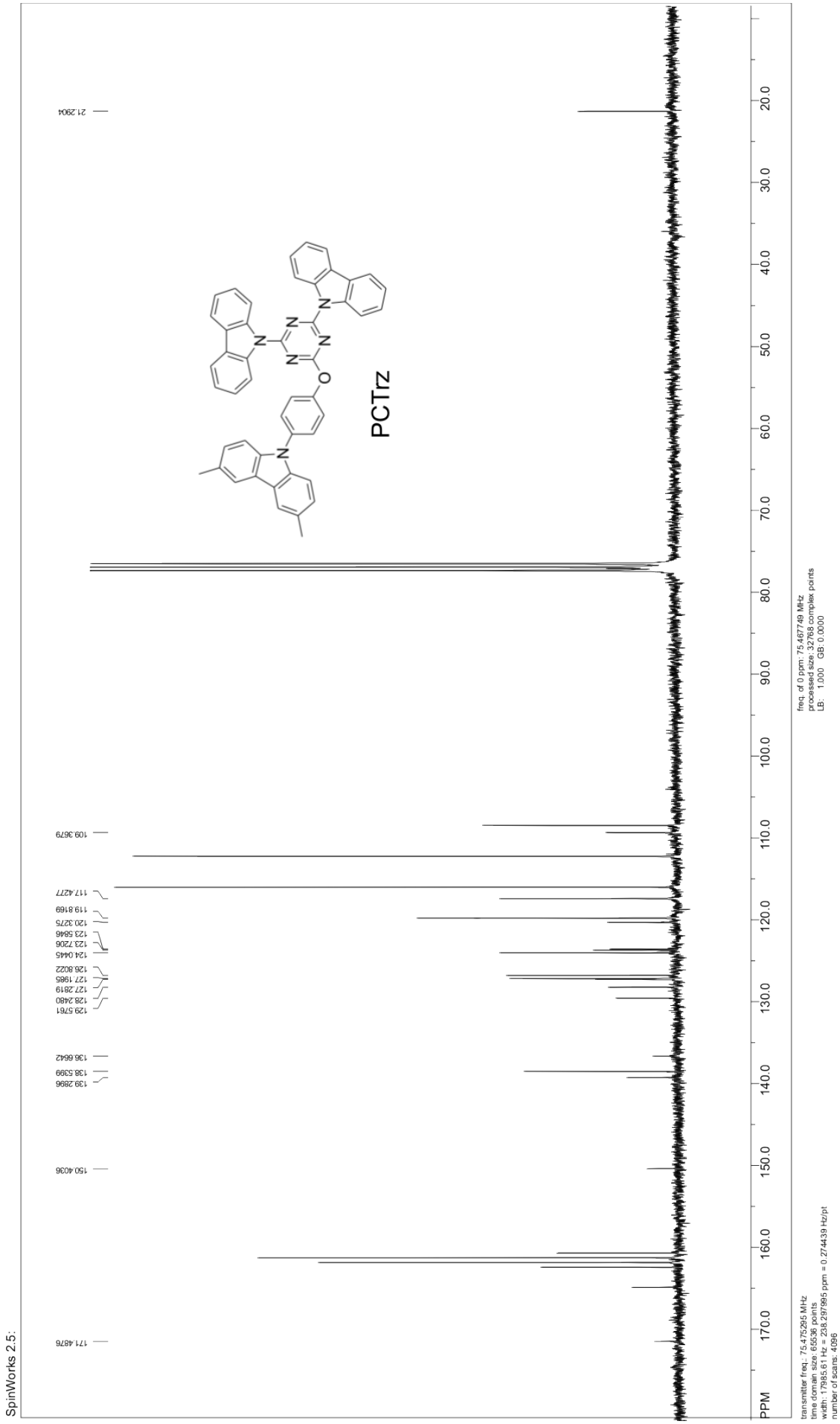
SpinWorks 2.5:
PCTrz
21.2904
109.3679
117.4277
119.8169
120.3275
123.5846
123.7206
124.0445
126.8022
127.1985
127.2819
128.2480
129.5761
136.6642
138.5399
139.2896
150.4036
171.4876
PPM
20.0
30.0
40.0
50.0
60.0
70.0
80.0
90.0
100.0
110.0
120.0
130.0
140.0
150.0
160.0
170.0
transmitter freq.: 75.475295 MHz
time domain size: 65536 points
width: 17985.61 Hz = 238.297995 ppm = 0.274439 Hz/pt
number of scans: 4096
freq. of 0 ppm: 75.467749 MHz
processed size: 32768 complex points
LB: 1.000 GB: 0.0000

References

[1] M. M. Rothmann, S. Haneder, E. Da Como, C. Schildknecht, C. Lennartz and P. Strohriegl, *Chem. Mater.*, submitted.

[2] Perdew, J. P.; *Phys. Rev. B* **1986**, *3319*, 8822.

[3] Becke, A. D.; *Phys. Rev. A* **1988**, *36*, 3098.

[4] Schäfer, A.; Horn, H.; Ahlrichs, R.; *J. Chem. Phys.* **1992,** *9*, 2571.

[5] Andrae, D.; Haeussermann, U.; Dolg, M.; Stoll, H.; Preuss, H.; *Theor. Chim. Acta* **1990**, *77*, 123.

[6] Schäfer, A.; Huber, C.; Ahlrichs, R.; *J. Chem. Phys.* **1994**, *100*, 5829.

[7] Klamt, A.; *J. Phys. Chem.* **1995**, *99*, 2224.

[8] Ahlrichs, R.; Bär, M.; Häser, M.; Horn, H.; Cölmel, C.; *Chem. Phys. Lett.* **1989**, *162*, 165.

9 Designing bipolar host materials for blue phosphorescent OLEDs: A Series of Phenoxy-carbazole substituted 1,3,5-Triazines

Michael M. Rothmann,[a] Sebastian T. Hoffmann,[b] Anna Köhler, [b] Gerhard Wagenblast, [c] Christian Lennartz,[c] Soichi Watanabe,[c] and Peter Strohriegl,[a]*

[a] Makromolekulare Chemie I and Bayreuther Institut für Makromolekülforschung, University of Bayreuth, 95440 Bayreuth, (Germany),

[b] *Experimentalphysik II, University of Bayreuth, Universitätsstraße 30, 95444 Bayreuth, Germany. Tel: +49 921 55 2601;*

[c] *BASF SE, 67056 Ludwigshafen, Germany;*

* Corresponding author. Email: peter.strohriegl@uni-bayreuth.de

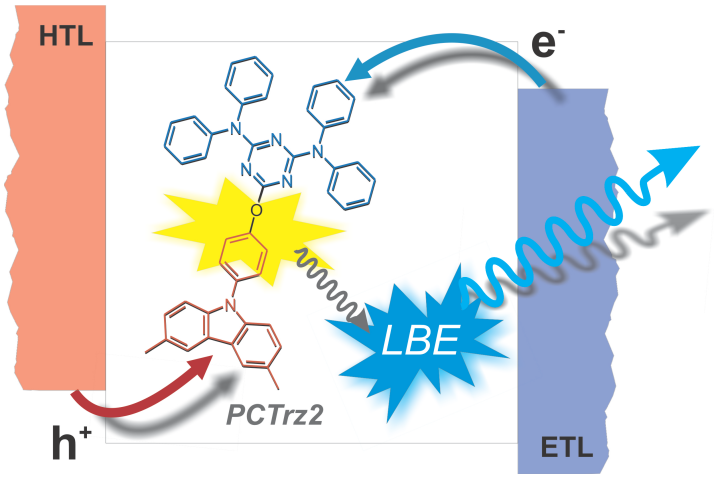

to be submitted to *Journal of Materials Chemistry*

Abstract.

A series of phenoxy-carbazole substituted triazine host materials (PCTrz, PCTrz2 and PCTrz3) were synthesized to investigate the influence of the different triazine moieties on thermal, photo physical and electronic properties. The non-conjugated ether bond successfully separates oxidation- and reduction-site in the molecule. However decreasing conjugation within the triazine moiety strongly influences the LUMO levels of the materials. Furthermore the impact reducing the conjugation on the phosphorescence and fluorescence of neat films is studied. The materials exhibit high glass transition temperatures up to 148 °C and high triplet bandgap up to 2.94 eV. Organic light-emitting diodes with a light blue emitter yield external quantum efficiencies of 11.5 %.

Introduction

Phosphorescent organic light emitting diodes (OLED) have been attracting much interest since they are capable of high efficiency and high brightness.[1,2] During the last decades OLED materials and device setups have undergone many improvements. [2,3,4] Nowadays full color displays and OLED lighting applications are in the focus of research.[5] One major advantage of high efficiency phosphorescent OLEDs is the fact that they can harvest both singlet and triplet excitons and therefore reach theoretical quantum efficiencies (QE) of 100%.[6] To reach such high QEs the emitter value has to be embedded in a suitable host.[7] In order to confine all excitons to the emitter the triplet energy of the host has to exceed that of the emitter, which is still a rather challenging task especially for blue emitters. Further requirements like thermal, chemical and morphological stability are essential to provide easy processing and long term stability. Additionally, a well balanced charge carrier transport and a broad recombination zone are desirable. This task is most likely solved by the design of a bipolar material. However, when donor and acceptor moieties form one conjugated molecule the triplet energy will drop dramatically.[8] This is often prevented by *meta* linkage of the two moieties.[9] The use of electron accepting N-heterocyclic compounds like triazines as electron transporters in OLEDs is well investigated.[10,11] One approach to enhance the hole conduction properties of 1,3,5-triazines and yield bipolar transport properties involves the introduction of three donor substituents.[12,13] Recently we reported a series of unsymmetrical donor substituted triazine host materials with high triplet energies and their performance in blue phosphorescent OLED.[14] However, the ionization potentials of carbazolyl substituted triazines might be too low (IP ~ 6.0 eV) for an efficient hole injection and therefore results in an excess of electrons in the emission layer and a recombination zone close to the hole transporting layer. Therefore bipolar host materials with ionization potentials higher than 6.0 eV would improve the hole injection properties. Up to now, only few bipolar hosts with high enough triplet energies for blue phosphorescent emitters (E > 2.8 eV) are known.[15]

In a recent communication we presented the design of bipolar host material for blue phosphorescent OLEDs.[16] The basic idea of this work was to introduce a hole transporting

phenylcarbazole moiety in a triazine electron transporter via a non-conjugated ether bond. This yielded 2-(4-(3,6-dimethylcarbazol-9-yl)-phenoxy)-bis-4,6-biscarbazolyl-1,3,5-triazine PCTrz, a bipolar host material. The injection and transport properties were improved compared to preceding donor substituted triazines.[14]

In this work we present a series of phenoxycarbazole-substituted triazines, including PCTrz, which follow the idea of designing bipolar organic hosts. The electron-conducting triazine unit is varied from a biscarbazolyl-triazine to a bis(diphenylamino)-triazine and a bisphenoxy-triazine. The hole transporting phenoxy-carbazole unit is kept constant. Therefore the electron injection properties can be studied for different triazine moieties. The glass forming properties and the thermal stability of the compounds are investigated. Furthermore the photo physical properties in neat films and different solvents as well as the PL quantum efficiency with different emitters are studied. Finally a blue phosphorescent OLED with PCTrz2 as host and a light blue phosphorescent emitter is presented.

Experimental

Materials. All commercially available reagents were purchased from Aldrich and used without further purification. The synthesis of 2,4-biscarbazolyl-6-chloro-1,3,5-triazine, 2,4-bis(diphenylamino)-6-chloro-1,3,5-triazine, 2,4-bis(3,5-dimethylphenoxy)-6-chloro-1,3,5-triazine and 9-(4-hydroxyphenyl)-3,6-dimethylcarbazole are described.[14,16] The synthesis of tris[(3-phenyl-1H-benzimidazol-1-yl-2(3H)-ylidene)-1,2-phenylene]-Iridium (DPBIC) is described in the literature.[17]

Characterisation. ^{1}H-NMR spectra were recorded on a Bruker AC-300 at 300 MHz. All NMR-data given are given as chemical shifts δ (ppm) downfield from $Si(CH_3)_4$. MS spectra were obtained on a Finnigan Mat 8500, MAT 112 S Varian machine using EI-ionization. Melting points and glass transition temperature determination was carried out on a Perkin Elmer Diamond DSC at a heating/cooling rate of 10 K/min in nitrogen atmosphere. Thermographimetric analysis (TGA) was performed on a Mettler Toledo TGA/SDTA851e machine at a heating rate of 10 K/min in nitrogen atmosphere.

UV-Vis absorption spectra were recorded on a Hitachi U-3000 spectrometer. Photoluminescence spectra were obtained using a Shimadzu Spectrofluorophotometer RF-5301PC. UVASOL solvents purchased from Merck were used to prepare solutions and films for optical characterization. The phosphorescence spectra were taken with 100-130 nm thick neat films prepared by spin-coating onto quartz substrates. The samples were mounted in a continuous flow helium cryostat. The temperature was controlled with an Oxford Intelligent temperature controller-4 (ITC-502). For the purely organic compounds, excitation was provided by a pulsed, frequency-tripled NdYAG laser at 355 nm (3.49 eV) (Spectron SL401) with a duration of the laser pulses of 6 ns. The light emitted by the sample was dispersed and subsequently detected by a time gated intensified CCD camera (Andor iStar DH734-18F-9AM). The measurements were taken with a delay time of 500ns and a gate width of 60 ms. OLED fabrication. The organic layers were deposited by thermal evaporation in high vacuum ($<10^{-6}$ mbar) onto indium-tin-oxide (ITO, 10 ohm/square) precoated glass substrates. Prior to use the ITO glass was degreased using organic solvents

and cleaned using an UV-ozon oven for 30 minutes. The organic layers and the metal cathode were evaporated without breaking the vacuum.

Computational Calculations. The transport levels of the materials used were determined via density functional calculations. For the ionization potential and the electron affinity first the geometry of the neutral as well as the charged states were optimized using the BP86-functional[18,19] in combination with a split-valence basis set (SV(P)) including polarization functions on all heavy atoms[20]. For iridium an effective core potential was employed.[21] For the energetics single point calculations at the optimized geometries using the same functional in combination with a valence triple zeta basis set (TZVP)[22] were conducted. To account for dielectric solid state effects a UPS/IEPS-calibrated version of the conductor like screening model (COSMO)[23] was used in conjunction with the single point calculations. All calculations were carried out with the turbomole program package.[24]

2,4-Biscarbazolyl-6-(4-(3,6-dimethylcarbazol-9-yl)phenoxy)-1,3,5-triazine (PCTrz). 4-Hydroxyphenyl-3,6-dimethylcarbazole (PC) (0.77 g, 2.67 mmol) and sodium hydroxide (0.10 g, 2.5 mmol) were dissolved in a water/dioxane mixture (20 ml, 1/1 (V/V)) at room temperature and stirred for 10 minutes until the solution was added to a solution of 2,4-biscarbazolyl-6-chloro-1,3,5-triazine (Trz) (0.99 g, 2.23 mmol) in dioxane (40 ml). The mixture is stirred for 8 hours at 70°C. After cooling to room temperature and addition of water (20 ml) the solid is filtered and washed with water and ethanol. The crude product is further purified by recrystallization from a hexane/ toluene mixture and sublimation to yield 2,4-Biscarbazolyl-6-(4-(3,6-dimethylcarbazol-9-yl)phenyoxy)-1,3,5-triazine (PCTrz) (1.24 g, 80 %) as white crystalline solid. ^{1}H NMR (300 MHz, $CDCl_3$-F_3CCOOD, δ): 8.73-8.70 (m, 4H), 8.08-8.05 (m, 4H), 7.96 (s, 2H), 7.78 (d, 2H), 7.64 (d, 2H), 7.44-7.40 (m, 10H), 7.28-7.25 (m, 2H), 2.59 (s, 6H); ^{13}C NMR (75 MHz, $CDCl_3$-F_3CCOOD, δ): 171.5, 164.9, 150.4, 139.2, 138.5, 136.6, 129.6, 128.2, 127.3, 127.2, 126.8, 124.0, 123.7, 123.6, 120.3, 119.8, 117.4, 109.4, 21.3; EI-MS (m/z (%)): 696 (100) [M^+], 530 (30) [$M^+ - C_{12}H_8N$], 348 (30) [M^{2+}], 166 (30) [$C_{12}H_8N$ (carbazole)]; T_m: 301 °C; T_g: 147 °C.

2,4-Bis(diphenylamino)-6-(4-(3,6-dimethylcarbazol-9-yl)phenoxy)-1,3,5-triazine (PCTrz2). This compound was synthesized by a procedure similar as described for PCTrz. Instead of

2,4-biscarbazolyl-6-chloro-1,3,5-triazine, 2,4-bis(diphenylamino)-6-chloro-1,3,5-triazine was used. Yield: 1.28 g, (75 %). ^{1}H NMR (300 MHz, $CDCl_3$, δ): 7.90 (s, 2H), 7.33-7.30 (m, 2H), 7.26-7.19 (m, 20H), 7.16-7.12 (m, 6H), 2.56 (s, 6H). ^{13}C NMR (75 MHz, $CDCl_3$, δ): 170.7, 167.0, 150.9, 143.0, 139.5, 134.5, 128.9, 128.6, 127.6, 127.2, 126.9, 125.8, 123.2, 123.2, 120.1, 109.5, 21.4. EI-MS (m/z (%)): 700 (100, M+), 415 (15), 287 (20). T_m: 274 °C; T_g: 109 °C.

2,4-Bis(3,5-dimethylphenoxy)-6-(4-(3,6-dimethylcarbazol-9-yl)phenoxy)-1,3,5-triazine (PCTrz3). This compound was synthesized by a procedure similar as described for PCTrz. Instead of 2,4-biscarbazolyl-6-chloro-1,3,5-triazine, 2,4-bis(3,5-dimethylphenoxy)-6-chloro-1,3,5-triazine. The product was purified by liquid column chromatography (silica gel) using a hexane/THF eluent (10/1, V/V). Yield: 2.35 g, (86 %). ^{1}H NMR (300 MHz, $CDCl_3$, δ): 7.90 (s, 2H), 7.48 (d, 2H), 7.32 (d, 2H), 7.23 (s, 4H), 6.88 (s, 2H), 6.78 (s, 4H), 2.55 (s, 6H), 2.30 (s, 12H). ^{13}C NMR (75 MHz, $CDCl_3$, δ): 173.9, 173.4, 151.5, 150.0, 139.3, 139.2, 135.7, 129.5, 127.8, 127.6, 127.0, 123.4, 122.8, 120.2, 118.9, 109.3, 21.4, 21.3. EI-MS (m/z (%)): 606 (100) [M^+]. T_m:- °C; T_g: 89 °C.

Results and Discussion.

Synthesis.

The structures and the synthetic route to all substituted triazines (PCTRZ1-3) are summarized in Scheme 1. As described earlier the main aim is the design of bipolar host materials, which comprise a hole transporting phenylcarbazole moiety attached to an electron conducting triazine unit via a non-conjugated ether bond. Both counterparts, N-(4-hydroxyphenyl)-3,6-dimethylcarbazole and the respective 1,3,5-triazine, were synthesized in a total of four steps. While the triazine building blocks were obtained from a one step nucleophilic substitution of two chlorines of cyanuric chloride, the phenoxycarbazole synthesis involves 3 steps, which were described in a preceding communication.[14,16,25] The final assembling step comprises the substitution of the remaining chlorine with the phenoxycarbazole unit and yields 2,4-biscarbazolyl-6-(4-(3,6-dimethylcarbazol-9-yl)phenoxy)-1,3,5-triazine (PCTrz), 4-bis(diphenylamino)-6-(4-(3,6-dimethylcarbazol-9-yl)phenoxy)-1,3,5-triazine (PCTrz2), and 2,4-bis(3,5-dimethylphenoxy)-6-(4-(3,6-dimethylcarbazol-9-yl)phenoxy)-1,3,5-triazine (PCTrz3).

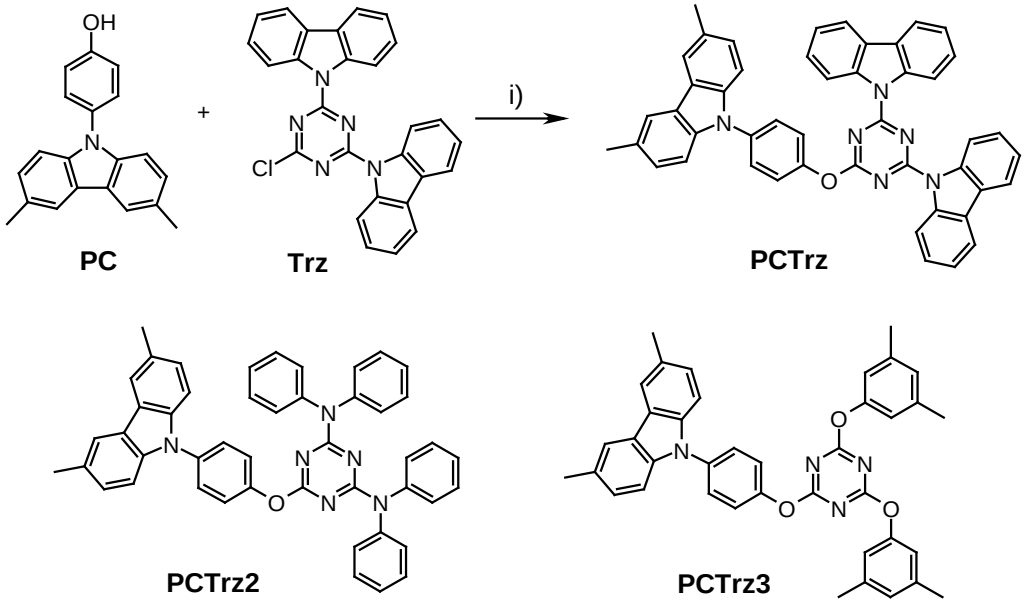

Scheme 1: Synthesis of 2-(4-(3,6-dimethylcarbazol-9-yl)-phenoxy)-bis-4,6-biscarbazolyl-1,3,5-triazine PCTrz: (i) NaOH, H_2O, dioxane, 100°C, 6h) and chemical structures of 2-(4-(3,6-dimethylcarbazol-9-yl)-phenoxy)-bis-4,6-diphenylamino-1,3,5-triazine PCTrz2 and 2-(4-(3,6-dimethylcarbazol-9-yl)-phenoxy)-bis-4,6-bis(3,5-dimethylphenoxy)-1,3,5-triazine PCTrz3 (synthesized using the same reaction conditions).

Thermal properties.

The thermal properties were investigated by thermogravimetric measurements (TGA) and differential scanning calorimetry (DSC) in nitrogen atmosphere. Figure 1 comprises the second heating DSC traces of all triazines. While PCTrz and PCTrz2 are obtained as crystalline material from the synthesis, PCTrz3 is an amorphous solid. Therefore the DSC scan of PCTrz3 shows no melting of the sample upon heating up to 240 °C. Instead, a glass transition is observed at a temperature of 89 °C. In further cooling and heating cycles only this glass transition is detected. In contrast to that, for PCTrz and PCTrz2 an endothermic peak in the first heating cycle is detected, which is attributed to the melting of the samples. Upon cooling with 40 K/min no crystallization of the materials can be observed. The subsequent heating cycles are illustrated in figure 1. We found that the materials exhibit glass transitions at temperatures of 109 °C (PCTrz2) and 148 °C (PCTrz). Upon further heating of the PCTrz2 sample, an exothermic transition (crystallization) at 170 °C followed by an endothermic melting peak at 280 °C is detected. PCTrz shows similar behavior. The sample crystallizes at 201 °C followed by an endothermic melting transition at 301 °C. The higher glass transition temperature of PCTrz is attributed to the more rigid carbazole substituents compared to the flexible diphenylamino groups of PCTrz2. We attribute the fully amorphous behavior of PCTrz3 to the presence of the methyl groups, which hinder crystallization. The relatively low glass transition temperature of 89 °C is mainly attributed to the lower molecular weight of PCTrz3.

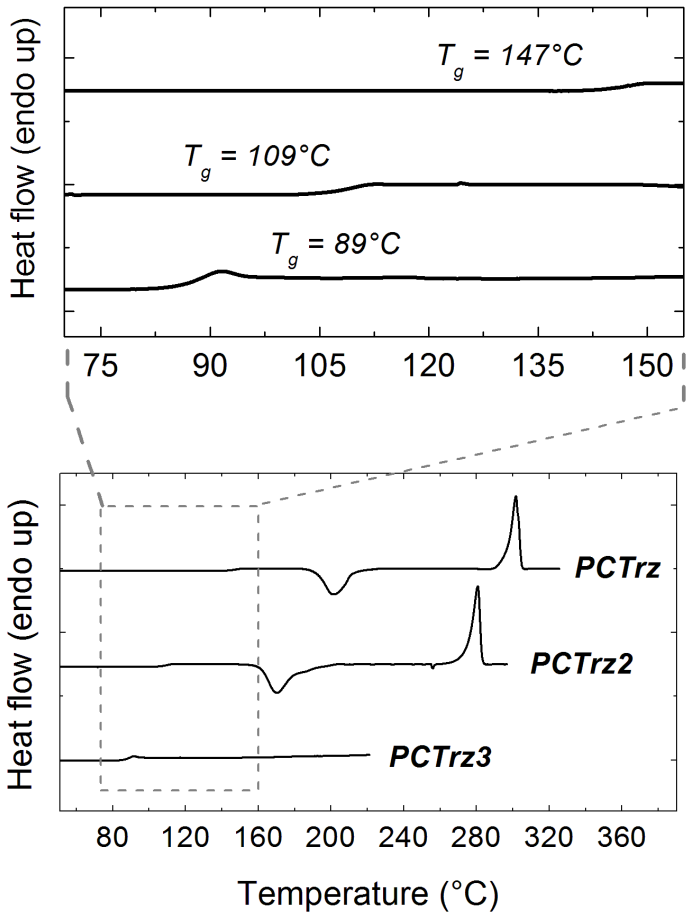

Figure 1: BOTTOM: Differential scanning calorimetry traces of PCTrz, PCTrz2 and PCTrz3 (top to bottom) (second heating scan; 10 K/min; N_2 atmosphere). **TOP:** Magnification of the DSC scans for a better visibility of the glass transitions at temperatures.

The TGA measurements evidence a high thermal stability of the triazines PCTrz and PCTrz2 up to at least 400 °C. For PCTrz, a weight loss of 1 % is observed at a temperature of T_D^1 = 425 °C. For PCTrz2 a T_D^1 temperatures of 370° can be detected. These T_D^1-values are more than 110 °C above the sublimation temperature of PCTrz and PCTrz2 and therefore substantiate the very high thermal stability. The thermal stability of PCTrz3 is lower with a T_D^1 temperature of 225 °C, which is very close to the sublimation temperature of the material.

Optical properties

The photophysical properties of the three triazine hosts have been investigated in solution and for neat films. The absorption and fluorescence spectra of PCTrz, PCTrz2 and PCTrz3 in cyclohexane solutions are given in figure 2a-c. Figure 2d-f comprises the thin film emission spectra of the three materials at different temperatures. The absorption of all materials is almost identical to the sum of the spectra of the respective phenoxy-carbazole and triazine moiety (grey lines in figures 2a-c). Since all materials comprise the same phenoxy-carbazole (PC) hole transporting unit, its characteristic pattern can be found in all spectra. Furthermore, this moiety defines the lowest energetic transition of the molecules at 349 nm, 351 nm and 350 nm for PCTrz. PCTrz2 and PCTrz3, respectively. Consequently, the optical bandgap, which is estimated from the absorption edge of this maximum, is essentially equal for the three hosts at a wavelength of about 359 nm (3.45 eV). The contribution of the triazine moieties is observed at shorter wavelengths. The absorption of biscarbazolyl-triazine (Trz), the triazine part of PCTrz (see scheme 1), ranges from 327 nm to 260 nm. For PCTrz2 a contribution of the bis(diphenylamino)-triazine part is detected below a wavelength of 310 nm. The bis(3,5-dimethyl)phenoxy-triazine unit of PCTrz3 features no absorption above 270 nm. Therefore the spectrum of PCTrz3 is almost equal to that of phenoxy-carbazole.

The fluorescence spectra of the three materials show a dominant 0-0 peak with two vibrational sidepeaks. This behavior is similar to that of phenylcarbazole with a small hypsochromic shift of 8 nm. The maxima of the PCTrz are situated at 353 nm, 370 nm and 390 nm. Those of PCTrz2 and PCTrz3 are red-shifted by 4 nm. For an excitation wavelength in the range of 260 to 355 nm, only this emission is observed. Thus, we suggest that the energy, which is absorbed by the triazine part, undergoes intramolecular transfer to the phenoxy-carbazole part. Therefore only the fluorescence of this moiety is detected.

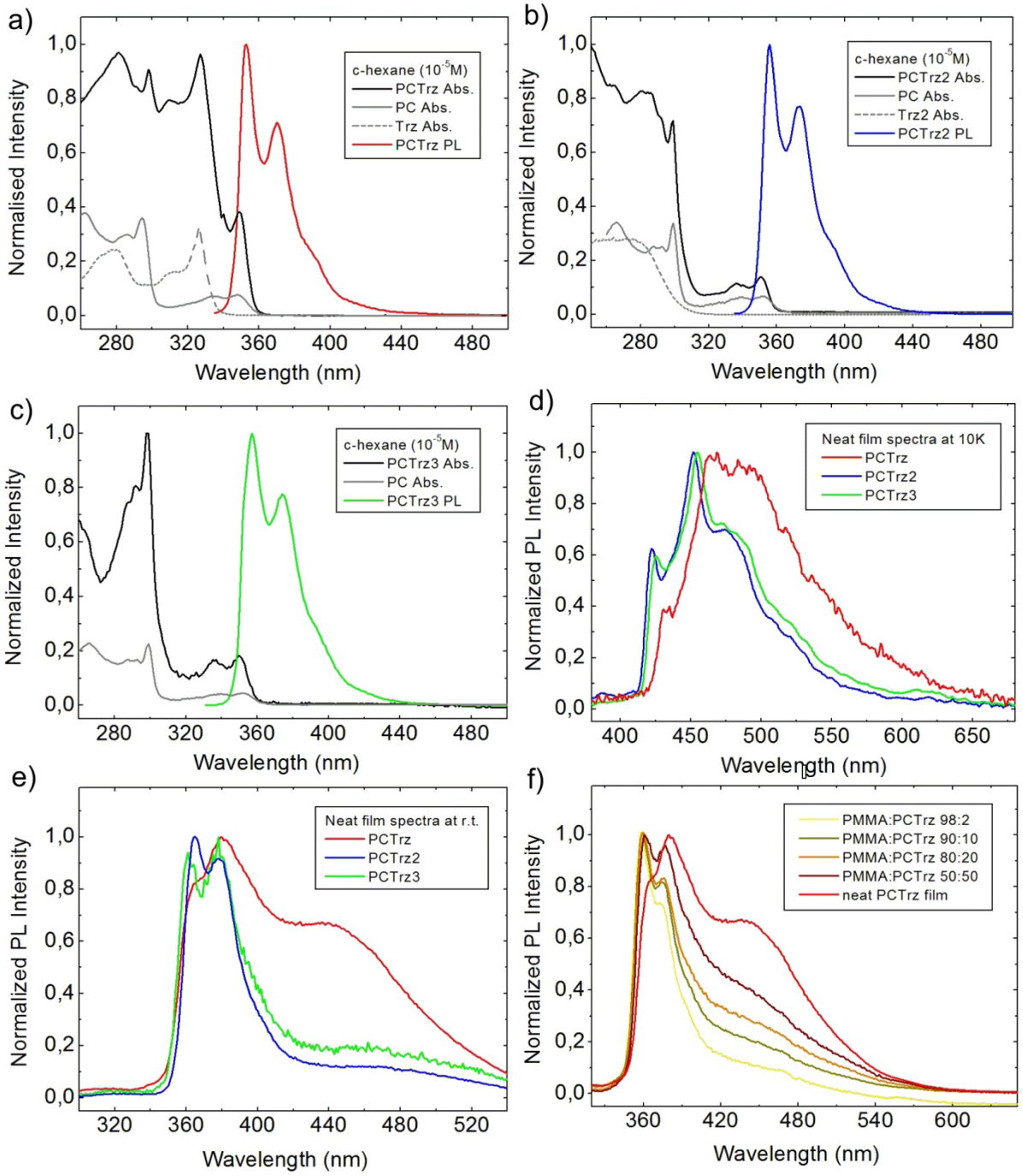

Figure 2: a-c) Optical properties of host materials PCTrz (**a**), PCTrz2 (**b**) and PCTrz3 (**c**) in cyclohexane solution (10^{-5}M) consisting of: absorption of the host material (black line), the absorption of the respective moieties PC (grey line) Trz and Trz2 (grey dotted line) and the fluorescence (colored line) of the host materials. **d-e)** Emission spectra of neat films of PCTrz (red line), PCTrz2 (blue line) and PCTrz3 (green line) at different temperatures. At 10K the phosphorescence (**d**) is recorded using time gated spectroscopy, while at room temperature the fluorescence (**e**) is detected**. f)** Emission spectra of PCTrz diluted in PMMA and of the neat film

For the application as host material in OLEDs, one essential requirement is that the triplet level of the host has to be higher than that of the guest. In order to record phosphorescence spectra, the emission of thin films was measured at 10K with a delay of 500ns after the excitation pulse. At this time after excitation, all prompt fluorescence is decayed, so that only long-lived excitation is detected. The low temperature reduces undesired non-radiative decay channels and so increases signal intensity. The spectra displayed in figure 2d show a peak with lower intensity at about 420-430 nm and a second, more intense peak at about 450-460 nm. This spectral shape and the energy of the emission of our compounds are very similar to the phosphorescence spectra reported for related carbazole derivatives.[26,27] The energy separation between the prompt emission we observe with a 0-0 around 355 nm (3.5 eV) and the longer-lived emission with a 0-0 peak around 420-430 nm (2.95-2.88) is about 0.55-0.67 eV, consistent with the S_1-T_1 energy gap reported by Brunner and co-workers.[26] Due to these similarities we attribute the emission observed after a delay time of 500 ns to phosphorescence from the carbazole moiety. The position of the 0-0 peaks yields the triplet energy. The exact values are 2.88 eV (430 nm), 2.94 eV (422 nm) and 2.93 eV (424 nm) for PCTrz , PCTrz2 and PCTrz3, respectively.

Although the 0-0 transitions are very similar for the three compounds the phosphorescence spectrum of PCTrz is broader and less structured than the other two spectra. In figure 2e the fluorescence spectra of evaporated neat films (thickness ~100 nm) of the three triazine hosts are plotted. Compared to the solution spectra, the fluorescence maxima of the films exhibit a red-shift. The smallest shift of 6 nm is observed for PCTrz3, while PCTrz and PCTrz2 have slightly larger shifts of 14 nm and 11 nm respectively. Beside this bathochromic shift of the major fluorescence peaks, the growth of an additional broad fluorescent peak between 410 nm and 520 nm can be found. The intensity of this contribution is strongly dependent on the triazine moiety and increases from PCTrz2 to PCTrz3 and PCTrz. The nature of this contribution is attributed to an intermolecular charge transfer complex (CT), which is ascribed to the aggregation of the molecules. To prove this statement the fluorescence spectra of PCTrz diluted in a polymer matrix were investigated. Figure 2f considers the emission of PCTrz embedded in PMMA in several concentrations. We found, that upon diluting PCTrz the emission of the CT-band decreases and almost vanishes at a

concentration of 2%. A further evidence for a CT-complex can be found in the broadening and the low intensity of the phosphorescence spectrum of PCTrz, due to the population of the CT-state instead of the triplet state. Since aggregates are potential loss pathways quantum efficiency measurement of host:guest system with two different emitters were carried out to quantify the effect. A light blue emitter (LBE) with a triplet energy of 2.61 eV and a deep blue emitter (DBE) with a triplet energy of 2.78 eV were used for this experiment. A typical concentration of 8 % doped into PCTrz and PCTrz2 was used. While the LBE-doped films showed similar efficiencies of 60 % (PCTrz2) and 55 % (PCTrz), the difference of the DBE-doped films was immense. The PCTrz films comprise a QE of only 12 % while the PCTrz2 film shows a QE of 55 %.

Electrochemical properties and computational calculations

The values for the highest occupied molecular orbital (HOMO) were determined with cyclic voltammetry. The values for the lowest unoccupied molecular orbital (LUMO) are calculated from the ionization potential and the optical bandgap. The cyclovoltagrams up on oxidation of PCTrz, PCTrz2 and PCTrz3 are shown in figure 3. Figure 3 also comprises a schematic of the measured HOMO and calculated LUMO values as well as the optical bandgap values. For each material a separate schematic for the phenoxy-carbazole and the triazinyl moieties is given The oxidation cycles of the three host exhibit reversible behavior in multiple cycles. The half-wave potentials (versus Fc/Fc^{+}) are determined at 0.68 V, 0.72 V and 0.70 V for PCTrz, PCTrz2 and PCTrz3 respectively. The ionization potential values were calculated as 5.48 eV, 5.52 eV and 5.50 eV. Since the oxidations of the triazine parts Trz, Trz2 and Trz3 are irreversible and occur at distinctly higher potentials (1.16 V, 1.26 V and 1.45 V, respectively) it is assumed that the oxidation of the host materials takes place at the phenoxy-carbazole moieties. This is supported by the similarity to the oxidation wave of the hte respective triazine host compared to that of 4-methoxyphenyl-3,6-dimethylcarbazole. The reversible CV-behavior upon oxidation can be explained by the protection of the 3,6-position of the phenoxy-carbazole unit with methyl groups, since side reactions of unprotected carbazoles are well known.[28,29]. Here, the methyl groups lead to lower oxidation potentials (~0.1 V-0.2 V) due to their inductive effect.

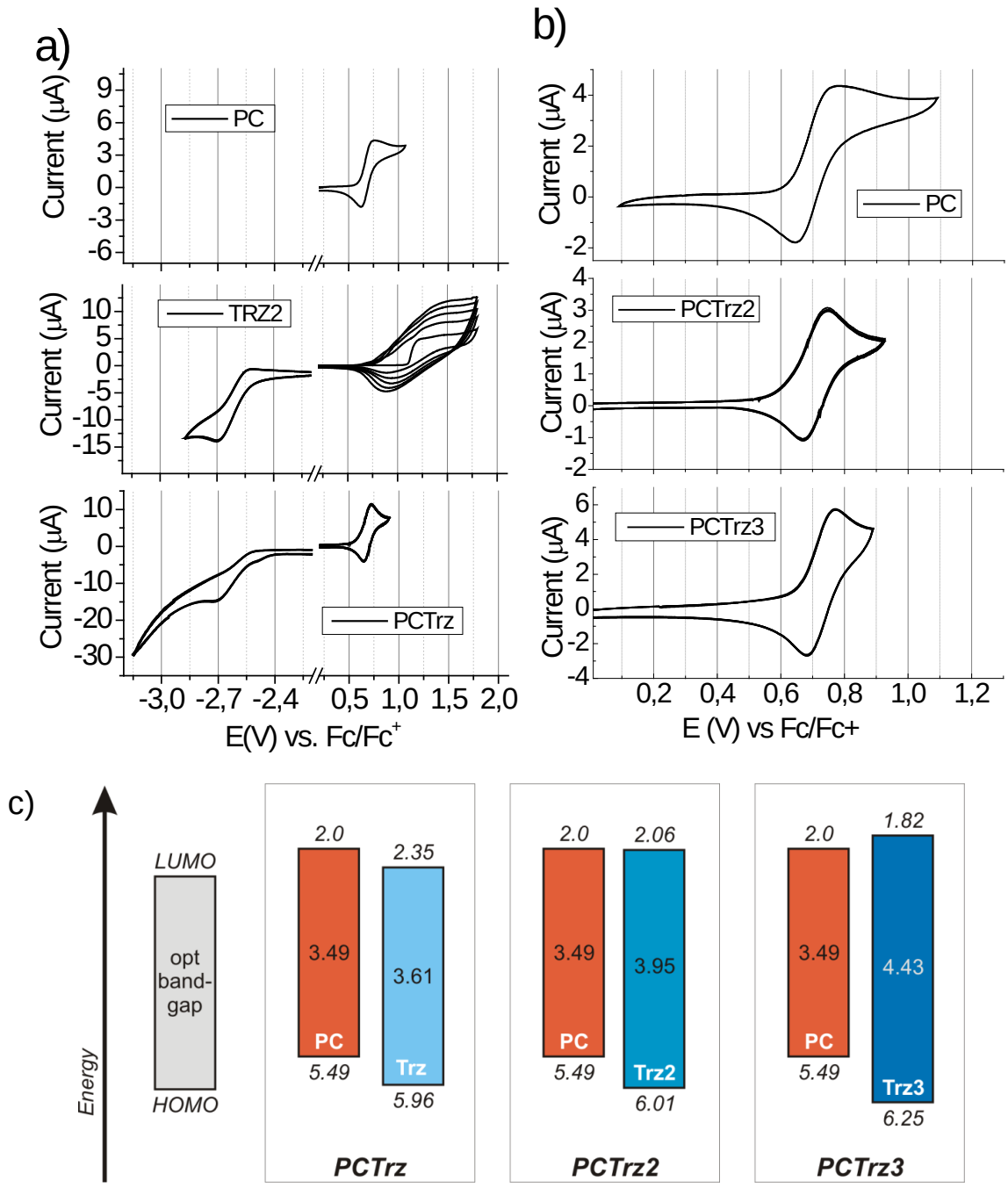

Figure 3: a) Oxidation and reduction waves of PCTrz compared to PC (no reduction detectable) and Trz. (5 cycles in dichloromethane; 50 mV/s). **b)** Oxidation waves of PCTrz2 and PCTrz3 compared to PC. (5 cycles in dichloromethane; 50 mV/s). **c** Schematic of the HOMO, LUMO and optical bandgap values for the respective moieties of each triazine host material. The HOMO values are measured by cyclic voltammetry, while the LUMO is estimated (HOMO minus opt. bandgap). Since the donor and acceptor parts of each host material are separated by a non-conjugated ether bridge they are regarded as isolated moieties. Therefore the two parts are individually characterized by cyclic voltammetry. The phenoxycarbazole moiety is more easily oxidized and therefore represents the hole conduction part of the molecule. In contrast to the LUMO values of the triazine moieties are different in each material.

However, the reduction of phenoxy-carbazole was not detected within potentials down to -3.1 V (corresponds to a LUMO of approximately 1.9 eV). For the reductions of the three host materials we found that only for PCTrz a reduction wave was observable at a half-wave potential of -2.6 V (LUMO = 2.2 eV). Since the reductive behavior of the carbazolyl-triazine intermediate Trz is similar, we conclude that the reduction of PCTrz only involves the triazine moiety. This is additionally supported by computational calculations of the HOMO and LUMO spatial electron distribution (figure 4a). It was found that the electron density is centered on the HOMO of the phenoxy-carbazole moiety, while the LUMO is mainly confined on the triazine ring. These results substantiate the successful separation of electron accepting and donating counterparts in PCTrz. Compared to the estimated LUMO (LUMO(est.)) value of 2.35 eV (from HOMO-bandgap) of PCTrz the measured LUMO level is 0.15 eV lower. The electro chemical investigations of PCTrz2 and PCTrz3 down to potentials of -3.1 V yielded no analyzable reduction wave. For PCTrz2, the LUMO(est.) of the phenoxy-carbazole and the triazine moiety are similar (2.06 eV, see figure 3). Since no reduction is observed in the CV experiment it can be assumed that the exciton binding energy is >0.15eV in this case. The spatial electron distribution of the LUMO (figure 4b) is mainly distributed over the triazine moiety. Therefore we assume that the electron transport in PCTrz2 favorably occurs on the diphenylamino-triazine part, although the energetic separation is not as clear as for PCTrz. PCTrz3 is the material, in which the triazine moiety exhibits the largest bandgap. In combination with the HOMO value at 6.25 eV, this results in a LUMO(est.) level that is higher compared to the phenoxy-carbazole moiety (figure 3). The calculated electron distribution of the LUMO (figure 4c) of PCTrz3 is no longer centered at the triazine moiety, but spread over the both moieties in equal parts. Therefore it can be assumed that the electron injection and transport properties of this material are decreased compared to PCTrz2.

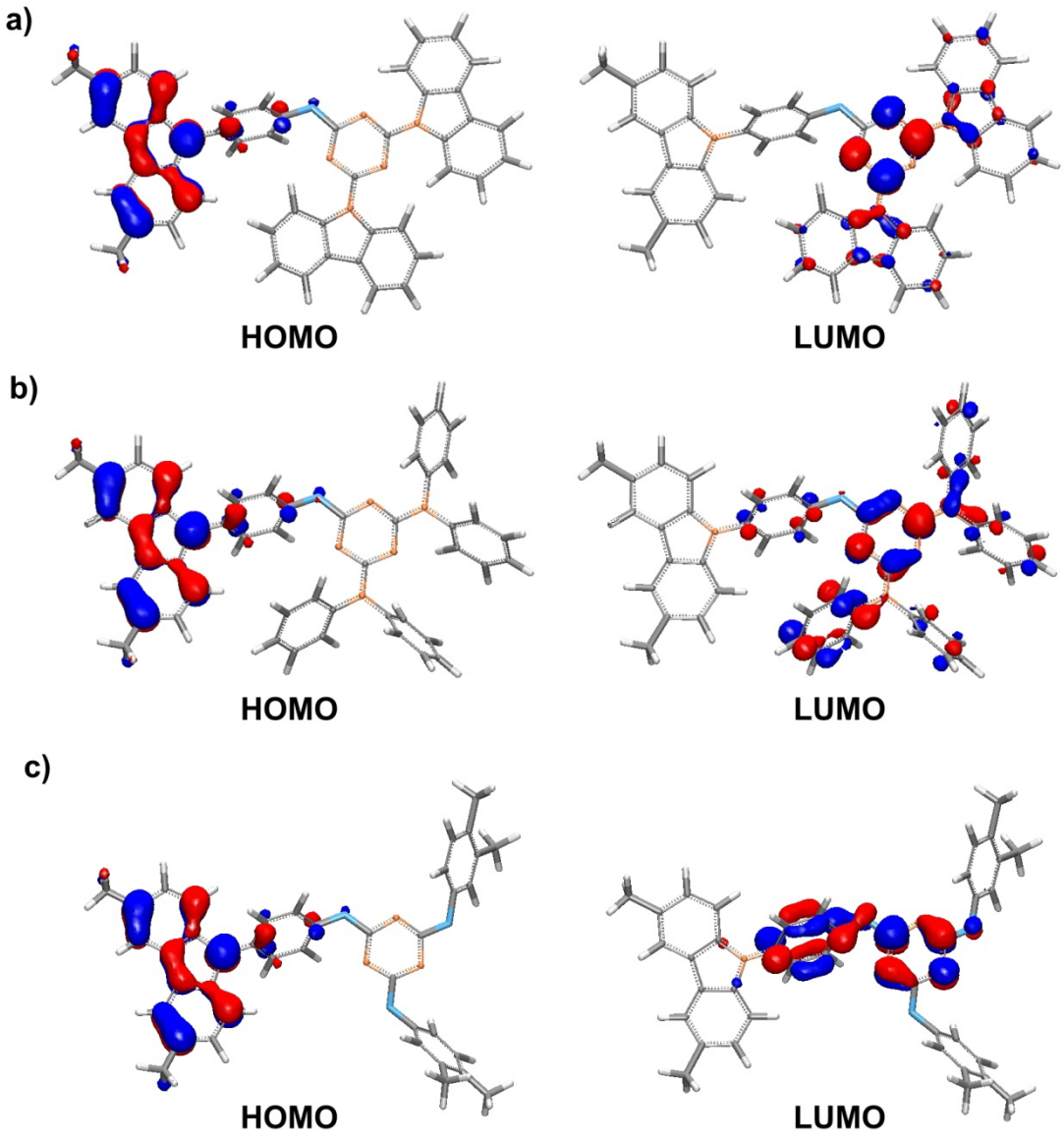

Figure 4: DFT-calculated spatial distribution of HOMO (left) and LUMO (right) electron densities of PCTrz (a), PCTrz2 (b) and PCTrz3 (c).

Phosphorescent Organic Light-Emitting Diodes

To demonstrate the potential of PCTrz2 as host material for blue phosphorescent emitters, an OLEDs with a light blue phosphorescent emitter (LBE) comprising the following configuration was fabricated. On top of indium-tin-oxide (ITO) poly(3,4-ethylenedioxythiophene):poly(styrenesulfonate) (PEDOT: PSS) was used as hole-injection layer followed by 35 nm of DPBIC p-doped with molybdenum(VI) oxide as hole-transporting layer. An additional 20 nm thick layer of DPBIC followed as exciton and electron blocker.

The 30 nm thick emission layer consisted of PCTrz2 doped with 15% light blue emitter LBE. 2,6-Dicarbazolyl-1,5-pyridine (PYD2)[30] was used as hole-blocking layer (10 nm) followed by 50 nm tris(8-hydroxyquinolinato)aluminum (Alq_3) as electron transporting material. The device was finalized by deposition of LiF (0.7 nm)/ Al (100 nm) cathode. In figure 5 the current density-voltage as well as current efficiency-voltage and EQE-voltage characteristics of this device are illustrated.

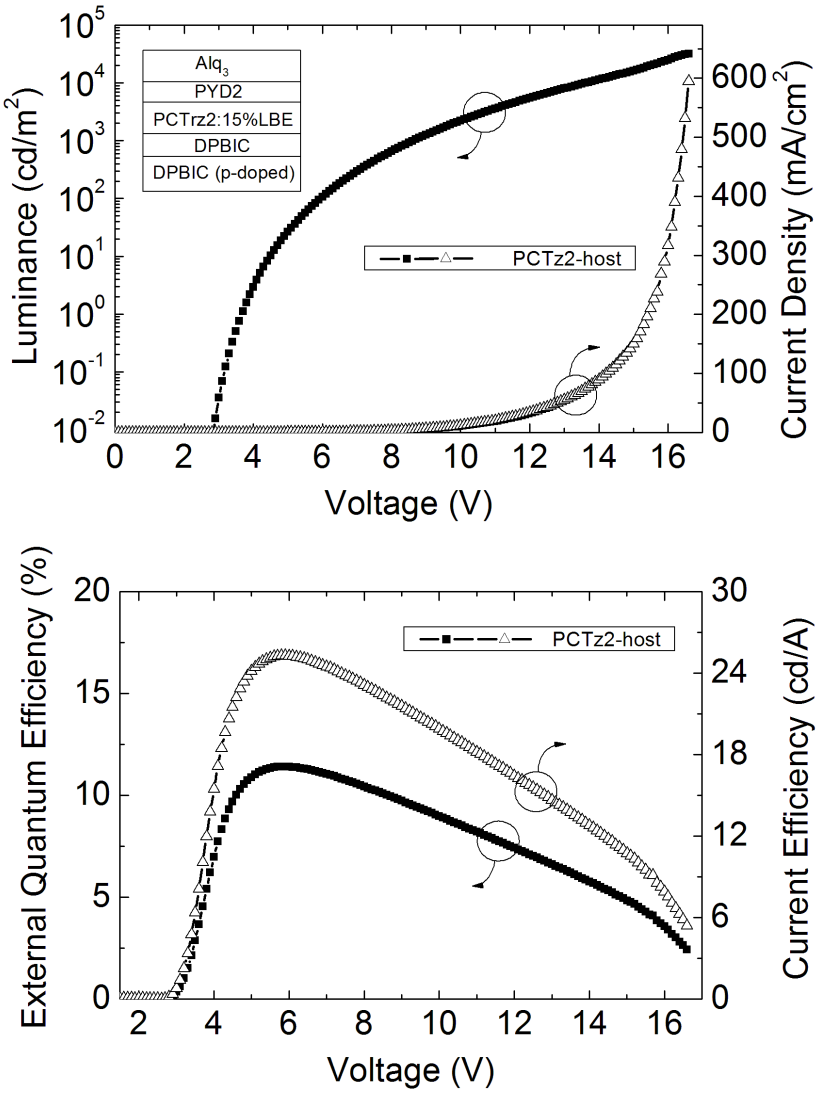

Figure 5: TOP: Luminance-voltage-current density characteristics of an OLED with PCTrz2 as host; **BOTTOM:** External quantum efficiency-voltage-current efficiency characteristics of an OLED with PCTrz2 as host; **INSET:** device configuration: ITO // PEDOT // p-doped DPBIC 35nm // DPBIC 20nm // 15% LBE:PCTrz2 30nm // PYD2 10nm // Alq_3 50nm // LiF/AL**.**

The electroluminescence spectrum of the device comprises a pure LBE emission with a maximum at 474 nm. The device reaches a maximum luminance of 32000 cd/m^2 at 16.6 V. The threshold voltage of 2.8 V is an excellent value for a light blue OLED and demonstrates the absence of injection barriers. The maximum external quantum efficiency of 11.5 % as well as the current efficiency maximum of 25.2 cd/A are reached at a luminance of 100 cd/m^2. It is notable that the EQE remains high over a wide voltage range and for 1000 cd/m^2 a value 10.2% is detected. These results demonstrate the potential of bipolar phenoxy-carbazole substituted triazines as host materials for blue phosphorescent OLEDs.

Conclusions.

We presented three host materials which consist of a hole-conducting phenoxy-carbazole and an electron-deficient substitute triazine moiety. The two parts are separated by a non-conjugated ether bond. For PCTrz and PCTrz2 this yields a separation of oxidation and reduction site. In contrast to that the bandgap of the triazine moiety of PCTrz3 is too large, so that the LUMO is spread of both, the phenoxy-carbazole and the triazine moiety. The excellent glass forming properties of the three triazines ensure morphological stability. From neat film phosphorescence spectroscopy of PCtrz, PCtrz2 and PCTrz3, the triplet energy values of 2.88 eV, 2.94 eV and 2.92 eV respectively, are obtained. The potential of this class of materials as hosts for blue phosphors has been tested. A maximum brightness of 32000 cd/m^2 and a maximum external quantum efficiency of 11.5 % were reached using a light blue emitter (474 nm).

Acknowledgement

The authors like to thank Dr. Ingo Münster, Dr. Evelyn Fuchs and Dr. Nicolle Langer for helpful discussions and the provision of the emitter LBE. Our special thanks go to I. Bauer for supporting us during synthesis and characterization of the host materials. We are grateful to the BMBF for financial support through the project OPAL 2008 (Grant No. 13N8992).

References

1 M. A. Baldo, D. F. O'Brian,Y. You, A. Shoustikov, S. Sibley, M. E. Thompson and S. Forrest, *Nature*, 1998, **395**, 151.

2 S. Reineke, F. Lindner, G. Schwartz, N. Seidler, K. Walzer, B. Luessem and K. Leo, *Nature*, 2009, **459**, 234.

3 H. Yersin (Ed.), *Highly Efficient OLED's with Phosphorescent Materials*; Wiley-VCH: Weinheim, Germany, **2008**.

4 M. Slootsky, S. R. Forrest, Appl. Phys. Lett. 2009, 94, 163302.

5 S. Tonzani, *Nature* 2009, **459**, 312-314.

6 M. Segal, M. A. Baldo, R. J. Holmes, S. R, Forrest, Z. G. Soos, *Phys. Rev. B*, **2003**, *68*, 075211.

7 C. Adachi, M. A. Baldo, M. E. Thompson, S. R. Forrest, J. Appl. Phys., 2001, 90, 5048-5051.

8 D. J. Cowley and I. Pasha, *J. Chem. Soc. Perkin Trans. II*, 1983, 1139.

9 S.-J. Su, T. Chiba, T. Takeda and J. Kido*, Adv. Mater*, 2008, **20**, 2125.

10 R. Fink, Y. Heischkel, M. Thelakkat, H.-W. Schmidt, C. Jonda and M. Hüppauff, *Chem. Mater.*, 1998, **10**,3620.

11 R. Klenker, H. Aziz, A. Tran, Z. D. Popovic and G. Xu, *Org. Elect.*, 2008, **9**, 285.

12 H. Inomata, K. Goushi, T. Masuko, T. Konno, T. Imai, H. Sasabe, J. J. Brown and C. Adachi, *Chem. Mater.*, 2004, **16**, 1285.

13 K. S. Son, M. Yahiro, T. Imai, H. Yoshizaki and C. Adachi, *Chem. Mater.*, 2008, **20**, 4439.

14 M. M. Rothmann, S. Haneder, E. Da Como, C. Lennartz, C. Schildknecht and P. Strohriegl, *Chem. Mater.*, submitted.

15 S. O. Jeon, K. S. Yook, C. W. Joo and J. Y. Lee, Adv. Funct. Mater., 2009, available online (DOI: 1002/adfm.200901274).

16 M. M. Rothmann, I. Münster, E. Fuchs, C. Schildknecht and P. Strohriegl, *Chem. Comm.*, submitted.

17 Bolt, M.; Lennartz, C.; Prinz, M.; Schmidt, H.-W.; Thelakkat, M.; Baete, M.; Neuber, C.; Kowalsky, W.; Schildknecht, C.; Johannes, H.-H.; WO Patent 2005 019373.

18 Perdew, J. P.; *Phys. Rev. B* **1986**, *3319*, 8822.

19 Becke, A. D.; *Phys. Rev. A* **1988**, *36*, 3098.

20 Schäfer, A.; Horn, H.; Ahlrichs, R.; *J. Chem. Phys.* **1992,** *9*, 2571.

21 Andrae, D.; Haeussermann, U.; Dolg, M.; Stoll, H.; Preuss, H.; *Theor. Chim. Acta* **1990**, *77*, 123.

22 Schäfer, A.; Huber, C.; Ahlrichs, R.; *J. Chem. Phys.* **1994**, *100*, 5829.

23 Klamt, A.; *J. Phys. Chem.* **1995**, *99*, 2224.

24 Ahlrichs, R.; Bär, M.; Häser, M.; Horn, H.; Cölmel, C.; *Chem. Phys. Lett.* **1989**, *162*, 165.

25 P. Schrögel, …….

26 K. Brunner, A. van Dijken,H. Börner, J. J. A. M. Bastiaansen, N. M. M. Kiggen, and B. M. W. Langeveld, *J. Am. Chem. Soc.,* **2004**, *126*, 6035-6042.

27 A. van Dijken, J. J. A. M. Bastiaansen, N. M. M. Kiggen, B. M. W. Langeveld, C. Rothe, A. Monkman, I. Bach, P. Stössel, and K. Brunner, *J. Am. Chem. Soc.,* **2004**, *126*, 7718-7727.

28 J. F. Ambrose, R. F. Nelson, *J. Electrochem. Soc.*, **1968**, *115*, 1159.

29 J. F. Ambrose, L. L. Carpenter, R. F. Nelson, *J. Electrochem. Soc.*, **1975**, *122*, 876.

30 K. S. Son, M. Yahiro, T. Imai, H. Yoshizaki, C. Adachi, J. Photopoly. Sci. Tech. 2007, 20, 47-50.

10 Appendix: Effect of Electric Field on Coulomb-Stabilized Excitons in Host/Guest Systems for Deep-Blue Electrophosphorescence

Stephan Haneder,[a] Enrico Da Como,[a] Jochen Feldmann,[a] Michael M. Rothmann,[b] Peter Strohriegl,[b] Christian Lennartz,[c] Ingo Münster,[c] Christian Schildknecht,[c] Gerhard Wagenblast[c]*

[a] Photonics and Optoelectronics Group, Department of Physics and CeNS Ludwig-Maximilians-Universität, 80799, Munich (Germany)

[b] Makromolekulare Chemie I and Bayreuther Institut für Makromolekülforschung, University of Bayreuth, 95440 Bayreuth, (Germany),

[c] BASF SE, 67056, Ludwigshafen (Germany)

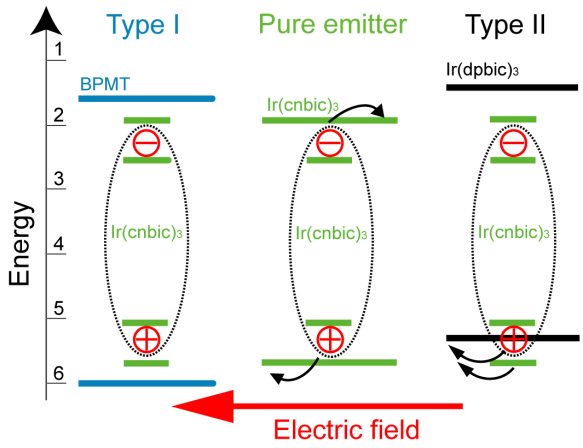

published in *Advanced Functional Materials*, ***2009***, *19*, 2416-2422.

Abstract.

Here, a study of the electric field induced quenching on the phosphorescence intensity of a deep-blue triplet emitter dispersed in different host materials is presented. The hosts are characterized by a higher triplet excitonic level with respect to the emitter, ensuring efficient energy transfer and exciton confinement, whereas they differ in the highest occupied molecular orbital (HOMO) alignment, forming type I and type II host/guest heterostructures. While the type I structure shows negligible electric field induced quenching, a quenching up to 25% for the type II at a field of 2 MV/cm is reported. A similar quenching behavior is also reported for thin films of the pure emitter, revealing an important luminescence loss mechanism for aggregated emitter molecules. These results are interpreted by considering Coulomb stabilized excitons in the type II heterostructure and in the pure emitter that become very sensitive to dissociation upon application of the field. These results clarify the role of external electric field quenching on the phosphorescence of triplet emitters and provide useful insights for the design of deep-blue electrophosphorescent devices with a reduced efficiency roll-off.

Keywords

OLED, electroluminescence, organometallic complexes, polaron

Introduction

Organic light emitting diodes (OLEDs) based on phosphorescent compounds represent a new promising way to produce efficient light sources with low costs.[1, 2] Among the various applications full color displays and lighting sources are demanding the use of emitters covering the complete visible spectral range. While red and green OLEDs have been developed with success, the blue part of the spectrum (λ < 470 nm) is still challenging.[3-5] Currently, most of the research is therefore focused on developing materials emitting in the deep-blue to be later combined with green and red emitters.[6, 7] Owing to the multi-stack architectures (transport and emitting layers) typically used in highly efficient OLEDs,[1, 8] efficient blue emission can be achieved by the design of several high band-gap materials making up the device. Large bandgaps are strictly necessary to guarantee the exciton confinement in the emitting layer, avoiding losses caused by back energy transfer from the emitter to the host.[9] Therefore, not only emitter molecules, but also high band-gap electron and hole transporting and host materials need to be developed. The challenges encountered so far in producing blue phosphorescent OLEDs can be summarized as follows: i) suitable deep-blue phosphors with short phosphorescence lifetimes and high efficiencies,[6, 7, 10] ii) development of host materials with good charge transport properties, maintaining high triplet level for blue triplet exciton confinement.[11, 12] iii) HOMO and lowest unoccupied molecular orbital (LUMO) levels of the host matching the ones of the adjacent charge transporting layers for optimal hole and electron injection, respectively.

In a recent publication we have investigated the physical parameters controlling the radiative rate of deep-blue emitters.[7] Here, we use one of these efficient emitters dispersed in various hosts to clarify the role of electric field quenching on the phosphorescence efficiency of the emitting layer. When organic molecules or polymers are used as hosts, the large exchange interaction (~800 meV) typical of these materials,[13-15] requires high band-gaps (>3.6eV) to assure triplet exciton confinement on blue phosphors (emission energy ~ 2.8 eV). Such large band-gaps can necessitate high operating voltages, in order to reach the current densities ensuring high external efficiencies. A second viable approach considers the use of molecules with an energy gap similar to the emitter. This

could lead to a good matching of levels with the HOMO and LUMO of the p-type and n-type transport layers. As discussed above, the triplet excitonic level should be maintained high to effectively confine the triplet excitons on the emitter molecule. An elegant way for obtaining host with such characteristics is the use of organometallic molecules, where the mixing of singlet and triplet states lead to a decreased exchange interaction.[7, 9] In this situation the triplet confinement can be reached without the need for a wide electronic band-gap. Such an approach has been recently exploited for red emitting OLEDs resulting in lower turn on voltages and higher efficiencies at a low current densities.[16] However, in contrast to this beneficial effect the use of host molecules with a narrower HOMO-LUMO gap can lead to type II energy level configurations between the emitter and the host,[16, 17] potentially impacting the radiative recombination of excitons during device operation at high brightness. We remind that type I, type II terminology, originally introduced for inorganic semiconductor heterostructures, refers to molecular heterojunctions, differing in the alignment of HOMOs and LUMOs. In the case of both the HOMO and LUMO of one material lying inside the ones of the other, one has a type I system. In type II, both the HOMO and LUMO are at higher energy with respect to the corresponding orbitals of the other material (Fig.1(b)).

Here, we present a new series of molecular hosts with the goal in mind of understanding the role of type I and type II host/emitter energy level alignment on the electric field induced quenching. While other quenching processes occurring in OLEDs, like triplet-triplet exciton annihilation, are well documented[18, 19] and can be limited with an appropriate design of the organic layers in the device, electric field induced quenching has been only partially investigated, sometimes with diverse conclusions.[20, 21] Such an effect appears to be significant for deep-blue emitters, where operating voltages are higher than for green and red. We demonstrate that the type II alignment results in a significant electric-field induced quenching (up to 25 %) at a field of 2 MV/cm. In addition, we show a strong dependence of the quenching on the emitter aggregation which represents an important finding for the interpretation of the efficiency roll-off in OLEDs. The results are interpreted by considering the presence of Coulomb stabilized excitons in the type II system and in the aggregated molecules. Indeed, in these two systems the exciton binding energy keeps

electron and hole bound for radiative recombination. Upon application of the electric field electrons and holes dissociate via a favorable transfer to the host. The dissociation results in the formation of long lived polaron pairs or free polarons according to the density of states available for the escape of charge carriers from the Coulomb potential. In contrast for the type I system carriers remain confined on the emitter, resulting in negligible quenching at field magnitudes relevant for OLEDs.

Results

Figure 1(a) shows the phosphorescence spectra of the three molecular compounds considered in our experiments, together with the chemical structures in the respective insets. Methods for synthesis along with the chemical characterization are reported in the supporting information. In the top panel the spectrum of the iridium complex iridium *tris*(1-cyanophenyl-3-methylbenzimidazolin-2-yilidene-*C*,$C^{2'}$) ($Ir(cnbic)_3$) shows emission in the deep-blue region of the visible spectrum peaking at 450 nm. The high quantum efficiency (~80%) and short phosphorescence lifetime (<10 μs)[7] make this material an ideal emitter in the deep-blue. $Ir(cnbic)_3$ will be hereafter referred as *emitter* and dispersed at low concentration (7% w/w) in various hosts. The host materials, iridium *tris*(1,3-diphenyl)benzimidazolin-2-yilidene-*C*,$C^{2'}$) ($Ir(dpbic)_3$) and 2,4-Bis(phenoxy)-6-(3-methyldiphenylamino)-1,3,5-triazine (BPMT), are reported in the middle and lower panel of Figure 1(a), respectively. The phosphorescence spectrum of BPMT, a namely fluorescent compound, was observed exclusively by low temperature gated spectroscopy.[13] While both the energy levels of host triplet excitons are higher with respect to the one of the emitter (Fig.1(a)), the alignment of the HOMO levels differs, creating type I and type II configurations in the case of BPMT and $Ir(dpbic)_3$, respectively (Fig. 1(b)). Our material combinations are, therefore, ideal for efficient triplet exciton transfer and confinement on the emitter, while potentially showing diverse behaviours for the dynamics of one type of charge carriers, i.e. holes. The exciton confinement is verified by the detection of exclusively emitter PL, upon excitation of the host/emitter films. This demonstrates that despite the type II configuration, excitons on the emitter are capable of emitting light, being stabilized by the strong binding energy in the triplet exciton. Fig. 1(b) shows in

addition the level alignment for a sample made of only $Ir(cnbic)_3$ molecules, in which the emitter is its own host.

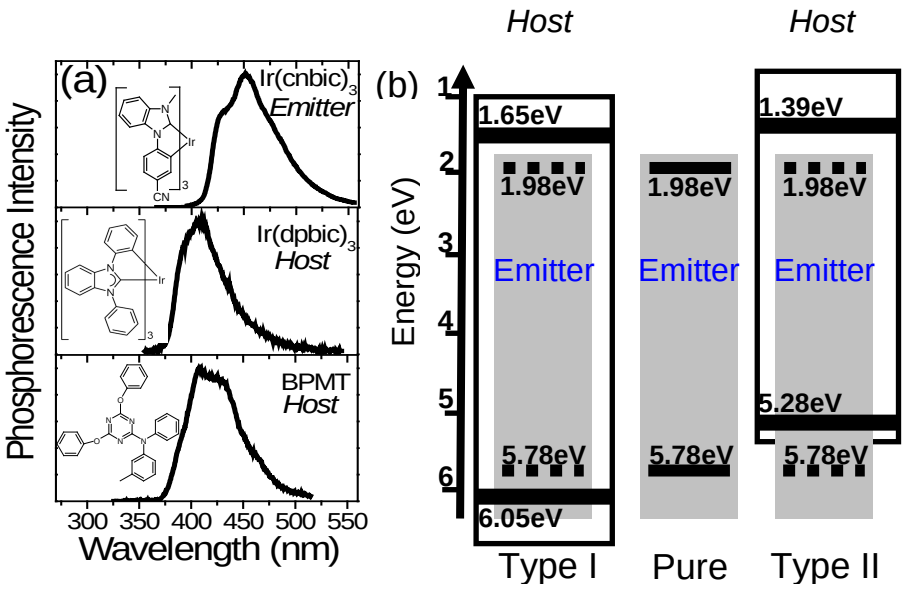

Figure 1: a) Phosphorescence spectra of the emitter $Ir(cnbic)_3$ and the two hosts $Ir(dpbic)_3$ and BPMT. All the spectra were obtained with the molecules dispersed in a thin film of PMMA. The spectra of $Ir(cnbic)_3$ and $Ir(dpbic)_3$ were recorded at room temperature for BPMT (T = 5K). Excitation was performed at 337 nm. The insets show the chemical structures of the compounds. b) Energy level diagram of the samples used to investigate electric field quenching. The HOMO and LUMO levels for the different materials are indicated. Solid lines are for the host, the dashed lines represent the levels of the dispersed emitter molecules. When the emitter molecule ($Ir(cnbic)_3$) is dispersed in the host BPMT a type I heterostructure is formed. In the case of the pure emitter film, molecules with the same HOMO and LUMO are closed packed. For $Ir(cnbic)_3$ in $Ir(dpbic)_3$ a type II heterojunction is formed. The HOMO and LUMO levels were extracted from density functional theory (DFT) calculations

In order to study the modulation of the emitter phosphorescence intensity upon the application of an electric field, we prepared sandwich structures, where the emitter is dispersed in the hosts at low concentration (7% w/w). We have observed that this is well below the threshold concentration (20%) at which emitter-emitter aggregation influences the electric field induced quenching (see Fig. S2 in supporting information). The different films were prepared by spin coating from chloroform solutions on top of silicon oxide (SiOx) (thickness 10 nm) coated indium-tin-oxide (ITO) substrates. A second SiOx layer was deposited on the organic thin film (thickness ~125 nm) before the evaporation of the top Al electrode. A scheme of the structure is shown in the inset of Fig. S2. The SiOx layers and a

reverse bias configuration assured a low current density, not exceeding 1 A/m^2 at 2MV/cm. This was necessary to study the effect of the electric field in the absence of carrier injection and therefore exciton-polaron quenching. Indeed several reports have shown how exciton-polaron quenching starts to be relevant (>3%) for larger currents typically 10 A/m^2 [[20, 22]]. In addition to the two host/emitter samples, thin films of pure and dispersed in polymethyl-methacrylate (PMMA) Ir(cnbic)$_3$ were studied, for a total of four samples.

Figure 2 shows relative field induced changes in the Ir(cnbic)$_3$ PL intensity ([PL-PL(*F*)]/PL=ΔPL(*F*)/PL), excited at 337 nm, as a function of the electric field amplitude *F*. The relative changes were calculated integrating the intensity on the overall emitter PL spectrum. The inset shows an example of PL spectra for the type II combination, in the presence (red line) and absence (black line) of the external electric field. The data points in the main figure summarize the experiments for the four previously described samples. While a negligible quenching (ΔPL(F)/PL<2%) is observed for the type I configuration (blue triangles), a quenching up to 23% is observed for the type II (black dots) at 2 MV/cm. This apparently high electric field corresponds to an applied voltage of 25 V on a ~125 nm thin film, an experimental configuration potentially reached in OLEDs when operated at high brightness,[9] or in the presence of charge accumulation at the interfaces of thin emitting layers.[23] Interestingly, also the thin film obtained from the pristine emitter (green stars) shows a pronounced quenching (12%) at the same field amplitude. This last result is similar to what observed in films of pristine conjugated polymers, where intrachain excitons can be separated in electrons and holes localized onto two adjacent conjugated segments.[24, 25] An intermolecular exciton separation is supported by the flat PL quenching curve of the sample Ir(cnbic)$_3$/PMMA (orange squares) and by the concentration dependent measurements of Fig. S2. Therefore, emitter molecules which are close packed or aggregated give rise to exciton separation and PL quenching in the presence of an external electric field. We note that the relative quenching is not linear with the applied field but tends to saturate after 1.75 MV/cm for pure emitter and type II. While the absence of a linear behaviour excludes space charge effect, the saturation is a typical feature explained by the field induced separation of polaron pairs.[21, 26] The saturation can be effectively fitted according to the

Onsager model, which has been extensively used to describe the effect of the external field on the luminescence of organic materials[21, 27] (see supporting information). We have fitted the quenching with this model extracting an average value for the polaron pairs radius. We obtained 2.16 nm and 2.70 nm for type II and the pure emitter, respectively.

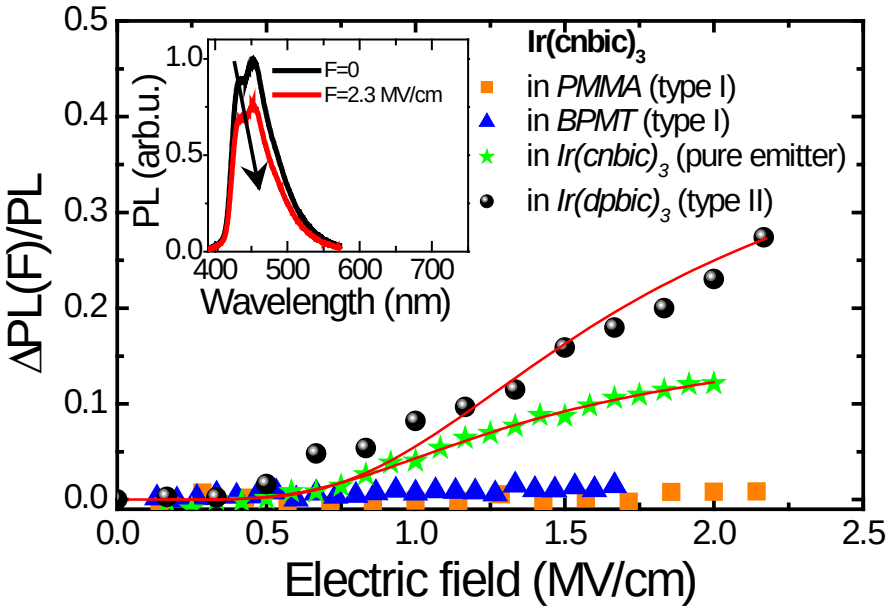

Figure 2: Field induced relative quenching (ΔPL(*F*)/PL) plotted as a function of the applied electric field. The data points are obtained by integrating the PL spectrum of the emitter molecule ($Ir(cnbic)_3$). Four different samples are reported in which $Ir(cnbic)_3$ is dispersed in: PMMA (type I (orange squares)), BPMT (type I (blue triangles)), Ir(cnbic) (pure emitter (green stars)) and $Ir(dpbic)_3$ (type II (black dots)). The red lines represent fits according to the Onsager model. See text for details. The inset shows an example of PL spectra in the presence (red solid line) and absence (black solid line) of the external electric field for the type II structure. Excitation is performed at 337 nm

The results of figure 2 have clear implications for the design of OLEDs based on deep-blue emitters operating at high voltages. A major consequence is the choice of host materials with a type I alignment with respect to the emitter HOMO and LUMO, beside the established guideline of higher triplet energy levels.[28] More importantly, focusing on the behaviour of the pure emitter, we note that aggregated molecules can have an important role in the electric field quenching phenomena. Considering more generally effects of quenching on the efficiency of OLEDs, researchers have considered several processes. Beside the well documented triplet-triplet exciton annihilation,[18, 29, 30] exciton-polaron quenching together with electric field induced quenching have been proposed. According to our results the electric field induced quenching can be very sensitive to the emitter

concentration and host/guest combination, an issue which was not systematically discussed in previous reports.[20, 21, 27, 31] We stress here that a complete modelling of the quenching phenomena contributing to the roll-off of electroluminescence in devices, should in addition consider exciton-exciton and exciton-polaron annihilation phenomena.

We now turn our attention on the mechanism of field induced quenching. In all the experiments reported in figure 2 excitons were created preferentially on the emitter but also on the host material (excitation at 337 nm). As a consequence the phosphorescence quenching could originate both from excitons dissociating in highly excited states before relaxation to the emitting level and also from the dissociation of thermalized emitter excitons. To clarify the mechanism involved in the emitter PL quenching we have analyzed the time resolved decays of the PL, in the presence and absence of the field. The inset of Figure 3(a) show the effect of the field on the decay curves for the type II alignment ($Ir(cnbic)_3$ in $Ir(dpbic)_3$). Upon application of the electric field both the PL lifetime (τ) and the signal amplitude (I_0) are influenced. In the presence of the field, we have noticed a slight deviation from a mono-exponential decay. The decays can be better fitted with two time constants which, however, remain very similar. We note that the second decay component is probably originating from a delayed recombination of polaron pairs (see below). Therefore, for our analysis we have considered the first component, which is more sensitive to field variations. Changes in amplitude can be better observed by focusing on the shorter time scale displayed in the inset of Fig.3(b). Amplitude quenching suggests the dissociation of part of the excitons, during the thermalization process, while the shortening of the lifetime is witnessing exciton dissociation once thermalization to the emitting level is completed. We performed this kind of experiment also for the pure emitter and the emitter in the type I configuration and plotted the relative variation of the lifetime ($\Delta\tau(F)/\tau$) and amplitude ($\Delta I_0(F)/I_0$) as a function of the applied field (Fig. 3 main figures). For the type I configuration (blue triangles) the variation in lifetime and amplitude intensity is negligible. This is consistent with the steady state measurements (Fig.2). In contrast the type II structure shows large changes (black dots). As commented above, we observe a decrease in the amplitude I_0 suggesting a separation of excitons precursors. In addition, the

shortening of the emitter lifetime is a clear indication of exciton separation after thermalization. The data points for the pristine emitter are shown as green stars. For low values of the electric field (> 1 MV/cm), $\Delta I_0(F)/I_0$ shows a small change which saturates at about 2% (Fig.3(b)), whereas $\Delta\tau(F)/\tau$ is increasing after 1.2 MV/cm (Fig.3(a)).

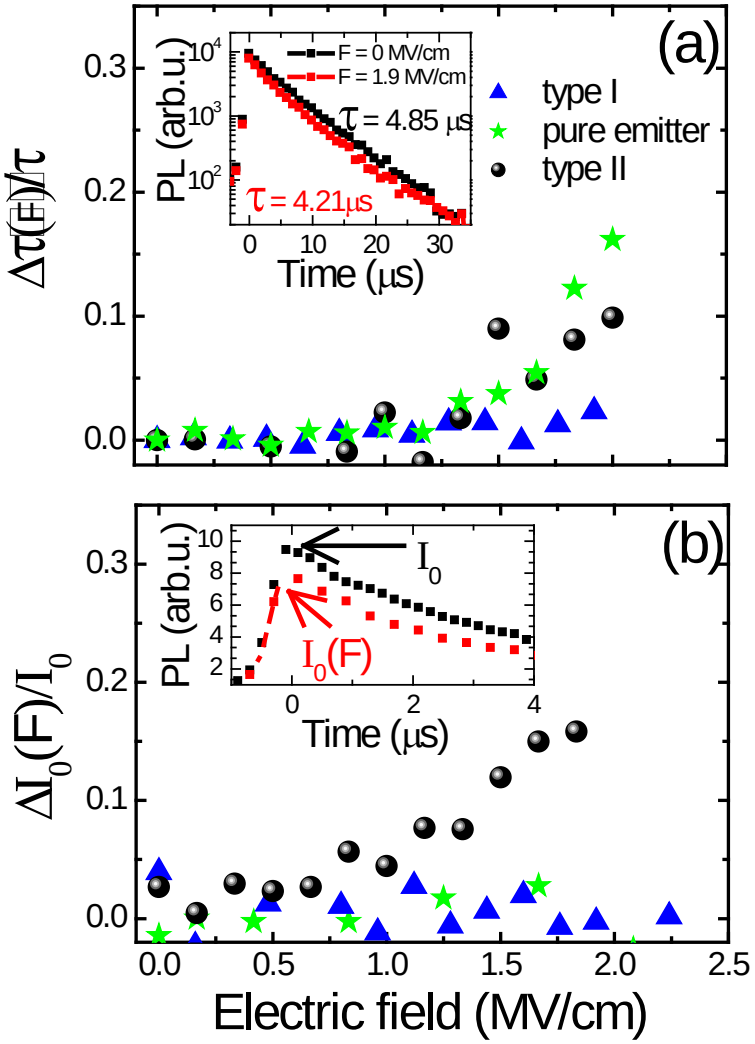

Figure 3: a) Relative change in the emitter PL lifetime ($\Delta\tau(F)/\tau$) as a function of the applied electric field in type II (black dots), pure emitter (green stars) and type I (blue triangles). The inset shows two decay curves in the presence (red squares) and absence (black squares) of the external field for the type II sample. b) Relative change in the intensity of PL at zero delay time $\Delta I_0(F)/I_0$ (amplitude quenching) for the same three samples of panel a. The inset shows an example of quenching in the intensity at zero delay for the type II sample, black squares represent data at zero applied field while the red at 1.9 MV/cm.

Discussion

The results reported in figure 2 clarify the role of energy level alignment in controlling the electric field induced quenching of phosphorescent emitters. While this issue has attracted much interest,[20, 21, 27] our experiments demonstrate that the quenching is strongly dependent on host/emitter energy level alignment and field amplitude. Both the type II and the pure emitter configurations lead to a strong quenching, which is likely due to exciton dissociation. This is supported by observing a lower PL quantum yield for the type II structure (50%) when compared to the type I (~80%), in the absence of the external field. This is due to a non negligible probability of exciton dissociation in the initial non-thermalized state, i.e. before relaxation to the emitting level and formation of a Coulomb stabilized exciton. Therefore, our results should be interpreted according to the differences in host/emitter energy level alignment in the presence of the field.

Field induced quenching of luminescence has been extensively studied in thin films of pristine and dispersed conjugated polymers.[24, 32] In such fluorescent materials the lifetime of singlet excitons is typically in the sub-nanosecond time range. Therefore a fast (~10 ps) field dissociation time has been invoked to explain the quenching phenomena with magnitudes up to 30%. In contrast to polymers, triplet emitters show microsecond recombination times for the spin-forbidden phosphorescent transitions. Assuming a similar time scale for field quenching, it should be possible to dissociate very efficiently the long lived excitons populating the triplet state. Our data on the pure and type II sample show, however, a comparable or lower quenching magnitudes with respect to conjugated polymers. To understand this issue and interpret the origin of the significant differences reported in our experiments, we have considered the energy level configurations of the different samples.

Figure 4 shows a simplified scheme in a *one-particle picture*, for the energy of an electron and a hole building an exciton on the emitter molecule in the three most relevant samples. To consider non thermalized states we have drawn two levels for the hole and the electron, respectively. The closest ones are stabilized by the Coulomb interaction (here schematically shown as a black dotted line) and correspond to the emitting triplet exciton. The exciton

binding energy was estimated subtracting the emission energy from the HOMO and LUMO gap of Fig.1. We start by considering the type I configuration, where the HOMO and LUMO of the emitter (green levels) are both at lower energy with respect to the ones of BPMT (blue levels). The effect of the external electric field is to modify the Coulomb potential profile destabilizing the excitonic levels.[33] In this situation the exciton can dissociate, provided that a density of states for charge transfer is available in the surrounding of the emitter molecule. This last condition is not satisfied for the type I alignment. Therefore, the absence of available states for electron or hole escape, both in the non-thermalized and in the excitonic level, results in a negligible quenching for the field strengths investigated in our experiments.

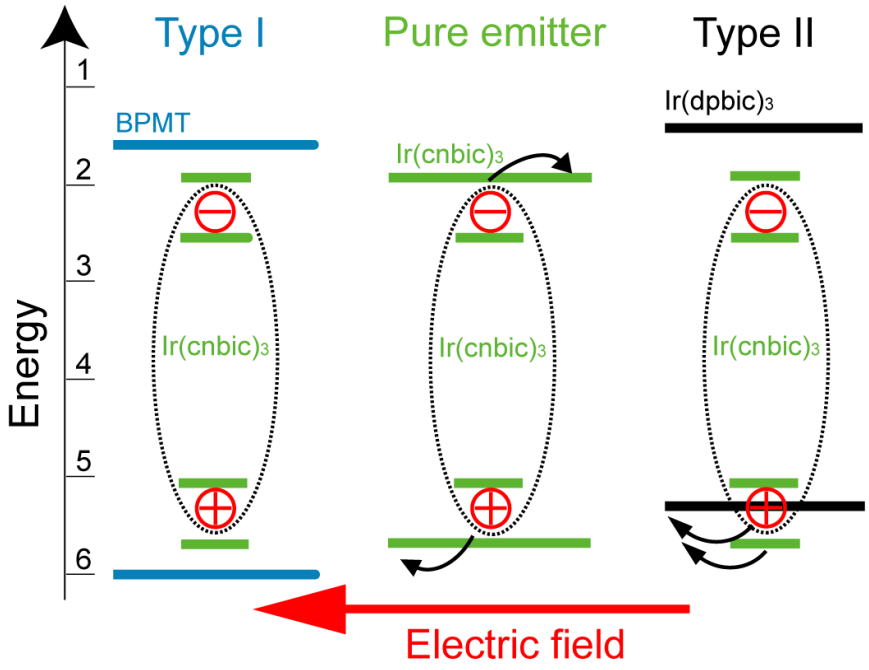

Figure 4: Schematic representation of the energy levels for the different host/emitter combinations. The HOMO and LUMO levels of the hosts and emitter are shown together with the *excitonic levels*. These levels are inside the black dotted circle indicating their excitonic nature. Their closed spacing with respect to the HOMO and LUMO of the emitter is due to the binding energy. The curved arrows show possible exciton separation processes upon application of the external electric field. This results in the transfer of an electron or a hole to the surrounding molecules that constitute the host material. In the pure emitter both the HOMO and LUMO of the surrounding emitter molecules provide a density of states for charge separation. The type II structure promotes exciton dissociation by hole transfer.

We now turn to the case of the film formed exclusively by emitter molecules (pure emitter). From the energy scheme we identify two possibilities for charge separation in the pristine emitter film, i.e. hole as well as electron transfer to the surrounding acceptor

molecules. In a similar way to conjugated polymers the charge separation may be promoted by energetic disorder in the system.[25] We have indeed observed a red shifted component in the PL spectrum of this film (not shown), witnessing the presence of low energy sites. Such low energy states might facilitate charge separation in the presence of the field. The limited *amplitude quenching* reported in Fig. 3 is correlated to a more pronounced exciton separation in the emitting state. A specific scheme describes the type II material combination. The host HOMO (black solid line) is at higher energy with respect to the one of the emitter, while the excitonic levels keep the exciton bound. Therefore, the external field by destabilizing the exciton promotes the separation with hole transfer to the host (curved arrow). As indicated in the figure and confirmed by the time resolved experiments (Fig.3) the transfer can occur both in the emitting and in the precursor states. From an energetic point of view, the type II structure increases the density of available states for the hole to escape. The larger contribution of amplitude quenching at low fields (Fig.3b) is confirmed in our picture, since non thermalized states require only a small field for the separation to occur. We stress that the quenching in the type II combination, where electrons remain trapped on the emitter molecule and only holes have available states for the separation may differ from the pure emitter. In the latter case exciton dissociation should generate both electrons and holes, which are free to drift by hopping among the different molecular sites. Summarizing the mechanism reported in Fig. 4, we note that electric field induced quenching strongly depends on the density of available states for charge separation. Because of the peculiar energy alignment this makes exciton dissociation highly probable for type II and pure emitter structures.

To further investigate the products resulting from exciton separation, we performed quenching measurements in the presence of a pulsed electric field. Such a technique proved to be sensitive to the formation of polaron pairs or free polarons, according to the recovery of PL intensity after the field pulse. In the case of field stabilized polaron pairs, excitons should be regenerated after the release of the field and part of the quenched PL intensity is recovered in a PL burst.[25, 34] The inset of Figure 5 shows a timing scheme for such kind of transient experiment. In brief, the field is applied during the photoexcitation

event and turned off after 80 μs. A scanning gated detection of 3 μs temporal width (black rectangle in the inset) is shifted in time to record point by point the PL intensity from the emitter. In the main panel of Fig. 5 we present typical data for the type II combination $Ir(cnbic)_3$ in $Ir(dpbic)_3$ (dots). Corresponding to the instant in which the electric filed pulse ends (80 μs) a burst in the PL intensity is observed. This result implies the creation of polaron pairs partially stabilized by a long range Coulomb potential. The pairs appear as a burst of emission due to the regeneration of triplet excitons, once the electric field is turned off. For the type II structure shown here, it is conceivable that holes are trapped in the $Ir(dpbic)_3$ HOMO levels, while the electrons remain localized on the emitter molecule (see energy scheme in Fig. 4). In contrast to this behaviour, the pure emitter sample shows an almost undetectable PL burst (stars). From these results we infer that polaron-pair states are much less stable in this sample. Interestingly, this correlates with the larger values of the polaron pair radius we reported above, extracted from the Onsager fit. Apparently the presence of localization sites for at least one type of charge carrier is a necessary condition to observe polaron pairs.

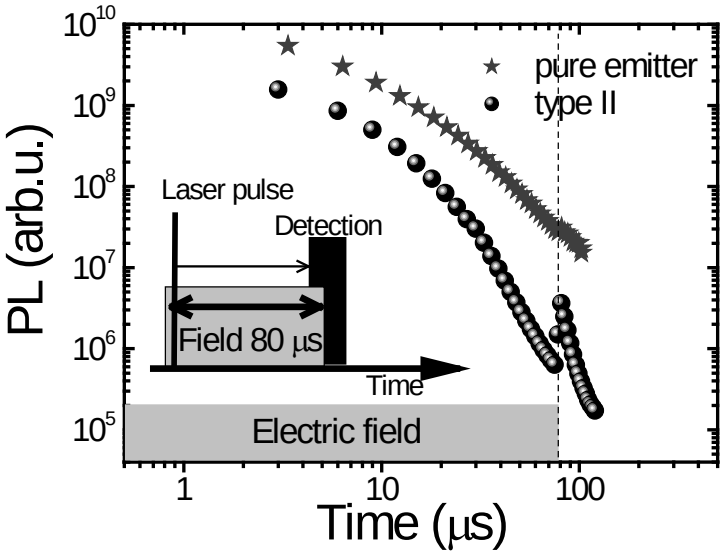

Figure 5: PL decay in the presence of an electric field pulse for the pure emitter (stars) and the type II structure (dots). The field pulse is applied for 80 μs starting in correspondence of the laser pulse. The detection window (3 μs) is moved at different delays with respect to the laser pulse during the field pulse and after its turning off. The inset shows a timing scheme for the experiment. The laser pulse is indicated as a vertical line, the grey rectangle indicates the electric field pulse duration and the black rectangle the detection window.

We discuss now the discrepancy between the fast induced quenching (ps) observed in conjugated polymers and the comparable quenching, though with three orders of magnitude longer excited state lifetimes, observed here in a triplet emitter. We remind that charge separation in organic semiconductors can involve two steps. An initial separation of the electron and hole resulting in the formation of polaron pairs (see above) and the subsequent generation of free polarons.[35] The first step is limited by the exciton binding energy which is about 0.4 eV for most studied conjugated polymers.[36, 37] In the presence of loosely bound polaron pairs (pristine emitter), the exciton dissociation is likely to be the limiting step. The exciton binding energy of small molecules is known to be larger than the value reported for conjugated polymers.[38] For $Ir(cnbic)_3$ the HOMO LUMO difference predicts an electronic bandgap of 3.8 eV (Fig.1(b)). By considering the optical gap of the emitting state (2.91 eV from Fig.1(a)) we can estimate an exciton binding energy of about 0.9 eV. This relatively large value should influence the rate of escape of charge carriers from the mutual Coulomb potential of the excitonic level (Fig.4). Figure 6 show the escape rate ($k_e(F)$) as a function of the electric field for the pure emitter and the type II. The rate has been evaluated considering that the exciton recombination rate is described by the following equation:

$$k(F) = k_r + k_{nr} + k_e(F) \qquad (1)$$

where k_r and k_{nr} are the radiative and non radiative rate, respectively. In this equation all the values apart from the escape rate are known, with the reasonable assumption that k_r and k_{nr} are not influenced by the field amplitudes considered in our experiments. Such an assumption is supported by the negligible quenching of the emitter in PMMA (Fig. 2). Similarly to the case of polymers, the escape rates reported in Fig. 6 are of the same order of magnitude with respect to the recombination rate (for our emitter ~10^5 s^{-1}). It is therefore not surprising that the quenching is similar or lower to the one observed in polymers, though the recombination rate is at least four orders of magnitude longer (phosphorescence). The long escape rate of our blue emitter can be interpreted taking into account the high binding energy. Since an exponential dependence of the escape rate on

the binding energy (E_b) has to be expected $k_e \sim e^{-E_b/kT}$, a factor of two in the binding energy, readily results in a difference of seven orders of magnitude in the escape rate between the two material systems.

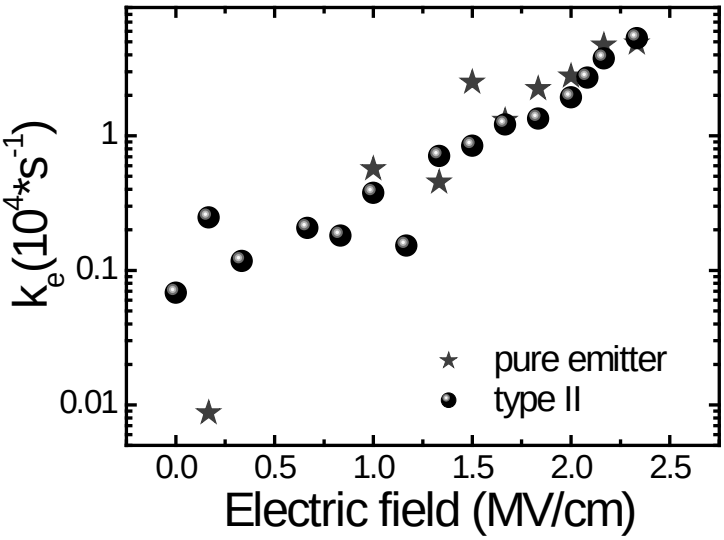

Figure 6: Escape rate k_e as a function of the external electric field. Data points were obtained from equation (1) in the text. Stars indicate data for the pure emitter and dots for the type II structure.

Conclusions

In conclusion, we have investigated the electric field induced quenching in the PL intensity of the deep-blue emitter $Ir(cnbic)_3$ in combination with several host materials building type I and type II molecular heterostructures. We report a strong field dependent quenching of the phosphorescence for thin films of the pure emitter and the type II heterostructure. These results highlight the importance of energy level alignment in the choice of suitable matrix materials for hosting deep-blue phosphors, in addition to the well-known guideline of a higher triplet level. By time resolving the PL in the presence of the field we provide useful insights in the quenching mechanism. In particular, we demonstrated that dissociation occurs preferentially for Coulomb stabilized excitons, when the external field overcomes the binding energy and accepting states are available for charge transfer. Additionally, we report a long lasting formation of polaron pairs, if one of the two charge carriers forming the exciton remains trapped on the emitter. The phosphorescence

quenching has immediate consequences for the optimization of deep-blue emitting OLEDs. While several aspects contribute to the efficiency of electroluminescence, such as charge injection, carrier balance, triplet-polaron quenching[20, 22] and exciton annihilation,[11, 20] electric field induced quenching becomes critical when large local field are building up at interfaces[23] and for particular HOMO-LUMO alignment between emitter and host, as demonstrated in this study. For deep-blue emitters the design of interfaces becomes critical as a consequence of high band-gap materials. While triplet-polaron quenching has been recognized as less critical in explaining the roll-off of the electroluminescence efficiency with respect to TTA, this might not hold true for deep-blue emitters where charge accumulation at organic heterojunctions or high driving voltages could results in high field We conclude that type I structures can reduce substantially the quenching for fields up to 2 MV/cm. On the contrary an effect can be observed at relatively low driving voltages (6.25V = 0.5 MV/cm) in the case of type II configurations. These experiments should provide valuable insights for the design of blue electrophosphorescent OLEDs and more generally other organic electroluminescent devices, where large driving electric fields are involved and high electroluminescence efficiencies are critical.[39, 40]

Experimental

Details about synthesis and purification of the materials can be found in the supporting information. The HOMO and LUMO of the materials used were determined via density functional calculations. For the ionization potential (HOMO) and the electron affinity (LUMO) first the geometry of the neutral as well as the charged states were optimized using the BP86-functional[41, 42], in combination with a split-valence basis set (SV(P)) including polarization functions on all heavy atoms.[43] For iridium an effective core potential was employed.[44] For the energetics single point calculations at the optimized geometries using the same functional in combination with a valence triple zeta basis set (TZVP) were conducted. To account for dielectric solid state effects a ultraviolet photoelectron spectroscopy/inverse electron photoemission spectroscopy UPS/IEPS-calibrated version of the conductor like screening model (COSMO)[45] was used in conjunction with the single point calculations. All calculations were carried out with the

turbomole program package.[46] These data were compared with cyclic voltammetry curves and UPS showing a reasonable agreement, with a variance smaller than 0.3 eV.

Sample preparation was carried on in a nitrogen glove-box equipped with a vacuum chamber for the evaporation of the SiOx and Al layers. As mentioned above SiOx blocking layers were used to minimize charge carrier injection upon the application of voltage and to avoid quenching by the surface plasmons at the metallic interfaces. Similar results in the PL intensity modulation were obtained using 10 nm of LiF instead of SiOx (not shown) clarifying the intrinsic nature of the effects in contrast to interfacial phenomena.[47] For the solubilization of the materials before spin-coating only spectroscopic grade solvents were used. The average thickness of the organic films (100 ± 20 nm) was determined by a scanning profilometer. PL excitation was performed at 337 nm with a nitrogen pulsed laser (500 ps, 50 Hz rep. rate) exciting both the emitter and the matrix molecules. Light excitation and detection was performed on the ITO side of the structures. Such an excitation wavelength, well above the emitter first excited state, mimics the electroluminescence processes taking place in real devices, where hot excitons are formed on the emitter, after electron and hole capture from the host material. All the measurements were performed at low excitation power and in absence of bi-excitonic quenching processes, as proved by the monoexponential decays of phosphorescence (see inset of Fig. 3(a)). Therefore, all the experiments were performed in the absence of triplet-triplet annihilation and exciton-polaron quenching, in order to provide a genuine estimation of electric field induced effects.

For the all the PL measurements samples were kept under a dynamic vacuum of 10^{-6} mbar at room temperature, only the spectrum in the lower panel of Fig. 1(a) was measured at T = 5K. PL spectra were recorded using an intensified CCD camera or a single sweep streak camera for the time resolved decays. PL quantum yield was measured with an integrating sphere saturated with nitrogen at room temperature. The application of an electric field was accomplished by Keithley source or a pulse generator in the case of the data reported in Fig.5.

References

[1] Y. R. Sun, N. C. Giebink, H. Kanno, B. W. Ma, M. E. Thompson, S. R. Forrest, *Nature* **2006**, *440*, 908.

[2] M. A. Baldo, D. F. O'Brien, Y. You, A. Shoustikov, S. Sibley, M. E. Thompson, S. R. Forrest, *Nature* **1998**, *395*, 151.

[3] S. J. Su, E. Gonmori, H. Sasabe, J. Kido, *Advanced Materials* **2008**, *20*, 4189.

[4] N. Chopra, J. Lee, Y. Zheng, S. H. Eom, J. G. Xue, F. So, *Applied Physics Letters* **2008**, *93*.

[5] M. E. Thompson, *Materials Research Bulletin* **2007**, *32*, 694.

[6] T. Sajoto, P. I. Djurovich, A. Tamayo, M. Yousufuddin, R. Bau, M. E. Thompson, R. J. Holmes, S. R. Forrest, *Inorganic Chemistry* **2005**, *44*, 7992.

[7] S. Haneder, E. Da Como, J. Feldmann, J. M. Lupton, C. Lennartz, P. Erk, E. Fuchs, O. Molt, I. Münster, C. Schildknecht, G. Wagenblast, *Advanced Materials* **2008**, *20*, 3325.

[8] B. W. D'Andrade, S. R. Forrest, *Advanced Materials* **2004**, *16*, 1585.

[9] H. Yersin, *Highly efficient OLEDs with Phosphorescent Materials*, Wiley-VCH, Weinheim, Germany, **2008**.

[10] S. J. Yeh, M. F. Wu, C. T. Chen, Y. H. Song, Y. Chi, M. H. Ho, S. F. Hsu, C. H. Chen, *Advanced Materials* **2005**, *17*, 285.

[11] M. A. Baldo, C. Adachi, S. R. Forrest, *Physical Review B* **2000**, *62*, 10967.

[12] F. C. Chen, G. F. He, Y. Yang, *Applied Physics Letters* **2003**, *82*, 1006.

[13] Y. V. Romanovskii, A. Gerhard, B. Schweitzer, U. Scherf, R. I. Personov, H. Bässler, *Physical Review Letters* **2000**, *84*, 1027.

[14] A. P. Monkman, H. D. Burrows, L. J. Hartwell, L. E. Horsburgh, I. Hamblett, S. Navaratnam, *Physical Review Letters* **2001**, *86*, 1358.

[15] A. Zahlan, *The Triplet State*, Cambridge University Press, London, **1967**.

[16] T. Tsuzuki, S. Tokito, *Advanced Materials* **2007**, *19*, 276.

[17] T. Tsuzuki, S. Tokito, *Applied Physics Express* **2008**, *1*, 021805.

[18] M. A. Baldo, S. R. Forrest, *Physical Review B* **2000**, *62*, 10958.

[19] J. C. Ribierre, A. Ruseckas, K. Knights, S. V. Staton, N. Cumpstey, P. L. Burn, I. D. W. Samuel, *Physical Review Letters* **2008**, *100*, 017402.

[20] S. Reineke, K. Walzer, K. Leo, *Physical Review B* **2007**, *75*, 125328.

[21] J. Kalinowski, W. Stampor, J. Mezyk, M. Cocchi, D. Virgili, V. Fattori, P. Di Marco, *Physical Review B* **2002**, *66*, 235321.

[22] D. Hertel, K. Meerholz, *Journal of Physical Chemistry B* **2007**, *111*, 12075.

[23] B. Ruhstaller, S. A. Carter, S. Barth, H. Riel, W. Riess, J. C. Scott, *Journal of Applied Physics* **2001**, *89*, 4575.

[24] R. Kersting, U. Lemmer, M. Deussen, H. J. Bakker, R. F. Mahrt, H. Kurz, V. I. Arkhipov, H. Bässler, E. O. Göbel, *Physical Review Letters* **1994**, *73*, 1440.

[25] B. Schweitzer, V. I. Arkhipov, H. Bässler, *Chemical Physics Letters* **1999**, *304*, 365.

[26] D. Hertel, E. V. Soh, H. Bassler, L. J. Rothberg, *Chemical Physics Letters* **2002**, *361*, 99.

[27] J. Kalinowski, W. Stampor, J. Szmytkowski, D. Virgili, M. Cocchi, V. Fattori, C. Sabatini, *Physical Review B* **2006**, *74*, 085316.

[28] K. Brunner, A. van Dijken, H. Borner, J. Bastiaansen, N. M. M. Kiggen, B. M. W. Langeveld, *Journal of the American Chemical Society* **2004**, *126*, 6035.

[29] W. Staroske, M. Pfeiffer, K. Leo, M. Hoffmann, *Physical Review Letters* **2007**, *98*, 197402.

[30] Y. Kawamura, J. Brooks, J. J. Brown, H. Sasabe, C. Adachi, *Physical Review Letters* **2006**, *96*, 017404.

[31] J. Mezyk, F. Meinardi, R. Tubino, M. Cocchi, *Applied Physics Letters* **2008**, *93*, 093301.

[32] M. Deussen, P. H. Bolivar, G. Wegmann, H. Kurz, H. Bässler, *Chemical Physics* **1996**, *207*, 147.

[33] M. Schwoerer, H. C. Wolf, *Organic molecular solids*, Wiley-VCH, Weinheim, **2007**.

[34] M. Reufer, M. J. Walter, P. G. Lagoudakis, B. Hummel, J. S. Kolb, H. G. Roskos, U. Scherf, J. M. Lupton, *Nature Materials* **2005**, *4*, 340.

[35] J. G. Müller, U. Lemmer, J. Feldmann, U. Scherf, *Physical Review Letters* **2002**, *88*, 147401.

[36] S. F. Alvarado, P. F. Seidler, D. G. Lidzey, D. D. C. Bradley, *Physical Review Letters* **1998**, *81*, 1082.

[37] S. Barth, H. Bässler, *Physical Review Letters* **1997**, *79*, 4445.

[38] C. Rothe, S. M. King, A. P. Monkman, *Physical Review B* **2005**, *72*, 085220.

[39] F. Cicoira, C. Santato, *Advanced Functional Materials* **2007**, *17*, 3421.

[40] M. Muccini, *Nature Materials* **2006**, *5*, 605.

[41] A. D. Becke, *Physical Review A* **1988**, *38*, 3098.

[42] J. P. Perdew, *Physical Review B* **1986**, *33*, 8822.

[43] A. Schafer, H. Horn, R. Ahlrichs, *Journal of Chemical Physics* **1992**, *97*, 2571.

[44] D. Andrae, U. Haussermann, M. Dolg, H. Stoll, H. Preuss, *Theoretica Chimica Acta* **1990**, 77, 123.

[45] A. Klamt, *Journal of Physical Chemistry* **1995**, *99*, 2224.

[46] R. Ahlrichs, M. Bar, M. Haser, H. Horn, C. Kolmel, *Chemical Physics Letters* **1989**, *162*, 165.

[47] C. Rothe, A. Monkman, *Journal of Chemical Physics* **2005**, *123*, 244904.

Supporting information for:

Effect of Electric Field on Coulomb-Stabilized Excitons in Host/Guest Systems for Deep-Blue Electrophosphorescence

Stephan Haneder,[a] Enrico Da Como,[a] Jochen Feldmann,[a] Michael M. Rothmann,[b] Peter Strohriegl,[b] Christian Lennartz,[c] Ingo Münster,[c] Christian Schildknecht,[c] Gerhard Wagenblast[c]*

[a] Photonics and Optoelectronics Group, Department of Physics and CeNS Ludwig-Maximilians-Universität, 80799, Munich (Germany)

[b] Makromolekulare Chemie I and Bayreuther Institut für Makromolekülforschung, University of Bayreuth, 95440 Bayreuth, (Germany),

[c] BASF SE, 67056, Ludwigshafen (Germany)

Synthesis of the compounds.

Iridium tris(1-cyanophenyl-3-methylbenzimidazolin-2-yilidene-C,C2´) ($Ir(cnbic)_3$) and iridium tris(1,3-diphenyl)benzimidazolin-2-yilidene-C,C2´) ($Ir(dpbic)_3$).

The organometallic synthesis is performed by combining carbene ligands with Iridium ionic complexes. This type of synthesis was first demonstrated by Hitchcok et al. [J. Organometallic Chem. 239, C 26 (1982)] for homoleptic complexes. For the specific synthesis of the compound ($Ir(cnbic)_3$) and ($Ir(dpbic)_3$), we refer to the work of Bold et al. [WO 2005/019373 A2, WO2005/019373 A3] which is available for download at http://www.freepatentsonline.com.

The two compounds were purified extensively by column chromatography (as described in the synthetic procedures) and subsequent gradient sublimation. The final purity of the compounds is 99.5%. The compounds were further characterized by high pressure liquid chromatography (HPLC) and ^{13}C-NMR spectroscopy.

$Ir(dpbic)_3$ ^{13}C NMR spectrum:

^{13}C-NMR (CD2Cl2, 125 MHz, δ): 188.7 (NCN), 149.7, 148.7, 138.0, 137.8, 132.6 (C), 136.8, 128.7, 128.2, 127.9, 127.5, 127.3, 124.5, 122.8, 121.7, 121.2, 112.5, 110.8, 110.4 (CH).

HPLC chromatography

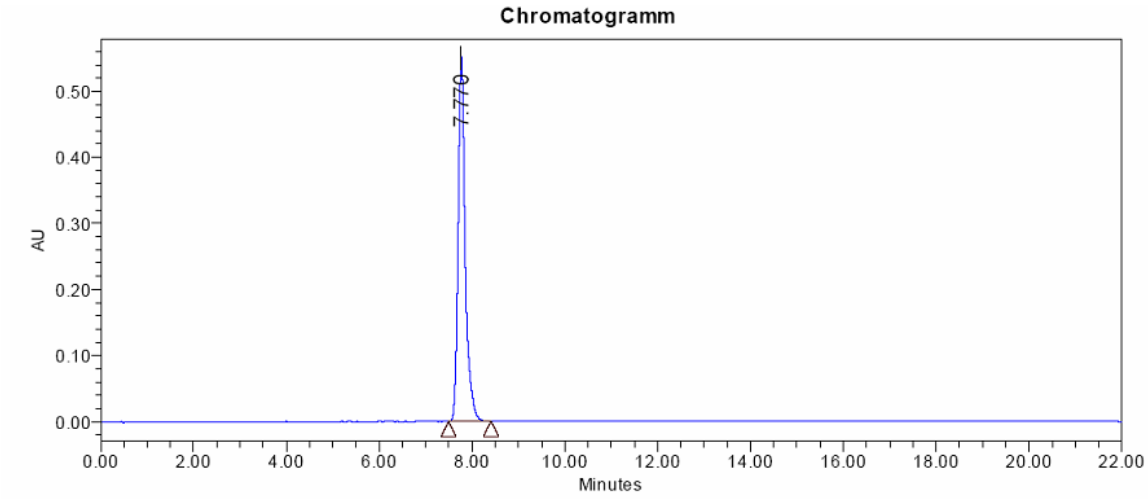

Figure S1: HPLC spectrum of Ir(dpbic)3. Tetrahydrofuran (THF) was used as eluent.

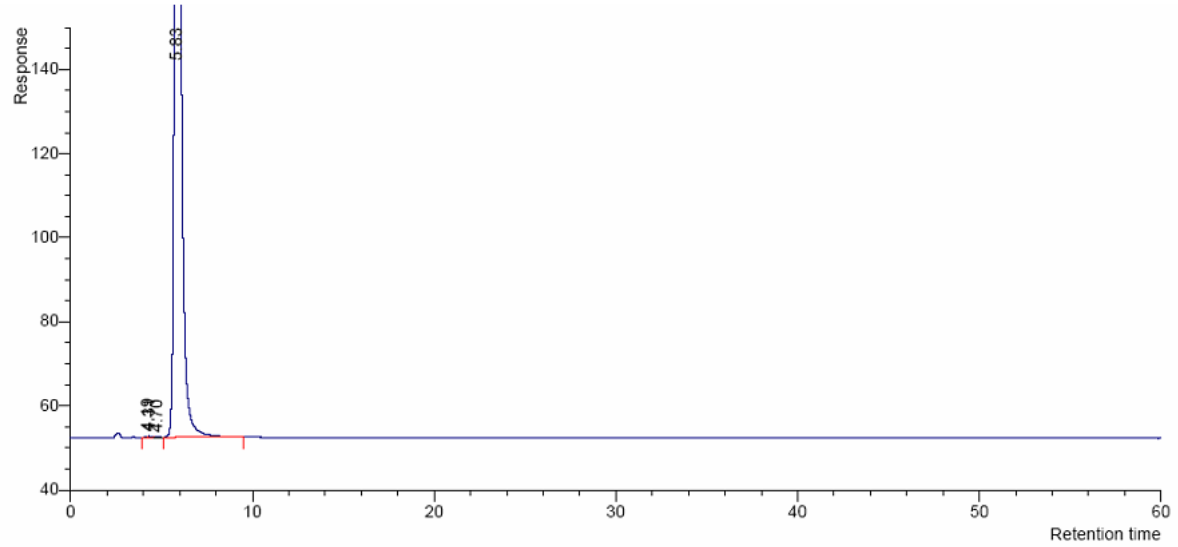

RT	Area %
4.187	0.027
4.315	0.055
4.704	0.036
5.829	99.881

Figure S2: HPLC spectrum of Ir(cnbic)3. Tetrahydrofuran (THF) was used as eluent

The HPLC spectrum for $Ir(dpbic)_3$ (Fig. S1) shows a single peak at a retention time of 7.77 minutes. Additional peaks are not detectable. For $Ir(cnbic)_3$ the HPLC spectrum of Fig. S2 shows a few peaks with different retention times, together with the main peak due to $Ir(cnbic)_3$. These are evaluated carefully by integrating the curves. The calculated areas are shown in the table at the bottom of Fig. S2. Numbers are given as percent of the overall signal. As described above the purity of these compounds is higher than 99.5%

2,4-Bisphenoxy-6-(3-methyldiphenylamino)-1,3,5-triazine (BPMT).

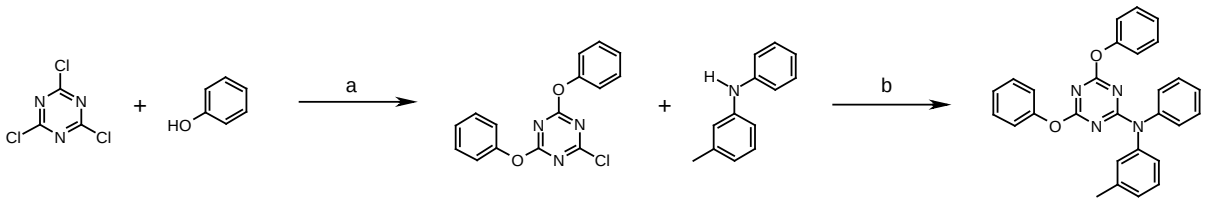

Conditions: a) NaOH, Aceton, H_2O, 15°C, 8h; b) n-BuLi, THF, 70°C, 6h;

2,4-Bisphenoxy-6-chloro-1,3,5-triazine (BPCT). 3.68 g (20 mmol) cyanuric chloride were dissolved in 200 ml acetone and cooled below 15°C. In a separate flask 3.76 g (40 mmol) phenole are reacted with 1.60 g (40 mmol) sodium hydroxide in 200 ml of water. After the formation of the sodium phenolate was complete the solution was cooled below 15°C and added drop wise to the solution of cyanuric chloride. The reaction mixture was stirred at temperatures below 15°C for 8 hours before 200 ml of water were added. The white precipitate is filtered and washed with water and ethanol. The product was purified by recrystallisation from hexane to yield 5.8 g (85%) as white crystals. ^{1}H NMR (250 MHz, $CDCl_3$): δ (ppm) 7.42-7.35 (m, 4H), 7.28-7.22 (m, 2H), 7.13 (d, 4H). EI-MS: m/z 299 (100, M^+).

2,4-Bisphenoxy-6-(3-methyldiphenylamino)-1,3,5-triazine (BPMT). 1.34 g (7.3 mmol) 3-Methyldiphenylamine were dissolved in 50 ml of dry THF under argon atmosphere in a two-necked round bottom flask equipped with a septum inlet and three way stopcock. 4.44 ml (7.1 mmol) of a n-buthyllithium/hexane solution (1.6 M) were added drop wise to the methyldiphenylamine solution and the mixture is stirred for 10 minutes. In a separate three-necked round bottom flask equipped with a septum inlet, three way stopcock and condenser 1.78 g (6.0 mmol) 2,4-bisphenoxy-6-chloro-1,3,5-triazine (BPCT) are dissolved in 50 ml dry THF under argon atmosphere. The lithium diphenylamine solution is added drop wise to the triazine solution within 10 minutes using a transfer canula. The reaction mixture is refluxed for 6 hours. After cooling to room temperature 40 ml of water are added. The product is filtered, washed with water, hexane and diethyl ether and further purified by liquid chromatographie using a hexane/thf eluent (10/1, V/V), to yield 1.35 g (51%) of **BPMT** as white solid. ^{1}H-NMR (250 MHz, $CDCl_3$) δ (ppm): 7.12-7.24 (m, 10H), 7.03-7.12 (m, 6H), 6.93-7.01 (m, 3H), 2.24 (s, 3H). ^{13}C NMR (62.5 MHz, CDCl3): δ (ppm) 172.0, 165.3, 151.9, 135.9, 128.9, 128.7, 128.6, 127.3, 127.2, 125.2, 124.5, 124.2, 121.5, 120.7, 120.6, 116.6, 17.4. EI-MS: m/z = 446 (100, M+), 353 (30).

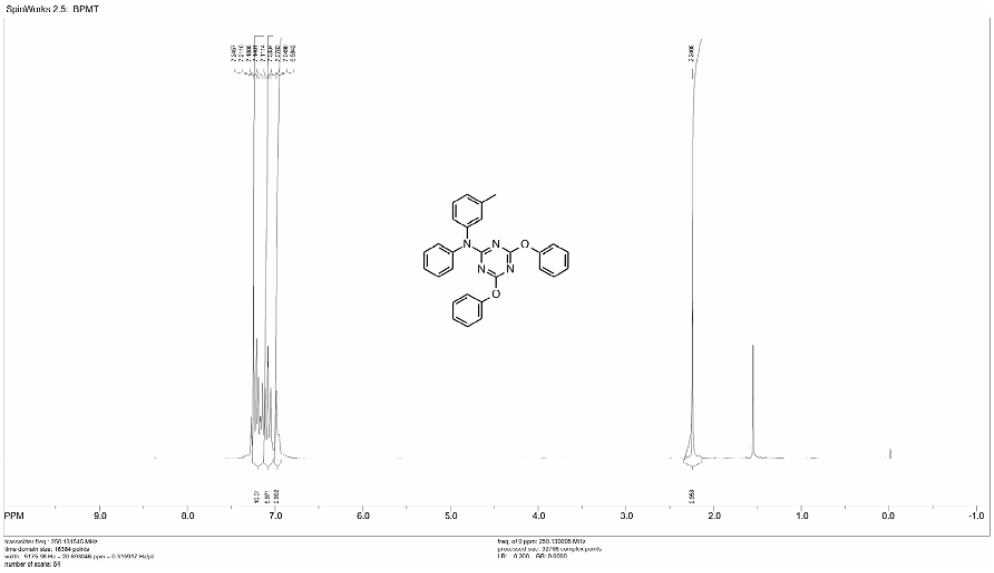

Figure S3: ^{1}H-NMR (250 MHz, CDCl3) spectrum of BPMT

The purity of BPMT has been carefully checked by HPLC (Agilent 1100 HPLC with Agilent Zorbax Bonus RP (4.6 x 150 mm; 5 micron) column). The eluent was acetonitril/H2O (8/2, V/V) Figure S4 shows the HPLC spectrum.

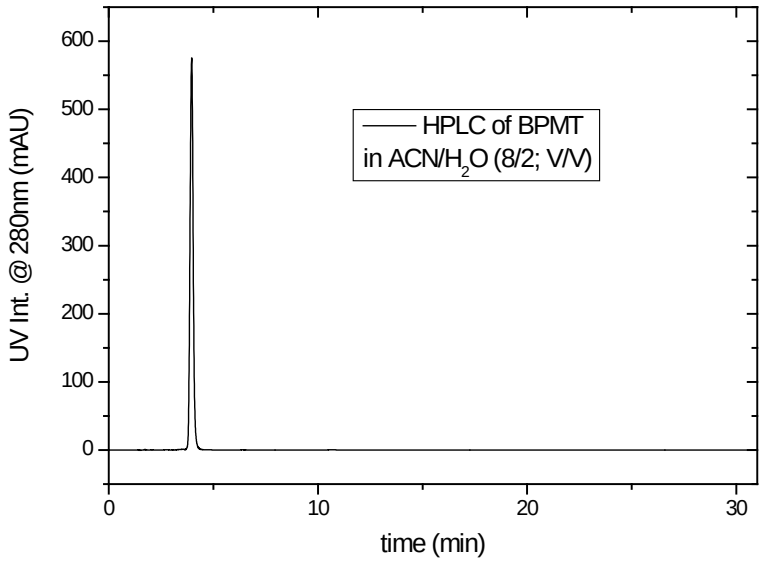

Figure S4: HPLC spectrum of BPMT**.**

OLED structures and concentration dependence of quenching Fig. S5 shows the concentration depends of the electric field induced quenching for different samples containing a different amount of Ir(cnbic)3 in PMMA. The data show a clear trend between the amount of quenched PL and the emitter concentration. As shown effective quenching sets at concentrations beyond 20%. The quenching curves have been modelled according to the Onsager model for the dissociation of Coulombically bound electron hole pairs. The model is described in more detail in the section below. The red curves superimposed on the data points show the results of the fitting.

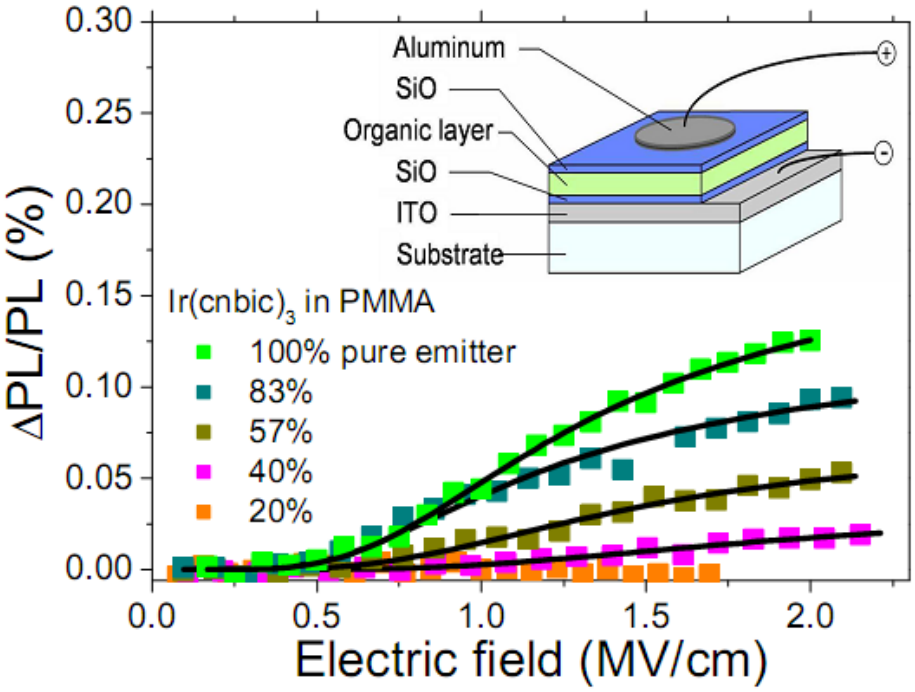

Figure S5: Electric field induced quenching for $Ir(cnbic)_3$ dispersed in PMMA. Different weight ratios were investigated: 20% (orange), 40% (violet), 57% (olive), 83% (blue) and 100% (green). The inset illustrates the typical sandwich structure used to perform the quenching experiments. Solid black lines are fitting curves according to the Onsager model.

To fit the field dependence of the quenching in figure 2 and figure S5 we used the Onsager model, which has been described in detail elsewhere [Phys. Rev. **54**, 554 (1938), J. Appl. Phys. **49**, 4035 (1978), Phys. Rev. B. **74**, 085316 (2006)]. Assuming a isotropic distribution and the same separation distance r_0 for all polaron pairs, the field dependent dissociation probability is given by:

$$\Delta PL/PL(r_0,F)=\Phi_0\left[1-\left(\frac{kT}{eFr_0}\right)\sum_{j=0}^{\infty}I_j\left(\frac{e^2}{\varepsilon_r\varepsilon_0 kTr_0}\right)I_j\left(\frac{eFr_0}{kT}\right)\right],$$

here Φ_0 denotes the initial probability of formation of polaron pairs, and F the electric field strength. $I_j(x)$ is given by

$$I_j(x)=I_{j-1}(x)-\frac{x^j\exp(-x)}{j!}\text{ and }I_0=1-\exp(-x).$$

The experimental data are in good agreement with the Onsager model (figure S5). The values obtained for the fit of the different samples are listed in table S1.

	Φ_0	r_0 (nm)
40% Emitter in PMMA	0.05	1.88
60% Emitter in PMMA	0.06	2.51
80% Emitter in PMMA	0.14	3.17
100% Emitter in PMMA	0.22	2.70
8% Emitter in $Ir(dpbic)_3$	0.54	2.16

Table S1: Values for the initial probability of formation of polaron pairs Φ_0 and for the distance of the polaron pairs r_0 obtained for fitting the experimental data to the Onsager model using the parameters $\varepsilon_r = 3.5$ and T = 296K.

11 List of Publications

6. **M. M. Rothmann**, S. Haneder, E. Da Como, C. Lennartz, C. Schildknecht, P. Strohriegl
„ Donor-substituted 1,3,5-Triazines as Host Materials for Blue Phosphorescent Organic Light-Emitting Diodes"
submitted to *Chemistry of Materials*, **2009***.*

5. **M. M. Rothmann**, E. Fuchs, C. Schildknecht, N. Langer, C. Lennartz, I. Münster, P. Strohriegl
„Designing a bipolar host material for blue phosphorescent OLEDs: Phenoxy-carbazole substituted triazine"
submitted to *Chemical Communications*, **2009**.

4. S. Haneder*,* E. Da Como*,* J. Feldmann*,* **M.M. Rothmann**, P. Strohriegl, C. Lennartz*,* I. Münster*,* C. Schildknecht , G. Wagenblast,
„Effect of Electric Field on Coulomb-Stabilized Excitons in Host/Guest Systems for Deep-Blue Electrophosphorescence",
Advanced Functional Materials, **2009**, *19*, 2416-2422.

3. O. Werzer, K. Matoy, D.M. Smilgies**, M. M. Rothmann**, P. Strohriegl, R. Resel,
„Uniaxially aligned poly[(9,9-dioctylfluorenyl-2,7-diyl)-co-bithiophene] thin films characterized by the X-ray diffraction pole figure technique"
Journal of Applied Polymer Science, **2008**, *107*, 1817-1821.

2. H. Thiem, **M. M. Rothmann**, P. Strohriegl,
„New fluorene-bithiophene based oligomers for the use in OFETs"
Des. Monomers Polym., **2005**, *8*, 619-628.

1. W.E. Lindsell, G.M. Rosair, **M. M. Rothmann**
„Reactions of α,ω-dithiolate ligands with bis(cyclopentadienyl)molybdenum dichloride; crystal structures of $Mo(\eta\text{-}C_5H_5)_2\ S(CH_2)_nS)$ (n = 2, 3) and a layered hydrate, $Mo(\eta\text{-}C_5H_5)_2(SCH_2CH_2O) \cdot 4.5\ H_2O$"
J. Organometallic Chem., **2005**, *690*, 126–133.

Patent applications

2. E. Fuchs, N. Langer, C. Lennartz, P. Strohriegl, **M. Rothmann**
„Use of substituted tris(diphenylamino)-triazine compounds in OLEDs ";
WO 2009/053278 A1, BASF SE, Germany.

1. E. Fuchs, N. Langer, C. Lennartz, P. Strohriegl, **M. Rothmann**:
„Use of diphenylamino-bis(phenoxy) and bis(diphenylamino)-phenoxytriazine compounds in OLEDs "
WO 2009/053346 A1, BASF SE, Germany.

Danksagung

Die vorliegende Arbeit wurde im Zeitraum von Januar 2006 bis November 2009 unter der Leitung von Prof. Dr. Peter Strohriegl am Lehrstuhl für Makromolekulare Chemie I an der Universität Bayreuth angefertigt. Ihm möchte ich besonders danken für die sehr interessante und anwendungsbezogene Aufgabenstellung sowie seine fortwährende Bereitschaft zur Diskussion.

Herrn Prof. Dr. Hans-Werner Schmidt danke ich für die Überlassung eines gut ausgestatteten Labor- und Messplatzes an seinem Lehrstuhl.

Für die finanzielle Unterstützung sei dem Bundesministerium für Bildung und Forschung (BMBF) und der BASF SE im Rahmen des Projektes OPAL 2008 gedankt.

Meinen Labor- und Projektkolleginnen Pamela Schrögel und Andrea Jahreis danke ich für die große Diskussionsbereitschaft während meiner Doktorarbeit, durch die der eine oder andere Gedanke erst gefasst wurde.

Bei Irene Bauer möchte ich ganz herzlich bedanken für die großartige Unterstützung bei der Synthese und Aufreinigung der Verbindungen. Weiterhin gedankt sei Bastian Wedel, Christian Pester, Christoph Hanske und Lisa Rollny die während ihrer Praktika auf diesem Gebiet mitgearbeitet haben.

Ich möchte mich bei allen Mitarbeitern des Lehrstuhls MC1 bedanken, die durch ihre fachliche Kompetenz zum Gelingen dieser Arbeit beigetragen haben. Besonders hervorzuheben sind hierbei Dr. Klaus Kreger, Dr. Christian Neuber und Robin Pettau für ihre ungebrochene Unterstützung durch ihr großes Interesse und Wissen.

Sebastian Hoffmann und Prof. Dr. Anna Köhler vom Lehrstuhl EP2 sowie Stephan Haneder und Dr. Enrico Da Como von der LMU München danke ich für die tieftemperatur-spektroskopischen Untersuchungen meiner Verbindungen.

Ein ganz großer Dank auch an die vielen Kooperationspartner außerhalb der Universität Bayreuth, die mir in wichtigen Fragen weiterhelfen und durch zahlreiche Messungen diese Arbeit mitgestaltet haben. Dr. Nicolle Langer, Dr. Evelyn Fuchs, Dr. Ingo Münster, Dr. Christian Lennartz, Dr. Christian Schildknecht, Dr. Gerhard Wagenblast und Dr. Soichi Watanabe von der BASF. Dr. Herbert Börner von Philips Research Aachen. Hassan Gargouri und Dr. Matthias Hoping von der TU Braunschweig. Dr. Heiko Thiem von Evonik Degussa für die unkomplizierte Bereitstellung des Photoelektronenspektrometers.

Meinen Eltern und meinen Schwestern möchte ich für die tolle Unterstützung während der gesamten Zeit danken. Vielen lieben Danke.

Der größte Dank gilt meiner Freundin Esther, die mir während des gesamten Studiums und der Promotion stets bei mir war und mich in jeder Situation mit allen Kräften unterstützt hat. :P

Erklärung

Die vorliegende Arbeit wurde selbstständig von mir verfasst. Ich habe keine anderen als die angegeben Hilfsmittel verwendet.

Ferner erkläre ich, dass ich nicht versucht habe, anderweitig mit oder ohne Erfolg eine Dissertation einzureichen oder mich der Doktorprüfung zu unterziehen.

Bayreuth, November 2009

(Michael Rothmann)

Quod lumen lumen.